Homogeneous, Heterogeneous, and Heterogenized-Homogeneous Catalytic Hydrogenation for the Cascade Conversion of Carbon Dioxide to Methanol

by

Danielle Christine Samblanet

A dissertation submitted in partial fulfillment
of the requirements for the degree of
Doctor of Philosophy
(Chemistry)
in The University of Michigan
2018

Doctoral Committee:

Professor Melanie S. Sanford, Co-Chair
Professor Levi T. Thompson, Co-Chair
Professor Bart M. Bartlett
Professor Vincent L. Pecoraro

Danielle Christine Samblanet

dsambla@umich.edu

ORCID iD: 0000-0002-0886-6859

DEDICATION

To the little ones in my life,

Elizabeth Mae,

Joshua Laurence,

Amelia Elizabeth,

&

Louis Paul.

Wherever you go, whatever you do,

work hard to make your dreams come true.

ACKNOWLEDGEMENTS

My graduate career would not have been possible without the support of my lab, friends, and family. In my second year of graduate school, I decided I was going to leave with my master's degree to pursue a law degree. I had spent many months talking to my husband, my brother and sister-in-law, my cousins, and my closest friends about my future plans. I proceeded to gain the courage to knock on Melanie's office door and tell her. I was confident and straight forward, "I'm leaving in December." I recall the utter silence that followed as Melanie stared at me with an expression of shock. Finally, after what must have been at least three minutes, she looked at me and said "No." This reply caught me so off guard, I replied "okay," tail-between my legs, ready to run out of the office and back to the safety and comfort of my hood. Of course, Melanie would never have let that happen. We proceeded to have an hour-long conversation about why I wanted to leave, what I was going to do, etc. There were multiple knocks on her door during that time, all of which were completely ignored. Melanie was focused on helping me and making sure I was making the right choice for me. Over the next few weeks we had multiple conversations about what was the best route to get where I wanted in life. Melanie may have initially said no to my bombshell, but in reality, she was a 100% supportive of whatever decision I made. She made me feel like she truly and honestly just wanted me to be happy with where I was going to end up, science or not.

With that story in mind, I'd like to thank my research advisor, Melanie. She is undoubtedly the most supportive research advisor I could have ever asked for. Through each research up and down she was there to help. I've learned so much chemistry from her and through her guidance have developed my analytical, writing, and communication skills to prepare me for a career in patent law. When people think of scientists, let alone geniuses, they think of a socially-awkward and hard-to-talk old guy. Well, Melanie contradicts every single one of those stereotypes. Most people in chemistry know Melanie is an utter genius, but what many may not realize is that she is an even a better person; she is one of the nicest and most caring people I've ever met. Beyond the plethora of Melanie stories I could tell ranging from hilarious to inspirational to downright insane (she's a hypochondriac), my favorite Melanie moment is certainly when she said, "The point of grad school is to not be in grad school." She

really gets it. Thank you, Melanie, for all of the chemistry and life lessons you taught me, and for sharing in my germaphobia when someone coughs in lab.

I would also like to thank my committee members Vincent Pecoraro, Levi Thompson, and Bart Bartlett. Each member has contributed to my scientific development and for that I am truly grateful. I will never forget Professor Pecoraro calling himself and s-orbital to teach us about bond angles. I learned so much from him in just a few short weeks that I considered rotating in his very bioinorganic lab just to continue to learn from him. I had the chance to work closely with Professor Thompson through CENTC where I learned a great deal about heterogeneous catalysis. Finally, in my second year I took a materials class from Professor Bartlett to learn more about the mythical topic of materials (or at least that was it was to me). The class ended up being one of the most useful I took at the University of Michigan and prepared me for a full project on MOFs. Additionally, I would like to thank Professor Bartlett for refreshing my baseball terminology during my candidacy exam where he pitched questions such as, “This project is a base-hit, maybe a double. How will you develop this into a homerun?” and “This could either be a pop fly or a grand slam. What are your plans if it is a pop fly?” Each of these professors were instrumental in my development as a chemist.

Based on my calculations, I’ve had at least 45 full time lab members in the Sanford lab. Although I have seen many post-docs come and go, there are a few I really need to thank. Thanks to Dr. Rachel Brooner who always observed sweatpants Sundays with me and always cheered me up with a great Daisy story. A special thanks to my MOF-boss Dr. Doug Genna who took a confused organic chemist under his wing and was always there to answer any of my questions about MOFs. Finally, my upmost favorite Australian, Outback James (Dr. James Suttil). I remember you were the first person in lab I told about leaving grad school and you always listened without judgment. I can’t express how much I appreciated that. You were such a great colleague to have in lab and I missed you daily since you left.

To the 2017 Sanford lab students, Sharmila, Sydonie, Pablo, Nomaan, and Nicole, you guys were the absolute best group of people to work with for four years. To my dearest little pup, Sharmila. You’ve grown into such a wonderful young lady and I am so proud of you. I miss feeding you dinner and snacks and chocolate. I miss our hair styling dates. Really, I just miss you. I can’t wait to see where you go in life, and I do know for sure, I will be right there cheering you on. Thank you to Sydonie who always provided the most phenomenal baked goods, shared a passion for LOTR, and understood how much I loathe gas equilibration. Pablo was always there to cheer me up and make me laugh no matter the circumstances. To my mentor Nomaan, I can’t thank you enough, you taught me so much and were always there to

empathize on the CO_2 project. Finally, to Noodle Seaver, much more of a dear friend than a colleague. From Charley's visits to grandma Ester days, from wedding cruise to Indy, from Pablo's wedding to Nicholsongiving, we have the most fun together. I can't express how happy I am to have met you. I know we will forever be friends.

To my current 2018 labmates, thank you all. To Christian and Devin who literally always make me laugh. A special thanks to Katarina and Mark who read thesis chapters and were always there to talk to over the years. To my fellow fifth years, James, BJ, and Melissa, I couldn't have asked for a more diverse or better group of people to go through grad school with. Little Melissa Lee, I will miss you so much after grad school. You are such a joy to be around and I admire you so much. Thanks for sharing in the crazy the last 5 years and for always being there no matter how stressed or busy you were. Finally, to Kuam Cakes, you've made my last year of grad school so much better than I thought it could be. You kept me sane through thesis writing and helped with my thesis so much more than I could have expected. Thank you, I will miss you.

The past five years were filled with life events beyond professional development. I made life-long friends. I watched twelve dear friends tied the knot. I got two sisters-in-law, an almost sister-in-law, and a brother-in-law. I was privileged to welcome two nephews and one niece. I got married. So much of life happened during grad school.

I had such a great internal support system through graduate school, but haven't even mentioned my external support system. A special shout out to my Indy family, Wedding Cruise people, and Cruise 2017 crew for making my vacations the best. I was so fortunate to have my local friends, Rachel and Beeper. Thank you, Rachel for being up for an adventure to Universal or Disney, unplanned lunch date, or double date dinner at Zingerman's. To Beeper, for the unregulated corgi cuddles before late night sushi, always spending July 4th together (some went better than others), and for loving Harry Potter just as much as I do. My Michigan family, the Meadows have been amazing over the last five years. Lynda and Keith always let us crash their holidays, helped with life events, and are really our second parents. To my little sister, Jaclyn who always listens, makes me smile, and knows my true inner crazy. I long for the day when we reside in the same state and don't have to travel hundreds of miles for a hug or shopping adventure. It's amazing that even though I've moved an hour further away from my hometown, I feel so much closer to my Louisville family. Thank you to Chris and Brad. I can't even express how much I love you guys and your kids or how thankful I am to have you guys in my life. You are truly irreplaceable.

Finally, to my immediate family, I am so thankful to have you guys and for everything you do for me. I love every one of you. Thank you, mom and dad, for raising me, always supporting me through the years, dealing with my stubbornness, and being up for an intense game of Monopoly. I look forward to our upcoming adventures together. Thank you, Jason, for getting me the best sister I could ever ask for (queue Kara), letting Sean and I crash your weekends at least once a month, and for letting us be apart of Amelia's and Louis's lives. The four of you bring me so much joy and happiness. You guys are the best siblings I could ever ask for. At last, I would like to thank my husband, Sean. We made it. What a rollercoaster. Thank you for going through grad school a second time. I really couldn't have done it without you. You are the best life partner. I can't wait to see where our adventure takes us next.

TABLE OF CONTENTS

LIST OF SCHEMES

LIST OF FIGURES

LIST OF TABLES

LIST OF EQUATIONS

ABSTRACT

This thesis focuses on the catalytic cascade conversion of carbon dioxide to methanol. Two cascade pathways were studied involving either an amide or ester intermediate. In the amide cascade pathway carbon dioxide is converted to formic acid. The formic acid undergoes an amidation reaction with a dimethylamine to produce an amide, which is ultimately hydrogenated to give methanol. In the ester cascade system, carbon dioxide is hydrogenated to formic acid which undergoes an esterification reaction with an equivalent of alcohol to generate a formate ester. Finally, the ester is hydrogenated to methanol.

Chapter 2 of this thesis focuses on finding improved homogeneous amide hydrogenation catalysts for ultimate application in the amide cascade system. Five Ru-PNP^{R} catalysts with varying substitutions on the phosphorus of the PNP were studied (R= Cy > iPr > Ph > tBu > Ad). A combination of batch reactions and *in situ* Raman monitoring showed that the three best catalysts gave high yields (>95%), selectivity (C-N bond cleavage), and exhibited fast rates (reactions complete in <6 hours under various conditions). Additionally, Ru-PNP^{Cy} and its 1st row analog, Fe-PNP^{Cy} were directly compared to one another. It was found that Ru was superior to its Fe analog, but Ru was only 1.7 as fast as Fe. This was surprising as computational studies have suggested 1st row analogs to be orders of magnitude slower than their 2nd counterpart.

Using the information from Chapter 2, Chapter 3 revolves around applying new homogeneous catalysts to the amide cascade system. Two new catalysts, Ru-PNP^{Cy} and Ru-PNP^{iPr} were applied to the amide cascade system and under certain conditions, outperformed the original catalyst used, Ru-PNP^{Ph}. Notably, Ru-PNP^{Cy} gave the highest CO_2 conversions

while Ru-PNP^{Ph} produced the highest turnovers of methanol. Cooperative cascade catalysis wherein Ru-PNP^{Cy} or Ru-PNP^{iPr} was coupled with Ru-PNP^{Ph} in the same pot yielded more methanol than the sum of the two catalysts individually, suggesting a synergistic effect between the catalysts. Variability in the amide cascade system was seen and many routes were attempted to eliminate it.

Chapter 4 focuses on coupling a homogeneous and heterogeneous catalyst in the ester cascade pathway. Three heterogeneous catalysts (Cu/Mo_2C, Mo_2C, CZA) were studied to find a superior ester hydrogenation catalyst in order to generate an improved second-generation ester cascade system. The heterogeneous catalysts were active for ethyl formate hydrogenation at low temperatures (80–135 °C) and pressures (≤40 bar). Despite the excellent reactivity of the heterogeneous catalysts, when coupling a heterogeneous catalyst with any one of five homogeneous catalysts, inhibition rather than synergy was seen between the two. Post-catalysis characterization suggested that the homogeneous catalyst was deposited on the heterogeneous catalyst.

Chapter 5 investigates heterogenizing a homogeneous ester hydrogenation catalyst inside of a metal-organic framework (MOF) via ionic interactions. The MOF utilized was MIL-101-SO_3 which contains an anionic linker and the cationic homogeneous complex used was [IrCp*Bpy(H_2O)][OTf]$_2$. The heterogenized-homogeneous catalyst (Ir@MIL) was active for ester hydrogenation, and even outperformed the homogeneous analog. Excitingly, the homogeneous catalyst could be ion-exchanged out of Ir@MIL either pre- or post-catalysis to straightforwardly study the catalytic active site and confirm that the Ir had maintained both its Cp* and bpy ligands. Ultimately, Ir@MIL is not a good candidate for the ester cascade system due to Ir leaching from Ir@MIL during catalysis, which likely the result of the cationic hydrogenation mechanism.

CHAPTER 1

Introduction

1.1. Global Climate Change and CO_2

An impasse arises when trying to preserve the current environment and its resources, while also facing continued population growth. The ever-increasing population results in a corresponding increased need for electricity, fuel, and plastics. Alternative sources of electricity and fuel are constantly sought, as these items are currently derived from non-renewable fossil fuel feedstocks, which take tens of thousands of years to naturally regenerate.[1] These fossil fuels also threaten the Earth's livelihood as many of them produce carbon dioxide when consumed.[1] The question eventually becomes whether the availability of these resources will be able to keep up with the growing population, and will the environment be destroyed in the process? These questions have no definitive answer, but the outlook on both is quite unsettling.

It is apparent that the environment is significantly suffering from human activities.[1] Climate change can be seen globally, but especially in Greenland.[1,2] Greenland's landmass is currently comprised of approximately 80% ice.[2] In 2014 alone, nearly 40% of the mass experienced melting due to increased temperatures.[2] Southern Greenland has recorded average temperatures approximately 2 °C above the 1981-2010 averages.[2] Moving just 400 miles north, temperatures have increased by about 8 °C on average.[2]

Many factors contribute to global climate change including carbon dioxide (CO_2) emissions.[1] Atmospheric CO_2 concentrations have dramatically increased over the past

800,000 years with the highest concentration in 2016 at 402 ppm (Figure 1.1).[3] In 2017, the average CO_2 concentration further increased to 403.96 ppm.[4] The correlation between increased atmospheric CO_2 concentrations and increased global temperatures is clear (Figure 1.2).[5] Although there are temperature fluctuations from year to year, the global temperature has increased by 1.4 °C since the start of the 1900s.[5] The twenty warmest years have all occurred since 1980 with the five warmest years on record occurring since 2010.[6]

Figure 1.1. CO_2 Concentrations Over the Past 800,000 years[3]

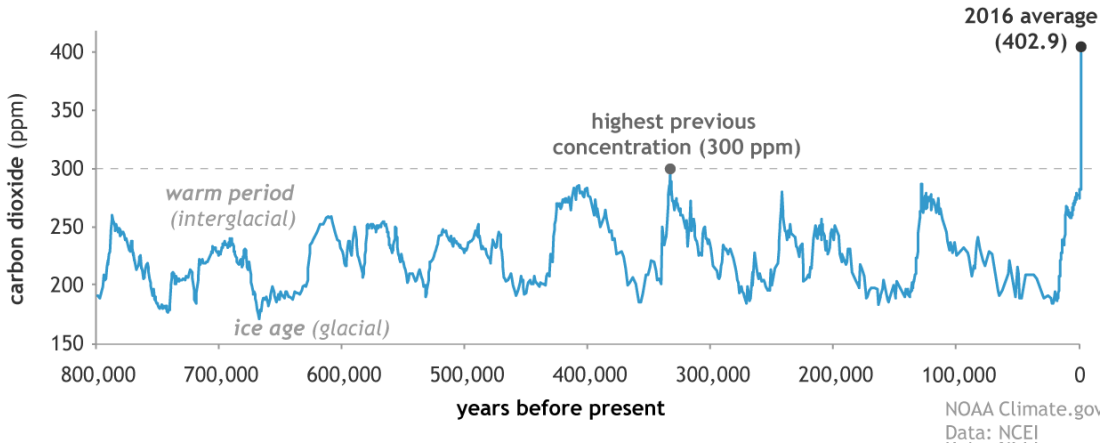

Figure 1.2. Relationship Between Global Temperature and CO_2 Concentrations[5]

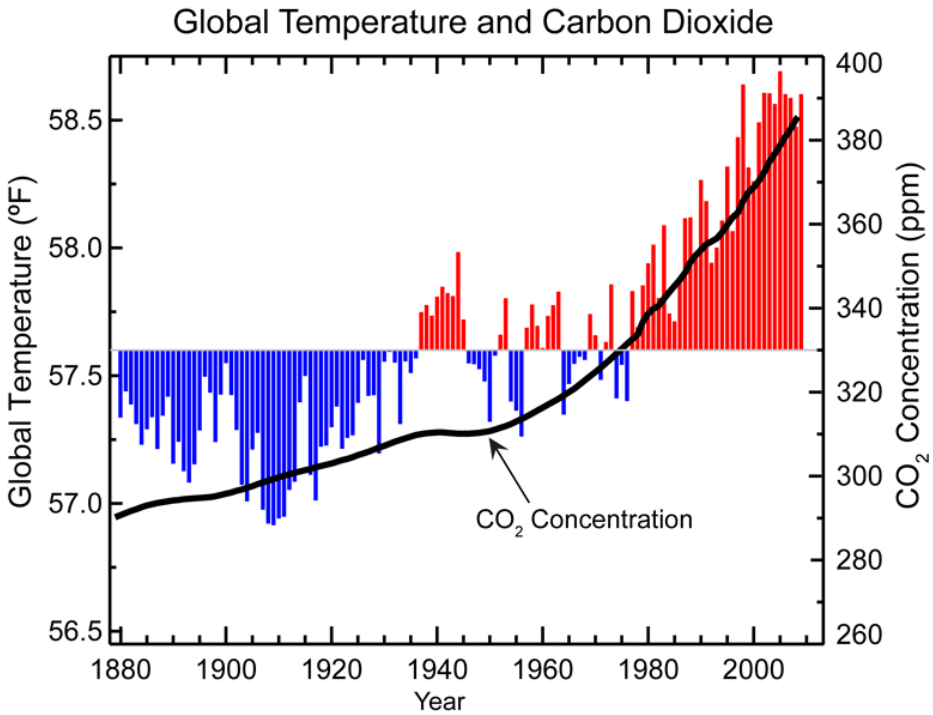

Although carbon dioxide is not the only gas contributing to climate change, its production and release into the atmosphere is the most profound (Figure 1.3).[1,7] Additionally, even though CO_2 absorbs less heat per molecule compared to methane,[3] it is significantly more abundant accounting for 82% of United States greenhouse gas emissions in 2012.[7] Carbon dioxide is further problematic as it absorbs energy at a different wavelength than water.[3] This results in more heat being retained by the atmosphere which would otherwise not be present.[3]

Figure 1.3. Influence of Select Greenhouse Gases[3]

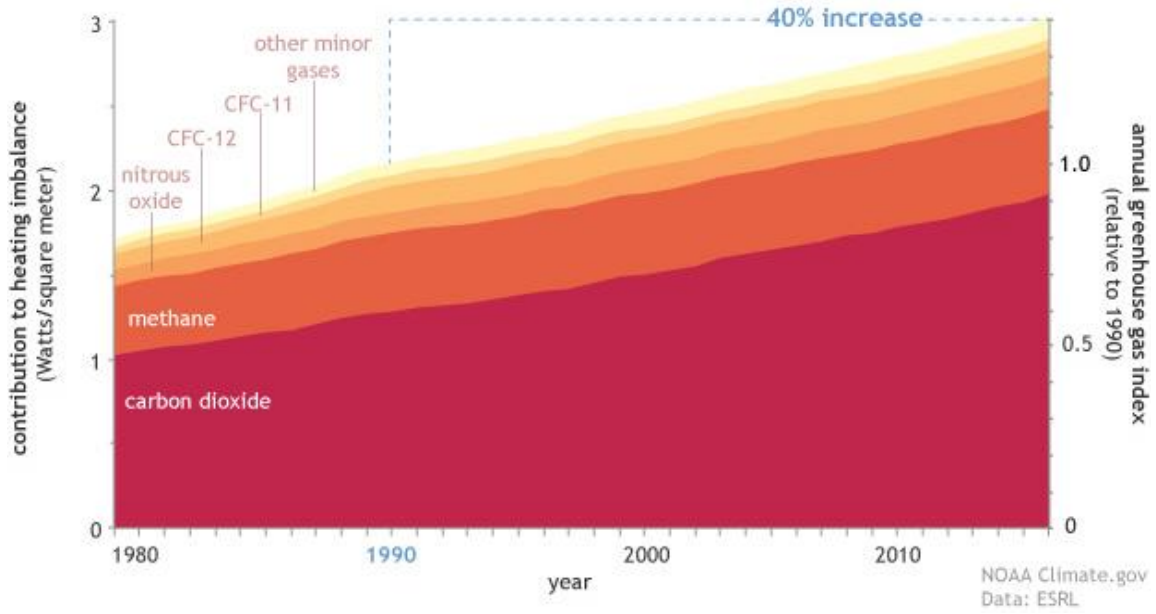

Even though CO_2 is a naturally occurring greenhouse gas, anthropogenic CO_2 emissions are causing an imbalance in the natural carbon cycle (Figure 1.4). Anthropogenic CO_2 emissions are emissions that originate from human activities such as the burning of coal and oil. Anthropogenic CO_2 emissions have spiked since the age of industrialization, taking the concentration of CO_2 in the atmosphere from 270 ppm to over 400 ppm, a 50% increase in just 200 years.[8] Human processes produce nearly 29 billion tons per year.[8] Major carbon sinks include plants, soil, and oceans.[9] Plants utilize CO_2 for photosynthesis, but widespread deforestation coupled with increased CO_2 emissions are allowing for further accumulation of

CO_2 in the atmosphere.[1,9] Oceans are a major carbon sink, but unfortunately, there are serious repercussions, namely, ocean acidification.[1,3,9] Since industrialization, the pH of the ocean has changed from 8.21 to 8.10.[3] This has had profound impacts on ocean-dwelling organisms, including the depletion of coral reefs.[1] Ultimately, CO_2 emissions are contributing to global climate change.

Figure 1.4. Global Carbon Cycle Flux[9]

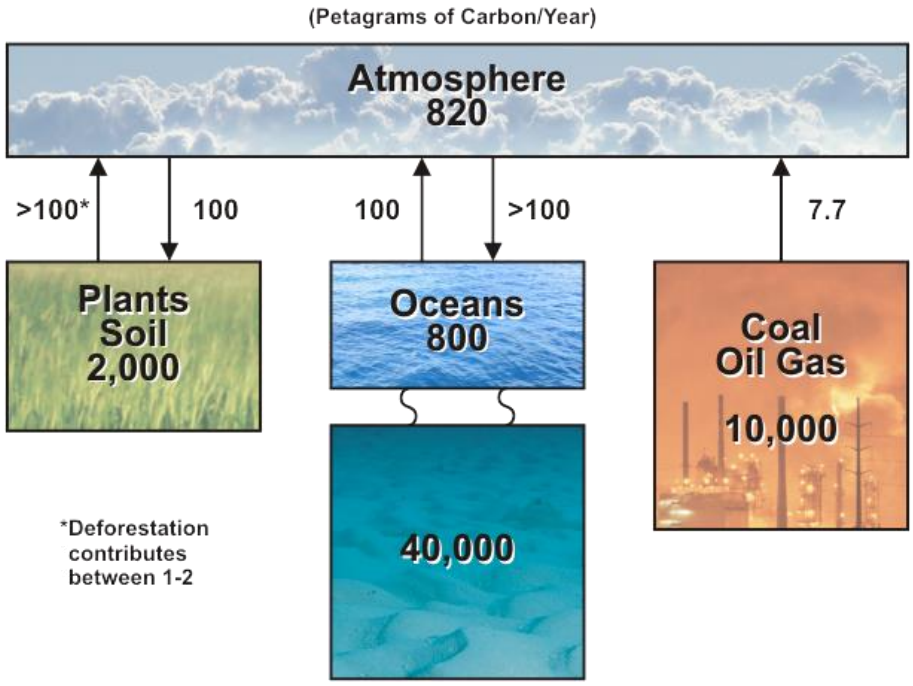

1.2. Conversion of CO_2 to Value-Added Methanol

One possible solution to the conundrum of maintaining the current standard of living while conserving the environment lies in the utilization of carbon dioxide as a chemical feedstock.[8] Instead of continuously releasing carbon dioxide into the atmosphere and adding to the building concentrations, why not take CO_2 from the atmosphere and utilize it as a chemical feedstock?[8] Olefins, ethylene glycol, ethanol, and methanol are all consumed on large scale and currently produced from fossil fuels. These four important products may be alternatively produced from CO_2 (Figure 1.5).[8]

Figure 1.5. Instead of Releasing CO_2 into the Atmosphere, CO_2 May Instead be Utilized

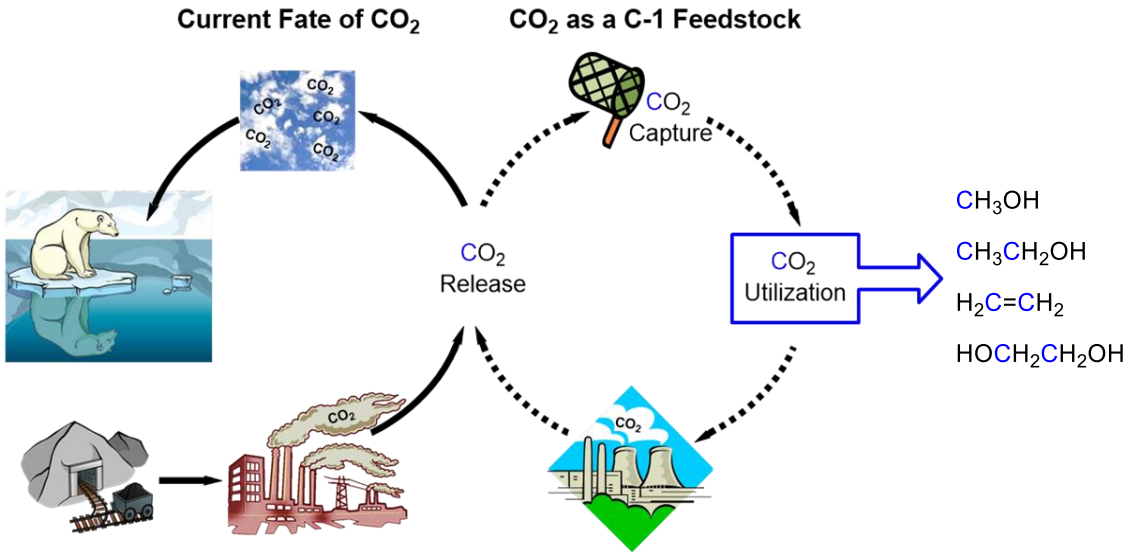

One of the most practical uses of carbon dioxide would be the production of methanol. Approximately 100,000 tons of methanol are consumed daily and are ultimately manufactured into paints, resins, silicones, adhesives, antifreeze, and plastics.[8] Nearly 40% of methanol is used to create formaldehyde, which is a vital feedstock for the polymer industry.[8] Furthermore, there are processes to take methanol to olefins and even gasoline length hydrocarbons (C_5-C_{10}).[8] Methanol derived from CO_2 would constitute a significant reduction in the amount of CO_2 in the atmosphere while also producing valuable products.

An idealized advantage of converting CO_2 to methanol lies in the Methanol Economy (Scheme 1.1).[8] The Methanol Economy presents a carbon neutral solution to CO_2 generation and fossil fuel consumption.[8] In this cycle, atmospheric CO_2 is captured and used to produce methanol. Methanol is then used as fuel and combusted to release CO_2. The released CO_2 can be captured and utilized, completing the cycle. Although this carbon neutral cycle presents an ideal solution to the increasing atmospheric CO_2 concentrations, as well as the depleting fossil fuel reserves, this cycle is far from global realization. The capture of CO_2 from the atmosphere is well studied, though the release of CO_2 is energetically inefficient.[10] Capturing CO_2 after generation at industrial plants, but before release into the atmosphere will not mitigate global

climate change from the CO_2 already in the atmosphere.[10] Additionally, methanol cannot be directly used in most combustion engines, particularly in vehicles.[8] Methanol would need to be up-converted to more complex molecules such as dimethyl ether or hydrocarbons; although, these technologies do exist, this would require a break in the Methanol Economy resulting in a non-carbon neutral cycle.[8] Furthermore, the Methanol Economy relies on efficient water electrolysis from renewable resources for true carbon neutrality.[10] Unfortunately, the most accessible form of energy to spilt water typically relies on coal or oil.[10] The Methanol Economy is not globally realistic at this point in time, but striving to advance the technologies present within the Methanol Economy are critical research topics, which may aid in climate change mitigation in addition to advancing science in other ways.[10]

Scheme 1.1. The Methanol Economy

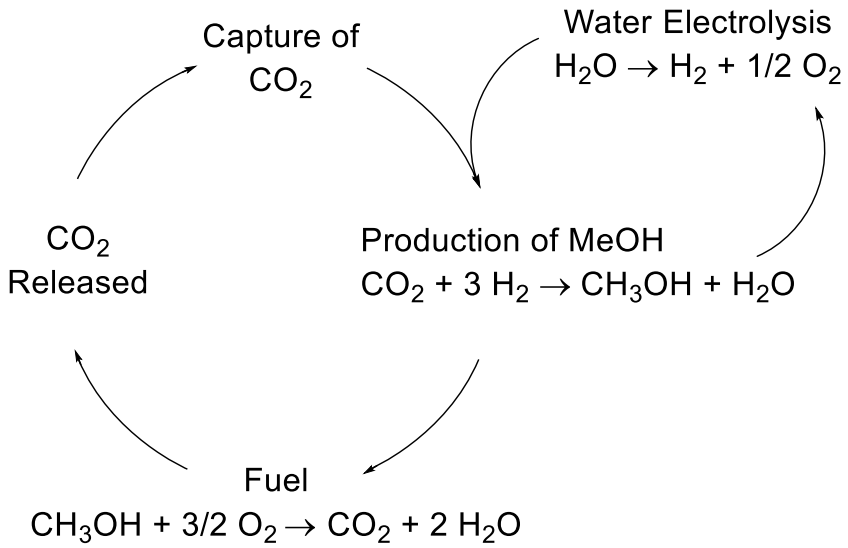

1.3. Current Industrial Production of Methanol

Current industrial production of methanol is accomplished via heterogeneous catalysts. In the early 1900s, some of the first methanol production plants utilized CO_2 as their carbon source; however, most of it derived from other processes within the chemical plant, not the atmosphere.[8] Some of the first catalysts employed were chromium oxides and zinc oxides with

reaction temperatures ranging from 300 to 400 °C and pressures of 250 to 300 atm.[8,11] These catalysts later spawned the development of other metal oxide based heterogeneous catalysts. During the 1960s, Imperial Chemical Industries developed copper zinc aluminum oxide and used it extensively for methanol production from syngas.[8] This catalyst enabled the use of significantly lower temperatures (200-300 °C) and pressures (50-100 atm).[8,12] Current industrial catalysts for methanol production are still copper based.[8,10,13]

Currently, nearly 90% of methanol is derived from methane. Methane is used to create syngas via steam reforming to yield CO and H_2 (syngas) (Scheme 1.2).[8] The CO and water in the system undergo the water gas shift reaction creating CO_2 and H_2 as products. As such, all three gases, CO_2, CO, and H_2 are fed into the reactor containing heterogeneous catalysts.[8] Through a series of studies, a general consensus has been reached that significant amounts of methanol are derived from CO_2 generated via the water gas shift reaction (although, the exact amount is still regularly disputed, with computational methods predicting around 70% of methanol being derived from CO_2, while experimental studies have reported greater than 90%).[8,11-14] This is advantageous since as CO_2 and H_2 react with one another to form methanol and water, the water can then react with the CO in the system to generate more CO_2, thus constantly pushing the reaction in the forward direction and not allowing the system to reach equilibrium.

Scheme 1.2. Steam Reforming of Methane and the Water Gas Shift Reaction to Form the Feed Gas for Methanol Production

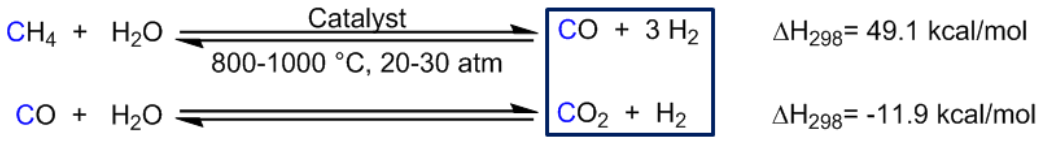

Scheme 1.3. Industrial Production of Methanol Over a Heterogeneous Catalyst ($Cu/ZnO/Al_2O_3$ as an example)

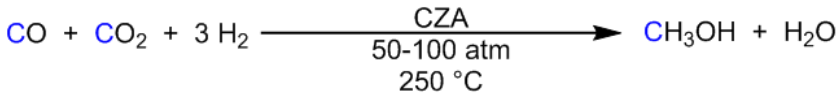

Recently, there is much interest around the world to employ CO_2 as a feedstock to produce methanol. In Iceland, the George Olah Plant built by Carbon Recycling International utilizes CO_2 from geothermal sources and industrial processes, while the H_2 is derived from water electrolysis.[10] The plant is capable of producing 5 million liters of methanol and utilizes 5,500 tons of CO_2 each year.[15] Plans for similar plants have been released, such as one in Japan with H_2 derived from photochemical splitting of water, but it is not currently in operation, even though completion was planned to occur in 2010.[10]

Although technologies do exist to industrially convert CO_2 directly to methanol, an underlying challenge of methanol synthesis from CO_2 is that the reaction becomes more thermodynamically unfavorable as temperature is increased. The reaction is enthalpically favorable ($\Delta H = -131$ kJ/mol), but entropically unfavorable ($\Delta S = -409$ J/(mol·K)).[8] This results in the two values opposing one another in terms of Gibbs free energy [$\Delta G = (\Delta H) - T(\Delta S)$], resulting in the reaction becoming less spontaneous as the temperature increases.[8] This temperature restraint is a major issue, as industrial heterogeneous catalysts typically utilize high temperatures to overcome high activation barriers and kinetic limitations.[11] Lower operating temperatures would be beneficial for favoring the equilibrium towards the desired product, methanol. Additionally, the rational design and selective tuning of heterogeneous catalysts remains non-trivial.[11,16] The heterogeneous catalysts employed have a further disadvantage in that they are typically difficult to study.[11,16]

Ultimately, homogeneous catalysis presents solutions to each of the challenges faced in the heterogeneous conversion of CO_2 to methanol. Homogeneous catalysts are often operable at lower temperatures compared to heterogeneous catalysts with relatively smaller activation barriers.[16] This would allow for low temperature CO_2 conversion where the reaction is much more favorable.[16] Compared to heterogeneous catalysts, homogeneous catalysts tend to be much easier to study allowing for the elucidation of the reaction mechanism, which in

turn leads to rational design of catalyst variations.[16] Advantageously, homogeneous catalysts can be straightforwardly amended and appended to generate multiple analogs.[16] The homogeneous conversion of CO_2 to methanol holds much promise in solving many of the limitations of heterogeneous catalysts.

1.4. Homogeneous Conversion of CO_2 to Methanol

The first homogeneous conversion of carbon dioxide to methanol was accomplished via cascade catalysis in 2011.[17] Instead of direct conversion of CO_2 to methanol with a single catalyst, Huff and Sanford utilized three separate homogeneous catalysts in tandem (Scheme 1.4).[17] This idea was inspired by nature, where CO_2 is functionalized through a series of proton coupled electron transfers utilizing multiple enzymes.[18] Instead of inventing a single new catalyst, each individual step utilized a previously reported catalyst with a comparatively smaller activation barrier for the individual step. When used in combination, this series of catalysts converted CO_2 to methanol at relatively low temperature (135 ºC).[17] First, Catalyst A produced formic acid by hydrogenation of CO_2.[19] Next, Catalyst B, a Lewis acid that acts as an esterification catalyst, transformed the formic acid in the presence of methanol to methyl formate.[20] Finally, methyl formate was reductively cleaved by Catalyst C, an ester hydrogenation catalyst, yielding methanol.[21] Overall, the only materials consumed are CO_2, and H_2, while the only species produced are methanol (21 turnovers), and naturally abundant and benign, water.[17]

Though this methodology holds much promise, there is significant room for improvement. The main roadblock encountered with this system was the fact that Catalyst C was poorly compatible with Catalyst B,[22,23] requiring Catalysts A and B to be physically separated from C within the reactor.[17] Ideally, all three catalysts would be combined in a single pot to allow for the facile reaction of intermediates with each catalyst, in turn yielding the final

products. Additionally, there was a significant amount of methyl formate, approximately 70 turnovers, remaining at the end of the reaction, thus indicating that Catalyst C is not performing as well as the other catalysts in the system.[17] With the combination of compatibility issues and modest performance, Catalyst C was determined to be the limitation of the cascade system.

Scheme 1.4. Cascade Conversion of CO_2 to Methanol via and Ester Intermediate

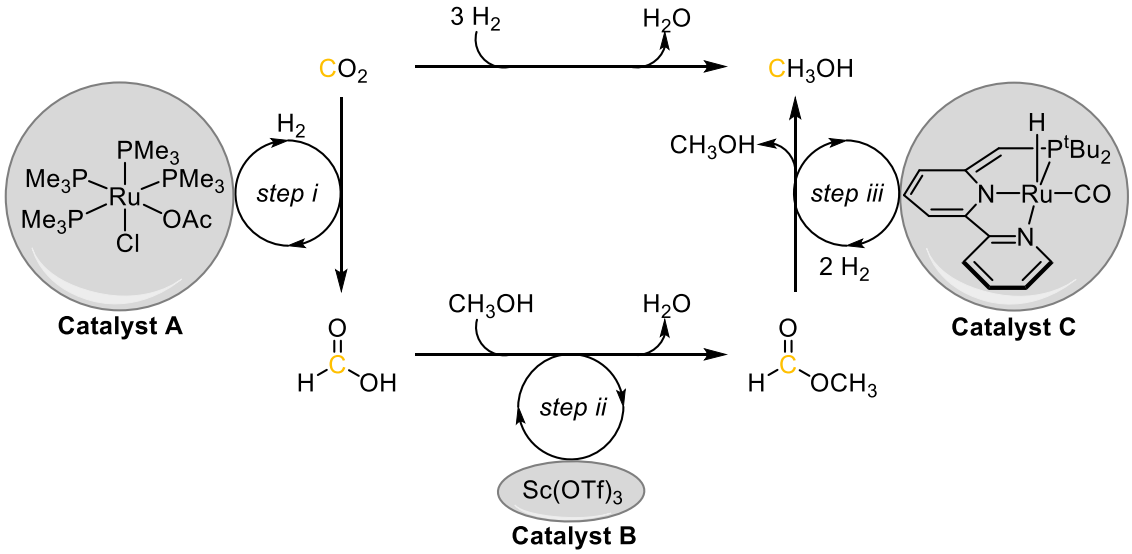

In 2012, Klankermayer and Leitner published a homogeneous conversion of CO_2 to methanol utilizing a single catalyst based on Ru and baring a triphos ligand.[24] They were able to generate 221 turnovers of methanol (Scheme 1.5).[24] Two years later, with the help of mechanistic and computational studies, they found that the alcohol in their original reaction was actually impeding the catalyst reactivity.[25] By eliminating ethanol from the reaction, they were able to produce 442 turnovers of methanol (Scheme 1.6).[25]

Scheme 1.5. Ru-Triphos Homogeneous Conversion of CO_2 to Methanol

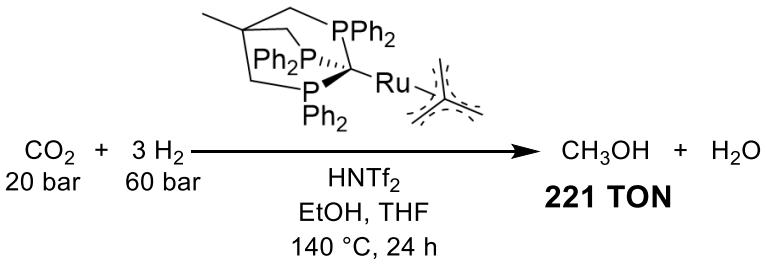

Scheme 1.6. Improved Ru-Triphos Homogeneous Conversion of CO_2 to Methanol

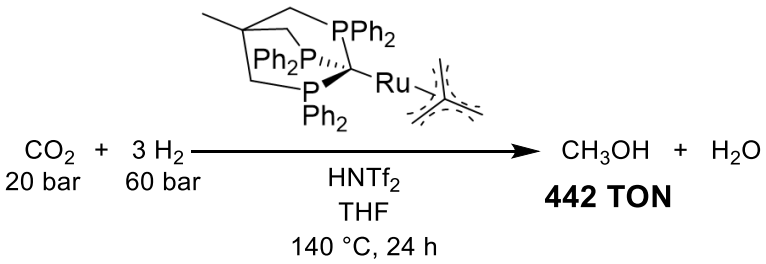

In 2015, the Sanford group followed up on their original cascade catalytic system, instead accessing an amide intermediate and utilizing a single metal-based catalyst.[26] In this amide cascade system, a ruthenium catalyst hydrogenates CO_2 to formic acid (Scheme 1.7, step i). The generated formic acid undergoes an amidation reaction (Scheme 1.7, step ii) with dimethylamine ($HNMe_2$) producing N,N-dimethylformamide (DMF). The same ruthenium catalyst hydrogenates DMF producing methanol while regenerating dimethylamine (Scheme 1.7, step iii). This system generated up to 550 turnovers of methanol and over 95% conversion of CO_2.[26]

Scheme 1.7. Cascade Conversion of CO_2 to Methanol via and Ester Intermediate

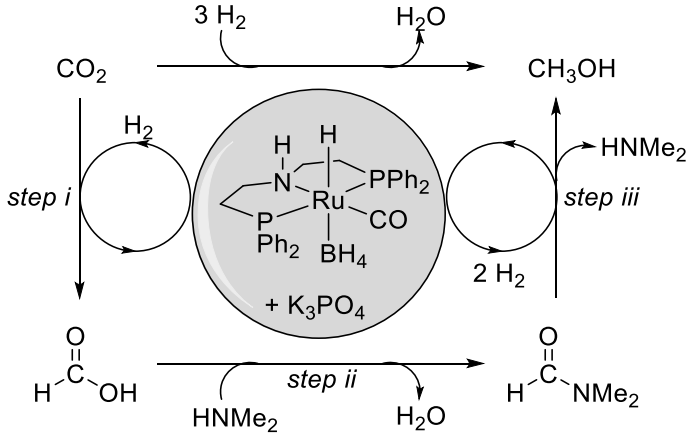

Since the advent of these ground-breaking homogeneous catalytic CO_2 to methanol systems, many other homogeneous catalysts and systems have been developed. Notably, Milstein and co-workers used a Ru-PNN catalyst coupled with an alkanolamine to generate modest turnovers of methanol (21).[27] This methodology was attractive in that ethanol amine,

an alkanolamine, is industrially used to capture CO_2 from flue gas.[10] At the same time, this system left much to be desired utilizing long reaction times and requiring the process to be carried out in a two-step process.[27] In the two-step process, once the CO_2 was hydrogenated, the system was vented releasing unreacted CO_2 and repressurized with H_2 only. Ding and co-workers generated a system very similar to the amide cascade system wherein a slight variation on the Ru-PNP catalyst used by Sanford and co-workers was employed, but instead of dimethylamine, morpholine was used as the amine.[28] By applying a two-step process similar to Milstein, Ding and co-workers were able to generate 3600 turnovers of methanol and 6300 turnovers of the intermediate formamide.[28] Finally, Olah and Prakash further expanded upon the Sanford lab's amide cascade system employing a slight variation of the Ru-PNP catalyst and a polyamine pentaethylenehexamine instead of dimethylamine.[29] Under optimized conditions, they were able to generate 520 turnovers of methanol.[29] Excitingly, this system could also be used to capture and hydrogenate CO_2 from a mixture of gases found in air (400 ppm of CO_2 in 80:20 N_2 to O_2) producing up to 79% yield.[29]

1.5. Further Investigations into the Ester and Amide Cascade Systems

This thesis expands upon the Sanford group's original reports of cascade conversion of CO_2 to methanol via either an ester[17] or amide intermediate (Scheme 1.8).[26] Chapter 2 of this thesis explores different homogeneous catalysts for DMF hydrogenation, as this was the limiting step in the original amide cascade system. Applying the catalysts from Chapter 2, Chapter 3 revolves around generation of an improved amide cascade system. Chapter 4 investigates utilizing a tandem catalytic system consisting of both a homogeneous and heterogeneous catalyst in the ester cascade system. Finally, Chapter 5 discusses heterogenizing homogeneous catalysts inside of metal-organic frameworks for ester hydrogenation, ultimately

for application in the ester cascade system. The over-arching goal throughout remains generating improved catalytic systems for the conversion of CO_2 to methanol.

Scheme 1.8. Amide and Ester Cascade Systems Throughout Each Chapter

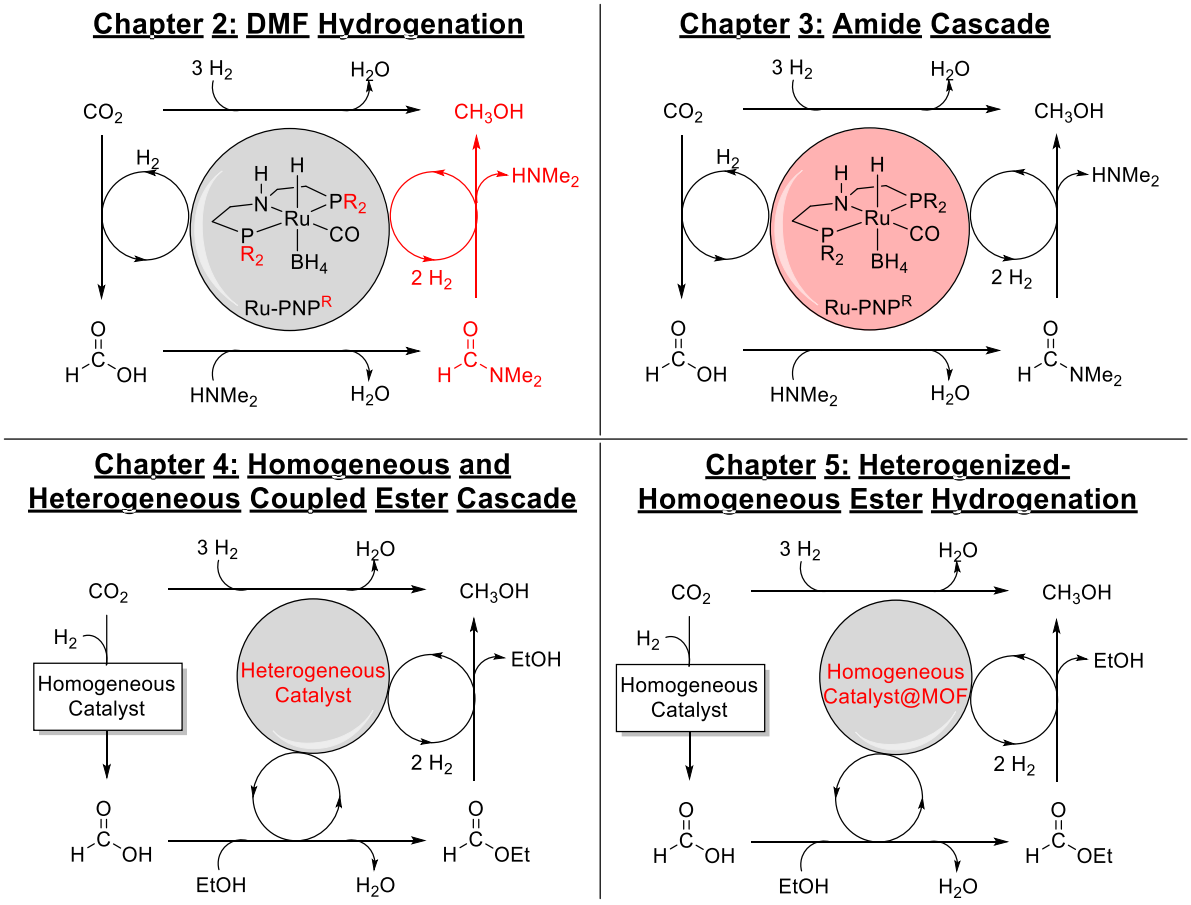

1.6. References

1. Baird, C.; Cann, M. *Environmental Chemistry*, W.H. Freeman and Company, New York, **2012**.

2. Tedesco, M.; Box J. E.; Cappelen, J.; Fettweis, X.; Mote, T.; van de Wal, R.S.W.; Smeets, C.J.P.P.; Wahr, J. *Greenland Ice Sheet.* http://www.arctic.noaa.gov/reportcard /greenland _ice_sheet.html, January 27, 2015.

3. Lindsey, R. *Climate Change: Atmospheric Carbon Dioxide.* https://www.climate.gov /news-features/understanding-climate/climate-change-atmospheric-carbon-dioxide, October 17, 2017.

4. Dlugokencky, E.; Tans, P. *Trends in Atmospheric Carbon Dioxide.* https://www.esrl. noaa.gov/gmd/ccgg/trends/global.html#global_growth, January 5, 2018.

5. National Centers for Environmental Information, National Oceanic and Atmospheric Administration. *Global Climate Change Indicators.* https://www.ncdc.noaa.gov/ monitoring -references/ faq/indicators.php (accessed January 31, 2018).

6. Phillips, B. *NOAA: 2017 as 3rd warmest year on record for the globe.* http://www.noaa.gov/news/noaa-2017-was-3rd-warmest-year-on-record-for-globe, January 18, 2018.

7. Environmental Protection Agency. *Carbon Dioxide*. http://www.epa.gov/climatechange/ ghgemissions/gases /co2.html, August 7, 2014.

8. Olah, G.A.; Goeppert, A.; Prakash, G.K.S. *Beyond Oil and Gas: The Methanol Economy*, Wiley-VCH, **2006**.

9. Carbon Dioxide Information Analysis Center. *The Carbon Cycle.* http://cdiac.ess-dive. lbl.gov/carbon_cycle.html (accessed January 31, 2018).

10. Olah, G. A.; Goeppert, A.; Prakash, G. K. S. *J. Org. Chem.* **2009**, *74*, 487.

11. Hansen, J.B.; Nielsen, P.E.H. *Handbook of Heterogenous Catalysis*, 2nd ed.; Wiley-VCH, **2008**.

12. Waugh, K.C. *Catal. Letters*, **2012**, *142*, 1153.

13. Grabow, L.C.; Mavrikakis, M. *ACS Catal.* **2011**, *1*, 365.

14. Behrens, M.; Studt, F.; Kasatkin, I.; Kühl, S.; Hävecker, S.; Abild-Pedersen, F.; Zander, S.; Girgsdies, F.; Kurr, P.; Kniep, B.; Tovar, M.; Fischer, R.W.; Nørskov, J.K.; Schlögl, R. *Science*, **2012**, *336*, 893.

15. Carbon Recycling International. *George Olah Plant.* http://carbonrecycling.is/george-olah/, February 14, 2016.

16. Miessler, G. L.; Fischer, P. J.; Tarr, D. A. *Inorganic Chemistry*, 5th ed.; Pearson, **2013.**

17. Huff, C. A.; Sanford, M. S. *J. Am. Chem. Soc.* **2011**, *133*, 18122.

18. Berg, I. A. *Appl. Environ. Microbiol.* **2011**, *77*, 1925.

19. Munshi, P.; Main, A.D.; Linehan, J.C.; Tai, C.C.; Jessop, P. G. *J. Am. Chem. Soc*. **2002**, *124*, 7963.

20. Barrett, A.G.M.; Braddock, D.C. *Chem. Commun*. **1997**, 351.

21. Zhang, J.; Leitus, G.; Ben-David, Y.; Milstein, D. *Angew. Chem. Int. Ed.* **2006**, *45*, 1113.

22. Huff, C. A.; Kampf, J. W.; Sanford, M. S. *Organometallics* **2012**, 3*1*, 4643

23. Huff, C. A.; Kampf, J. W.; Sanford, M. S. *Chem. Comm*. **2013**, *49*, 7147

24. Wesselbaum, S.; von Stein, T.; Klankermayer, J.; Leitner, W. *Angew. Chem. Int. Ed.* **2012**, *21*, 7499.

25. Wesselbaum, S.; Moha, V.; Markus, M.; Brosinski, S.; Thenert, K.M.; Kothe, J.; von Stein, T.; Englert, U.; Holscher, M.; Klankermayer, J.; Leitner, W. *Chem. Sci.*, **2015**, *6*, 693.

26. Rezayee, N. M.; Huff, C. A.; Sanford, M. S. *J. Am. Chem. Soc*. **2015**, *137*, 1028.

27. Khusnutdinova, J. R.; Garg, J. A.; Milstein, D. *ACS Catal.*, **2015**, *5*, 2416.

28. Zhang, L.; Han, Z.; Zhao, X.;Wang, Z.; Ding, K. *Angew. Chem. Int. Ed.* **2015**, *54*, 6186.

29. Kothandaraman, J.; Goeppert, A.; Czaun, M.; Olah, G. A.; Prakash, G. K. S. *J. Am. Chem. Soc.*, **2016**, *138*, 778.

CHAPTER 2

Catalytic Hydrogenation of N,N-Dimethylformamide en Route to Methanol Generation[1]

2.1. Introduction

The catalytic hydrogenation of N,N-dimethylformamide (DMF) is a critical step in the cascade conversion of carbon dioxide (CO_2) to methanol (CH_3OH) via an amide intermediate (Scheme 2.1).[2] In this pathway, CO_2 is hydrogenated to formic acid by a Ru-PNP catalyst (Scheme 2.1, step i). Formic acid then undergoes an amidation reaction with dimethylamine to generate the corresponding formamide, DMF (Scheme 2.1, step ii). Finally, the same Ru-PNP catalyst is used to hydrogenate DMF to methanol and regenerate the co-catalytic amine (Scheme 2.1, step iii). The amide cascade system utilizing Ru-PNP^{Ph} gave excellent conversions of CO_2 (>95%).[2]

Scheme 2.1. Conversion of CO_2 to Methanol via an Amide Cascade Pathway

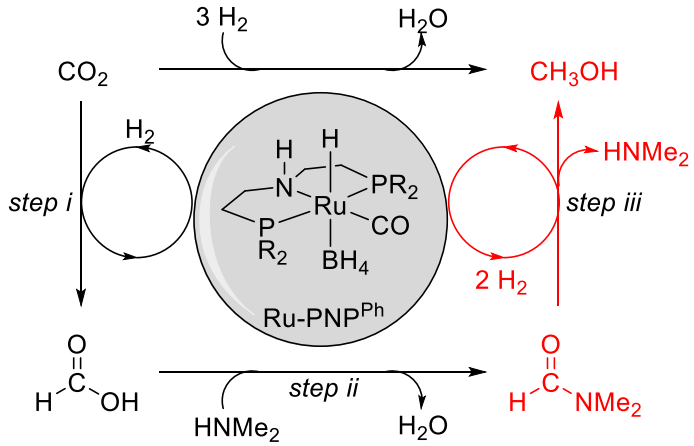

A major limitation to this previously reported amide cascade system is the fact that approximately 75-80% of the converted CO_2 is in the form of formic acid and DMF.[2] Ideally,

a high CO_2 conversion would correspond to high yields of methanol. To increase the amount of methanol obtained, our primary focus shifted to thoroughly studying DMF hydrogenation (Scheme 2.1, step iii). We hypothesized that by identifying a superior DMF hydrogenation catalyst, we would be able to increase the amount of methanol formed. Concurrently, the hydrogenation of DMF will release $HNMe_2$, thus allowing for the conversion of more CO_2. Ultimately, a better DMF hydrogenation catalyst should provide increased amounts of the hydrogenation product, methanol.

Beyond our interest in finding a better DMF hydrogenation catalyst for application in the cascade amide system, amide hydrogenation itself is an important reaction in organic synthesis. There is much interest both academically and industrially on the catalytic hydrogenation of amides.[3,4] The reduction of amides presents an interesting selectivity issue where either C–O or C–N bond cleavage can occur to yield two different products (Scheme 2.2).[5] Traditional methods for the hydrogenation of amides utilize stoichiometric reductants such as lithium aluminum hydride and samarium iodide.[5] The transition-metal-catalyzed hydrogenation of an amide is not only more atom-economical, but often employs milder conditions to generate the desired bond scission products.[3,4]

Scheme 2.2. Bond Scission Products for Amide Reduction

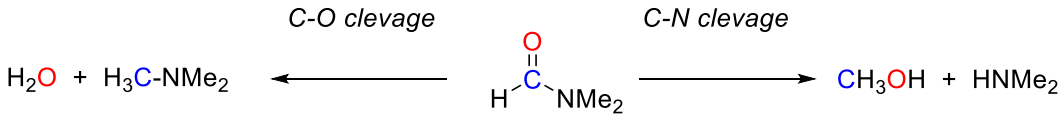

2.2. Results and Discussion

2.2.1. Ruthenium-PNP Catalyzed Hydrogenation of N,N'-Dimethylformamide

We began our studies by evaluating a variety of Ru-PNP complexes with different substituents on the PNP backbone (Figure 2.1).[6,7,8,9,10,11] The original system utilized phenyl

groups on the phosphine (Ru-PNP^{Ph}); however, other variations are known, including isopropyl (Ru-PNP^{iPr}), cyclohexyl (Ru-PNP^{Cy}), tert-butyl (Ru-PNP^{tBu}), and adamantyl (Ru-PNP^{Ad}) derivatives.[7] The original Ru-PNP^{Ph} was commercially available, and the synthesis of the other complexes was straightforward following literature procedures and utilizing commercially available PNP ligands (Scheme 2.3).[12,13,14] With the complexes in hand, we set out to study their reactivity in DMF hydrogenation.

Figure 2.1. Ru-PNP Variations with Different Substituents on the PNP Ligand

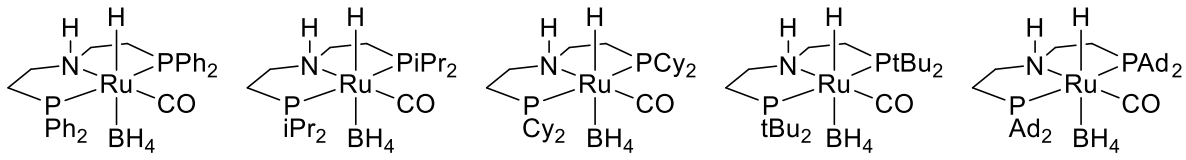

Scheme 2.3. Synthesis of Ru-PNP^{R} Complexes

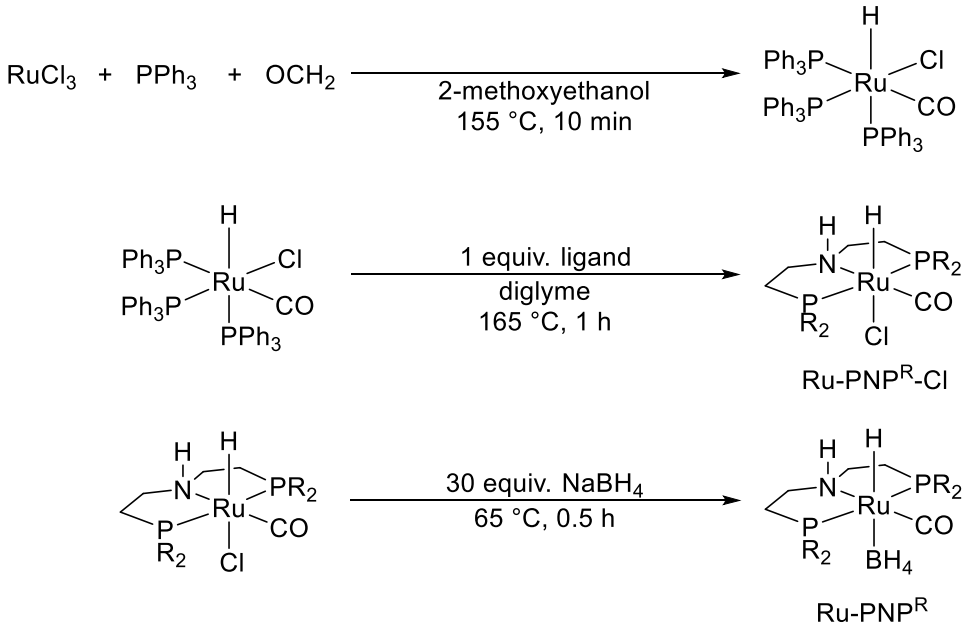

We first focused on utilizing the hydridochloride (Ru-PNP^{R}-Cl) complexes as catalysts for DMF hydrogenation (Table 2.1). These complexes are generated en route to the Ru-PNP^{R} complexes bearing a -BH_4 ligand (Scheme 2.3). Running the reactions under the previously optimized conditions for the cascade amide pathway,[2] we found that in the presence of K_3PO_4, Ru-PNP^{iPr}-Cl and Ru-PNP^{Cy}-Cl afforded near quantitative yields of methanol (Table 2.1,

Entries 1-4). Additionally, Ru-PNP^{tBu}-Cl and Ru-PNP^{Ad}-Cl gave moderate yields under analogous conditions (Table 2.1, Entries 5-8). Notably, all of these complexes selectively afforded the C–N bond scission products (*e.g.*, methanol and dimethylamine) rather than the C–O bond cleavage products (*e.g.*, trimethylamine and water; see Scheme 2.2).

Table 2.1. Hydrogenation of DMF via Ru-PNP-Cl complexes

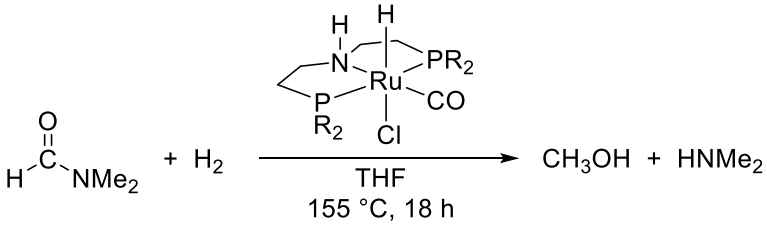

Entry	R	Additive	Yield (%)[a]
1	iPr	None	0
2	iPr	K_3PO_4	>99
3	Cy	None	0
4	Cy	K_3PO_4	>99
5	tBu	None	0
6	tBu	K_3PO_4	80
7	Ad	None	0
8	Ad	K_3PO_4	74

[a]**Conditions:** 1 mmol DMF, 1.5 mL THF, 1 mol% Ru-PNP catalyst, 250 μmol K_3PO_4, 50 bar H_2, 155 °C, 18 h. Yields determined by ^{1}H NMR spectroscopy.

While very similar to the Ru-PNP^R complexes with -BH_4, the Ru-PNP^R-Cl complexes require the use of exogenous base to generate the catalytically active *trans*-dihydride (Scheme 2.4).[15] On the other hand, the -BH_4 complexes can easily lose -BH_3 at elevated temperatures in THF to generate the active catalyst (Scheme 2.4).[14,16,17,18,19,20] The requirement for exogeneous base is the reason that the Ru-PNP^R-Cl species do not show reactivity in the absence of K_3PO_4.

Scheme 2.4. Generation of Catalytically Active *trans*-Dihydride

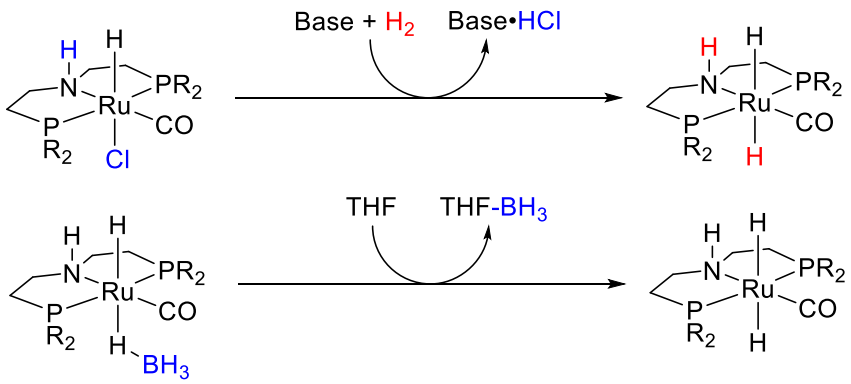

Encouraged by the reactivity of the Ru-PNP^{R}-Cl complexes, the -BH_4 complexes were next tested (Table 2.2). Ru-PNP^{Ph}, Ru-PNP^{iPr}, and Ru-PNP^{Cy} all gave full conversion of DMF and quantitative yields of methanol with and without base (Table 2.2, Entries 1-6). Conversely, Ru-PNP^{tBu} and Ru-PNP^{Ad} both performed better in the absence of base as compared to when K_3PO_4 was present (Table 2.2, Entries 7 vs 8 and 9 vs 10, respectively). The overall lower decrease of Ru-PNP^{tBu} and Ru-PNP^{Ad} versus the other complexes could be due to a combination of increased steric crowding around the metal center. Once again, these complexes were fully selective for C–N bond scission and no C–O bond cleavage products were detected.

Table 2.2. Hydrogenation of DMF via Ru-PNP-BH_4 complexes

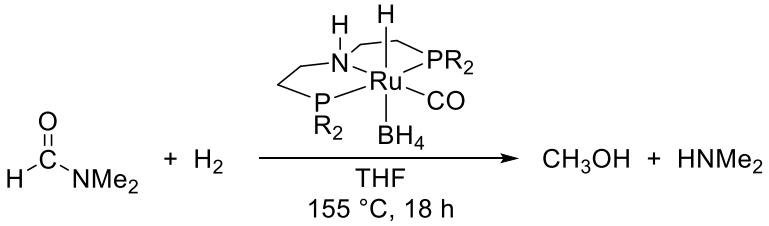

Entry	R	Additive	Yield (%)[a]
1	Ph	None	>99
2	Ph	K_3PO_4	>99
3	iPr	None	>99
4	iPr	K_3PO_4	>99
5	Cy	None	>99
6	Cy	K_3PO_4	>99
7	tBu	None	>99
8	tBu	K_3PO_4	88
9	Ad	None	70
10	Ad	K_3PO_4	33

[a]**Conditions:** 1 mmol DMF, 1.5 mL THF, 1 mol% Ru-PNP catalyst, 250 µmol K_3PO_4, 50 bar H_2, 155 °C, 18 h. Yields determined by ^{1}H NMR spectroscopy.

In an attempt to establish the relative reactivity of the three best Ru-PNP^{R} complexes (R=Ph, iPr, Cy), reaction times were decreased without base present (Table 2.3). Surprisingly, Ru-PNP^{Ph}, Ru-PNP^{iPr}, and Ru-PNP^{Cy} all gave quantitative yields of methanol even when dropping the reaction time from 18 down to just 3 hours. The Ru-PNP^{tBu} and Ru-PNP^{Ad} complexes produced the same amount of methanol in 3 hours; however, at 18 hours it was clear that Ru-PNP^{tBu} was the superior catalyst. This difference in reactivity may be indicative of

enhanced longevity of the Ru-PNP^{tBu} complex. The overall lower reactivity of Ru-PNP^{tBu} and Ru-PNP^{Ad} is likely due to the steric congestion around the metal center with these ligands.

Table 2.3. Decreasing Reaction Time for DMF Hydrogenation

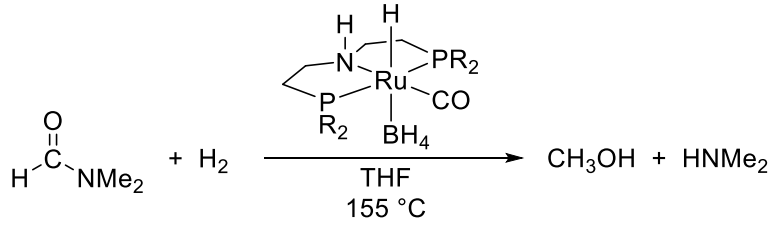

Entry	R	Time (h)	Yield (%)[a]
1	Ph	18	>99
2	Ph	3	>99
3	iPr	18	>99
4	iPr	3	>99
5	Cy	18	>99
6	Cy	3	>99
7	tBu	18	>99
8	tBu	3	30
9	Ad	18	70
10	Ad	3	33

[a]**Conditions:** 1 mmol DMF, 1.5 mL THF, 1 mol% Ru-PNP catalyst, 50 bar H_2, 155 °C. Yields determined by ^{1}H NMR spectroscopy.

In a further effort to distinguish the reactivity of Ru-PNP^{Ph}, Ru-PNP^{iPr}, and Ru-PNP^{Cy}, the reaction temperature was dropped from 155 ºC to 80 ºC (Table 2.4). With such a large decrease in temperature, we expected the corresponding slower reaction rates to be reflected in the yield; however, each complex still afforded quantitative yield of methanol (Table 2.4).

Table 2.4. Decreasing Reaction Temperature for DMF Hydrogenation

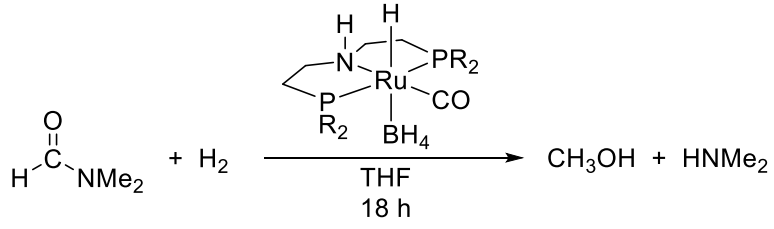

Entry	R	Temperature (°C)	Yield (%)[a]
1	Ph	155	>99
2	Ph	135	>99
3	Ph	100	>99
4	Ph	80	>99
5	iPr	155	>99

6	iPr	135	>99
7	iPr	100	>99
8	iPr	80	>99
9	Cy	155	>99
10	Cy	135	>99
11	Cy	100	>99
12	Cy	80	>99

[a]**Conditions:** 1 mmol DMF, 1.5 mL THF, 1 mol% Ru-PNP catalyst, 50 bar H_2, 18 h. Yields determined by ^{1}H NMR spectroscopy.

A difference in reactivity between Ru-PNP^{Ph}, Ru-PNP^{iPr}, and Ru-PNP^{Cy} was finally observed upon dropping the reaction temperature to 80 °C while decreasing the reaction time for DMF hydrogenation (Table 2.5). In 3 hours at 80 °C, Ru-PNP^{Cy} was the superior catalyst for DMF hydrogenation, affording 83% yield of methanol (Table 2.5, Entry 6). The other two complexes, Ru-PNP^{Ph} and Ru-PNP^{iPr}, were still quite reactive affording 67% yield of methanol (Table 2.5, Entries 2 and 4). Again, in all cases, selective formation of C–N bond cleavage products (methanol and dimethylamine) with no C–O bond scission products (trimethylamine and water) was observed.

Table 2.5. Decreasing Reaction Time and Temperature for DMF Hydrogenation

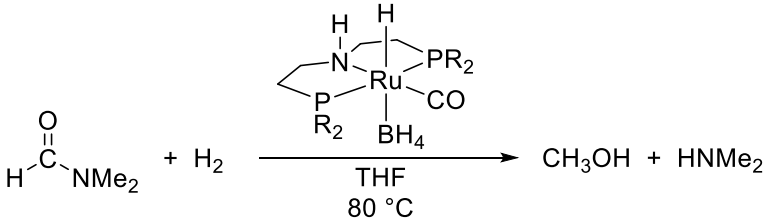

Entry	R	Time (h)	Yield (%)[a]
1	Ph	18	>99
2	Ph	3	67
3	iPr	18	>99
4	iPr	3	67
5	Cy	18	>99
6	Cy	3	83

[a]**Conditions:** 1 mmol DMF, 1.5 mL THF, 1 mol% Ru-PNP catalyst, 50 bar H_2, 80 °C. Yields determined by ^{1}H NMR spectroscopy.

Knowing that Ru-PNP^{Ph}, Ru-PNP^{iPr}, and Ru-PNP^{Cy} are all excellent catalysts for the hydrogenation of DMF under mild conditions, we next sought to study how these three

complexes react in the presence of CO_2 (Table 2.6). Ideally, these complexes will retain their reactivity even if CO_2 is present, as ultimately these complexes will be applied to the cascade amide system where CO_2 is present as a substrate. In the original cascade amide system, we observed that CO_2 inhibited DMF hydrogenation, thus requiring optimization of reaction conditions in order to fully consume the CO_2.

Our initial studies on the influence of just 1 bar of CO_2 on the hydrogenation of DMF showed that all three complexes (Ru-PNP^{Ph}, Ru-PNP^{iPr}, and Ru-PNP^{Cy}) were strongly inhibited by CO_2 (Table 2.6). Indeed, the most reactive complex for DMF hydrogenation, Ru-PNP^{Cy} was the most inhibited by CO_2, dropping the yield of methanol in 18 hours at 155 °C from quantitative down to 56% yield at 1 bar of CO_2 (2 mmol, 200 equivalents compared to [Ru]) (Table 2.6, Entries 1 and 2). Ru-PNP^{iPr}, the second most active complex, also saw significant inhibition, resulting in a drop from 99% to 47% yield of methanol (Table 2.6, Entries 3 and 4). On the other hand, Ru-PNP^{Ph} retained more of its reactivity, as the yield of methanol only dropped from 99% to 73% in the presence of CO_2 at 155 °C (Table 2.6, Entries 5 and 6).

Table 2.6. Influence of CO_2 on the Hydrogenation of DMF

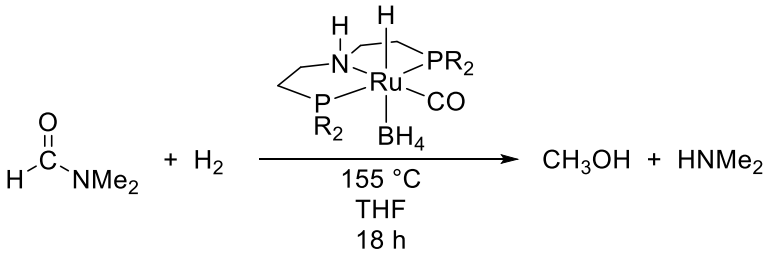

Entry	R	CO_2 (bar)	Yield (%)[a]
1	Ph	—	>99
2	Ph	1	73
3	iPr	—	>99
4	iPr	1	47
5	Cy	—	>99
6	Cy	1	56

[a]**Conditions:** 1 mmol DMF, 1.5 mL THF, 1 mol% Ru-PNP catalyst, 1 bar CO_2, 50 bar H_2, 18 h. Yields determined by ^{1}H NMR spectroscopy.

There is extensive literature precedent for pincer complexes capable of hydrogenating carboxylic acid derivatives being inhibited by CO_2. [2,21,22,23] Our group has reported the formate complexes, **1** and **2**, as stable intermediates of CO_2 hydrogenation in related systems (Figure 2.2).[21,24] Furthermore, Bernskoetter, Hazari, and Holthausen have reported that Fe-PNP^{Cy} reacts with CO_2 to generate the formate adduct, Fe-PNP^{Cy}-OOCH (Figure 2.2).[25] We hypothesize that in the presence of CO_2, our Ru-PNP^{R} complexes are generating the analogous formate complex, Ru-PNP^{R}-OOCH. The formate ligand occupies the open coordination site at the metal and thus inhibits subsequent H_2 activation and subsequent DMF hydrogenation. Additionally, once undergoing a hydrogenation and before splitting of H_2 across the Ru–N bond, Hazari and Bernskoetter also proposed that the backbone nitrogen of Fe-PNP^{Cy} is sufficiently nucleophilic enough to attack CO_2 and generate Fe-PNP^{Cy}-OCO (Figure 2.2).[26] Importantly, they note that in the presence of H_2, the formate-complex Fe-PNP^{Cy}-OOCH is favored and Fe-PNP^{Cy}-OCO speciation is likely of "minimal consequence" as an off-cycle intermediate.[26] Nonetheless, it is worth nothing that this pathway is likely accessible with the Ru-PNP^{R} complexes under certain conditions.

Figure 2.2. CO_2 Inhibition in Pincer Complexes for Carboxylic Acid Hydrogenation

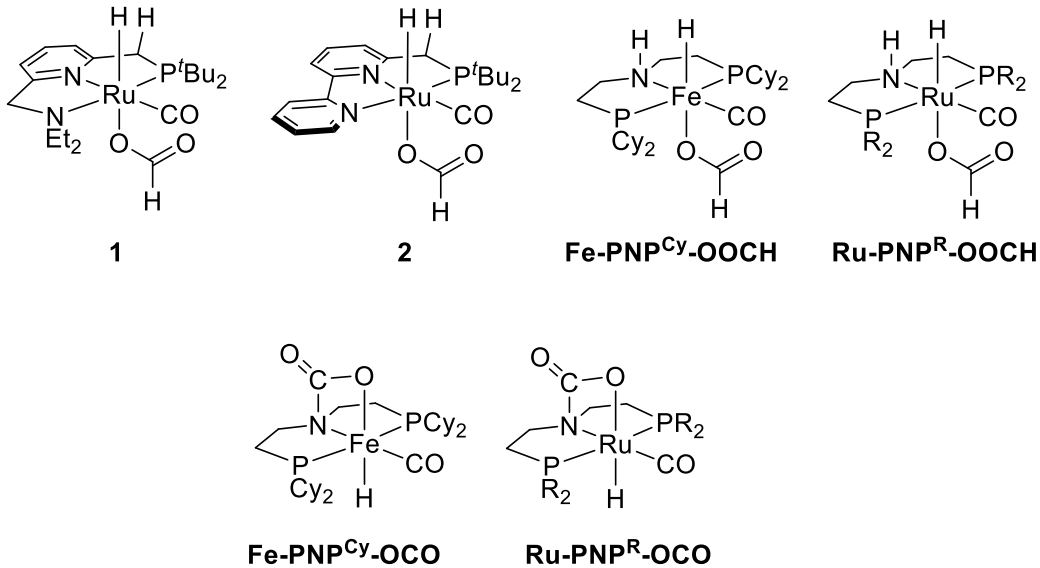

Scheme 2.5. Amide Cascade System Proposed Ru-PNP^R Hydrogenation Mechanism

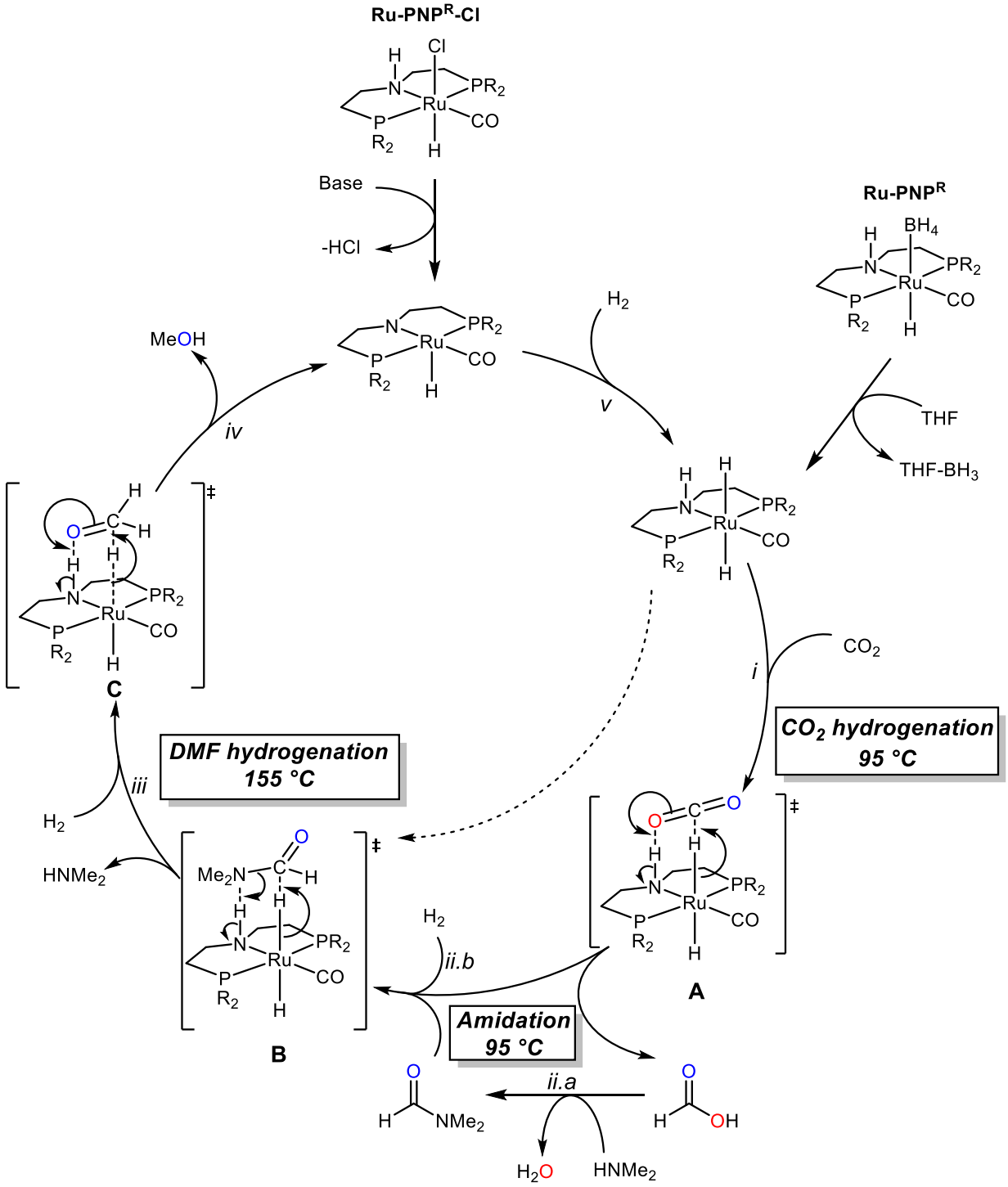

Overall, CO_2 inhibition of Ru-PNP^R catalyzed DMF hydrogenation is likely occurring through CO_2 interacting with Ru-PNP^R to generate a formate complex. This would result in the active site of complex being occupied, thus preventing H_2 activation and subsequent DMF hydrogenation. The mechanism shown in Scheme 2.5 shows the concerted hydrogenation[15] of

CO_2 and DMF, but it should be noted that a step-wise mechanism is also possible.[10,15,25,27,28,29,30] Either Ru-PNP^R-Cl or Ru-PNP^R can enter the catalytic cycle. The Ru-PNP^R-Cl complexes must be activated by base to remove HCl while the -BH_3 of the Ru-PNP^R complexes can be removed with or without base (as mentioned above). A trans-dihydride complex is generated via activation of H_2. Next, CO_2 coordinates and undergoes hydrogenation to give formic acid (Scheme 2.5, step i via **A**). Next, in step ii formic acid undergoes an amidation reaction while Ru-PNP^R splits H_2 across the Ru-N bond regenerating the trans-dihydride (not shown). The amide can then be hydrogenated via **B**. Another equivalent of H_2 regenerates the trans-dihydride (step iii), before a final hydrogenation (**C**). Methanol is formed and released (iv) before a final equivalent of H_2 regenerates the active complex (v), completing the catalytic cycle.

When focusing only on DMF hydrogenation and not the full amide cascade system, only steps iii-v occur, but the mechanism is ultimately the same (Scheme 2.5). Additionally, it is critical to note the thermodynamics of CO_2 hydrogenation. The hydrogenation of CO_2 is more favorable at low temperatures due to the reaction being entropically unfavorable ($\Delta S = -409$ Jmol-1K-1) and enthalpically favorable ($\Delta H = -131$ kJmol-1). At higher temperatures, such as those used for DMF hydrogenation (155 °C), the hydrogenation of CO_2 is much harder than at 95 °C which is employed in the amide cascade system. We propose that the inhibition in Table 2.6 is the result of formation of the corresponding formate complex. At elevated temperatures, it is extremely hard to generate formic acid from the formate complex, thus making the Ru-complex unavailable for DMF hydrogenation.

In addition to the formate complex being extremely stable, in the cases where the formate complex is generated, there is an additional step the catalyst must go through before it can hydrogenate DMF (Scheme 2.6, showing a possible concerted mechanism for hydrogenation and formation of the formate complex). It would be most straightforward for

the CO_2 adduct to directly deprotonate the N-H of the PNP ligand to generate formic acid and the open Ru-complex, both of which can directly enter step ii in Scheme 2.5. However, it is also possible that direct deprotonation does not occur and instead, generation of the formate complex occurs. This complex must still deprotonate the N-H (or can be removed via base as mentioned above), thus resulting in an additional step along the hydrogenation pathway.

Scheme 2.6. Formate Complex Results in an Additional Step

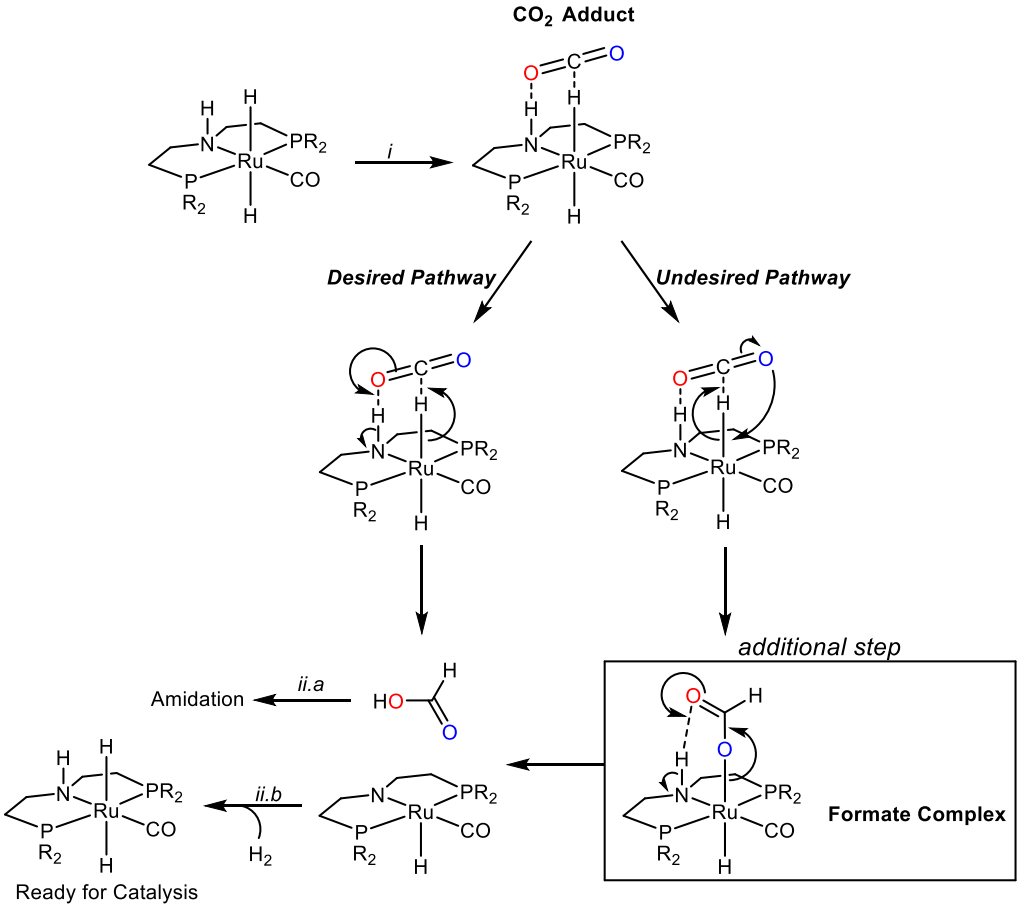

We propose that the reason Ru-PNP^{Ph} is the least inhibited by CO_2 has to do with the deprotonation of the N-H bond on the PNP backbone (Scheme 2.7). Due to steric crowding around the metal center in the case of Ru-PNP^{Cy} and Ru-PNP^{iPr}, we propose that deprotonation of the N-H bond would be more difficult than in the case of the less sterically congested Ru-PNP^{Ph}. Additionally, based on calculations, the predicted pKa of PNP^{Ph} is 9.44 while PNP^{Cy} is 10.01 and finally, PNP^{iPr} is 10.42.[31,32,33] Ultimately, this difference becomes important when the catalyst gets stuck as the formate complex. For Ru-PNP^{Ph} the N-H bond will be more

susceptible to deprotonation by the formate species (or base), thus making it easier to release formic acid from the catalyst while for Ru-PNP^{Cy} and Ru-PNP^{iPr}, the N-H bond will be more difficult to access and less acidic, slowing the release of formic acid and regeneration of the catalyst.

Scheme 2.7. N-H Deprotonation as Key Step in Opening the Active Site of Ru-PNP^{R}

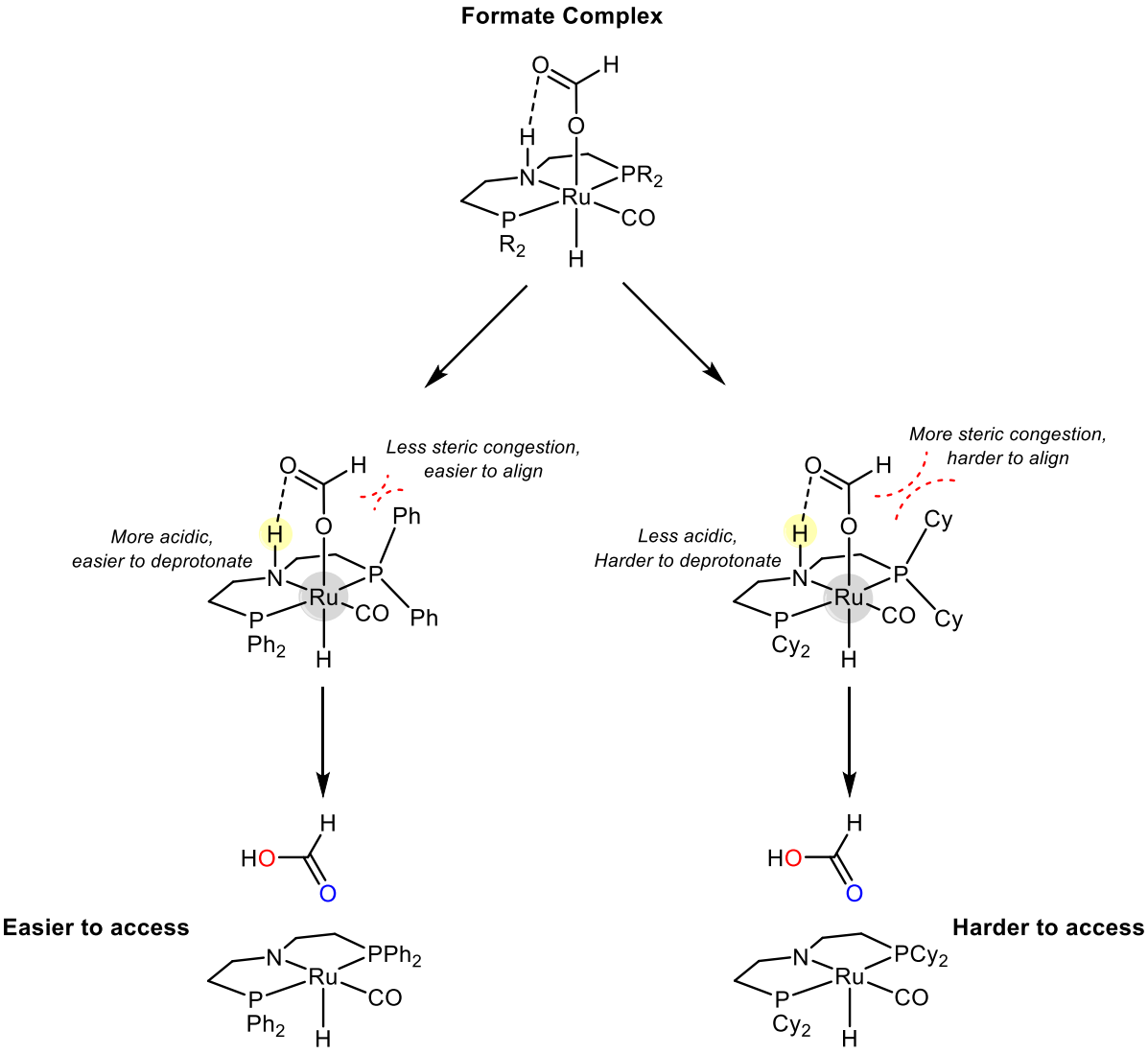

In summary, a suite of Ru-PNP^{R} complexes was studied for the hydrogenation of DMF. Five different Ru-PNP complexes bearing PNP-ligands with varying substitution at the phosphine (phenyl, isopropyl, cyclohexyl, tert-butyl, and adamantyl) were studied. Overall, these studies show that Ru-PNP^{Cy} and Ru-PNP^{iPr} are excellent candidates to use in the amide

cascade system to improve the DMF hydrogenation step due to their excellent reactivity, while noting that they are also strongly inhibited by the presence of CO_2.

2.2.2. Kinetics of Ruthenium-PNP Catalyzed Hydrogenation of N,N'-Dimethylforamide

We next sought to compare Ru-PNP^{Ph}, Ru-PNP^{iPr}, and Ru-PNP^{Cy}-catalyzed DMF hydrogenation using *in situ* kinetics experiments. Most commonly our lab conducts kinetic studies using NMR spectroscopy; however, this is not possible for these Ru-catalyzed DMF hydrogenation reactions, as they require relatively high temperatures and pressures and are typically carried out in Parr reactors. In order to obtain kinetic information about DMF hydrogenation, we constructed a set-up that uses *in situ* Raman monitoring. A reactor was built wherein a Raman probe with a sapphire window was inserted directly into a Parr reactor, allowing for *in situ* Raman monitoring at pressures up to 200 bar and temperatures up to 450 °C (see 2.4.1, Figure 20).[34,35] It is important to note that due to the length of the Raman probe, at least 7 mL of solvent are necessary to fully submerge the sapphire window of the probe. Ultimately, the concentration of DMF in THF was kept constant (0.66 M) with the studies described above, thus requiring the volume of solvent to be scaled up accordingly (from 1.5 mL to 8.5 mL, unless otherwise noted). On the other hand, the amount of catalyst was kept constant resulting in the concentration of catalyst for the kinetics studies significantly decreasing (0.0063 M in Tables 2.1-2.6 versus 0.0011 M in Raman reactions).

Initially, we monitored the formation of methanol during DMF hydrogenation. The Raman spectra of methanol and our reaction solvent, THF, show a number of non-overlapping peaks (Figures 2.3 and 2.4). When placing reaction quantities amount of methanol in THF and obtaining the Raman spectrum, the methanol in THF spectrum appears identical to the THF spectrum, with no new peaks being observed (Figure 2.5). Indeed, the detection limit of

methanol in THF is 12.35 mmol of methanol (or approximately 0.5 mL) in 1.4 mL of THF (Figure 2.6). This represents a 6.5 M concentration of MeOH, which is an order of magnitude higher than that produced in our reaction (0.66 M ; 5.87 mmol in 8.5 mL of THF, 8.95 mL total solution).

Figure 2.3. Raman Spectrum of Methanol

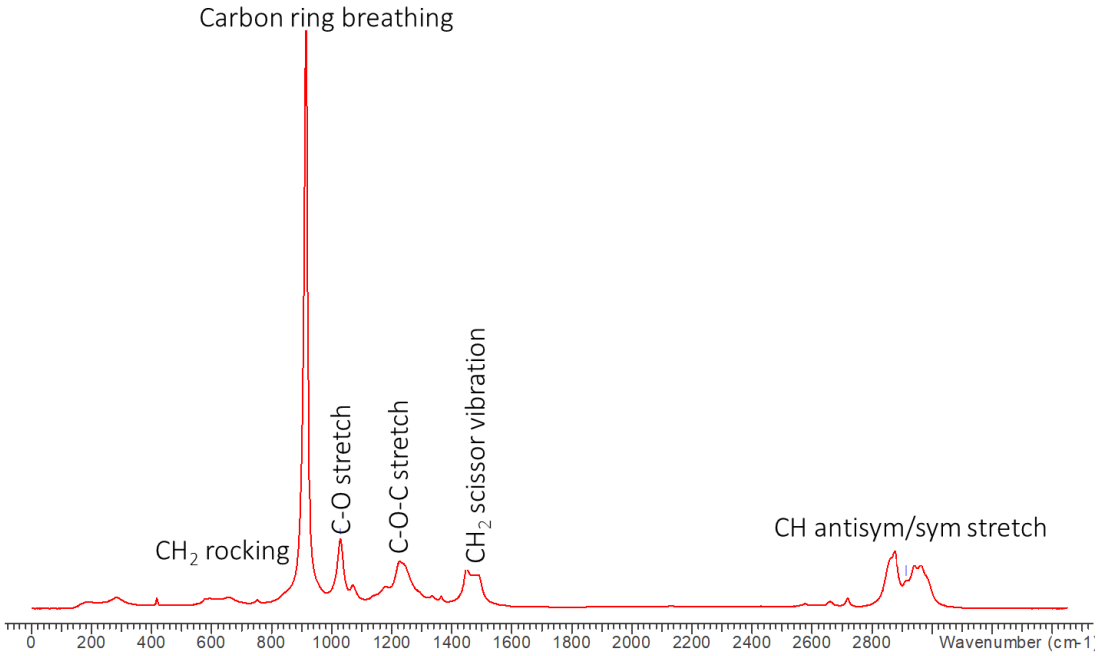

Figure 2.4. Raman Spectrum of THF

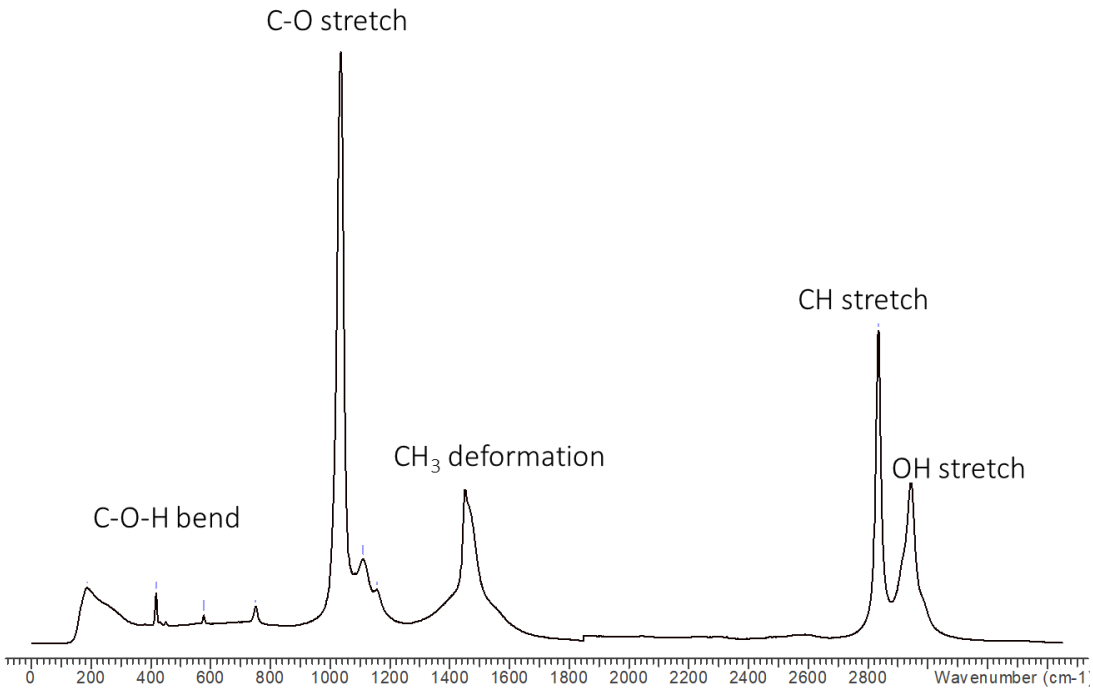

Figure 2.5. Raman Spectrum of Methanol in THF (black) vs Raman Spectrum of THF (red)

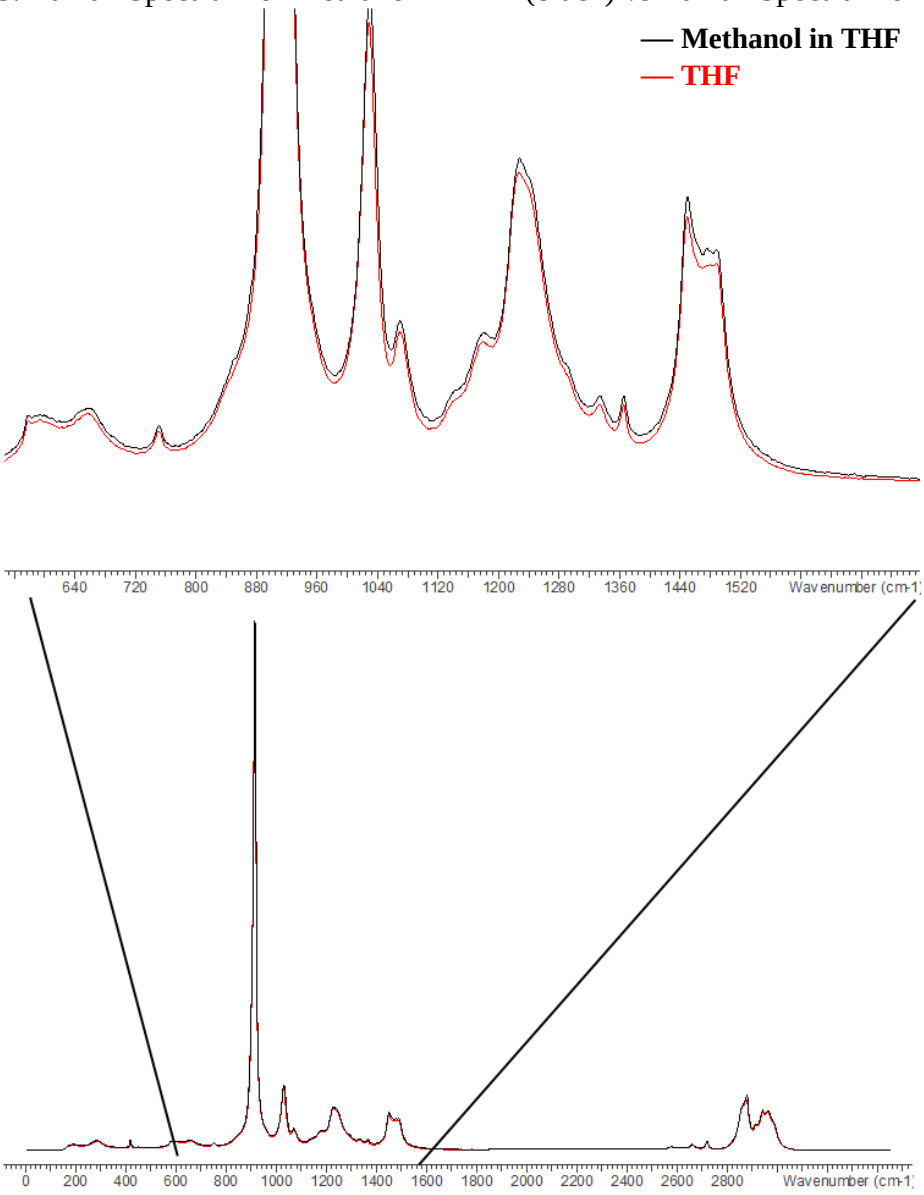

Figure 2.6. Determination of the Detection Limit of Methanol in THF

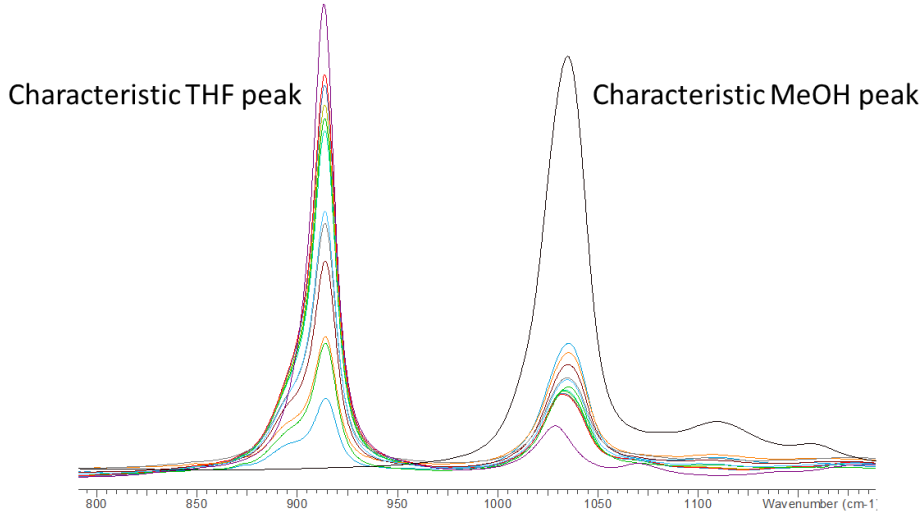

Since detecting methanol in THF at low concentrations was not possible via Raman spectroscopy, we next turned our attention to monitoring the consumption of DMF. It is important to note that under the DMF hydrogenation conditions presented herein, the reactions proceed cleanly with no side products; thus, there is a direct relationship between DMF conversion and methanol production. All reactions were also analyzed via ^{1}H NMR spectroscopy to ensure that there were no side products and to confirm the yields. When comparing the Raman spectra of DMF and THF (Figures 2.7 and 2.4, respectively), the most intense peaks of DMF are in a region of the THF spectrum where there are only weak and non-overlapping peaks. Next, a series of solutions with varying concentrations of DMF in THF were prepared and their Raman spectra stacked. As shown in Figure 2.8, even at low concentrations, there are distinct peaks as compared to the THF (Figure 2.8). Indeed, the detection limit of DMF in THF was found to be 0.00067 M (0.8 µL in 15 mL of THF), which corresponds to about 1 turnover under our reaction conditions. As such, this is a useful approach for reaction monitoring (Figure 2.9).

Figure 2.7. Raman Spectrum of DMF

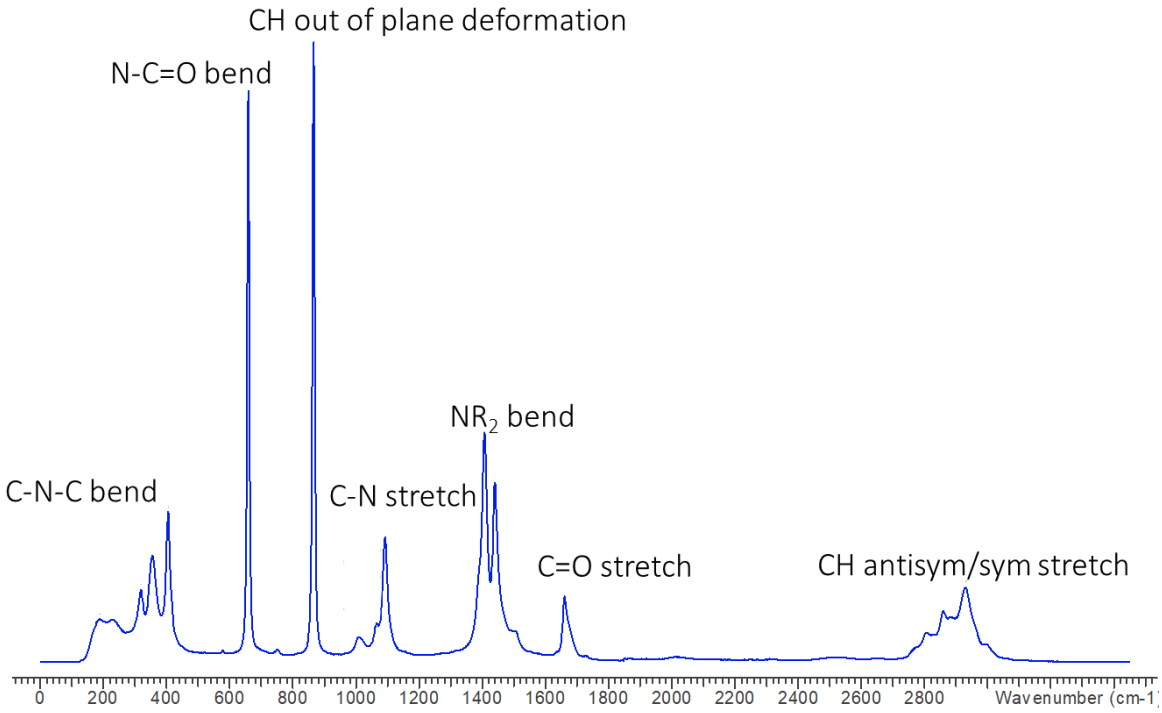

Figure 2.8. Raman Spectra of Different Concentrations of DMF in THF

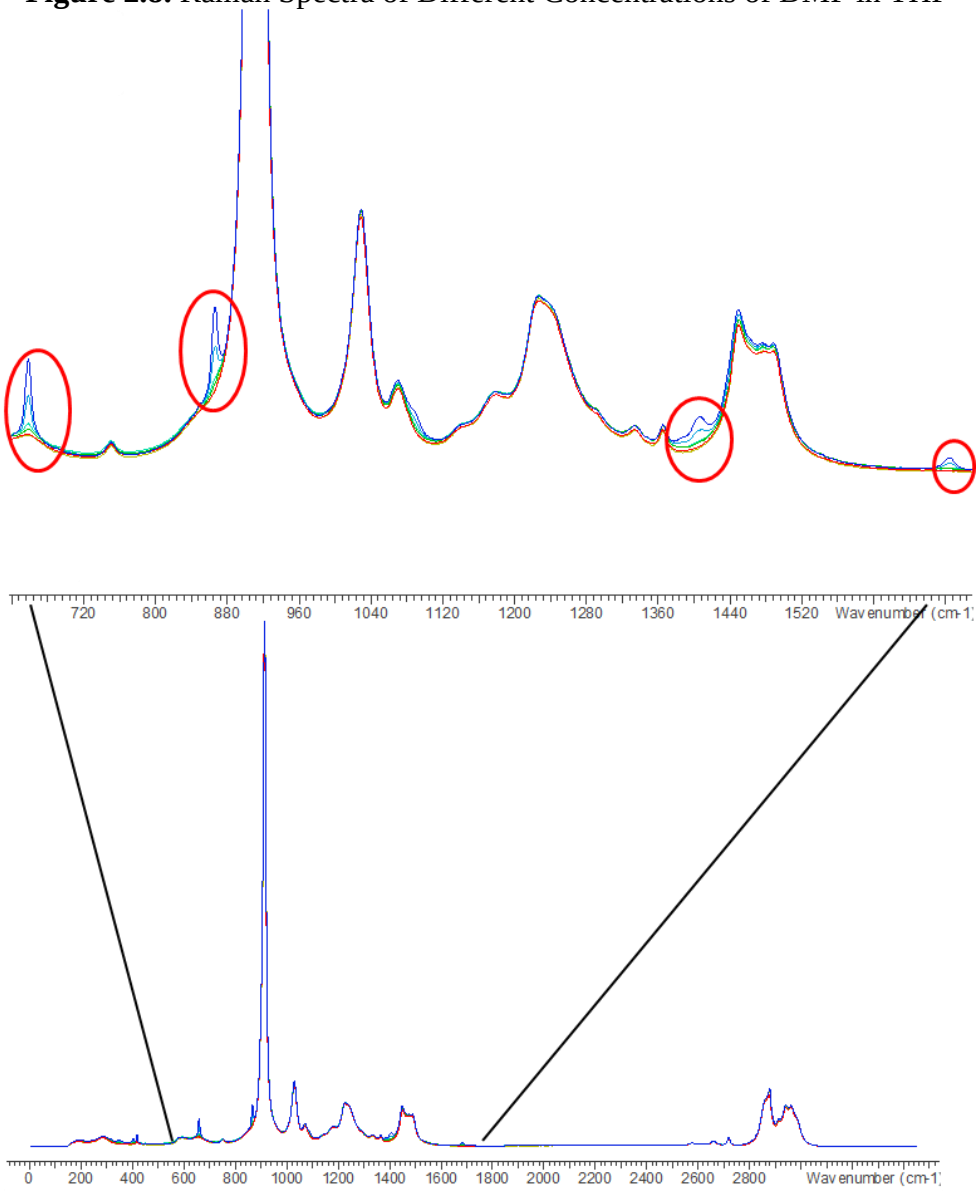

Figure 2.9. Determination of the Detection Limit of DMF in THF

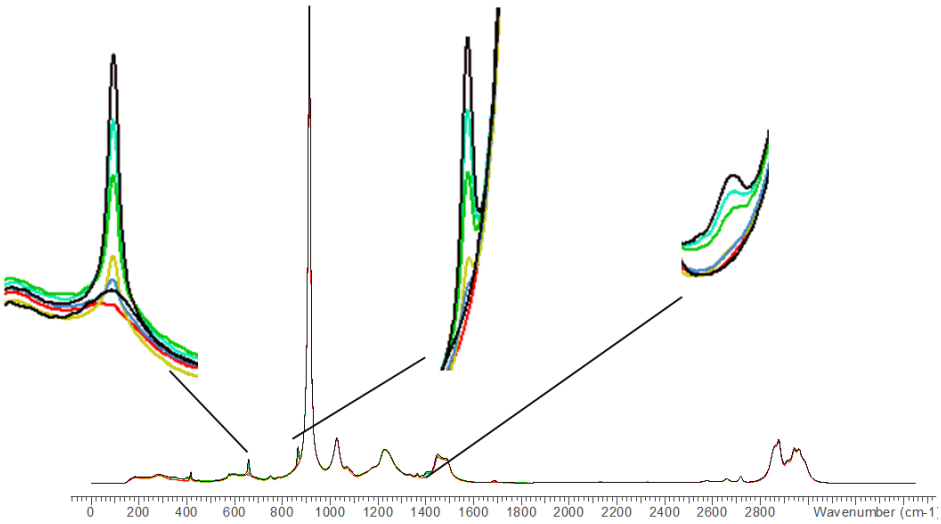

We set out to compare the rate of DMF hydrogenation catalyzed by Ru-PNP^{Ph}, Ru-PNP^{iPr}, and Ru-PNP^{Cy} via Raman spectroscopy. After loading the reactor with the necessary starting materials and placing it under hydrogen pressure, the reactor was placed in a preheated aluminum block and connected to the Raman instrument. It is important to note that the internal temperature of the reactor takes approximately 35 minutes to reach the temperature of the heating block; as such, all reaction profiles begin at 0.5 hours to eliminate the unequilibrated temperature points. However, notably, our previous studies indicated that all three complexes (Ru-PNP^{Ph}, Ru-PNP^{iPr}, and Ru-PNP^{Cy}) are catalytically active at temperatures of at least 80 °C, so some turnover of the catalyst was expected before Raman collection was started. A Raman spectrum of the reaction solution was collected every few minutes (between 3 and 7 minutes), and the peak area and peak intensity are used in conjunction with a calibration curve consisting of 6 points between 0 and 0.66 M to determine the concentration of DMF at each time point. A representative stack plot of all the spectra collected over the course of a reaction clearly shows the decrease in the DMF peak intensity and peak area as the reaction proceeds to completion (Figure 2.10). Both the 658 and 865 cm^{-1} peaks were used in analysis and compared to one another, but the 865 cm^{-1} peak tended to have less noise at the end of the reaction (once DMF was fully consumed) and thus, was the primary peak used for correlating the concentration of DMF to reaction progress.

Figure 2.10. Example Stack Plot of Raman Spectra Acquired During the Course of a DMF Hydrogenation Kinetics Experiment

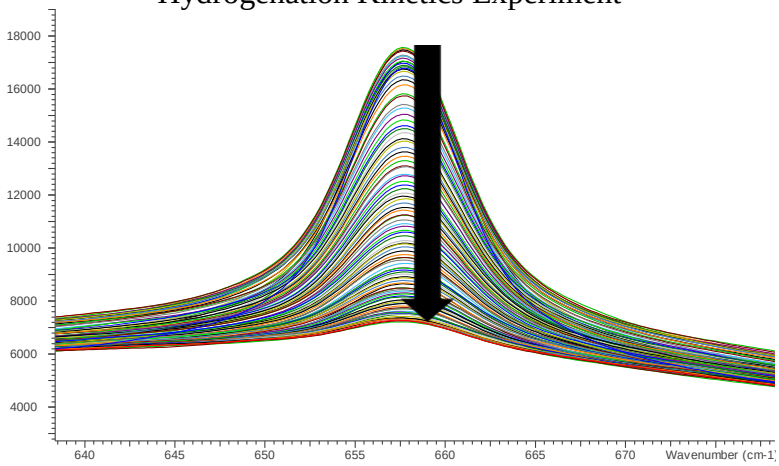

Using *in situ* Raman monitoring, we were able to directly compare Ru-PNP^{Ph}, Ru-PNP^{iPr}, and Ru-PNP^{Cy} (Figure 2.11). These studies show that Ru-PNP^{Cy} is the best catalyst with the ability to reach full conversions in under 2.5 hours. The other two catalysts fully converted DMF in under 4.5 hours for Ru-PNP^{iPr} and 5.5 hours for Ru-PNP^{Ph}.

Figure 2.11. Comparing DMF Hydrogenation by *in situ* Raman Monitoring

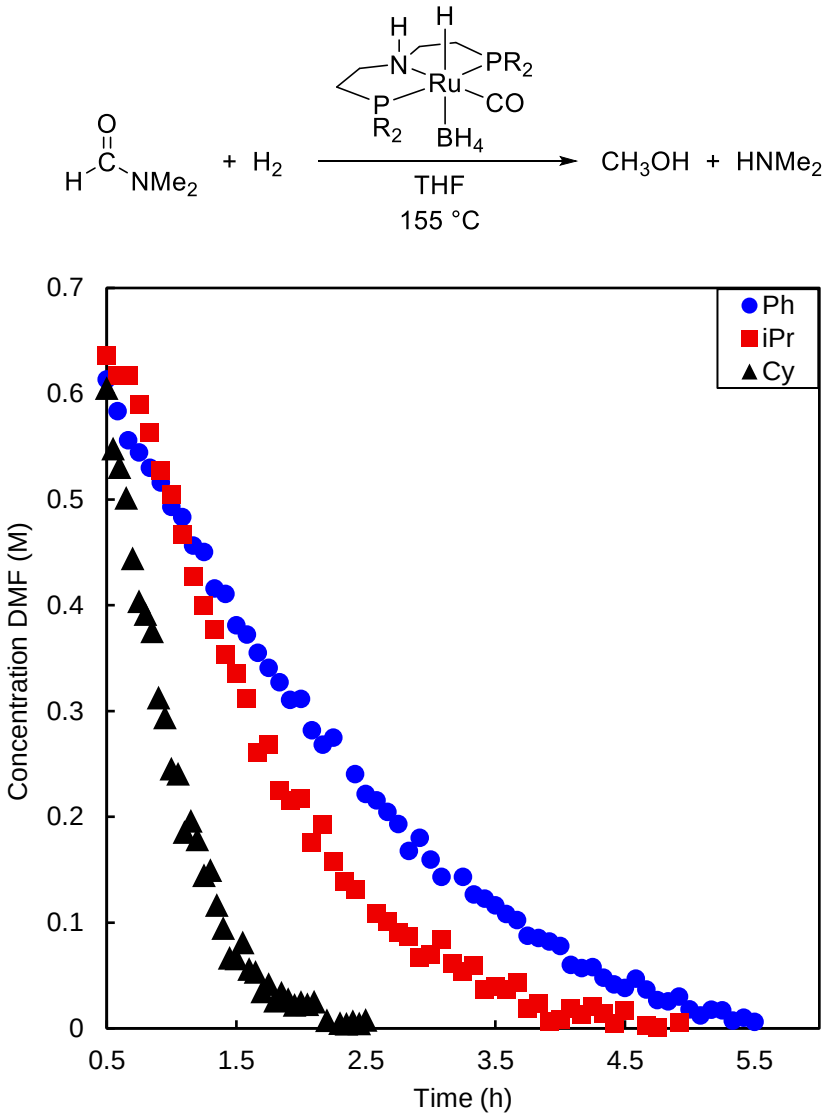

Conditions: 5.87 mmol of DMF, 0.01 mmol of catalyst, 8.5 mL of THF, 50 bar of H_2. The disappearance of DMF was monitored via the Raman peak at 865 cm^{-1}. Reactions were conducted in a high-pressure reactor fitted with a Raman probe, and the temperature was equilibrated to 155 °C (internal temperature) prior to data collection.

We next sought to study DMF hydrogenation catalyzed by Ru-PNP^{Ph}, Ru-PNP^{iPr}, and Ru-PNP^{Cy} in the presence of base. Although Ru-PNP^{Ph}, Ru-PNP^{iPr}, and Ru-PNP^{Cy} all

performed similarly with and without base at 155 °C in 18 hours (Table 2.2, Entries 1-6), Ru-PNP^{tBu}, and Ru-PNP^{Ad} afforded higher yields without base (Table 2.2, Entries 7-10). We hypothesized that Ru-PNP^{Ph}, Ru-PNP^{iPr}, and Ru-PNP^{Cy} might actually perform better without base as well, but due to their extremely high reactivity, a difference was not discernible after such a long reaction time (18 hours). Utilizing *in situ* Raman monitoring, we found that, with base present, the reaction with Ru-PNP^{Cy} is complete in 2.5 hours, while that with Ru-PNP^{iPr} is complete in 3.5 hours, and Ru-PNP^{Ph} is complete in 4.5 hours (Figure 2.12). Thus, the overall reactivity trend (Ru-PNP^{Cy} > Ru-PNP^{iPr} > Ru-PNP^{Ph}) is the same with and without base.

Figure 2.12. Comparing DMF Hydrogenation with Base by *in situ* Raman Monitoring

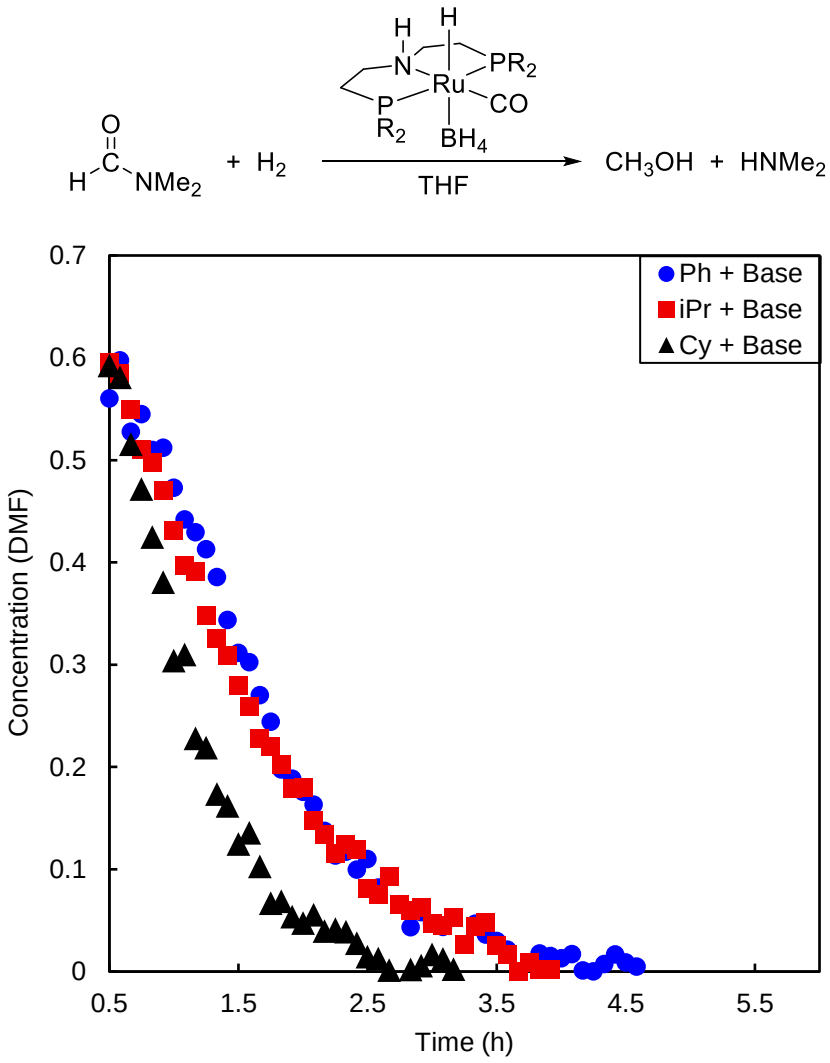

Conditions: 5.87 mmol of DMF, 0.01 mmol of catalyst, 250 μmol of K_3PO_4, 8.5 mL of THF, 50 bar of H_2. The disappearance of DMF was monitored via the Raman peak at 865 cm^{-1}. The temperature was equilibrated to 155 °C (internal temperature) prior to data collection.

Comparing Ru-PNP^{Ph} as a catalyst for DMF hydrogenation with and without base present, it is apparent that this complex performs better with base present, completing the reaction over an hour sooner as compared to in the absence of base (Figure 2.13). Similarly, Ru-PNP^{iPr} also performs better with base, albeit, with a smaller rate enhancement (Figure 2.14). In contrast, Ru-PNP^{Cy} performs slightly better without base present, converting all DMF in under 2.5 hours without base, as compared to over 2.5 hours with base (Figure 2.15). Ultimately, the reactivity of Ru-PNP^{iPr}, and Ru-PNP^{Cy} with and without base may be a critical distinction in determining which catalyst is most applicable to the cascade amide pathway.

Figure 2.13. Comparing DMF Hydrogenation with and without Base for Ru-PNP^{Ph} by *in situ* Raman Monitoring

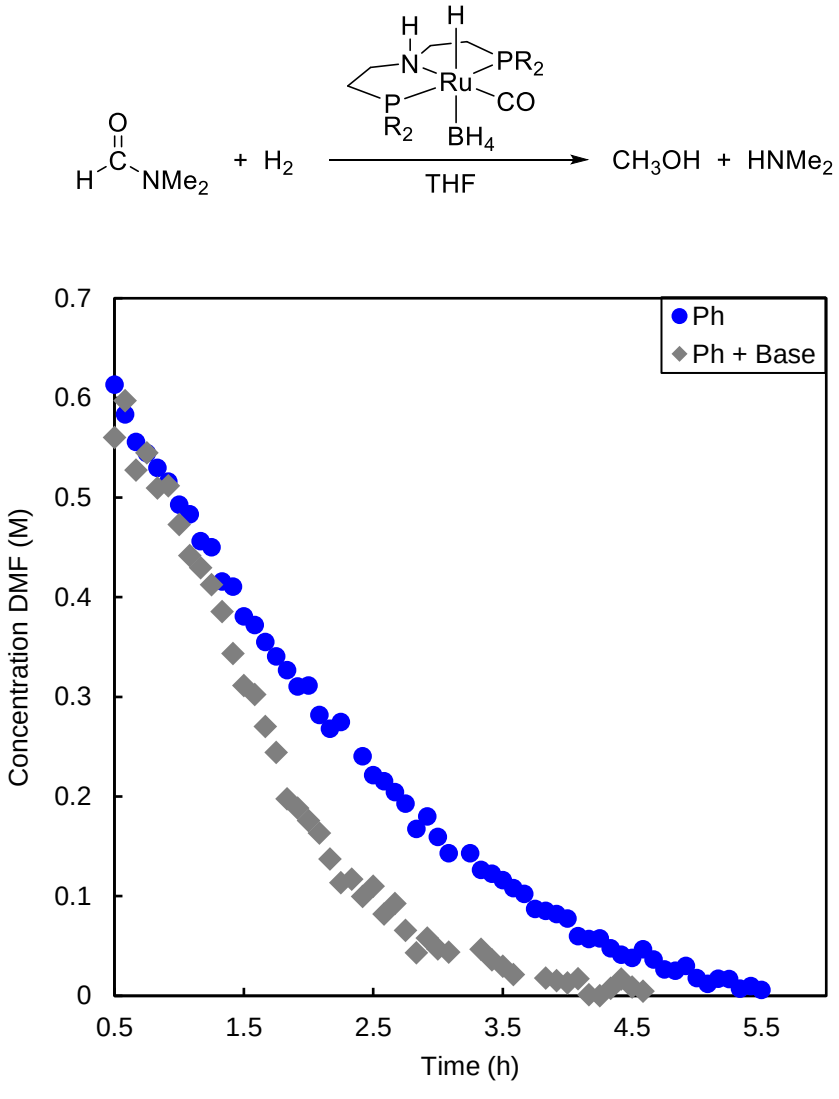

Conditions: 5.87 mmol of DMF, 0.01 mmol of catalyst, 250 μmol of K_3PO_4 (where appropriate), 8.5 mL of THF, 50 bar of H_2. The disappearance of DMF was monitored via the Raman peak at 865 cm^{-1}. Reactions were conducted in a high-pressure reactor fitted with a Raman probe, and the temperature was equilibrated to 155 °C (internal temperature) prior to data collection.

Figure 2.14. Comparing DMF Hydrogenation with and without Base for Ru-PNP^{iPr} by *in situ* Raman Monitoring

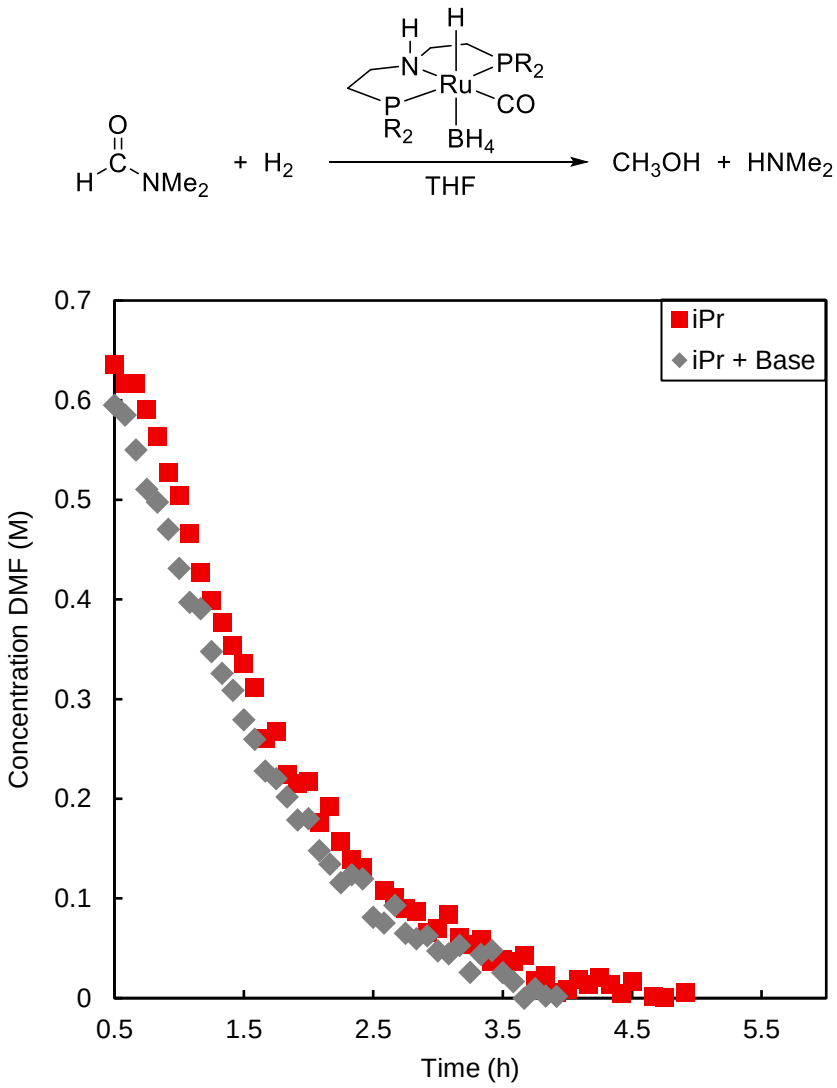

Conditions: 5.87 mmol of DMF, 0.01 mmol of catalyst, 250 μmol of K_3PO_4 (where appropriate), 8.5 mL of THF, 50 bar of H_2. The disappearance of DMF was monitored via the Raman peak at 865 cm^{-1}. Reactions were conducted in a high-pressure reactor fitted with a Raman probe, and the temperature was equilibrated to 155 °C (internal temperature) prior to data collection.

Figure 2.15. Comparing DMF Hydrogenation with and without Base for Ru-PNP^{Cy} by *in situ* Raman Monitoring

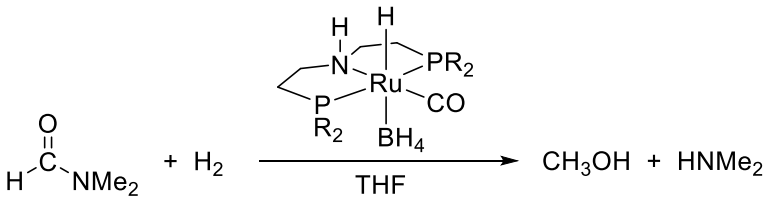

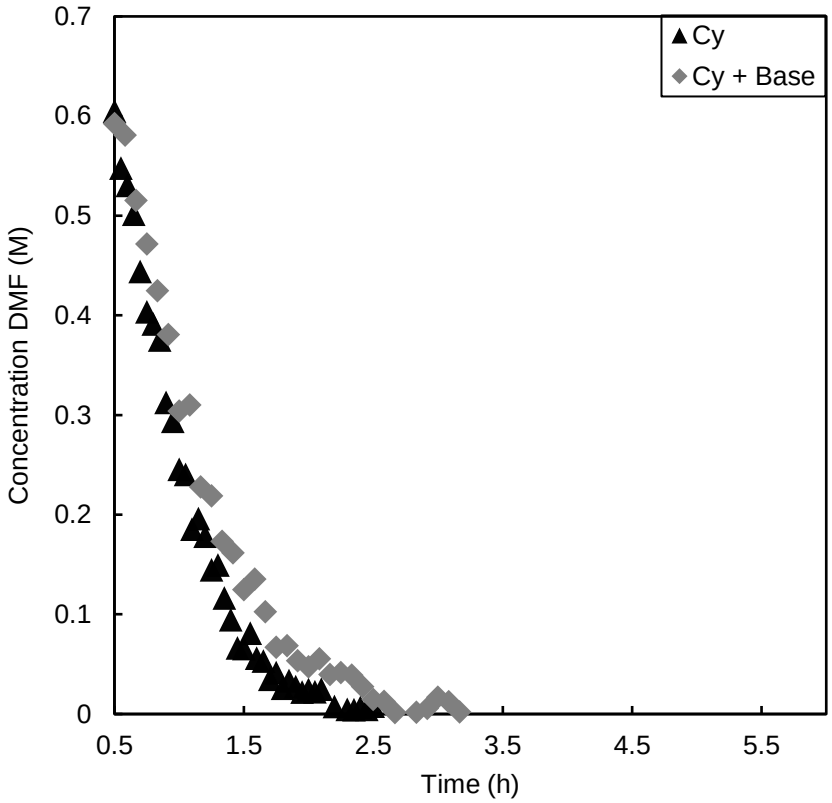

Conditions: 5.87 mmol of DMF, 0.01 mmol of catalyst, 250 μmol of K_3PO_4 (where appropriate), 8.5 mL of THF, 50 bar of H_2. The disappearance of DMF was monitored via the Raman peak at 865 cm^{-1}. Reactions were conducted in a high-pressure reactor fitted with a Raman probe, and the temperature was equilibrated to 155 °C (internal temperature) prior to data collection.

A final study probed the rate of DMF hydrogenation in the presence and absence of CO_2. Previous studies showed that Ru-PNP^{Ph} was the least inhibited by 1 bar of CO_2, dropping the yield from >99% down to 73% yield of methanol at 155 °C in 18 hours. Maintaining the concentration of the reaction but scaling the THF, DMF, and catalyst appropriately (0.66 M DMF and 0.0063 M Ru-PNP^{Ph}), resulted in a significant rate inhibition with just 1 bar of CO_2 (2 mmol, 36 equivalents to catalyst). At this high concentration of catalyst, Ru-PNP^{Ph} fully

hydrogenates DMF in about 2 hours. In contrast, in the presence of just 1 bar of CO_2, the rate of the reaction is much slower, with a significant amount of DMF remaining at the time when Raman monitoring was stopped. Less than one turnover of formic acid was detected (derived from CO_2 hydrogenation). Comparing the initial rates starting at 0.33 h for Ru-PNP^{Ph} reaction and 0.75 h for the reaction with base, the reaction with CO_2 is ~24 times slower than when no CO_2 is present. This significant different in rate is a testament to the stability of the Ru-formate complex.

Figure 2.16. Comparing DMF Hydrogenation with and without CO_2 for Ru-PNP^{Ph} by *in situ* Raman Monitoring

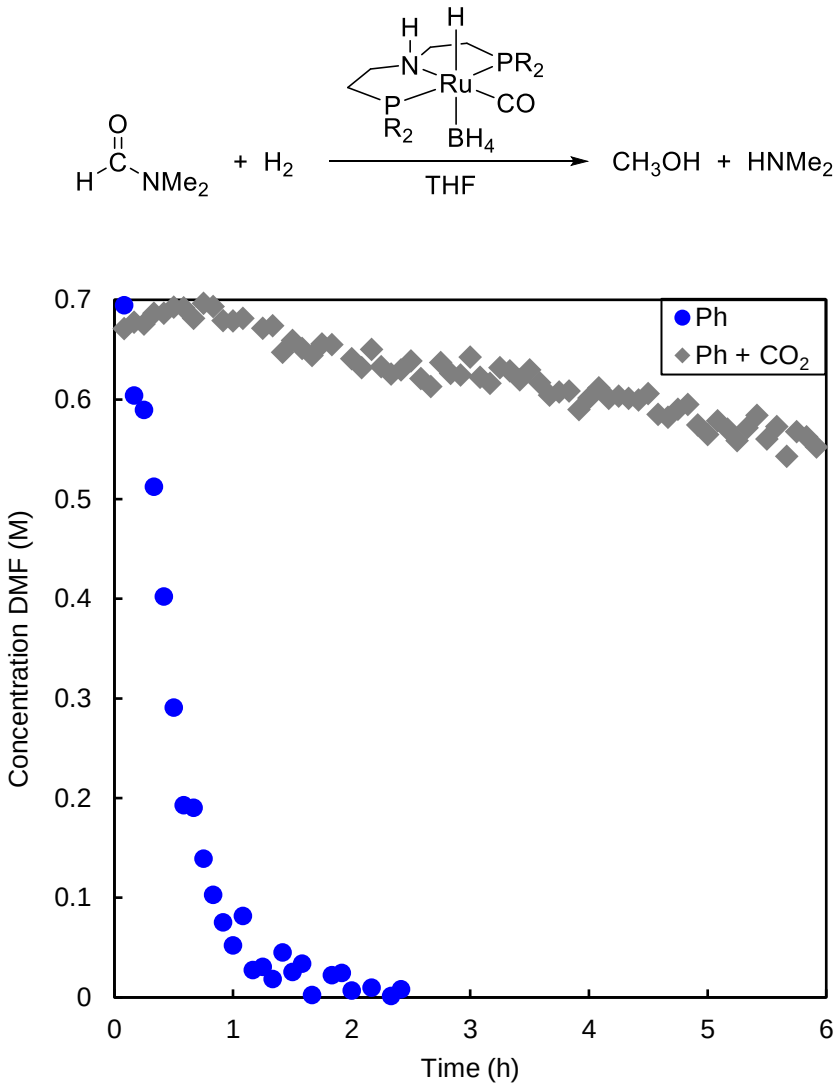

Conditions: 5.87 mmol of DMF, 0.056 mmol of catalyst, 8.5 mL of THF, 1 bar of CO_2, 50 bar of H_2. The disappearance of DMF was monitored via the Raman peak at 865 cm^{-1}. Reactions were conducted in a high-pressure reactor fitted with a Raman probe, and the temperature was equilibrated to 155 °C

(internal temperature) prior to data collection. Unequilibrated time points (<0.5 h) were included due to the extremely fast rates of hydrogenation at these concentrations.

Overall, *in situ* Raman monitoring provided additional information about the kinetics of DMF hydrogenation catalyzed by Ru-PNP^{Ph}, Ru-PNP^{iPr}, and Ru-PNP^{Cy}. First, these experiments allowed us to rank the relative reactivity of these catalysts as Ru-PNP^{Cy} > Ru-PNP^{iPr} > Ru-PNP^{Ph}, both in the presence and absence of K_3PO_4 base. This trend in reactivity cannot be easily explained by simply steric or electronic parameters and further experimentation and computation studies are necessary. Second, we were able to quantify the inhibition of Ru-PNP^{Ph}-catalyzed DMF hydrogenation in the presence of CO_2 (Figure 2.16). The rate of Ru-PNP^{Ph} without base is ~24 times faster than when CO_2 is present.

2.2.3. Directly Comparing Ruthenium-PNP and Iron-PNP Catalysts in the Hydrogenation of N,N'-Dimethylformamide[1]

Besides our interest in identifying a superior DMF hydrogenation catalyst for the cascade amide system, amide hydrogenation itself is an important reaction. The vast majority of homogeneous catalysts for these transformations contain second- or third-row transition metals (*e.g.*, Ru, Rh, Pd, Pt).[5,36,37] There are significantly fewer examples of the hydrogenation of carboxylic acid derivatives using earth-abundant first-row metal catalysts.[38,39] Recent efforts toward this goal have focused on Fe-based catalysts for the hydrogenation of aldehydes,[40,41,42,43]ketones,[40,41,42,43,44,45,46,47,48] and esters.[18,19,20,49,50] However, analogous Fe-catalyzed hydrogenations of less electrophilic amide derivatives remain largely unexplored.[51,52] These weakly electrophilic substrates are expected to be particularly challenging for Fe catalysts, due to the anticipated lower hydricity of first-row metal hydrides in comparison to their second- and third-row counterparts.[53,54] A number of reports have described homogeneous Ru catalysts for amide hydrogenation[55,56,57,58,59,60,61,62,63,64,65,66,67,68,69] and have demonstrated that selective C–N cleavage can be achieved by an appropriate choice

of supporting ligands. Scheme 2.8a shows one of the mildest and most general reported examples, involving catalyst Ru-1.[55]

Scheme 2.8. Examples of Ru and Fe-catalyzed amide hydrogenation

a) Ru-catalyzed hydrogenation of amides (***Milstein***)

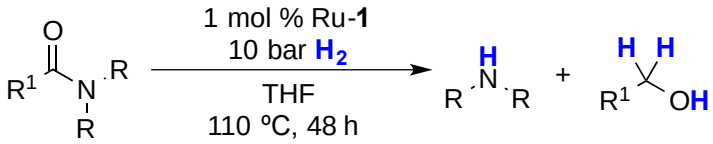

b) Fe-catalyzed hydrogenation of activated amides (***Milstein***)

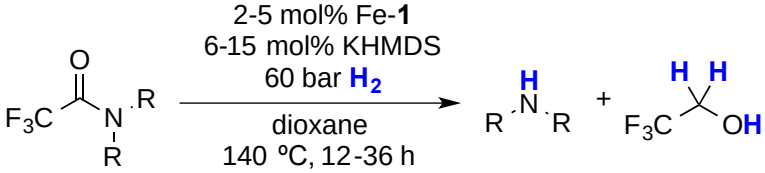

c) Fe-catalyzed hydrogenation of unactivated amides (***this work***)

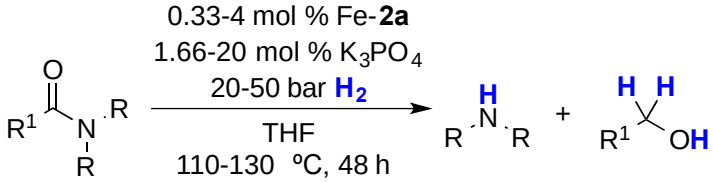

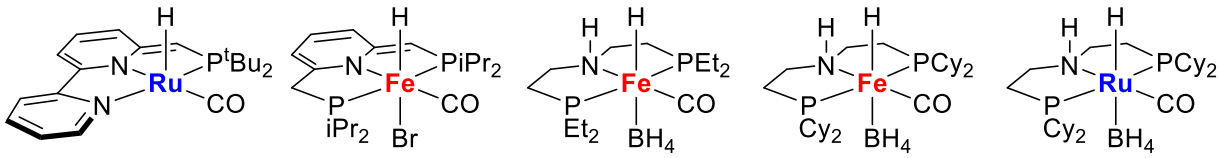

Ru-1 Fe-1 Fe-PNP^{Et} Fe-PNP^{Cy} Ru-PNP^{Cy}

We sought to develop an analogous Fe-catalyzed hydrogenation of unactivated amides and to conduct a detailed investigation of catalysts, conditions, and scope. Furthermore, we sought to benchmark the best Fe catalyst to its second-row congener. At the start of our investigation, there were no reported examples of homogeneous Fe-catalyzed amide hydrogenation. Over the course of our studies, two papers appeared describing Fe-catalyzed amide hydrogenation to yield C–N bond scission products using catalysts Fe-1[51] and Fe-PNP^{Et}.[52] However, these methods suffer from a limited substrate scope, modest TONs (up to 50),[51,52] and/or forcing conditions (Scheme 2.8b).[51] We demonstrate herein that Fe-PNP^{Cy} is an effective catalyst for the hydrogenation of unactivated amides. These transformations

selectively afford C–N cleavage products, and many substrates can be hydrogenated within 3 h at 110 °C. Further, we demonstrate that Fe-PNP^{Cy} catalyzes this reaction with an initial rate that is within a factor of 2 of that for its Ru analogue (Ru-PNP^{Cy}), under otherwise identical conditions.

Based on our ongoing interest in the reduction of C-1 starting materials,[2,24,70,71] we initially focused on the Fe-catalyzed hydrogenation of DMF. We selected Fe-PNP^{R} complexes to employ in DMF hydrogenation due to the excellent reactivity observed by their Ru-PNP^{R} analogues (*via supra*), as well as literature precedent.[2,19,26,49,50,72,73,74] Using research grade H_2 (20 bar) and 0.33 mol% Fe-PNP^{Cy} at 110 °C, we obtained a 59% yield of methanol after 3 h with high (>99%) selectivity for C–N cleavage (Scheme 2.9). The addition of base is known to promote metal-catalyzed hydrogenations,[75,76,77,78] and K_3PO_4 proved particularly effective in a related Ru-catalyzed hydrogenation of DMF.[2] Similarly, the addition of K_3PO_4 (25 equivalents relative to Fe) to the Fe-PNP^{Cy}-catalyzed hydrogenation of DMF under otherwise identical conditions boosted the yield to >99%.

Scheme 2.9. DMF Hydrogenation by Fe-PNP^{Cy} With and Without Base

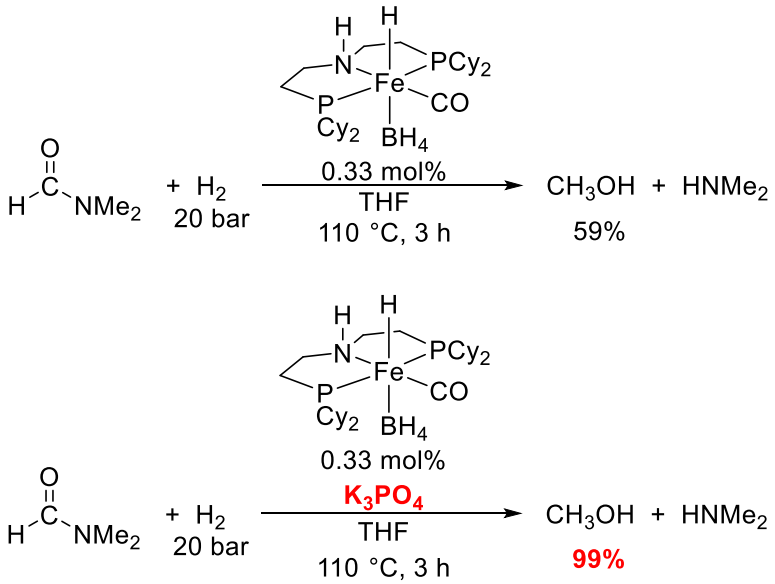

We next examined the scope of Fe-PNP^{Cy}-catalyzed hydrogenation of formamides (Scheme 2.10). Tertiary alkyl and aryl formamides underwent hydrogenation in quantitative yield with >95% selectivity for C–N cleavage. Secondary aryl formamides were also viable substrates affording yields of 57-95% of C–N cleavage products. The highest yields were obtained with substrates bearing electron-neutral or -withdrawing substituents on the aromatic ring. Alkyl- and aryl-substituted amides often required more forcing conditions than the formamides (higher temperatures, pressures, and catalyst loadings); however, they also underwent selective reduction in modest to high yields. Overall, the substrate scope, catalyst loading, and TONs obtained with Fe-PNP^{Cy} rival those of many Ru catalysts.[59,63,64,79]

Scheme 2.10. Overview of General Reaction Conditions used for Substrate Scope Study

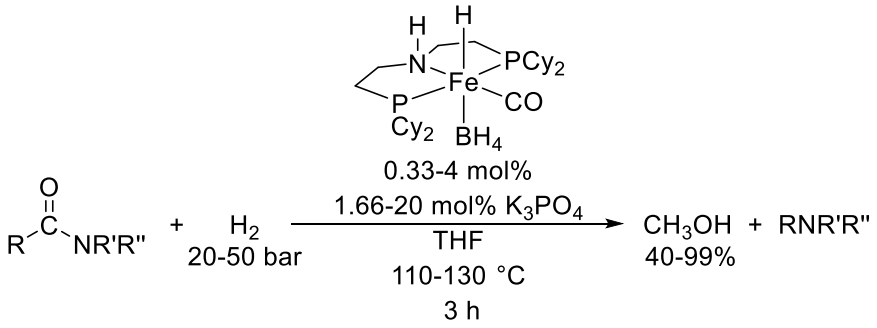

We next sought to compare the rate of amide hydrogenation with Fe-PNP^{Cy} to that of its Ru analogue, Ru-PNP^{Cy} by monitoring the hydrogenation of DMF via *in situ* Raman spectroscopy.[34] As shown in Figure 2.17, the complete consumption of DMF required ~5.5 h with Fe-PNP^{Cy}, while with Ru-PNP^{Cy} the amide substrate was fully converted within ~3 h. Comparison of the initial reaction rates shows that the Ru catalyst is ~1.7-fold faster than the Fe catalyst. These experimental and computational results are particularly noteworthy considering that previous studies have demonstrated orders of magnitude differences in the kinetic hydricity of first-row transition-metal hydrides versus their second-/third-row counterparts.[80]

Figure 2.17. Reaction progress of the hydrogenation of DMF with Fe-PNP^{Cy} vs Ru-PNP^{Cy}.

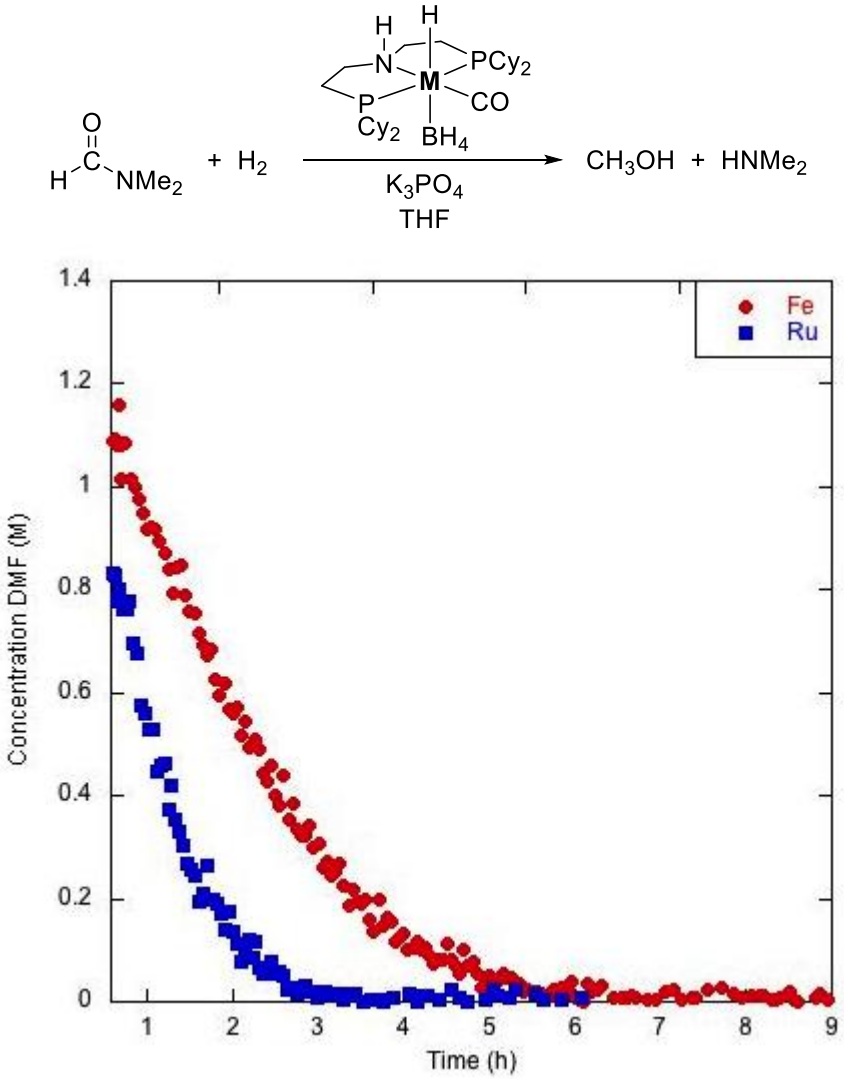

Conditions: 10.5 mmol of DMF, 35 μmol of Fe-PNP^{Cy} or Ru-PNP^{Cy}, 175 μmol of K_3PO_4, 7 mL of THF, 70 bar of H_2. The disappearance of DMF was monitored via the Raman peak at 865 cm^{-1}. Reactions were conducted in a high-pressure reactor fitted with a Raman probe, and the temperature was equilibrated to 110 °C (internal temperature) prior to data collection.

A plausible catalytic cycle for Fe-catalyzed amide hydrogenation is shown in Scheme 2.11. This mechanism is similar to those reported in the literature for carbonyl hydrogenation with related Ru and Fe catalysts.[54] In a catalyst initiation step, the loss of BH_3 from A leads to the active *trans*-dihydride complex B. The BH_3 is presumably captured by a Lewis base in solution (*e.g.*, solvent, PO_4^{3-}, etc.). Complex B then transfers a hydride and a proton to the amide substrate (step a) to yield a hemiaminal intermediate and C. Heterolytic cleavage of H_2 by C regenerates B (step b), while the hemiaminal intermediate extrudes the amine and

concomitantly generates the aldehyde. Finally, hydrogenation of the aldehyde by B (step c) yields the primary alcohol and re-forms C. Importantly, an exogeneous base is not necessary for this cycle to proceed; consistent with this, our results show that added base is not necessary to achieve efficient catalysis. We hypothesize that the enhanced TONs in the presence of relatively weak bases such as K_3PO_4 and NEt_3 are likely due to either base-promoted catalyst initiation (via sequestration of BH_3) and/or the base acting as a proton shuttle during reaction.

Scheme 2.11. Proposed mechanism for the Fe-catalyzed hydrogenation of DMF

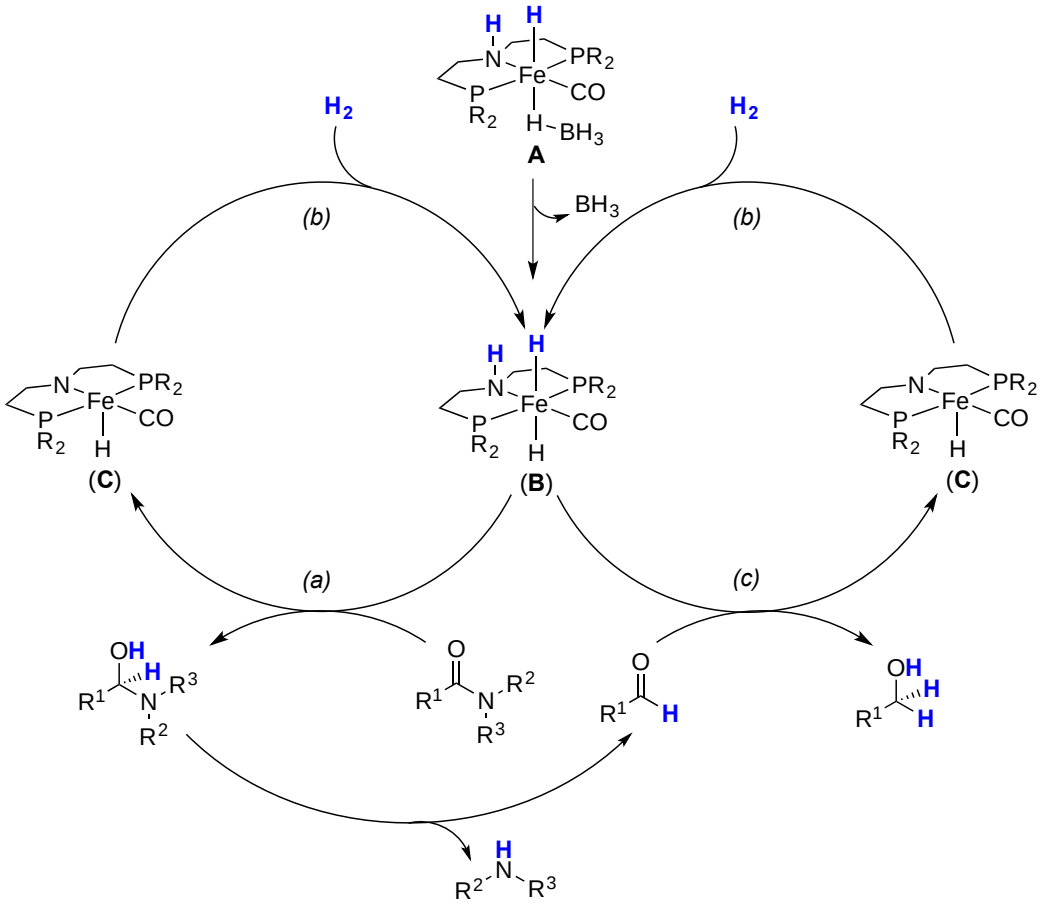

To gain additional mechanistic insights into this transformation, we monitored the reaction progress of the Fe-PNP^{Cy}-catalyzed DMF hydrogenation as a function of H_2 pressure via Raman spectroscopy. As shown in Figure 2.18, the reaction progress curves are nearly identical at 50 and 70 bar of H_2. In contrast, the reaction is significantly slower at 20 bar of H_2, and there appears to be an induction period at this lower pressure. While more detailed studies

will be necessary to fully interpret these findings, the preliminary results suggest that either the turnover-limiting step and/or the initiation rate change as a function of H_2 pressure.

Figure 2.18. Reaction progress of the hydrogenation of DMF with Fe-PNP^{Cy} at 20, 50, and 70 bar of H_2

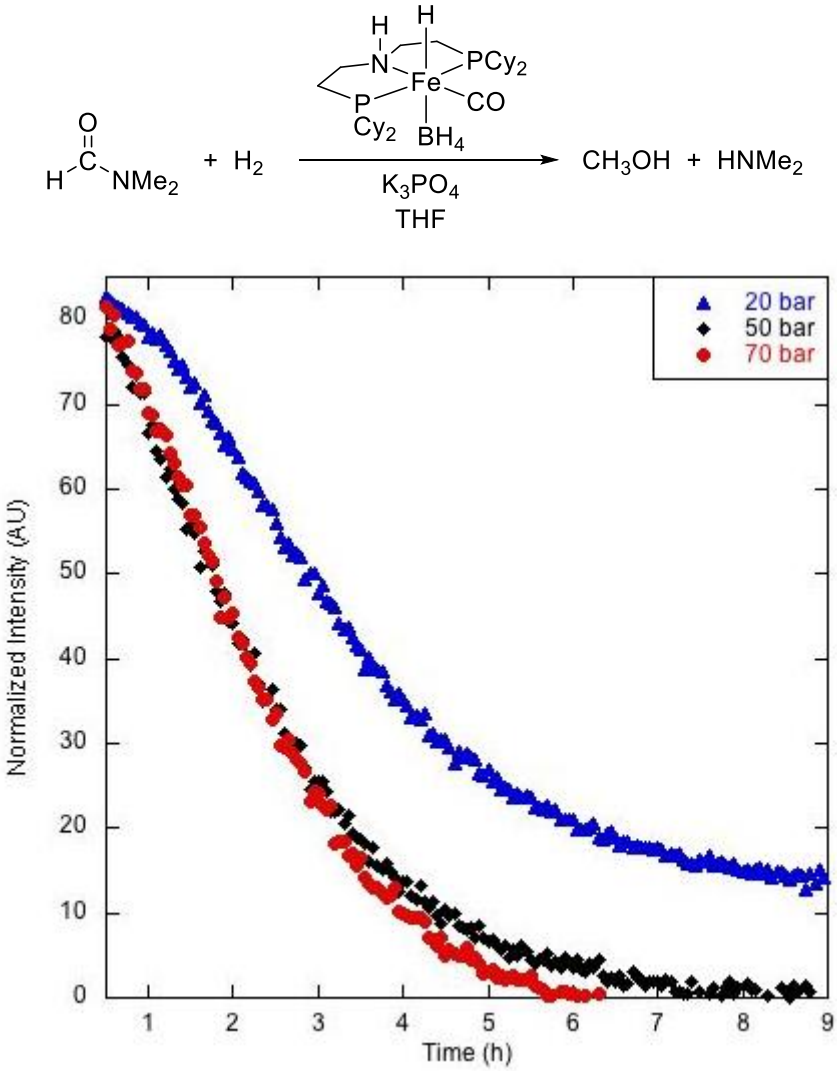

Conditions: 10.5 mmol of DMF, 35 μmol of Fe-PNP^{Cy}, 175 μmol of K_3PO_4, 7 mL of THF. The disappearance of DMF was monitored via the Raman peak at 865 cm^{-1}. Reactions were conducted in a high-pressure reactor fitted with a Raman probe, and the temperature was equilibrated to 110 °C (internal temperature) prior to data collection.

Overall, our findings show that that Fe-PNP^{Cy} is not only catalytically competent, but that it also performs similar to its Ru analogue, albeit with lower reactivity. Kinetic experiments using *in situ* Raman spectroscopy demonstrate that the rate of amide hydrogenation with Fe-PNP^{Cy} can approach that of its noble-metal Ru counterpart. Efforts to elucidate the mechanistic similarities/differences between the Fe and Ru catalysts in more detail, as well as to design

second-generation Fe catalysts with improved activity are currently underway in our laboratory and will be reported in due course.

2.3. Conclusions

The study of metal-PNP catalyzed DMF hydrogenation has demonstrated that Ru-PNP, as well as Fe-PNP are excellent catalysts for this reaction. Both Ru-PNP^{R} complex types, the hydridochloride (Ru-PNP^{R}-Cl) and -BH_4 (Ru-PNP^{R}) are competent for DMF hydrogenation; however, the hydridochloride complexes require the use of exogeneous base. As such, the -BH_4 complexes became the main area of focus. Using Ru-PNP^{R}-BH_4 complexes, milder conditions (80 °C) can be employed to reach high yields of methanol in short periods of time (3 hours). A clear ranking of the complexes became apparent after optimization and use of *in situ* Raman monitoring: Ru-PNP^{Cy} > Ru-PNP^{iPr} > Ru-PNP^{Ph} > Ru-PNP^{tBu} > Ru-PNP^{Ad}. Studies were undertaken to compare Ru-PNP^{Cy}, our best catalyst for DMF hydrogenation, to its first-row analogue, Fe-PNP^{Cy}. Interestingly, the two performed rather similarly with Ru-PNP^{Cy} having an initial rate of 1.7 times faster than Fe-PNP^{Cy} when computational studies had previously suggested first and second row congers to be orders of magnitude different. Overall, this thorough study of DMF hydrogenation has led to the identification of new catalysts to be tested in the amide cascade system in hopes of generating a more efficient system with higher yields of methanol.

2.4. Experimental Procedures

2.4.1. General Procedures and Materials and Methods

General Procedures

All manipulations were carried out under a nitrogen atmosphere using standard Schlenk line or glove box techniques unless otherwise noted. All high-pressure reactions were carried

out using a Parr Model 5000 Multiple Reactor system that includes six 45 mL vessels equipped with flat-gaskets and head mounting valves. The system was operated by a 4871 process controller and SpecView version 2.5 software. All pressures are reported from the SpecView interface at room temperature. NMR spectra were obtained on Varian VNMRs: 400 MHz (400 MHz for ^{1}H; 100 MHz for ^{13}C) or 700 MHz (700 MHz for ^{1}H; 176 MHz for ^{13}C). Chemical shifts are reported in parts per million (ppm) and are referenced to an internal standard. Unless otherwise noted, the NMR yields with formamide substrates were based on methanol (δ= 3.16 ppm, T_1 = 7.2 s) and were quantified using 1,3,5-trimethoxybenzene (δ= 6.02 ppm, T_1 = 2.8 s) as an internal standard in dimethylsulfoxide-d_6 (DMSO-d_6). For each NMR experiment, 4 scans were collected, a 35 s relaxation delay was used, and a pulse angle of 90° was applied.

High pressure Raman data were collected using a Kaiser Optical Systems, Inc. RamanRxn1 system. In situ Raman analysis was performed with a NIR Immersion Sampling Optic Probe with a sapphire window and alloy C276 body (6 inch length and 0.25 inch diameter) attached to the MR Filtered Probe Head of the RamanRxn1 system. The laser source was a 400 mW Invictus operating at 785 nm. The high pressure experiments were performed in a 45 mL Parr cylinder containing a 0.3 inch center port hole with a 0.25 inch Swagelock fitting at the top. The probe was swaged into a 0.25 inch Swagelok fitting, which was then attached to the top center port hole of the reactor. Calibration was performed using cyclohexane as a wavelength standard and a white light correction for spectral intensity. Spectra were collected via the NIR Immersion Sampling Optic Probe with a range of 0-3450 cm^{-1}. Spectra were analyzed using ACD Spectrus Processer 2015 Pack 2 software.

Reactor Descriptions

Two different types of reaction vessels were used. All are 45 mL and are composed of a well (in which the solid and liquid reagents are charged) and a head, which contains various

attachments as described below.

Reactors of type A variety are made of Hastelloy C, and the wells are 7.5 cm tall and 3 cm in diameter. The heads consist of a pressure transducer and two inlet/outlet valves that can connect to a Parr Model 5000 Multiple Reactor system described above, a safety release valve, and a well for a thermocouple (Figure 2.19).

Figure 2.19. Picture of reactor type A with the parts of the reactor labeled.

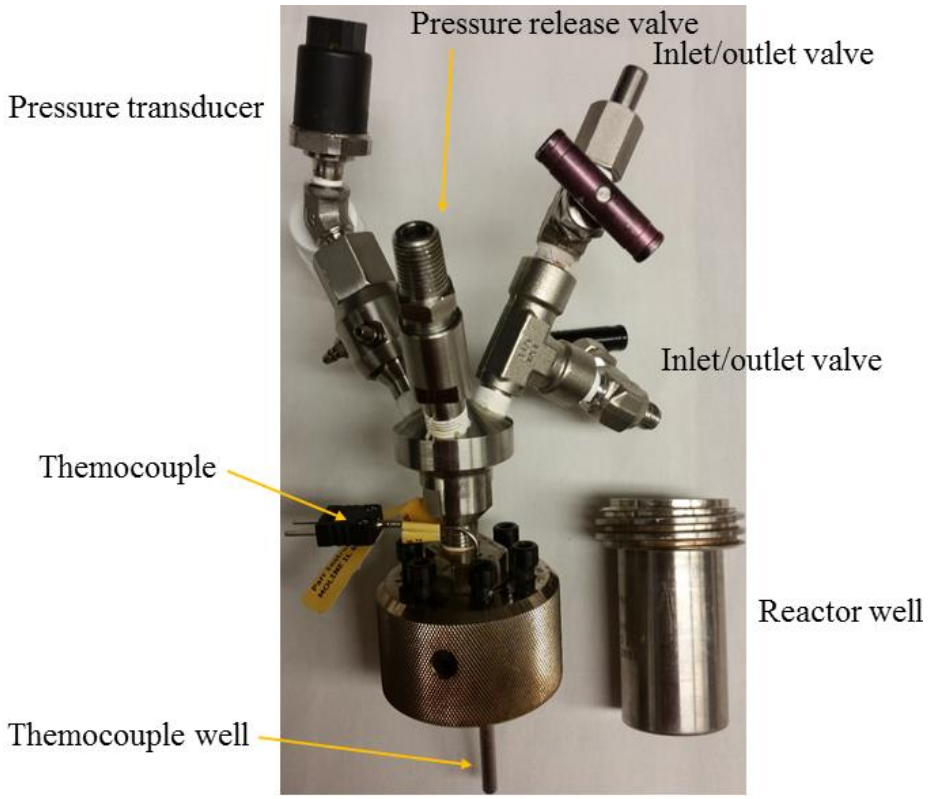

Reactor B (Hastelloy C) is identical to the type A reactors except that it has an additional attachment on the head. This attachment is an adaptor for a Raman probe that is submerged into the well of the reactor. This attachment is used for in situ Raman spectroscopy (Figure 2.20).

Figure 2.20. Picture of reactor type B with the parts of the reactor labeled.

Materials and Methods

The ligands bis(2-(dicyclohexylphosphino)ethyl)amine (PNP^{Cy}), bis(2-(diisopropylphospino)ethyl)amine (PNP^{iPr}), bis(2-(di-tert-butylphosphino)ethyl)amine (PNP^{tBu}), and bis(2-(diadmantylphosphino)ethyl)amine (PNP^{Ad}) were purchased from commercial sources (98%, Alfa Aesar). Catalysts Ru-PNP^{Cy}-Cl, Ru-PNP^{iPr}-Cl, Ru-PNP^{tBu}-Cl, Ru-PNP^{Ad}-Cl, Ru-PNP^{Cy}, Ru-PNP^{iPr}, Ru-PNP^{tBu}, Ru-PNP^{Ad}, and Fe-PNP^{Cy} were prepared according to a literature procedure.[12,13,14] The final catalyst, Ru-PNP^{Ph} was purchased from Strem Chemicals (98%). Anhydrous K_3PO_4 (Aldrich, 98%) was ground with a mortar and pestle before use. Ultra-high purity hydrogen (99.999%), research grade hydrogen (99.9999%), and carbon dioxide (99.9%) were purchased from Metro Welding. All catalytic experiments were set up under an oxygen-free atmosphere in a glovebox. All catalytic experiments were

conducted in triplicate, and the reported results represent an average of three runs (NMR yields). Anhydrous N,N-dimethylformamide (DMF, 99.8%) was obtained from Alfa Aesar and used without further purification. Tetrahydrofuran (THF) purified using an Innovative Technologies (IT) solvent purification system consisting of a copper catalyst, activated alumina, and molecular sieves. Dimethylsulfoxide-d_6 (DMSO-d_6), Cambridge Isotope Laboratories) was purchased from the respective supplier and used as received.

2.4.2. Hydrogenation Reactions

General Procedure for the Hydrogenation of DMF (Tables 2.1–2.5)

In a N_2-atmosphere dry box, [Ru] (10 µmol, 1 mol%) was dissolved in 1 mL of THF, and this solution was added to the metal well of a pressure vessel containing the appropriate quantity of base (0 or 53 mg, 250 µmol) and a micro magnetic stirbar (3 x 10 mm). DMF (80 µL, 1.0 mmol, 100 equiv relative to Ru) was then added, and the vessel (Reactor-type A) was sealed and removed from the dry box. The vessel was connected to the Parr Multiple Reactor System, and the manifold was thoroughly purged with ultra-high purity H_2 (99.999%). The vessel was then pressurized to 50 bar with ultra-high purity grade H_2 at room temperature, and the reaction was heated at the desired temperature with a stir rate of 800 RPM. The heating was conducted using Specview software. After the proper amount of time of heating, the reaction mixture was allowed to cool to room temperature. The pressure vessel was placed in a –84 °C bath (ethyl acetate/LN_2) for 15 min and then carefully vented using a metering valve. THF (0.5 mL) was added through the venting valve of the pressure vessel to wash any residual liquids/solids into the vessel. The vessel was then opened, 1,3,5-trimethoxybenzene (0.178 mmol, 300 µL of 0.593 M solution in DMSO-d_6) was added as a ^{1}H NMR standard, and the contents of the vessel were diluted with DMSO-d_6. Approximately 50 µL of the resulting solution was added to an NMR tube, diluted further with DMSO-d_6. The sample was then analyzed by ^{1}H NMR spectroscopy (see Figure 2.31 for representative sample).

Figure 2.21. Representative ^{1}H NMR Spectrum of Post-DMF Hydrogenation

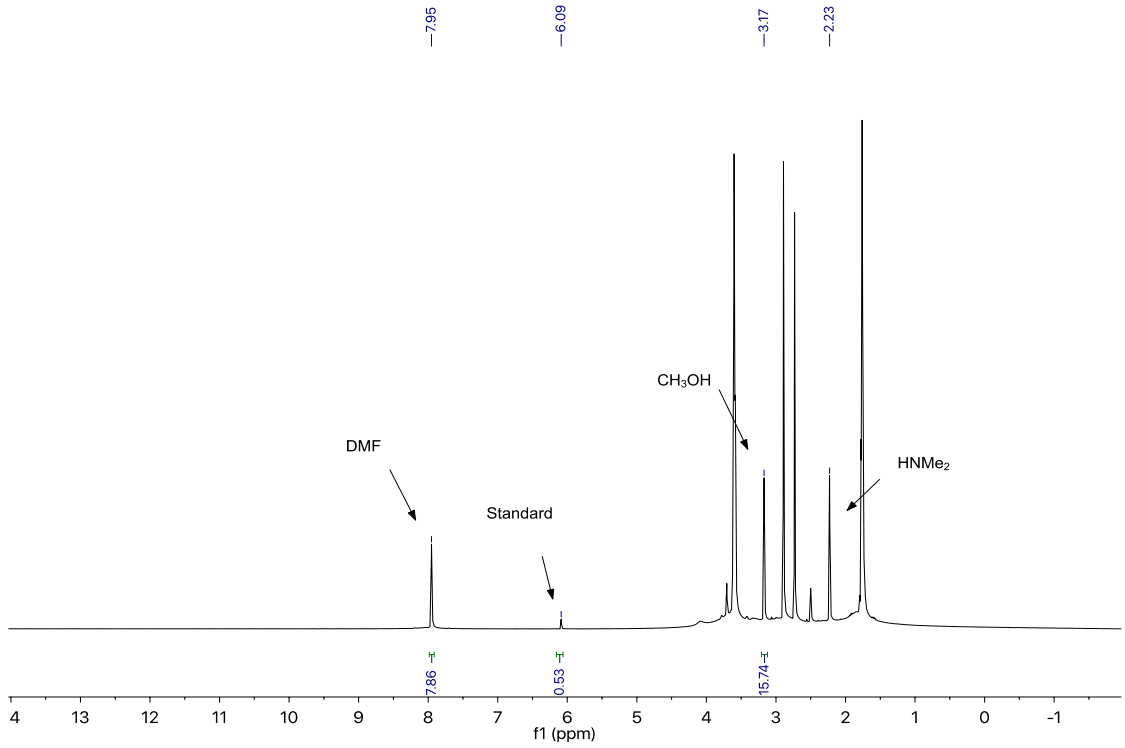

Procedure for the Hydrogenation of DMF in the Presence of CO_2 (Table 2.6)

In a N_2-atmosphere dry box, [Ru] (10 µmol, 1 mol%) was dissolved in 1 mL of THF, and this solution was added to the metal well of a pressure vessel containing a micro magnetic stirbar (3 x 10 mm). DMF (80 µL, 1.0 mmol, 100 equiv relative to Ru) was then added, and the vessel (Reactor-type A) was sealed and removed from the dry box. The vessel was connected to the Parr Multiple Reactor System, and the manifold was thoroughly purged with bone dry grade CO_2 (99.9%). The vessel was then pressurized to 1 bar with CO_2. The manifold was then thoroughly purged with ultra-high purity H_2 (99.999%). The vessel was then pressurized with 50 bar with ultra-high purity grade H_2 at room temperature to reach a total pressure of 51 bar. The reaction was heated at the desired temperature with a stir rate of 800 RPM. The heating was conducted using Specview software. After 18 hours of heating, the

reaction mixture was allowed to cool to room temperature. The pressure vessel was placed in a –84 °C bath (ethyl acetate/LN_2) for 15 min and then carefully vented using a metering valve. THF (0.5 mL) was added through the venting valve of the pressure vessel to wash any residual liquids/solids into the vessel. The vessel was then opened, 1,3,5-trimethoxybenzene (0.178 mmol, 300 μL of 0.593 M solution in DMSO-d_6) was added as a ^{1}H NMR standard, and the contents of the vessel were diluted with DMSO-d_6. Approximately 50 μL of the resulting solution was added to an NMR tube, diluted further with DMSO-d_6, and neutralized with HCl. The sample was then analyzed by ^{1}H NMR spectroscopy.

2.4.3. In situ Raman Hydrogenation Reactions

Procedure for In Situ Raman Kinetics for Comparing Ru Catalysts (Figures 2.11–2.15)

In a N_2-atmosphere dry box, the appropriate Ru catalyst (10 μmol) and K_3PO_4 (53 mg, 250 μmol, if appropriate) were added to the metal well of Reactor B which also contained a micro magnetic stirbar (3 x 10 mm) and a glass cylinder to displace solvent volume toward the Raman probe. THF (8.5 mL) and DMF (453 μL, 5.87 mmol) were then added, and the vessel was sealed and removed from the dry box. The vessel was connected to the Parr Multiple Reactor System, and the manifold was thoroughly purged with ultra-high purity H_2 (99.999%). The vessel was then pressurized to 50 bar with ultra-high purity grade H_2 at room temperature. The Raman probe was attached to the instrument. A dark spectrum was acquired at the onset. The reactor was then placed into a preheated block to obtain a reactor internal temperature of 155 °C. Once the reactor's internal temperature was at 155 °C ± 5 °C (after 35 min), Raman spectra were collected for 4 exposures (1 accumulation for 3 s) every 3 to 7 minutes (depending on catalyst) until the reaction had reached completion. Savitzky-Golay smoothing (using a 5th order polynomial constructed from 7 points with distortion being removed) and normalization was applied to each spectrum. A background spectrum of THF was also treated with Savitzky-Golay smoothing and normalized before being subtracted from each spectrum. The data was

truncated to include the region between 240-1800 cm^{-1}. Baseline correction was applied between endpoints, and peak areas were determined by peak picking for DMF peaks at ~658 cm^{-1} (integration area between 629–687 cm^{-1}) and ~865 cm^{-1} (integration area 852-878 cm^{-1}). A constant factor was subtracted from each spectrum determined from the value of the computed areas after full conversion. This removes the constant contribution of noise to the peak areas. Peak areas were converted to concentrations based on a calibration curve constructed at six different concentrations ranging from 0-1 M DMF in THF.

After heating, the reaction mixture was allowed to cool to room temperature. The pressure vessel was placed in a –84 °C bath (ethyl acetate/LN_2) for 15 min and then carefully vented using a metering valve. THF (0.5 mL) was added through the venting valve of the pressure vessel to wash any residual liquids/solids into the vessel. The vessel was then opened, 1,3,5-trimethoxybenzene (0.178 mmol, 300 µL of 0.593 M solution in DMSO-d_6) was added as a ^{1}H NMR standard, and the contents of the vessel were diluted with DMSO-d_6. Approximately 50 µL of the resulting solution was added to an NMR tube, diluted further with DMSO-d_6. The sample was then analyzed by ^{1}H NMR spectroscopy to confirm the results.

Procedure for In Situ Raman Kinetics for Influence of CO_2 on Kinetics (Figure 2.16)

In a N_2-atmosphere dry box, the appropriate Ru catalyst (56 µmol) was added to the metal well of Reactor B which also contained a micro magnetic stirbar (3 x 10 mm) and a glass cylinder to displace solvent volume toward the Raman probe. THF (8.5 mL) and DMF (453 µL, 5.9 mmol) were then added, and the vessel was sealed and removed from the dry box. The vessel was connected to the Parr Multiple Reactor System, and the manifold was thoroughly purged with bone dry grade CO_2 (99.9%) and then the vessel was pressurized to 1 bar with bone dry grade CO_2 (99.9%). The manifold was thoroughly purged with ultra-high purity grade H_2 (99.999%). The vessel was then pressurized with 50 bar of ultra-high purity grade H_2 at room temperature to a total pressure of 51 bar. The Raman probe was attached to the

instrument. A dark spectrum was acquired at the onset. The reactor was then placed into a preheated block to obtain a reactor internal temperature of 155 °C. Once the reactor's internal temperature was at 155 °C ± 5 °C (after 35 min), Raman spectra were collected for 4 exposures (1 accumulation for 3 s) every 5 minutes until the reaction had reached completion. Savitzky-Golay smoothing (using a 5th order polynomial constructed from 7 points with distortion being removed) and normalization was applied to each spectrum. A background spectrum of THF was also treated with Savitzky-Golay smoothing and normalized before being subtracted from each spectrum. The data was truncated to include the region between 240-1800 cm^{-1}. Baseline correction was applied between endpoints, and peak areas were determined by peak picking for DMF peaks at ~658 cm^{-1} (integration area between 629–687 cm^{-1}) and ~865 cm^{-1} (integration area 852–878 cm^{-1}). A constant factor was subtracted from each spectrum determined from the value of the computed areas after full conversion. This removes the constant contribution of noise to the peak areas. Peak areas were converted to concentrations based on a calibration curve constructed at six different concentrations ranging from 0-1 M DMF in THF.

After heating, the reaction mixture was allowed to cool to room temperature. The pressure vessel was placed in a –84 °C bath (ethyl acetate/LN_2) for 15 min and then carefully vented using a metering valve. THF (0.5 mL) was added through the venting valve of the pressure vessel to wash any residual liquids/solids into the vessel. The vessel was then opened, 1,3,5-trimethoxybenzene (0.178 mmol, 300 µL of 0.593 M solution in DMSO-d_6) was added as a ^{1}H NMR standard, and the contents of the vessel were diluted with DMSO-d_6. Approximately 50 µL of the resulting solution was added to an NMR tube, diluted further with DMSO-d_6, and neutralized with HCl. The sample was then analyzed by ^{1}H NMR spectroscopy to confirm the results.

Procedure for In Situ Raman Kinetics for Ru vs. Fe (Figure 2.17)

In a N_2-atmosphere dry box, Ru-PNP^{Cy} (21.4 mg, 35 μmol) or Fe-PNP^{Cy} (19.6 mg, 35 μmol) and K_3PO_4 (37.1 mg, 175 μmol, 5 equiv relative to Ru-PNP^{Cy} or Fe-PNP^{Cy}) were added to the metal well of Reactor B which also contained a micro magnetic stirbar (3 x 10 mm) and a glass cylinder to displace solvent volume toward the Raman probe. THF (7 mL) and DMF (805 μL, 10.5 mmol, 300 equiv relative to Ru-PNP^{Cy} or Fe-PNP^{Cy}) were then added, and the vessel was sealed and removed from the dry box. The vessel was connected to the Parr Multiple Reactor System, and the manifold was thoroughly purged with research grade H_2 (99.9999%). The vessel was then pressurized to 70 bar with research grade H_2 at room temperature. The Raman probe was attached to the instrument. A dark spectrum was acquired at the onset. The reactor was then placed into a preheated block to obtain a reactor internal temperature of 110 °C. Once the reactor's internal temperature was at 110 °C ± 5 °C (after 35 min), Raman spectra were collected for 4 exposures (1 accumulation for 3 s) over a period of 6 min with collections every 1.5 min, at which time spectra were then collected every 3 min until the reaction had reached completion (for to Ru-PNP^{Cy}, an additional 122 spectra were collected over 6.1 h; for Fe-PNP^{Cy}, an additional 168 spectra were collected over 8.4 h). Savitzky-Golay smoothing (using a 5th order polynomial constructed from 7 points with distortion being removed) and normalization was applied to each spectrum. A background spectrum of THF was also treated with Savitzky-Golay smoothing and normalized before being subtracted from each spectrum. The data was truncated to include the region between 240-1800 cm^{-1}. Baseline correction was applied between endpoints, and peak areas were determined by peak picking for DMF peaks at ~658 cm^{-1} (integration area between 629–687 cm^{-1}) and ~865 cm^{-1} (integration area 852-878 cm^{-1}). A constant factor was subtracted from each spectrum determined from the value of the computed areas after full conversion (–30.06 for peaks at 658 cm^{-1} and –21.25 for 865 cm^{-1}). This removes the constant contribution of noise to the peak areas. Peak areas were converted

to concentrations based on a calibration curve constructed at six different concentrations ranging from 0-1.34 M DMF in THF.

General Procedure for Variable Pressure In Situ Raman Kinetics for Fe (Figure 2.18)

In a N_2-atmosphere dry box, Fe-PNP^{Cy} (19.6 mg, 35 μmol) and K_3PO_4 (37.1 mg, 175 μmol, 5 equiv relative to Fe-PNP^{Cy}) were added to the metal well of Reactor B which also contained a micro magnetic stirbar (3 x 10 mm) and a glass cylinder to displace solvent volume toward the Raman probe. THF (7 mL) and DMF (805 μL, 10.5 mmol, 300 equiv relative to Fe-2a) were then added, and the vessel was sealed and removed from the dry box. The vessel was connected to the Parr Multiple Reactor System, and the manifold was thoroughly purged with research grade H_2 (99.9999%). The vessel was then pressurized to either 20, 50, or 70 bar with research grade H_2 at room temperature. The Raman probe was attached to the instrument. A dark spectrum was acquired at the onset. The reactor was then placed into a preheated block to obtain a reactor internal temperature of 110 °C. Once the reactor's internal temperature was at 110 °C ± 5 °C (after 35 min), Raman spectra were collected for 3 exposures (1 accumulation for 3 s) over a period of 10 h with collections every 3 min. Savitzky-Golay smoothing (using a 5th order polynomial constructed from 7 points with distortion being removed) and normalization was applied to each spectrum. The data was truncated to include the region between 480-1137 cm^{-1}. Baseline correction was applied between endpoints, and peak intensities were determined by peak picking for DMF peaks at ~658 cm^{-1} and ~865 cm^{-1}. A constant factor was subtracted from each spectrum determined from the value of the computed intensities after full conversion. This removes the constant contribution of noise to the peak intensities. The resulting peak intensities were used to compare the reaction progress.

2.5. References

1. Adapted with permission from Rezayee, N. M.; Samblanet, D.C.; Sanford, M. S. *ACS Catal.* **2016**, *6*, 6377. © American Chemical Society

2. Rezayee, N. M.; Huff, C. A.; Sanford, M. S. *J. Am. Chem. Soc*. **2015**, *137*, 1028.

3. Roose, P.; Eller, K.; Henkes, E.; Rossbacher, R.; Höke, H. In *Ullmann's Encyclopedia of Industrial Chemistry; Wiley-VCH, Weinhma, Germany, Amines, Aliphatic*: **2000**. DOI: 10.1002/14356007.a02_001.pub2.

4. Jessop, P. G. In *The Handbook of Homogeneous Hydrogenation*; Wiley-VCH Verlag GmbH: **2006**, p 489-511.

5. Dodds, D. L.; Cole-Hamilton, D. J. In *Sustainable Catalysis*; John Wiley & Sons, Inc.: **2013**, p 1-36.

6. Kim, S. H.; Hong, S. H. *ACS Catal*., **2014**, *4*, 3630.

7. Han, Z.; Rong, L.; Wu, J.; Zhang, L.; Wang, Z.; Ding, K. *Angew. Chem. Int. Ed*. **2012**, *51*, 13041.

8. Younus, H. A.; Ahmand, N.; Su, W.; Verpoort, F. *Coord. Chem. Rev.* **2014**, *276*, 112.

9. Spasyuk, D.; Gusev, D. G. *Organometallics* **2012**, *31*, 5239.

10. Alberico, E.; Lennox, A. J. J.; Vogat, L. K.; Jiao, H.; Baumann, W.; Drexler, H.; Nielsen, M.; Spannenberg, A.; Checinski, M. P.; Junge, H.; Beller, M. *J. Am. Chem. Soc*. **2016**, *138*, 14890.

11. Li, Y.-N.; Ma, R.; He, L.-N.; Diao, Z.-F. *Catal. Sci. Technol*. **2014**, *4*, 1498.

12. Ahmad, N.; Levison, J. J.; Robinson, S. D.; Uttley, M. F.; Wonchoba, E. R.; Parshall, G. W. Complexes of Ruthenium, Osmium, Rhodium, and Iridium Containing Hydride Carbonyl, or Nitrosyl Ligands. In *Inorganic Syntheses*; Parshall, G. W. McGraw-Hill: New York, **1974**; Vol. 15, p 48.

13. Bertoli, M.; Choualeb, A.; Lough, A. J.; Moore, B.; Spasyuk, D.; Gusev, D. G. *Organometallics* **2011**, *30*, 3479.

14. Kuriyama, W.; Matsumoo, T.; Ino, Y.; Ogata, O. (Takasago International Corporation) Ruthenium carbonyl complex having tridentate ligand, its production method and use. U.S. Patent 8,471,048. June 25, 2013.

15. Nielsen, M.; Alberico, E. Haumann, W.; Drexler, H.; Junge, H.; Gladiali, S.; Beller, M. *Nature* **2013**, *495*, 85.

16. Monney, A.; Barsch, E.; Sponholz, P.; Junge, H.; Ludwig, R.; Beller, M. *Chem. Commun*. **2014**, *50*, 707.

17. Neumann, J.; Bornschein, C.; Jiao, H.; Junge, K.; Beller, M. *Eur. J. Org. Chem*. **2015**, *27*, 5944.

18. Fairweather N. T.; Gibson, M. S.; Guan, H. *Organometallics* **2015**, *34*, 335.

19. Werkmeister, S.; Junge, K.; Wendt, B.; Alberico, E.; Jiao, H.; Baumann, W.; Junge, H.; Gallou, F.; Beller, M. *Angew. Chem. Int. Ed*. **2014**, *53*, 8722.

20. Qu, S.; Dai, H.; Dang, Y.; Song, C.; Wang, Z.-X.; Guan, H. *ACS Catal*. **2014**, *4*, 4377.

21. Huff, C. A. "Cascade Hydrogenation of Carbon Dioxide to Methanol." Ph.D. Dissertation, University of Michigan, Ann Arbor, MI, 2014.

22. Zhang, L.; Han, Z.; Zhao, X.;Wang, Z.; Ding, K. *Angew. Chem. Int. Ed.* **2015**, *54*, 6186.

23. Khusnutdinova, J. R.; Garg, J. A.; Milstein, D. *ACS Catal.*, **2015**, *5*, 2416.

24. Huff, C. A.; Sanford, M. S. *ACS Catal.* **2013**, *3*, 2412.

25. Bielinski, E. A.; Förster, M.; Zhang, Y.; Bernskoetter, W. H.; Hazari, N.; Holthausen, M. C. *ACS Catal.* **2015**, *5*, 2404.

26. Zhang, Y.; MacIntosh, A. D.; Wong, J. L.; Bielinski, E. A.; Williard, P. G.; Mercado, B. Q.; Hazari, N.; Bernskoetter, W. H. *Chem. Sci*. **2015**, *6*, 4291.

27. Chakrabotry, S.; Lagaditis, P. O.; Förster, M.; Bielinski, E. A.; Hazari, N.; Holthausen, M. C.; Jones, W. D.; Schneider, S. *ACS Catal.* **2014**, *4*, 3994.

28. Xu, R.; Chakraborty, S.; Bellow, S. M.; Yuan, H.; Cundari, T. R.; Jones, W. D. *ACS Catal.* **2016**, *6*, 2127.

29. Lu, Y. Liu, Z.; Guo, J.; Qu, S.; Zhao, R.; Wang, Z.-X. *Chem. Commun.* **2017**, *53*, 12148.

30. Sordakis, K.; Tang, C.; Vogt, L. K.; Junge, H.; Dyson, P. J.; Beller, M.; Laurenczy, G. *Che*m. Rev. 2018, 118, 372.

31. SciFinder; Chemical Abstracts Service: Columbus, OH; pKa; RN 66534-96-1; https://scifinder.cas.org (accessed March 7, 2018); calculated using ACD/Labs software, version 11.01; ACD/Labs 1994-2018.

32. SciFinder; Chemical Abstracts Service: Columbus, OH; pKa; RN 131890-26-1; https://scifinder.cas.org (accessed March 7, 2018); calculated using ACD/Labs software, version 11.01; ACD/Labs 1994-2018.

33. SciFinder; Chemical Abstracts Service: Columbus, OH; pKa; RN 550373-32-5; https://scifinder.cas.org (accessed March 7, 2018); calculated using ACD/Labs software, version 11.01; ACD/Labs 1994-2018.

34. Cook, A. K.; Schimler, S. D.; Matzger, A. J.; Sanford, M. S. *Science* **2016**, *351*, 1421.

35. Rezayee, N. M.; Samblanet, D. C.; Sanford, M. S. *ACS Catal*. **2016**, *6*, 6377.

36. Smith, A. M.; Whyman, R. *Chem. Rev.* **2014**, *114*, 5477.

37. Yuan, M.-L.; Xie, J.-H.; Zhu, S.-F.; Zhou, Q.-L. *ACS Catal*. **2016**, *6*, 3665.

38. Zell, T.; Milstein, D. *Acc. Chem. Res*. **2015**, *48*, 1979.

39. Mérel, D. S.; Do, M. L. T.; Gaillard, S.; Dupau, P.; Renaud, J.-L. *Coord. Chem. Rev*. **2015**, *288*, 50.

40. Casey, C. P.; Guan, H. *J. Am. Chem. Soc*. **2007**, *129*, 5816.

41. Langer, R.; Leitus, G.; Ben-David, Y.; Milstein, D. *Angew. Chem. Int. Ed*. **2011**, *50*, 2120.

42. Gorgas, N.; Stöger, B.; Veiros, L. F.; Pittenauer, E.; Allmaier, G.; Kirchner, K. *Organometallics* **2014**, *33*, 6905.

43. Gorgas, N.; Stöger, B.; Veiros, L. F.; Kirchner, K. *ACS Catal*. **2016**, *6*, 2664.

44. Sui-Seng, C.; Freutel, F.; Lough, A. J.; Morris, R. H. *Angew. Chem. Int. Ed*. **2008**, *47*, 940.

45. Zuo, W.; Lough, A. J.; Li, Y. F.; Morris, R. H. *Science* **2013**, *342*, 1080.

46. Sonnenberg, J. F.; Lough, A. J.; Morris, R. H. *Organometallics* **2014**, *33*, 6452.

47. Zuo, W.; Prokopchuk, D. E.; Lough, A. J.; Morris, R. H. *ACS Catal*. **2015**, *5*, 301.

48. Zell, T.; Ben-David, Y.; Milstein, D. *Catal. Sci. Technol.* **2015**, *5*, 822.

49. Chakraborty, S.; Dai, H.; Bhattacharya, P.; Fairweather, N. T.; Gibson, M. S.; Krause, J. A.; Guan, H. *J. Am. Chem. Soc.* **2014**, *136*, 7869.

50. Elangovan, S.; Wendt, B.; Topf, C.; Bachmann, S.; Scalone, M.; Spannenberg, A.; Jiao, H.; Baumann, W.; Junge, K.; Beller, M. *Adv. Syn. Catal.* **2016**, *358*, 820.

51. Garg, J. A.; Chakraborty, S.; Ben-David, Y.; Milstein, D. *Chem. Commun.* **2016**, *52*, 5285.

52. Schneck, F.; Assmann, M.; Balmer, M.; Harms, K.; Langer, R. *Organometallics* **2016**, *35*, 1931.

53. Fox, D. J.; Bergman, R. G. *Organometallics* **2004**, *23*, 1656.

54. Jiao, H.; Junge, K.; Alberico, E.; Beller, M. J. *Comput. Chem*. **2016**, *37*, 168.

55. Kilner, M.; Tyers, D. V.; Crabtree, S. P.; Wood, M. A. W.O. Patent 093208, November 13, 2007.

56. Ito, M.; Sakaguchi, A.; Kobayashi, C.; Ikariya, T. *J. Am. Chem. Soc.* **2007**, *129*, 290.

57. Magro, A. A. N.; Eastham, G. R.; Cole-Hamilton, D. J. *Chem. Commun*. **2007**, 3154.

58. Ito, M.; Koo, L. W.; Himizu, A.; Kobayashi, C.; Sakaguchi, A.; Ikariya, T. *Angew. Chem. Int. Ed*. **2009**, *48*, 1324.

59. Balaraman, E.; Gnanaprakasam, B.; Shimon, L. J. W.; Milstein, D. *J. Am. Chem. Soc.* **2010**, *132*, 16756.

60. Ito, M.; Kobayashi, C.; Himizu, A.; Ikariya, T. *J. Am. Chem. Soc*. **2010**, *132*, 11414.

61. John, J. M.; Bergens, S. H. *Angew. Chem. Int. Ed*. **2011**, *50*, 10377.

62. Miura, T.; Held, I. E.; Oishi, S.; Naruto, M.; Saito, S. *Tetrahedron Lett*. **2013**, *54*, 2674.

63. Kita, Y.; Higuchi, T.; Mashima, K. *Chem. Commun*. **2014**, *50*, 11211.

64. John, J. M.; Loorthuraja, R.; Antoniuk, E.; Bergens, S. H. *Catal. Sci. Technol.* **2015**, **5**, 1181.

65. Coetzee, J.; Dodds, D. L.; Klankermayer, J.; Brosinski, S.; Leitner, W.; Slawin, A. M. Z.; Cole-Hamilton, D. J. *Chem. Eur. J*. **2013**, *19*, 11039.

66. Coetzee, J.; Manyar, H. G.; Hardacre, C.; Cole-Hamilton, D. J. *Chemcatchem* **2013**, *5*, 2843.

67. Meuresch, M.; Westhues, S.; Leitner, W.; Klankermayer, J. *Angew. Chem. Int. Ed*. **2016**, *55*, 1392.

68. vom Stein, T.; Meuresch, M.; Limper, D.; Schmitz, M.; Hölscher, M.; Coetzee, J.; Cole-Hamilton, D. J.; Klankermayer, J.; Leitner, W. *J. Am. Chem. Soc*. **2014**, *136*, 13217.

69. Cabrero-Antonino, J. R.; Alberico, E.; Junge, K.; Junge, H.; Beller, M. *Chem. Sci*. **2016**, *7*, 3432.

70. Huff, C. A.; Sanford, M. S. *J. Am. Chem. Soc.* **2011**, *133*, 18122.

71. Brewster, T. P.; Rezayee, N. M.; Culakova, Z.; Sanford, M. S.; Goldberg, K. I. *ACS Catal*. **2016**, *6*, 3113.

72. Kuriyama, W.; Matsumoto, T.; Ogata, O.; Ino, Y.; Aoki, K.; Tanaka, S.; Ishida, K.; Kobayashi, T.; Sayo, N.; Saito, T. *Org. Process Res. Dev.* **2012**, *16*, 166.

73. Lagaditis, P. O.; Sues, P. E.; Sonnenberg, J. F.; Wan, K. Y.; Lough, A. J.; Morris, R. H. *J. Am. Chem. Soc*. **2014**, *136*, 1367.

74. Zhang, L.; Han, Z.; Zhao, X.; Wang, Z.; Ding, K. *Angew. Chem. Int. Ed*. **2015**, *54*, 6186.

75. Noyori, R.; Ohkuma, T. *Angew. Chem. Int. Ed*. **2001**, *40*, 40.

76. Hamilton, R. J.; Bergens, S. H. *J. Am. Chem. Soc*. **2006**, *128*, 13700.

77. Clarke, M. L.; Diaz-Valenzuela, M. B.; Slawin, A. M. Z. *Organometallics* **2007**, *26*, 16.

78. Saudan, L. A.; Saudan, C. M.; Debieux, C.; Wyss, P. *Angew. Chem. Int. Ed*. **2007**, *46*, 7473.

79. Cabrero-Antonino, J. R.; Alberico, E.; Drexler, H.-J.; Baumann, W.; Junge, K.; Junge, H.; Beller, M. *ACS Catal.* **2016**, **6**, 47.

80. For example, see: Cheng, T.-Y.; Brunschwig, B. S.; Bullock, R. M. *J. Am. Chem. Soc.* **1998**, *120*, 13121.

CHAPTER 3

Cascade Conversion of Carbon Dioxide to Methanol via an Amide Intermediate

3.1. Introduction

In 2015, the Sanford group reported a ruthenium-catalyzed cascade conversion of carbon dioxide (CO_2) to methanol (CH_3OH) via an amide intermediate (Scheme 3.1).[1] In the first step, a ruthenium catalyst (Ru-PNP^{Ph}) hydrogenates CO_2 to formic acid (Scheme 3.1, step i). Formic acid then undergoes an amidation reaction with dimethylamine ($HNMe_2$) to produce N,N-dimethylformamide (DMF) (Scheme 3.1, step ii). The same ruthenium catalyst then hydrogenates DMF, yielding methanol and regenerating dimethylamine (Scheme 3.1, step iii). This system generated up to 550 turnovers of methanol and greater than 95% conversion of CO_2.[1]

Scheme 3.1. Conversion of CO_2 to Methanol via an Amide Cascade Pathway

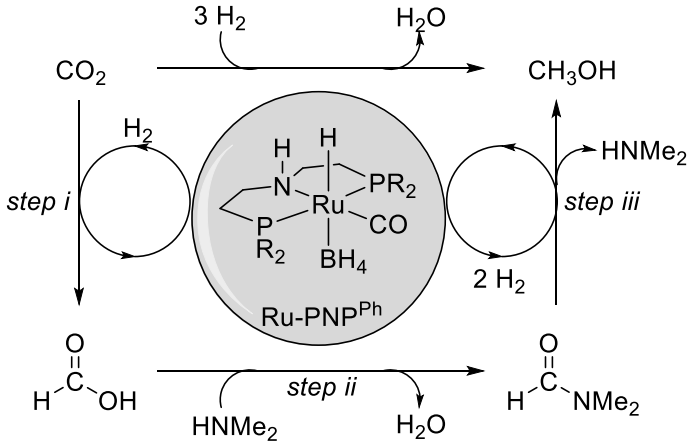

Scheme 3.2 shows a more detailed representation of the different competing pathways that are believed to be operating during catalysis.[1] Dimethylamine readily reacts with CO_2

(Scheme 3.2, step i.a) to generate dimethylammonium dimethylcarbamate (DMC), an ionic liquid. Indeed, amines are widely used for CO_2 capture and sequestration.[2,3,4] DMC is in equilibrium with free CO_2 and dimethylamine, with the equilibrium shifting towards CO_2 at elevated temperatures.[1] Once Ru-PNP^{Ph} hydrogenates CO_2 to formic acid (FA) (Scheme 3.2, step i), dimethylamine reacts with this intermediate to form dimethylammonium formate (DMFA) (Scheme 3.2, step i.b). Under these conditions, the equilibrium lies primarily towards the formation of DMFA.[1] The small population that exists as formic acid undergoes an amidation reaction to generate DMF as described above (Scheme 3.2, step ii).[1]

Scheme 3.2. Detailed Amide Cascade Pathway

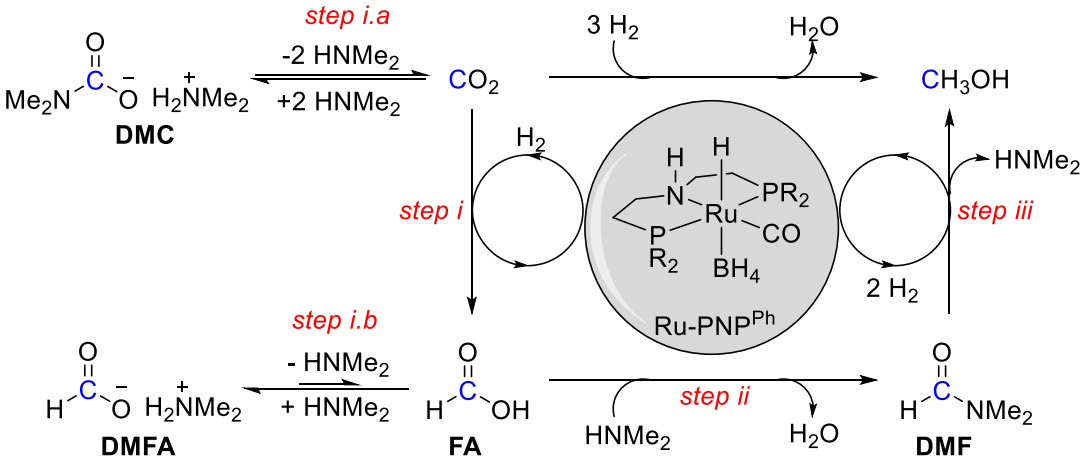

The original cascade amide system required the use of a temperature ramp.[1] At 95 °C, steps i and ii proceed. This relatively mild temperature was chosen because the hydrogenation of CO_2 is more favorable at low temperatures due to the reaction being entropically unfavorable (ΔS= –409 Jmol^{-1}K^{-1}) and enthalpically favorable (ΔH= –131 kJmol^{-1}).[5] At this temperature, near quantitative conversion of CO_2 was obtained, which is ideal, since CO_2 inhibits DMF hydrogenation.[1] Importantly, under the amide cascade conditions, no DMF hydrogenation is observed at 95 °C. The next step involved ramping the temperature to 155 °C, allowing for the conversion of DMF to methanol (step iii).[1] Conducting the reaction at a single temperature

(i.e., under isothermal conditions) resulted in either extremely low CO_2 conversions (at high temperatures) or little to no methanol formation (at low temperatures).[1]

Although the reported amide cascade system can reach high conversion of CO_2, a closer examination reveals that there is significant room for improvement. Under most conditions, only ~25% of the CO_2 is transformed into methanol.[1] Upon acidification during workup, the majority of the CO_2-derived products are intermediates FA and DMF. We sought to improve upon this initial cascade system by developing conditions to further hydrogenate the remaining DMF to generate methanol. In Chapter 2, we identified several ruthenium-based DMF hydrogenation catalysts that were more active than the original Ru-PNP^{Ph}. We sought to use these to develop a superior cascade amide system that shows not only high conversions of CO_2, but also high yields of methanol.

Our studies in Chapter 2, as well as our experience with the ester cascade system[6] made us consider applying cooperative tandem catalysis.[7,8,9,10,11] Notably, the ester cascade system described in Chapter 1 utilized tandem catalysis, with three separate catalysts sequentially performing each individual step to ultimately generate methanol.[6] In our original amide system, a single ruthenium catalyst was responsible for both CO_2 and DMF hydrogenation;[1] however, we hypothesized that two separate ruthenium catalysts (each optimized for an individual hydrogenation reaction) might be more effective.[7,9] Specifically, we reasoned that we could enhance the overall turnovers and conversion to methanol by coupling a Ru-PNP^{R} catalyst that is highly effective for CO_2 hydrogenation (Scheme 3.1 and 3.2, step i) with a second Ru-PNP^{R} catalyst that serves as a good DMF hydrogenation catalyst (Scheme 3.1 and 3.2, step iii). We anticipated that these could potentially operate synergistically, affording more methanol when the catalysts are in the same pot working cooperatively[10,11] compared to the sum of the two individually (Figure 3.1).

Figure 3.1. Cooperative vs. Additive Methanol Production

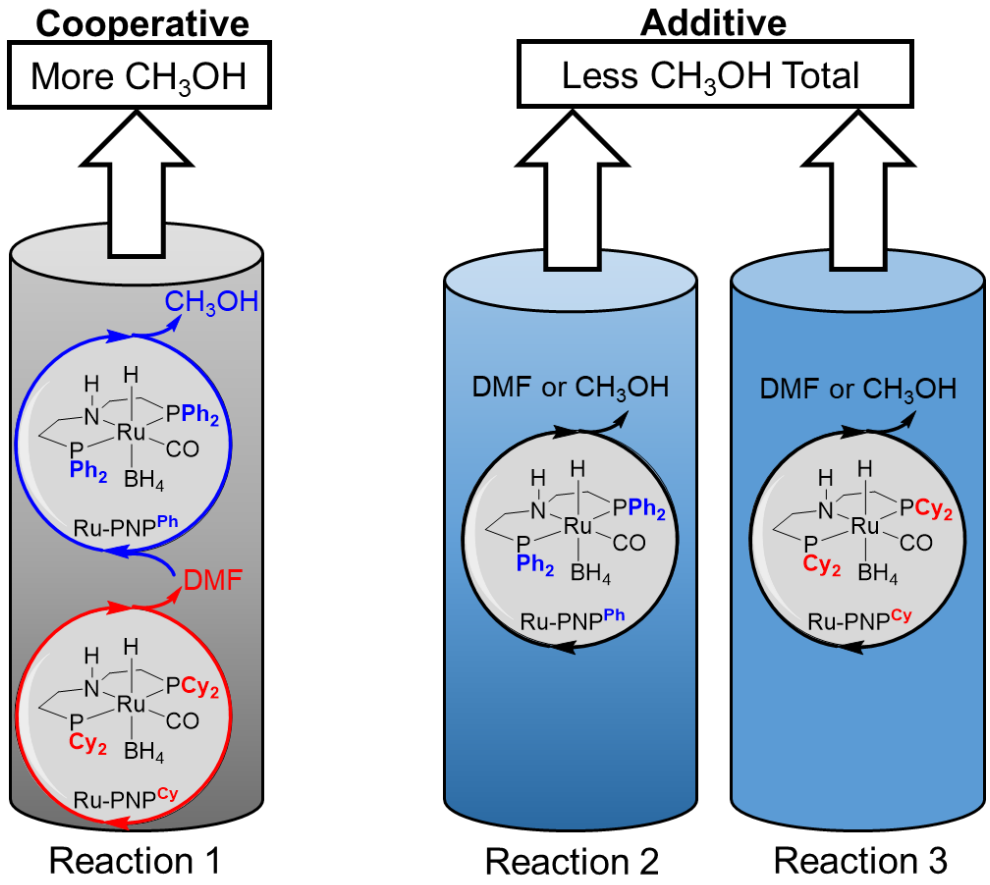

3.2. Results and Discussion

3.2.1. Ruthenium-PNP Catalyzed Cascade Conversion of CO_2 to Methanol with Commercial Dimethylamine Solution (2 M in THF)

We focused on applying the most active DMF hydrogenation catalysts identified in Chapter 2 (Ru-PNP^{Ph}, Ru-PNP^{iPr}, and Ru-PNP^{Cy}) to the amide cascade system (Figure 3.2). Our findings in Chapter 2 demonstrated that Ru-PNP^{Cy} is the fastest catalyst for DMF hydrogenation and typically gives very high yields of methanol. Unfortunately, its shortcoming lies in its sensitivity to CO_2. Ru-PNP^{iPr} is the second-best catalyst for DMF hydrogenation. Finally, our original catalyst, Ru-PNP^{Ph} is the least inhibited by CO_2, but is also the least active DMF hydrogenation catalyst. The original cascade amide system utilized Ru-PNP^{Ph}.

However, by balancing activity and sensitivity, Ru-PNP^{iPr} and Ru-PNP^{Cy} presented an opportunity to develop a second-generation system to produce more methanol.

Figure 3.2. Ru-PNP Variations with Different Substituents on the PNP Ligand

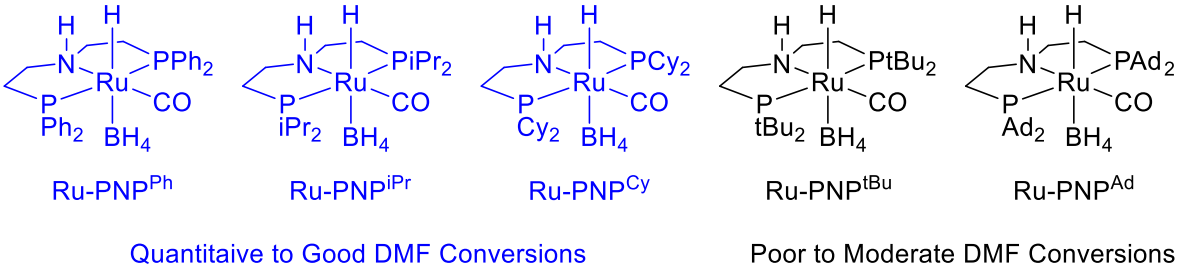

With this goal in mind, we first focused on replicating literature results with Ru-PNP^{Ph} as the catalyst. The original amide cascade system utilized a 3.8 M dimethylamine solution prepared in our lab via a time-consuming process and was subject to significant evaporative loss of dimethylamine. Thus, we chose to use a commercial 2 M dimethylamine solution for exploratory studies with the new catalysts Ru-PNP^{iPr} and Ru-PNP^{Cy}. Once establishing that Ru-PNP^{iPr} and Ru-PNP^{Cy} were active, we would then evaluate the 3.8 M dimethylamine solution to more closely match the literature report. Additionally, as these were exploratory and preliminary studies, the reactions presented in this section (3.2.1) were only run once.

We first confirmed that the reaction proceeded with the original Ru-PNP^{Ph} catalyst and 2 M dimethylamine (Table 3.1). In general, lower yields were obtained at this lower concentration of dimethylamine as this resulted in a lower concentration of $HNMe_2$ to perform the amidation reaction. We compared maintaining the same number of moles of dimethylamine relative to the 3.8 M reaction (Table 3.1, Entry 2), versus using less amine, but maintaining the same concentration of catalyst (Table 3.1, Entry 3). These preliminary results showed that maintaining the same number of moles of amine resulted in a higher yield and led us to adopting these as our standard conditions.

Table 3.1. Comparing Commercial $HNMe_2$ to Published Results in CO_2 Hydrogenation

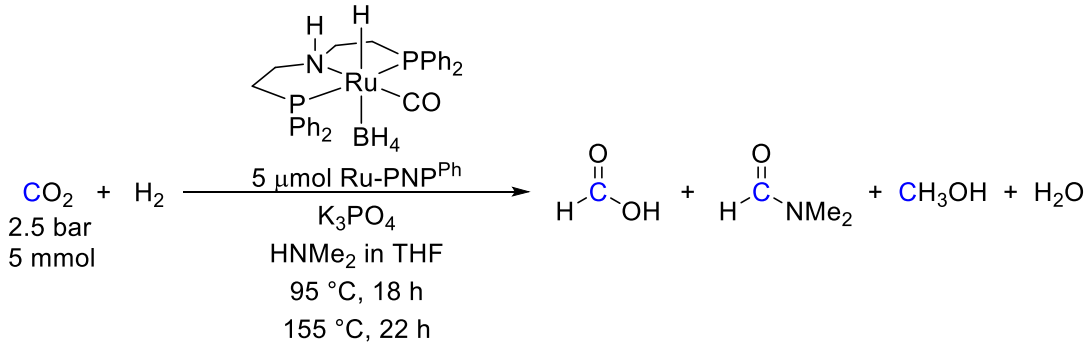

Entry	Concentration $HNMe_2$ (M)	$HNMe_2$ (mmol)	Total Volume (mL)	Conversion (%)[a]
1[b]	3.8	7.6	2	96
2[c]	2	7.6	4	39
3[d]	2	3.8	2	21

[a]**Conditions:** 5 μmol Ru-PNP catalyst, 250 μmol K_3PO_4, 2.5 bar CO_2, 50 bar H_2, 95 °C for 18 h followed by 155 °C for 22 h. Yields determined by ^1H NMR spectroscopy. [b]Entry obtained from ref 1, 2 mL of 3.8 M $HNMe_2$ in THF, 155 °C for 18 h. [c]3.8 mL of 2 M $HNMe_2$ in THF (commercial), 0.2 mL of THF added. [d]1.9 mL of 2 M $HNMe_2$ in THF (commercial), 0.1 mL of THF added.

We next compared Ru-PNP^{Ph}, Ru-PNP^{iPr}, and Ru-PNP^{Cy} with the 2 M amine solution. As shown in Table 3.2, all three catalysts were effective for the hydrogenation of CO_2 under these conditions. Our best DMF hydrogenation catalyst, Ru-PNP^{Cy}, gave the highest CO_2 conversion (76%), while Ru-PNP^{Ph} and Ru-PNP^{iPr} both afforded a 39% conversion of CO_2 (Table 3.2, Entries 1 and 5). These results are consistent with the data in Chapter 2, showing that Ru-PNP^{Ph} and Ru-PNP^{iPr} have comparable activity for DMF hydrogenation. These initial studies indicated that Ru-PNP^{Cy} may be the best complex and may ultimately provide a superior amide cascade system, thus prompting further studies.

Table 3.2. Hydrogenation of CO_2 with Ru-PNP^R complexes

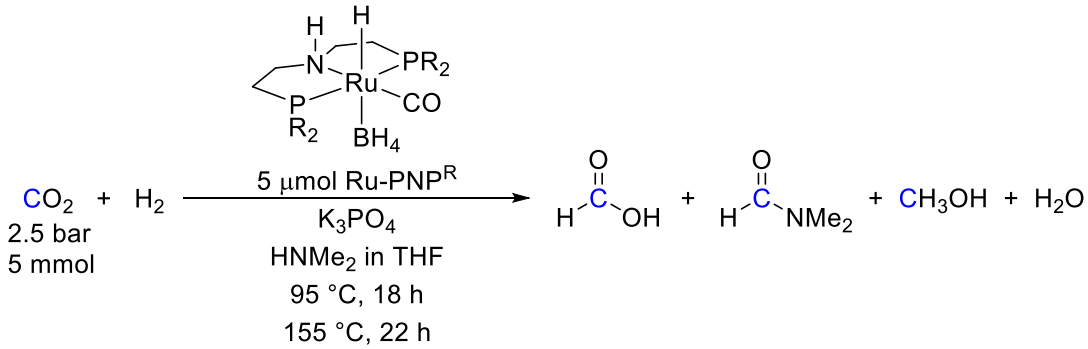

Entry	R	Concentration $HNMe_2$ (M)	$HNMe_2$ (mmol)	Total Volume (mL)	Conversion (%)[a]
1	Ph	2	7.6	4	39
2	Cy	2	7.6	4	76
3	iPr	2	7.6	4	39

[a]**Conditions:** 5 µmol Ru-PNP^R catalyst, 250 µmol K_3PO_4, 3.8 mL of 2 M $HNMe_2$ in THF (commercial), 0.2 mL of THF added, 2.5 bar CO_2, 50 bar H_2, 95 °C for 18 h followed by 155 °C for 22 h. Yields determined by ^{1}H NMR spectroscopy.

In addition to looking at the overall conversion of CO_2, the relative amounts of products formed also provided insight for comparing Ru-PNP^{Ph}, Ru-PNP^{iPr}, and Ru-PNP^{Cy} (Table 3.3). Although Ru-PNP^{Ph} gave a low conversion of CO_2 (39%), it produced the most methanol (104 turnovers), which represents 27% of the CO_2 converted (Table 3.3, Entry 1). Conversely, Ru-PNP^{Cy} converted the most CO_2, but only produced 40 turnovers of methanol along with 720 turnovers of formic acid and DMF combined (Table 3.3, Entry 2). As such, the amount of methanol produced by Ru-PNP^{Cy} represents a very small portion (5%) of the total CO_2 converted. Finally, Ru-PNP^{iPr} converted 39% of the CO_2, producing the least methanol and the second most intermediates (Table 3.3, Entry 3).

Table 3.3. Product Distribution of Ru-PNP^R Catalyzed CO_2 Hydrogenation

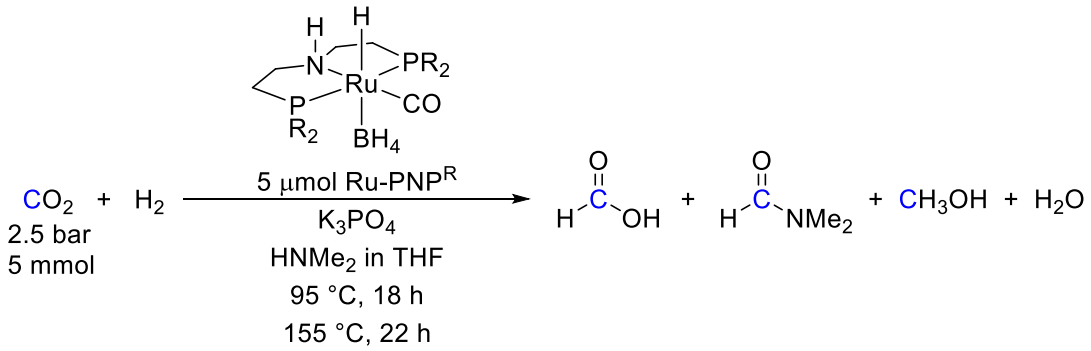

Entry	R	TON Intermediates[b]	TON Methanol	Conversion CO_2 (%)
1	Ph	282	104	39
2	Cy	720	40	76
3	iPr	368	18	39

[a]**Conditions:** 5 µmol Ru-PNP catalyst, 250 µmol K_3PO_4, 3.8 mL of 2 M $HNMe_2$ in THF (commercial), 0.2 mL of THF, 2.5 bar CO_2, 50 bar H_2, 95 °C for 18 h followed by 155 °C for 22 h. Yields determined by ^{1}H NMR spectroscopy. [b] Intermediates = formic acid + DMF.

The findings in Table 3.3 were consistent with Chapter 2 wherein Ru-PNP^{Cy} and Ru-PNP^{iPr} were most inhibited by CO_2 for DMF hydrogenation, while Ru-PNP^{Ph} was least inhibited by the present of CO_2 and maintained its reactivity the best when CO_2 was present (see section 2.2.1). This inhibition is reflected in Table 3.3 in the ratio of products formed; Ru-PNP^{Cy} and Ru-PNP^{iPr} are the most inhibited by CO_2 and thus only produce relatively small amounts of methanol. In comparison, Ru-PNP^{Ph}, which is the best DMF hydrogenation catalyst when CO_2 is present, and generates the highest amount of methanol.

In the original cascade system, the concentration of catalyst was found to be extremely important. As such, we next probed the impact of concentration on the performance of Ru-PNP^{iPr} and Ru-PNP^{Cy} (Table 3.4). In accordance with the reported cascade amide system, Ru-PNP^{Ph} gave higher turnovers of methanol at lower loadings (Table 3.4, Entries 1-3). This was also true for Ru-PNP^{iPr}, where the turnovers of methanol increase from 16 at 10 μmol to 64 at 2.5 μmol (Table 3.4, Entries 7-9). This same trend (higher turnovers with decreasing Ru) was also observed for the intermediates formed by Ru-PNP^{iPr} (Table 3.4, Entries 7-9). A decrease in CO_2 conversion was observed for both Ru-PNP^{Ph} and Ru-PNP^{iPr} as the concentration of Ru was dropped (Table 3.4, Entries 1-3 and 7-9). In contrast, the CO_2 conversion was nearly the same at 10 and 5 μmol of Ru-PNP^{Cy} before decreasing by half at 2.5 μmol (Table 3.4, Entries 4-6). In marked contrast, for Ru-PNP^{Cy}, the turnovers of methanol did not increase as the amount of catalyst was decreased. The results in Table 3.4 are consistent with those in Table 3.3: Ru-PNP^{Cy} converts the most CO_2 and results in the highest turnovers of intermediates at all loadings, while Ru-PNP^{Ph} produces the most turnovers of methanol at all loadings.

Table 3.4. Varying Concentration of Ru-PNP^{R} for CO_2 Hydrogenation

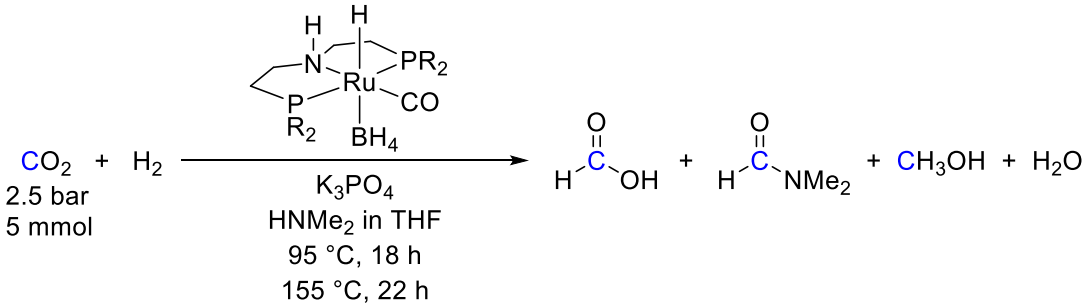

Entry	µmol Ru-PNP^{R}	R	TON Intermediates	TON Methanol	% Yield Methanol	Conversion CO_2 (%)
1	10	Ph	194	77	15	54
2	5	Ph	282	104	10	39
3	2.5	Ph	240	116	6	18
4	10	Cy	315	53	11	74
5	5	Cy	720	40	4	76
6	2.5	Cy	652	20	1	34
7	10	iPr	295	16	3	60
8	5	iPr	368	18	2	39
9	2.5	iPr	392	64	3	23

[a]**Conditions:** 2.5 – 10 µmol Ru-PNP catalyst, 250 µmol K_3PO_4, 3.8 mL of 2 M $HNMe_2$ in THF (commercial), 0.2 mL of THF, 2.5 bar CO_2, 50 bar H_2, 95 °C for 18 h followed by 155 °C for 22 h. Yields determined by ^{1}H NMR spectroscopy.

Another important factor to study in the cascade amide system was the influence of base (Table 3.5). When K_3PO_4 was present during Ru-PNP^{Ph}-catalyzed hydrogenation of CO_2, higher or equal turnovers of methanol were obtained compared to the reactions without base (Table 3.5, Entry 1 versus 2, Entry 3 versus 4, and Entry 5 versus 6). Interestingly, when base was present, the conversion of CO_2 decreased as the amount of Ru decreased (Table 3.5 Entries 1, 3, and 5) and the turnovers of intermediates formed remained relatively consistent. On the other hand, when no base was present, the CO_2 conversion dramatically increased when dropping below 10 µmol of Ru-PNP^{Ph} (Table 3.5, Entries 2, 4, and 6). Furthermore, there was a significant increase in the turnovers of intermediates, increasing by two orders of magnitude from 10 to 1152 as the Ru loading decreased (Table 3.5, Entries 2 and 6). Another interesting facet that can be extracted from Table 3.5 is the influence base has on product distribution. In the reactions with base (Table 3.5, Entries 1, 3 and 5), methanol represents approximately 30% of the products (32-27%). Base-free reactions that produced

moderate conversions of CO_2 (75% and 61%) resulted in a relatively smaller percentage methanol (16-6%) (Table 3.5, Entries 4 and 6). Overall, under these exploratory reaction conditions, base either has no impact or aids in increasing the turnovers of methanol. However, higher conversions can be reached by eliminating K_3PO_4.

Table 3.5. Influence of Base for Ru-PNP^{Ph} in CO_2 Hydrogenation

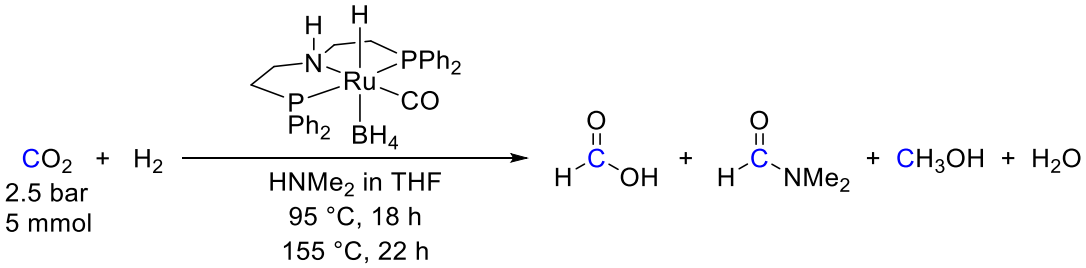

Entry	Ru-PNP^{Ph} (µmol)	K_3PO_4 (µmol)	TON Intermediates	TON Methanol	Conversion CO_2 (%)
1	10	250	194	77	54
2	10	0	10	30	9
3	5	250	282	104	39
4	5	0	648	104	75
5	2.5	250	240	116	18
6	2.5	0	1152	72	61

[a]**Conditions:** 2.5 – 10 µmol Ru-PNP catalyst, 250 µmol K_3PO_4 (where appropriate) 3.8 mL of 2 M $HNMe_2$ in THF (commercial), 0.2 mL of THF, 2.5 bar CO_2, 50 bar H_2, 95 °C for 18 h followed by 155 °C for 22 h. Yields determined by ^{1}H NMR spectroscopy.

These findings are particularly interesting in light of the published amide cascade system. It is important to note that the influence of K_3PO_4 on the reaction was studied only at 10 µmol and only for carbamate hydrogenation at 155 °C.[1] According to this original publication, when base was present, higher turnovers of methanol were obtained upon dropping the catalyst loading, which is generally consistent with the findings in Table 3.5. However, the published data was not studied in the absence of base, making Entry 4 in Table 3.5 particularly interesting.[1] The turnovers of methanol are maintained when removing K_3PO_4 (104), but the turnovers of intermediates more than double (282 to 648) when base is removed. Excitingly, this was the best result when considering both CO_2 conversion and turnovers of methanol!

Next, we examined the impact of base on Ru-PNP^{Cy}-catalyzed CO_2 hydrogenation. We observed that the presence of base led to higher conversions of CO_2, higher turnovers of methanol, and higher turnovers of intermediates (Table 3.6, Entries 1-6). The observation of added base increasing the turnovers of methanol is consistent with reactivity observed with Ru-PNP^{Ph} (Table 3.5). In accordance with Table 3.4, Ru-PNP^{Cy} produced a significantly smaller amount of methanol as compared to Ru-PNP^{Ph} in all cases (Table 3.5 vs Table 3.6). Conversely, Ru-PNP^{Cy} generally produced significantly higher turnovers of intermediates as compared to Ru-PNP^{Ph}. The exception to this was at very low loadings in the absence of base wherein Ru-PNP^{Ph} retained its reactivity better than Ru-PNP^{Cy} (only a 20% drop verses a 92% drop, respectively). This was consistent with Table 3.2 findings where Ru-PNP^{Cy} gave the highest turnovers of intermediates while Ru-PNP^{Ph} produced the highest turnovers of methanol.

Table 3.6. Influence of Base for Ru-PNP^{Cy} in CO_2 Hydrogenation

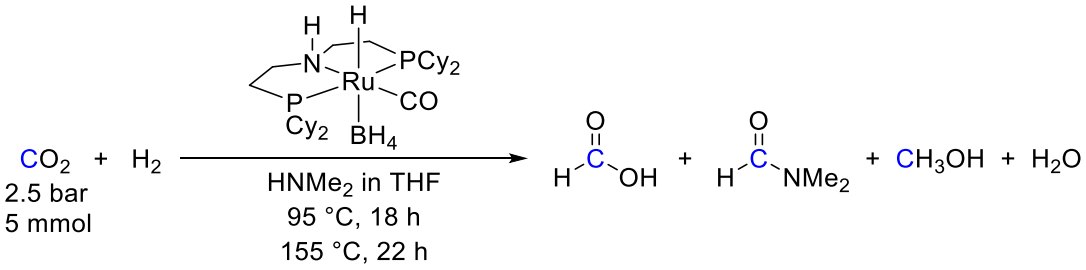

Entry	Ru-PNP^{Cy} (µmol)	K_3PO_4 (µmol)	TON Intermediates	TON Methanol	Conversion CO_2 (%)
1	10	250	315	53	74
2	10	0	203	30	23
3	5	250	720	40	76
4	5	0	664	14	68
5	2.5	250	652	20	34
6	2.5	0	228	3	12

[a]**Conditions:** 2.5 – 10 µmol Ru-PNP catalyst, 250 µmol K_3PO_4 (where appropriate) 3.8 mL of 2 M $HNMe_2$ in THF (commercial), 0.2 mL of THF, 2.5 bar CO_2, 50 bar H_2, 95 °C for 18 h followed by 155 °C for 22 h. Yields determined by ^{1}H NMR spectroscopy.

Finally, the reactivity of Ru-PNP^{iPr} was studied in the presence and absence of base. Interestingly, with this catalyst the presence of base did not always result in higher turnovers of methanol compared to base-free (Table 3.7, Entries 1 vs 2, 3 vs 4). This is a result unique to Ru-PNP^{iPr}, whereas Ru-PNP^{Ph} and Ru-PNP^{Cy} produced the same or more turnovers of

methanol when base was present. At high loadings of Ru (10 and 5 µmol), base led to both a decrease in the CO_2 conversion, as well as a decrease in the turnovers of intermediates and methanol (Table 3.7, Entries 1-4).

Table 3.7. Influence of Base for Ru-PNP^{iPr} in CO_2 Hydrogenation

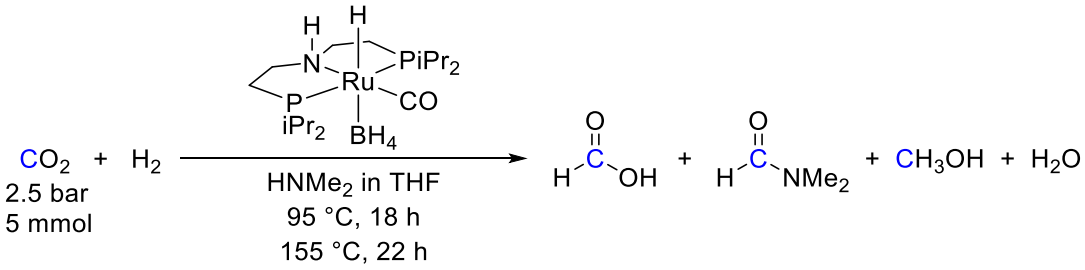

Entry	Ru-PNP^{iPr} (µmol)	K_3PO_4 (µmol)	TON Intermediates	TON Methanol	Conversion CO_2 (%)
1	10	250	295	16	60
2	10	0	422	41	93
3	5	250	368	18	39
4	5	0	578	60	64
5	2.5	250	392	64	23
6	2.5	0	216	28	12

[a]**Conditions:** 2.5 – 10 µmol Ru-PNP catalyst, 250 µmol K_3PO_4 (where appropriate) 3.8 mL of 2 M $HNMe_2$ in THF (commercial), 0.2 mL of THF, 2.5 bar CO_2, 50 bar H_2, 95 °C for 18 h followed by 155 °C for 22 h. Yields determined by ^{1}H NMR spectroscopy.

To obtain high conversions of CO_2 as well as high turnovers of methanol, we next examined cooperative tandem catalysis (Figure 3.1). Our earlier experiments indicated that Ru-PNP^{Ph} was the most reactive complex for methanol production followed by Ru-PNP^{iPr} then Ru-PNP^{Cy}. On the other hand, Ru-PNP^{Cy} gave the highest conversions of CO_2. As such, we hypothesized that utilizing two catalysts in the same reaction, where one normally results in high CO_2 conversions (Ru-PNP^{Cy}) and the other produces high turnovers of methanol (Ru-PNP^{Ph}), could produce a synergistic system where higher turnovers of methanol and higher conversions of CO_2 could be realized compared to the two catalysts individually.

We first studied our three catalysts in cooperative tandem catalysis where the additive turnovers of product were conducted at the same loading of Ru (Figure 3.3). For the cooperative reactions where two catalysts are working in tandem, 2.5 µmol of each catalyst was loaded into

the same reactor well, and the methanol and intermediates produced are represented below. In the additive reactions, 2.5 μmol of a single catalyst (such as Ru-PNP^{Ph}) was loaded into a reactor well, and the reaction was conducted under standard conditions. In a second reactor, 2.5 μmol of a second catalyst (such as Ru-PNP^{Cy}) was also used to perform the reaction under standard conditions. Upon work up, the total moles of each product were obtained via ^{1}H NMR spectroscopic analysis and divided by the appropriate catalyst loading (2.5 μmol) to obtain the turnovers for methanol and the intermediates. The turnovers of each product (methanol and intermediates) obtained from each catalyst were then added together to get the additive turnovers shown in Figure 3.3.

We were pleased to see that, consistent with our hypothesis, a synergistic effect was observed in many cases (Figure 3.3). When combining the best methanol production catalyst, Ru-PNP^{Ph}, with one of the high CO_2 converting catalysts (Ru-PNP^{Cy} or Ru-PNP^{iPr}), we observed an increase in methanol compared to the sum of the catalysts alone (Figure 3.3, Cooperative versus Additive). This cooperative effect resulted in more than double the amount of methanol relative to Ru-PNP^{Ph} and Ru-PNP^{iPr} alone. The second-best synergy was seen in the case of Ru-PNP^{Ph} and Ru-PNP^{Cy} with base, where again the amount of methanol obtained nearly doubles. On the other hand, neither Ru-PNP^{Cy} or Ru-PNP^{iPr} are particularly good at producing methanol, with Ru-PNP^{Cy} normally producing the least of the three complexes. Interestingly, when pairing these two catalysts together with base, a significant inhibition is seen in the cooperative case and the sum of the two catalysts separately yielded more turnovers of methanol (Figure 3.3, Ph + Cy + base Cooperative versus Additive).

Figure 3.3. Comparing Cooperative System and the Additive Single Catalysts for Methanol Production: Same Ru Loading[a]

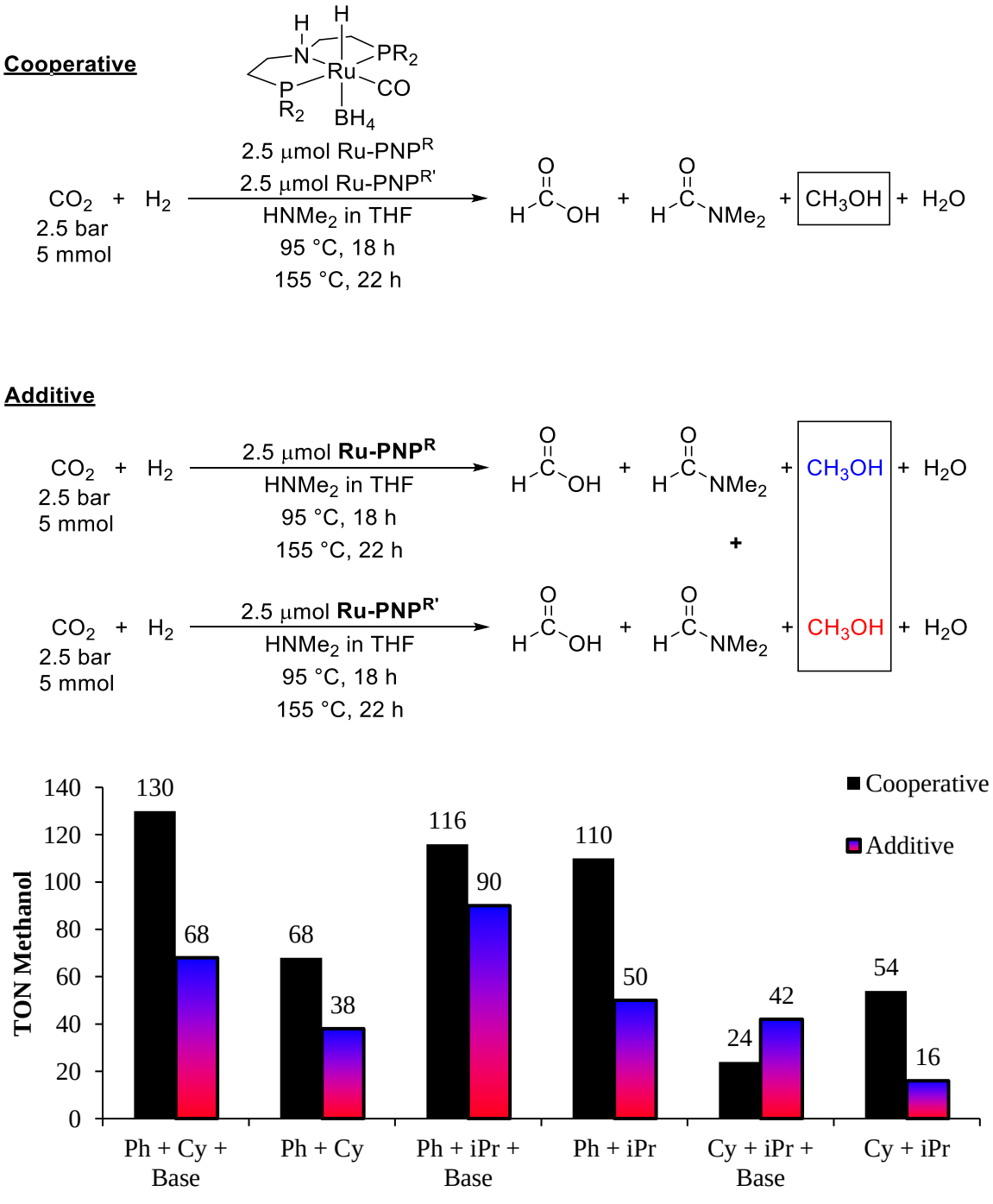

[a]**Conditions:** Cooperative reactions- 2.5 µmol Ru-PNP^R and 2.5 µmol Ru-PNP^R', 250 µmol K_3PO_4 (where appropriate) 3.8 mL of 2 M $HNMe_2$ in THF (commercial), 0.2 mL of THF, 2.5 bar CO_2, 50 bar H_2, 95 °C for 18 h followed by 155 °C for 22 h. Yields determined by ^{1}H NMR spectroscopy. Additive reactions- 2.5 µmol Ru-PNP^R or 2.5 µmol Ru-PNP^R', 250 µmol K_3PO_4 (where appropriate) 3.8 mL of 2 M $HNMe_2$ in THF (commercial), 0.2 mL of THF, 2.5 bar CO_2, 50 bar H_2, 95 °C for 18 h followed by 155 °C for 22 h. Yields determined by ^{1}H NMR spectroscopy.

A second way to study cooperative cascade catalysis in this two-catalyst system is by maintaining the same concentration of Ru in the individual reactions as is used in the cooperative studies. In these reactions, each individual catalyst was analyzed for CO_2 hydrogenation using 5 µmol of catalyst. Upon work up, the total moles of each product were obtained via ^1H NMR spectroscopic analysis and divided by the appropriate catalyst loading (5 µmol). From there, the turnovers of each product (methanol and intermediates) were halved to represent the amount of catalyst used in the cooperative reaction (See Figure 3.4 below for visual representation). The resulting turnovers of methanol and intermediates were added for the two catalysts and are represented in Figure 3.5 below as "Additive".

Once again, we observe a synergistic effect when comparing the cooperative reactions to additive reactions. Again, when combining Ru-PNP^{Ph} with either Ru-PNP^{Cy} or Ru-PNP^{iPr} increased turnovers of methanol are obtained compared to when the catalysts are alone (Figure 3.4 and 3.5). Consistent with the results in Figure 3.3, when combining Ru-PNP^{Cy} and Ru-PNP^{iPr} with base there is inhibition rather than an increase in methanol production.

Figure 3.4. Comparing Cooperative System and the Individual Single Catalysts[a]

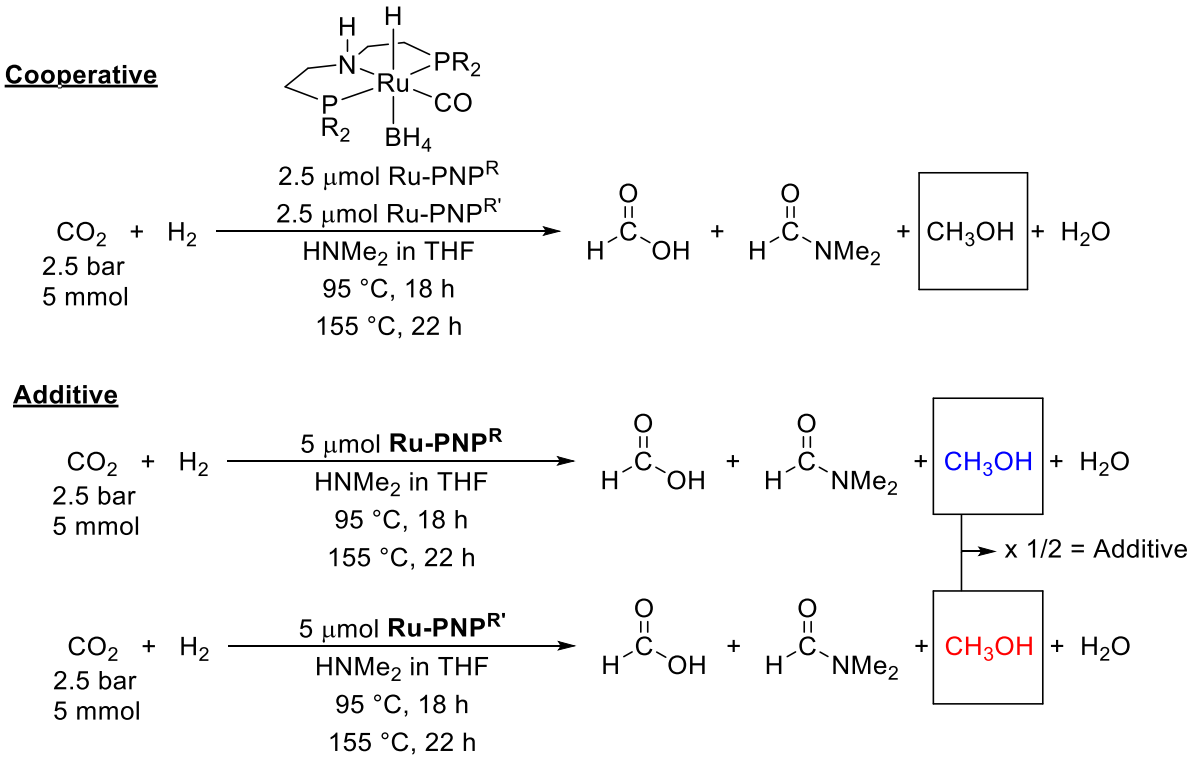

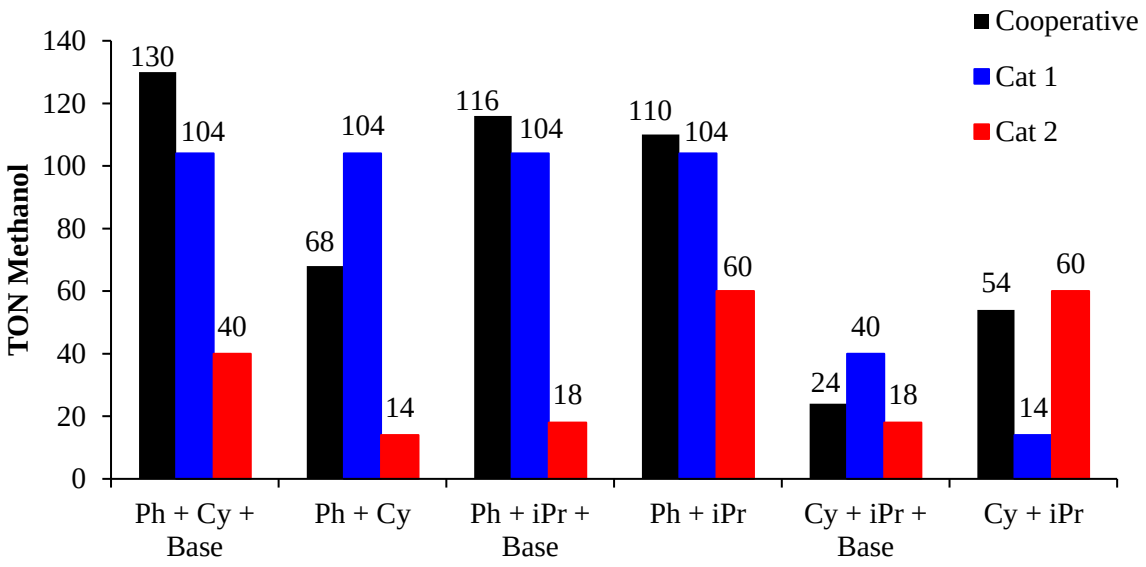

[a]**Conditions:** Cooperative reactions- 2.5 µmol Ru-PNP^R and 2.5 µmol Ru-PNP^R', 250 µmol K_3PO_4 (where appropriate) 3.8 mL of 2 M $HNMe_2$ in THF (commercial), 0.2 mL of THF, 2.5 bar CO_2, 50 bar H_2, 95 °C for 18 h followed by 155 °C for 22 h. Yields determined by ^{1}H NMR spectroscopy. Additive reactions- 5 µmol Ru-PNP^R or 5 µmol Ru-PNP^R', 250 µmol K_3PO_4 (where appropriate) 3.8 mL of 2 M $HNMe_2$ in THF (commercial), 0.2 mL of THF, 2.5 bar CO_2, 50 bar H_2, 95 °C for 18 h followed by 155 °C for 22 h. Yields determined by ^{1}H NMR spectroscopy.

Figure 3.5. Comparing Cooperative System and the Additive Single Catalysts for Methanol Production: Same Ru Concentration[a]

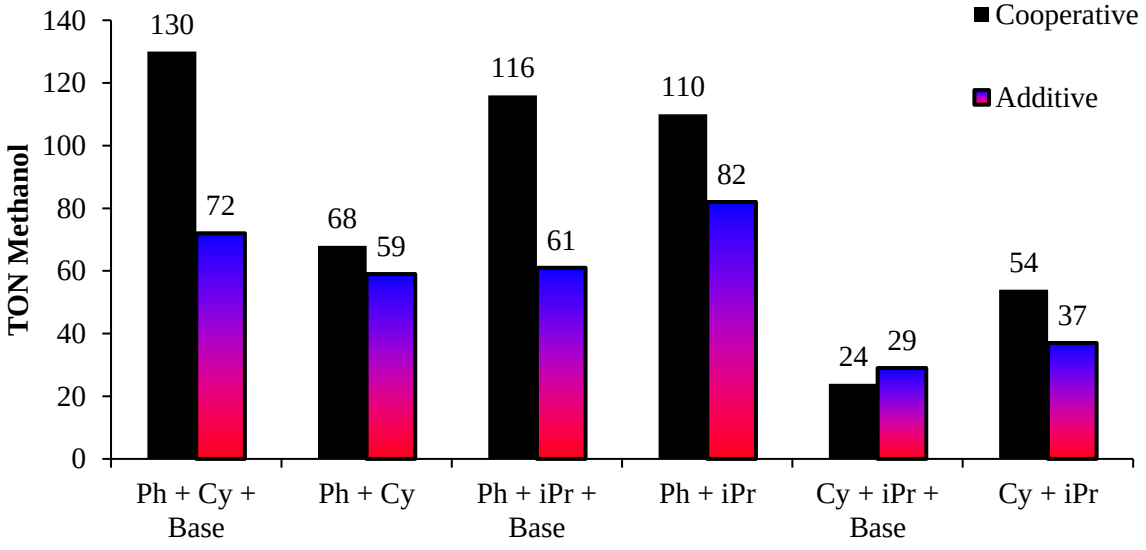

[a]**Conditions:** Cooperative reactions- 2.5 µmol Ru-PNP^R and 2.5 µmol Ru-PNP^R', 250 µmol K_3PO_4 (where appropriate) 3.8 mL of 2 M $HNMe_2$ in THF (commercial), 0.2 mL of THF, 2.5 bar CO_2, 50 bar H_2, 95 °C for 18 h followed by 155 °C for 22 h. Yields determined by ^{1}H NMR spectroscopy. Additive reactions- 5 µmol Ru-PNP^R or 5 µmol Ru-PNP^R', 250 µmol K_3PO_4 (where appropriate) 3.8 mL of 2 M $HNMe_2$ in THF (commercial), 0.2 mL of THF, 2.5 bar CO_2, 50 bar H_2, 95 °C for 18 h followed by 155 °C for 22 h. Yields determined by ^{1}H NMR spectroscopy.

All reaction conditions presented above utilize a temperature ramp. As discussed above, this was used to consume the CO_2 at lower temperatures were the reaction is most favorable.[1] The reaction temperature was then increased to convert DMF to methanol when there was little or no CO_2 present, as studies have shown that CO_2 inhibits DMF hydrogenation. However, once finding that higher amounts of methanol can be obtained by using cooperative catalysis, we next aimed to utilize isothermal reaction conditions to simplify the system (Table 3.8). At 100 °C, full conversion of CO_2 was achieved, but no methanol was formed (Table 3.8 Entry 1). At 135 °C, high CO_2 conversions were observed, and very small amounts of methanol were formed (Table 3.8, Entry 2). Upon increasing the temperature to 155 °C, lower CO_2 conversions were coupled with no change in methanol formation as well as lower turnovers of intermediates (Table 3.8). Next, we increased the reaction time at 155 °C to see if more of the intermediates were converted to methanol (Table 3.8, Entry 4). Unfortunately, even with nearly doubling the reaction time, only a small increase from 8 to 24 turnovers of methanol was obtained. Based on this data, we hypothesize that the catalysts have likely decomposed due to the very minimal improvement in methanol formation after such a long period of time.

Table 3.8. Isothermal CO_2 Hydrogenation by Ru-PNP^{Cy} and Ru-PNP^{Ph}

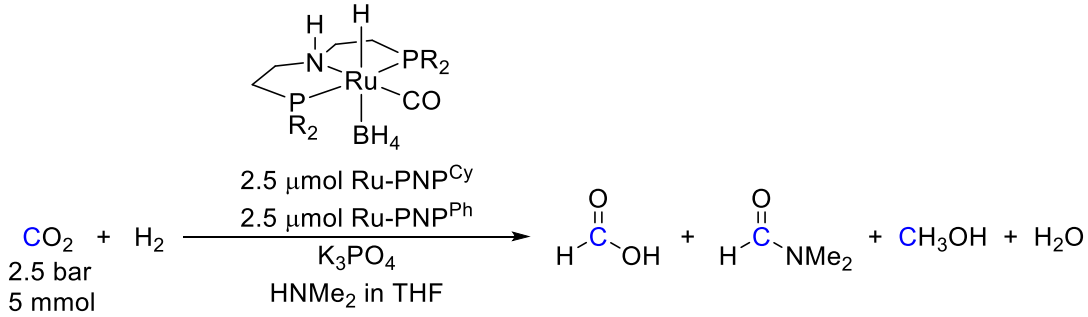

Entry	Temperature (°C)	Time (h)	TON Intermediates	TON Methanol	Conversion CO_2 (%)
1	100	24	1084	0	108
2	135	24	702	8	71
3	155	24	234	8	24
4	155	40	208	24	23

[a]**Conditions:** 2.5 μmol Ru-PNP^{Cy} and 2.5 μmol Ru-PNP^{Ph}, 250 μmol K_3PO_4, 3.8 mL of 2 M $HNMe_2$ in THF (commercial), 0.2 mL of THF, 2.5 bar CO_2, 50 bar H_2. Yields determined by ^{1}H NMR spectroscopy.

Although the reactions appearing in this section were all only performed a single time, these preliminary studies of Ru-PNP^{R}-catalyzed CO_2 hydrogenation at low dimethylamine concentrations provided a wealth of knowledge. Importantly, we found that both Ru-PNP^{Cy} and Ru-PNP^{iPr} were indeed active in the amide cascade system. Additionally, it was apparent that Ru-PNP^{Cy} and Ru-PNP^{iPr} were better at CO_2 hydrogenation as compared to DMF hydrogenation, while the opposite was true for Ru-PNP^{Ph}. Furthermore, cooperative cascade catalysis was attempted wherein two catalysts, one that gave high CO_2 conversions coupled with one that gave high turnovers of methanol, were used in the same pot. These preliminary reactions suggested that there was likely a synergistic effect when the catalysts were used cooperatively. As described in detail below, we later found that there were significant run-to-run variability in conversion/TON with related transformations at higher concentrations of dimethylamine. This made it challenging to definitively establish whether cooperative catalysis was operating under those conditions (since the error in the individual TON measurements was greater than the difference in TON between the additive and cooperative reactions). While we did not go back and repeat the 2M reactions to establish the errors in them, Table 3.9 below shows the error threshold for individual TON measurements in order for the differences in cooperative and additive catalysis in Figures 3.3, 3.4, and 3.5 to be statistically significant.

Table 3.9. Percent Error Needed for Cooperative and Additive Reactions to Give the Same TON of Methanol

	Ph + Cy + Base	Ph + Cy	Ph + iPr + Base	Ph + iPr
Same Ru Amount	31%	28%	13%	38%
Same Ru Concentration	29%	7%	31%	15%

3.2.2. Ruthenium-PNP Catalyzed Cascade Conversion of CO_2 to Methanol with Concentrated Dimethylamine (3.8 M in THF)

With these promising results in hand using 2 M dimethylamine solutions, we set out to study the conversion of CO_2 to methanol at the published concentration of dimethylamine (3.8

M). As described above, these conditions were anticipated to afford significantly higher TONs. We first focused on reproducing the literature results (96% conversion of CO_2 and >200 turnovers of methanol under the standard conditions), but our initial attempts resulted in low reactivity (11% conversion of CO_2 and 43-60 turnovers of methanol; Table 3.10). We initially hypothesized that the CO_2 source was the problem, as the tank was nearly empty and impurity concentrations in the gas tend to increase as the tank pressure decreases.[12]

Table 3.10. Reproducing Literature CO_2 Hydrogenation Results with Ru-PNP^{Ph}

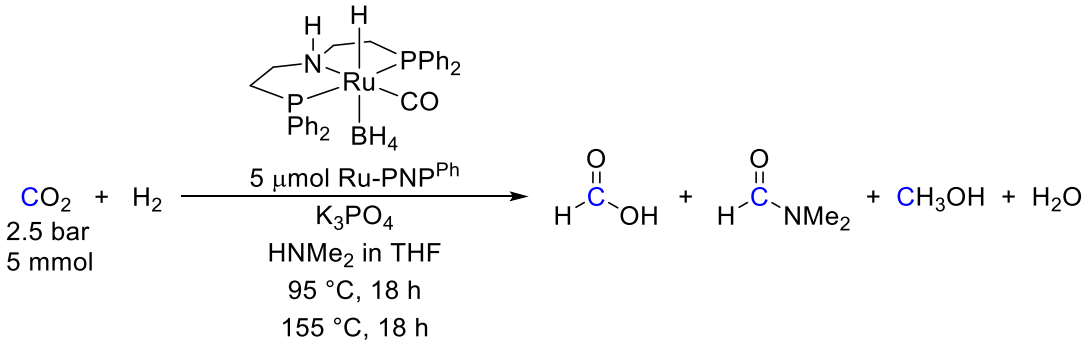

Entry	TON Intermediates	TON Methanol	Conversion CO_2 (%)
1[b]	740	220	96
2	45	43	9
3	81	60	14

[a]**Conditions:** 5 μmol Ru-PNP^{Ph}, 250 μmol K_3PO_4, 2 mL of 3.8 M $HNMe_2$ in THF, 2.5 bar CO_2, 50 bar H_2, 95 °C for 18 h followed by 155 °C for 18 h. Yields determined by ^{1}H NMR spectroscopy. [b]Values obtained from ref 1.

In order to determine if a CO_2 purity was causing the discrepancy between the published and current results, we next utilized dimethylammonium dimethylcarbamate (DMC) as the CO_2 source. This ionic liquid releases CO_2 at elevated temperatures and was also tested as a CO_2 source in the original cascade system. Comparing our results with the published DMC results, we saw good agreement in the CO_2 conversion and reasonable similarity in TON of intermediates and methanol (Table 3.11).

Table 3.11. Reproducing Literature Carbamate Hydrogenation Results with Ru-PNP^{Ph}

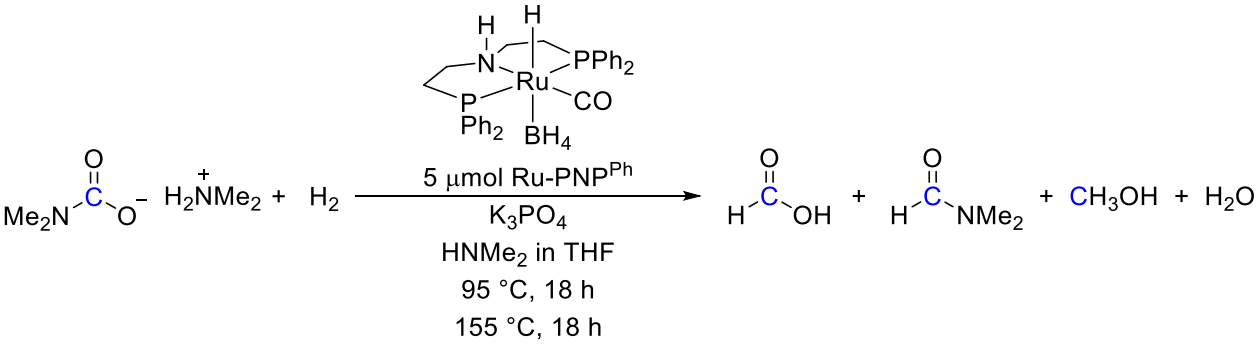

Entry	TON Intermediates	TON Methanol	Conversion CO_2 (%)
1[b]	306	270	58
2	328	214	57
3	420	146	54

[a]**Conditions:** 5 μmol Ru-PNP^{Ph}, 250 μmol K_3PO_4, 2.6 mL of 1.89 M DMC in THF, 2 mL of 3.8 M $HNMe_2$ in THF, 50 bar H_2, 95 °C for 18 h followed by 155 °C for 18 h. Yields determined by ^{1}H NMR spectroscopy. [b]Values obtained from ref 1.

Our preliminary studies with low concentration $HNMe_2$ indicated that a cooperative two-catalyst system comprising Ru-PNP^{Ph} and Ru-PNP^{iPr} outperformed the individual catalysts. Coupling these two catalysts together and running the reaction in triplicate, we discovered that the CO_2 conversions were once again very close between the three runs, but that the ratio between intermediates and methanol was substantially different (Table 3.12). Although each reaction gave nearly the same conversion of CO_2, Entry 3 gave over three times the amount of methanol compared to Entry 1 (Table 3.12).

Table 3.12. Variability in Conversion/TON in Carbamate Hydrogenation to Methanol via Cooperative Catalysis of Ru-PNP^{Ph} and Ru-PNP^{iPr}

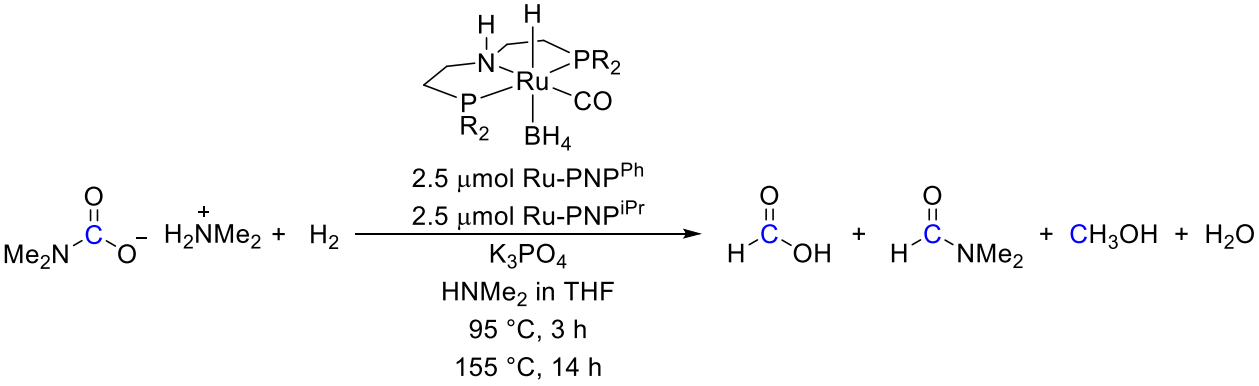

Entry	TON Intermediates	TON Methanol	Conversion CO_2 (%)
1	450	46	50
2	442	74	56
3	340	140	51

[a]**Conditions:** 2.5 µmol Ru-PNP^{Ph} and 2.5 µmol Ru-PNP^{iPr}, 250 µmol K_3PO_4, 2.6 mL of 1.89 M DMC in THF, 2 mL of 3.8 M $HNMe_2$ in THF, 2.5 bar CO_2, 50 bar H_2, 95 °C for 3 h followed by 155 °C for 14 h. Yields determined by ^{1}H NMR spectroscopy.

Since DMC did not resolve the high variability in conversion/TON, we next sought to simplify the system by removing K_3PO_4 and focusing on the first step of the reaction. This would allow us to identify whether the variability originated during the first step (i.e., CO_2 hydrogenation and generation of DMF). As shown in Table 3.13, the variability does appear to be in this first step. Within a single day (Entries 1 and 2), good agreement in the CO_2 conversion and product distribution was obtained; however, the CO_2 conversions and turnovers varied significantly on other days (for example: Table 3.13, Entries 3 & 4).

Table 3.13. Variability in Conversion/TON in CO_2 Hydrogenation via Cooperative Catalysis of Ru-PNP^{Ph} and Ru-PNP^{iPr}

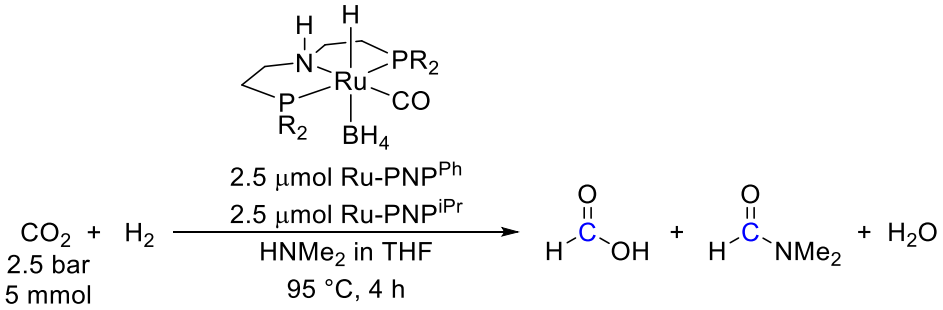

Entry	TON FA	TON DMF	Conversion CO_2 (%)
1	16	532	55
2	20	522	54
3	44	406	45
4	0	314	31

[a]**Conditions:** 2.5 µmol Ru-PNP^{Ph} and 2.5 µmol Ru-PNP^{iPr}, 2 mL of 3.8 M $HNMe_2$ in THF, 2.5 bar CO_2, 50 bar H_2, 95 °C for 4 h. Yields determined by ^{1}H NMR spectroscopy.

The system was further simplified to include just a single catalyst, and we increased the catalyst loading to 5.5 mg in order to decrease errors associated with weighing. We also

decreased the pressure of CO_2 in an effort to minimize variability in the pressurization process (since the CO_2 can react with dimethylamine during pressurization). However, once again, these changes did not resolve the high variability in conversion/TON (Table 3.14).

Table 3.14. Variability in Conversion/TON of CO_2 Hydrogenation with Ru-PNP^{Ph}

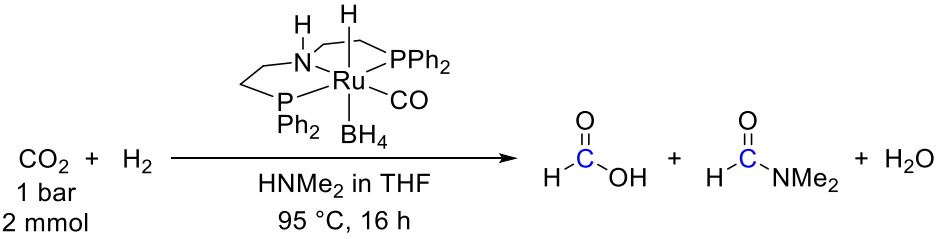

Entry	Ru-PNP Ph (μmol)	TON FA	TON DMF	Conversion CO_2 (%)
1	10	3	42	23
2	10	7	36	22
3	10	0	63	31
4	10	0	20	10
5	5	0	58	15
6	5	14	28	11
7	5	0	76	19
8	2.5	48	448	62
9	2.5	0	72	9

[a]**Conditions:** 2 mL of 3.8 M $HNMe_2$ in THF, 1 bar CO_2, 50 bar H_2, 95 °C for 16 h. Yields determined by ^{1}H NMR spectroscopy.

We next sought to compare the reactions with and without base. Even though early on we removed K_3PO_4 from the system for simplification, we now studied how variability in conversion/TON changed as a function of CO_2 source, catalyst, catalyst loading, CO_2 pressure, and phases of the reaction without finding any conclusive cause. As such, we decided it was imperative to thoroughly study reactions with K_3PO_4 as reported in the first cascade amide system, but using Research Grade H_2. This inspiration to change from Ultra High Purity (99.999%) to Research Grade (99.9999%) H_2 derived from our studies with Fe-PNP^{Cy} complexes, which were concurrently under investigation. With the Fe system, Research Grade (99.9999%) H_2 was required to obtain consistent results. To test this in the Ru system, we performed a series of eight reactions with Research Grade H_2 only to find similar variability in conversion/TONs as seen above (Table 3.15). Conversions ranged from 50% to nearly double

that at 92% (Table 3.15, Entries 1 and 8). Similarly, turnovers of DMF greatly varied between 360 and 688 (Table 3.15, Entries 1 and 7). A relative standard deviation of 23% for conversion of CO_2 was calculated for the results in Table 3.15.

Table 3.15. Variability in Conversion/TON of CO_2 Hydrogenation by Ru-PNP^{Ph} with K_3PO_4

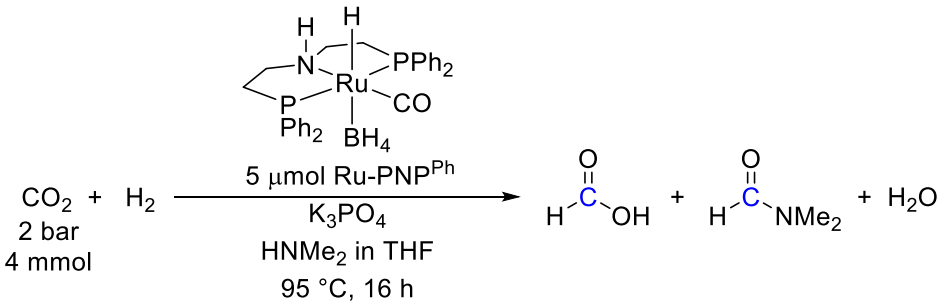

Entry	TON FA	TON DMF	Conversion CO_2 (%)
1	44	688	92
2	40	632	84
3	32	568	75
4	62	476	67
5	38	408	56
6	46	392	55
7	44	360	51
8	30	366	50

[a]**Conditions:** 5 μmol Ru-PNP^{Ph}, 250 μmol K_3PO_4, 2 mL of 3.8 M $HNMe_2$ in THF, 2 bar CO_2, 50 bar Research Grade H_2, 95 °C for 16 h. Yields determined by ^{1}H NMR spectroscopy. Results presented by CO_2 conversion and do not correspond to order in which the experiment was carried out.

We also studied reactions with Research Grade H_2 in the absence of base. As shown in Table 3.16, conversions ranged from 46% to 89% with turnovers of DMF spread between 676 and 324 (Table 3.16, Entries 1 and 13). The relative standard deviation for these conversions was 20%, nearly the same as the reactions with base (23%).

Table 3.16. Variability in Conversion/TON for CO_2 Hydrogenation by Ru-PNP^{Ph} without K_3PO_4

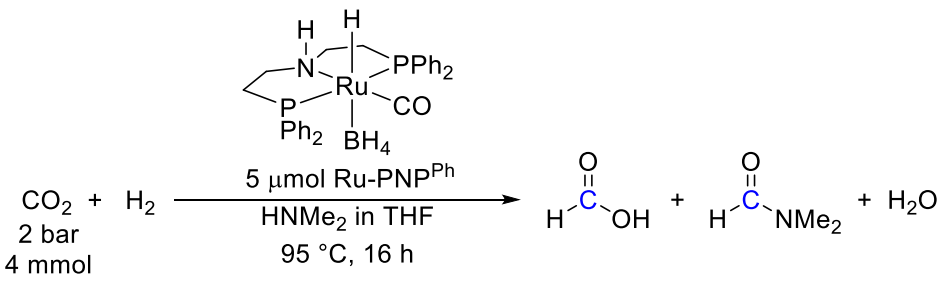

Entry	TON FA	TON DMF	Conversion CO_2 (%)
1	36	676	89
2	34	622	82
3	46	500	68
4	44	478	65
5	58	440	62
6	52	402	57
7	42	396	55
8	50	388	55
9	40	394	54
10	46	380	53
11	48	376	53
12	40	354	49
13	40	324	46

[a]**Conditions:** 5 µmol Ru-PNP^{Ph}, 250 µmol K_3PO_4, 2 mL of 3.8 M $HNMe_2$ in THF, 2 bar CO_2, 50 bar Research Grade H_2, 95 °C for 16 h. Yields determined by ^1H NMR spectroscopy. Results presented by CO_2 conversion and do not correspond to order in which the experiment was carried out.

As a final attempt to generate a better amide cascade system, we redirected our attention to our cooperative catalytic systems. We hypothesized we could show that a two-catalyst component system had a beneficial synergistic effect as long as the standard deviation of the cooperative system results were not within range of the standard deviation of the additive single catalyst results. Each catalyst individually, as well as the cooperative two-catalyst system were run six times (Figure 3.6). When considering the error associated with this system, the cooperative system produces less than 0.05 mmol more DMF compared to the additive system even though their averages are significantly different (Figure 3.6). However, in terms of methanol production, the additive and cooperative system are within error of one another (Figure 3.7).

Figure 3.6. DMF Produced via Cooperative CO_2 Hydrogenation at High $HNMe_2$ Loadings

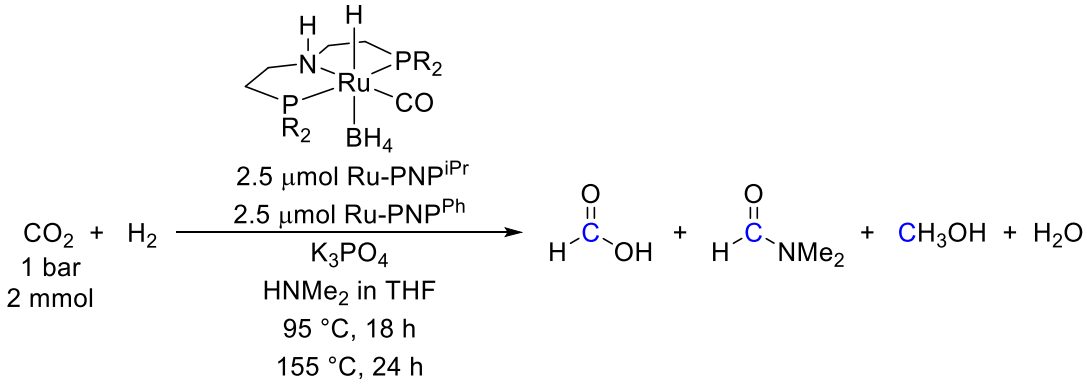

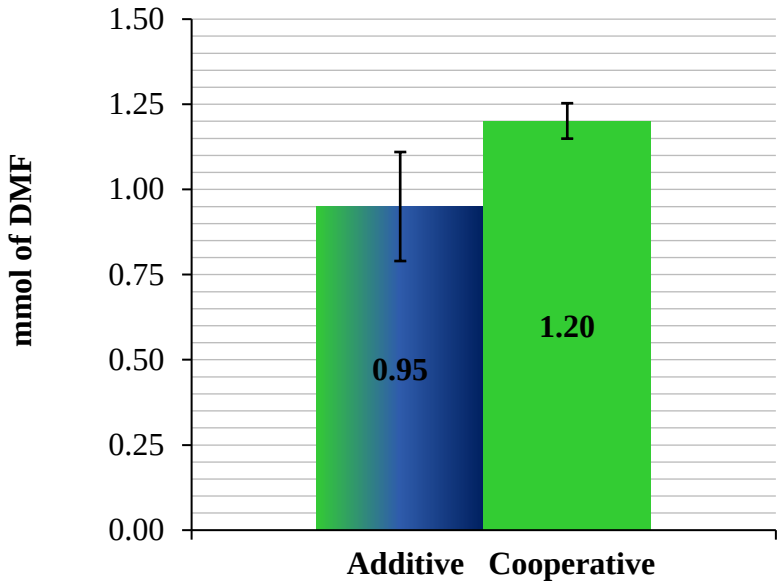

[a]**Conditions:** 2.5 µmol Ru-PNP^{iPr} and 2.5 µmol Ru-PNP^{Ph}, 250 µmol K_3PO_4, 2 mL of 3.8 M $HNMe_2$ in THF, 1 bar CO_2, 50 bar H_2, 95 °C for 18 h followed by 155 °C for 24 h. Yields determined by ^{1}H NMR spectroscopy. All reactions carried out 6 times.

Figure 3.7. Methanol Produced via Cooperative CO_2 Hydrogenation at High $HNMe_2$ Loadings

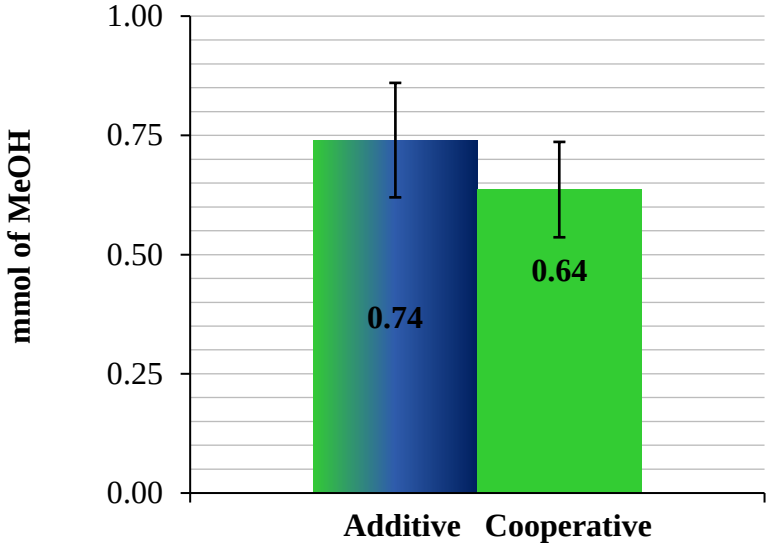

[a]**Conditions:** 2.5 µmol Ru-PNP^{iPr} and 2.5 µmol Ru-PNP^{Ph}, 250 µmol K_3PO_4, 2 mL of 3.8 M $HNMe_2$ in THF, 1 bar CO_2, 50 bar H_2, 95 °C for 18 h followed by 155 °C for 24 h. Yields determined by ^{1}H NMR spectroscopy. All reactions carried out 6 times.

Overall, high variability in conversion/TON at high dimethylamine concentrations resulted in an inability to definitively generate an improved amide cascade system. Many parameters were probed to identify the source of these issues, but all such explorations were

inconclusive. The studies mentioned above focused on probing the purity of H_2, CO_2 source, CO_2 pressure, catalyst, catalyst loading, K_3PO_4, and reaction step. Other potential factors were also probed, including $HNMe_2$ source, $HNMe_2$ concentration, $HNMe_2$ purity, $HNMe_2$ storage, K_3PO_4 source, THF purity, THF source, CO_2 purity, catalyst batch, extensive exploration with Ru-PNP^{Cy}, reaction time, reaction temperature, reaction pressure, reaction heating, pressurization technique, reaction preparation time, reaction preparation temperature, glovebox atmosphere, reactor cleaning, reactor drying, reactor cooling, and reaction stirring. Unfortunately, even after sequentially changing each of the mentioned reaction conditions, high variability in conversion/TONs was observed.

3.3. Conclusions

Although an improved amide cascade system could not be definitively realized, there were several important findings from the studies in this Chapter. The originally published catalyst, Ru-PNP^{Ph} was the most efficient catalyst for methanol generation. The catalysts identified in Chapter 2, Ru-PNP^{iPr} and Ru-PNP^{Cy} were also active in the amide cascade system. Ru-PNP^{Cy} afforded the highest CO_2 conversions as well as highest turnovers of intermediates. Under some conditions, Ru-PNP^{iPr} outperformed the other two catalysts with respect to balancing CO_2 conversions and turnovers of methanol. The impact of base was thoroughly studied and showed that Ru-PNP^{Cy} performs best with base, while Ru-PNP^{Ph} is largely unaffected by base, and Ru-PNP^{iPr} is inhibited by base. Like the originally reported amide cascade system, catalyst loading was extremely important, but the optimal loading was catalyst dependent. Ultimately, a tandem two-catalyst system where either Ru-PNP^{Cy} or Ru-PNP^{iPr} is coupled with Ru-PNP^{Ph} may be capable of producing a superior cascade amide system wherein high conversions of CO_2 are coupled with high turnovers of methanol due to their

cooperativity, resulting in a synergistic effect. However, the high variability in conversion/TON with these systems made definitive realization of this challenging.

3.4. Outlook on the Amide Cascade System

Although we were unable to definitely generate an improved cascade amide system, we believe that there is still much promise in this approach. After the Sanford lab's initial report of Ru-PNP^{Ph} catalyzed CO_2 hydrogenation to methanol under basic conditions, other groups have followed up with variations.[13,14,15,16,17] Many of these systems utilize the same Ru-PNP^{Ph} catalyst or a variation thereof, but instead of using $HNMe_2$, they employ different amines, in particular polyamine derivatives.[13,14] A notable example is that recently reported by Prakash and co-workers (Scheme 3.3).[18] In this follow-up paper, they utilized Ru-PNP^{Ph} to convert CO_2 to methanol using the polyamine PEHA in place of dimethylamine. After PEHA captures the CO_2, the CO_2 loaded PEHA solution is exposed to the catalyst under an H_2 atmosphere in 2-methyl-THF and the original water solution. Under optimized conditions, 95% yield of methanol was obtained. Under slightly different conditions, 411 turnovers of methanol could be achieved. The biphasic solvent system allowed for separation and recycling of the catalyst and the amine. By recycling only the catalyst, 810 turnovers total of methanol were formed, while when recycling both catalyst and amine, 582 turnovers of methanol were formed.

Scheme 3.3. Prakash's Biphasic Ru-PNP^{Ph} CO_2 Capture by PEHA and Hydrogenation

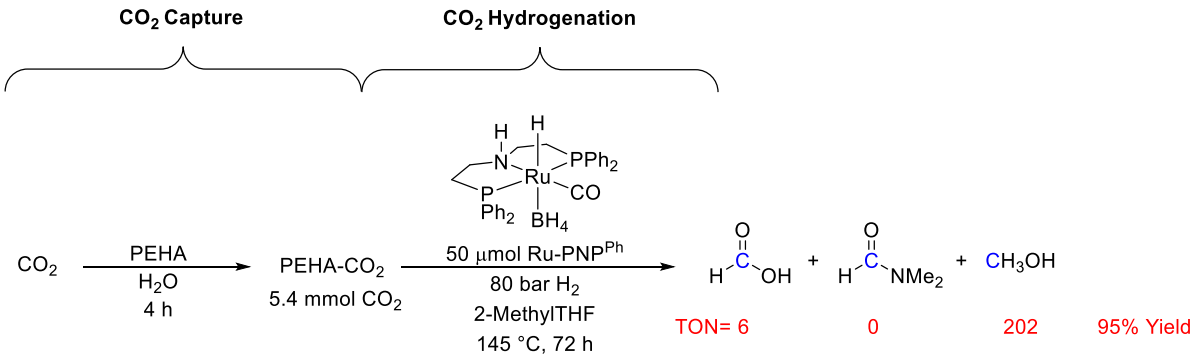

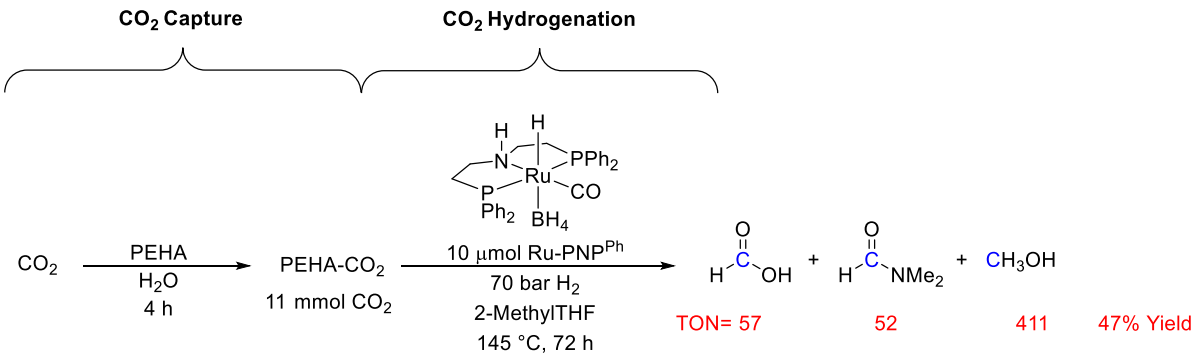

Overall, although the system with $HNMe_2$ afforded significant variability in conversion/TONs, the utilization of a different, non-gaseous amine could potentially resolve these issues and be amenable to cooperative catalysis. We propose that by utilizing both Ru-PNP^{Cy}, which was not investigated in the Prakash paper, in tandem with Ru-PNP^{Ph}, both high yields of methanol and high turnovers of methanol could be achieved through cooperative catalysis. Furthermore, the catalysts could then be recycled to continue to generate methanol in high yields and turnovers of methanol. Ultimately, the utilization of Ru-PNP^{Cy} and Ru-PNP^{Ph} with PEHA under Prakash's reaction conditions may generate the best amide cascade system yet.

3.5. Experimental Procedures

3.5.1. General Procedures and Materials and Methods

General Procedures

All manipulations were carried out under a nitrogen atmosphere using standard Schlenk line or glove box techniques unless otherwise noted. All high-pressure reactions were carried out using a Parr Model 5000 Multiple Reactor system that includes six 45 mL vessels equipped with flat-gaskets and head mounting valves. The system was operated by a 4871process controller and SpecView version 2.5 software. All pressures are reported from the SpecView interface at room temperature. NMR spectra were obtained on Varian VNMRs: 400 MHz (400

MHz for ^{1}H; 100 MHz for ^{13}C) or 700 MHz (700 MHz for ^{1}H; 176 MHz for ^{13}C). Chemical shifts are reported in parts per million (ppm) and are referenced to an internal standard. Unless otherwise noted, the NMR yields were based on methanol (δ= 3.16 ppm, T_1 = 7.2 s) and were quantified using 1,3,5-trimethoxybenzene (δ= 6.02 ppm, T_1 = 2.8 s) as an internal standard in dimethylsulfoxide-d_6 (DMSO-d_6). For each NMR experiment, 4 scans were collected, a 35 second relaxation delay was used, and a pulse angle of 90° was applied.

Reactor Descriptions

A single Parr reactor type was employed. All are 45 mL and are composed of a well (in which the solid and liquid reagents are charged) and a head, which contains various attachments as described below. Each is made of Hastelloy C, and the wells are 7.5 cm tall and 3 cm in diameter. The heads consist of a pressure transducer and two inlet/outlet valves that can connect to a Parr Model 5000 Multiple Reactor system described above, a safety release valve, and a well for a thermocouple (Figure 3.8).

Figure 3.8. Picture of reactor type A with the parts of the reactor labeled.

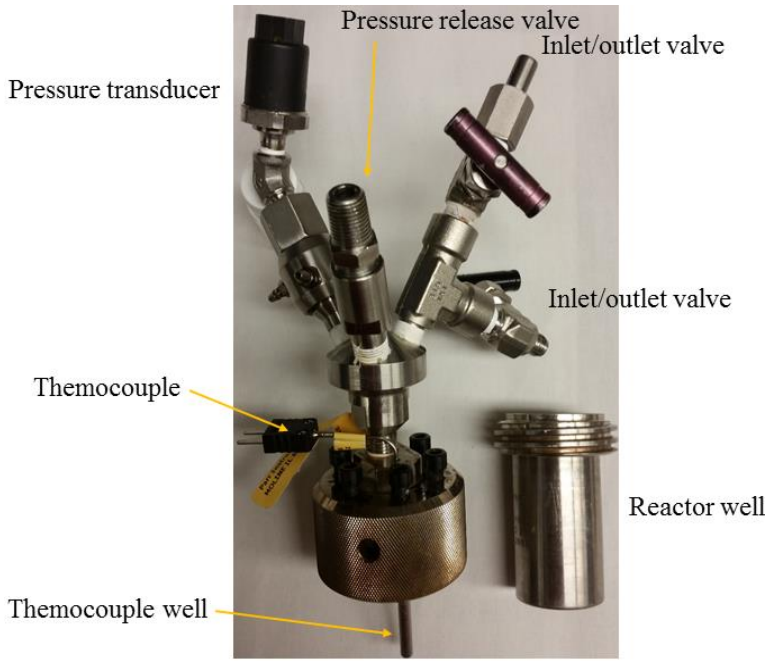

Materials and Methods

The ligands bis(2-(dicyclohexylphosphino)ethyl)amine (PNP^{Cy}) and bis(2-(diisopropylphospino)ethyl)amine (PNP^{iPr}) were purchased from commercial sources (98%, Alfa Aesar). Complexes Ru-PNP^{Cy} and Ru-PNP^{iPr} were prepared according to a literature procedure.[19,20,21] The catalyst, Ru-PNP^{Ph} was purchased from Strem Chemicals (98%). Anhydrous K_3PO_4 (Aldrich, 98%) was ground with a mortar and pestle before use. Dimethylamine in THF 2 M was purchased from Sigma Aldrich. Dimethylamine (99%) was purchased from Sigma Aldrich and used to prepare a 3.8 M in THF solution according to literature procedure.[1] Ultra-high purity hydrogen (99.999%), research grade hydrogen (99.9999%), and carbon dioxide (99.9%) were purchased from Metro Welding. All catalytic experiments were set up under an oxygen-free atmosphere in a glovebox. Catalytic experiments in section 3.2.1 wherein commercial dimethylamine was used for exploratory investigation and preliminary findings were spot-checked where each new catalyst was initially ran in triplicate in a single day to ensure reproducibility of <10% relative standard deviation. Tetrahydrofuran (THF) was purified using an Innovative Technologies (IT) solvent purification system consisting of a copper catalyst, activated alumina, and molecular sieves. Dimethylsulfoxide-d_6 (DMSO-d_6, Cambridge Isotope Laboratories) was purchased from the respective supplier and used as received.

3.5.2. Hydrogenation Reactions with Commercial 2 M Dimethylamine

Procedure for Comparing Commercial Dimethylamine to Published Results in the Hydrogenation of CO_2 to Methanol (Table 3.1 & 3.2)

In a N_2-atmosphere dry box, a Parr reactor bottom (containing an octagon magnetic stirbar), glass pipettes, a 1 mL syringe, a 5 mL syringe, and a 20 gauge needle were placed into the –37 °C freezer for 45 minutes. K_3PO_4 (250 μmol) was weighed and transferred to the reactor bottom that was placed back into the freezer. Next, Ru-PNP^{Ph} (5 μmol) was weighed

into a 4 mL vial and transferred to the reactor bottom. The reactor bottom and 4 mL vial were placed into the –37 °C freezer. THF (either 0.2 or 0.1 mL) that had been stored in the freezer was added to the 4 mL vial via a 1 mL syringe. Dimethylamine (either 3.8 mL or 1.9 mL of 2.0 M in THF and stored in the freezer in a sure seal) was then added to the 4 mL vial via a 5 mL syringe and needle before being transferred to the reactor bottom with a glass pipette. The reactor was immediately sealed and removed from the glovebox. The vessel was connected to the Parr Multiple Reactor System, and the manifold was thoroughly purged (1 minute and then vented 15 times) with bone dry grade CO_2 (99.9%). The vessel was then pressurized to 2.5 bar with CO_2. The manifold was then thoroughly purged (1 minute and then vented 15 times) with ultra-high purity H_2 (99.999%). The vessel was then pressurized with 50 bar with ultra-high purity grade H_2 at room temperature to reach a total pressure of 52.5 bar. The reaction was heated at 95 °C with a stir rate of 800 RPM. The heating was conducted using Specview software. After 18 hours of heating, the temperature was increased to 155 °C for 22 hours before the reaction mixture was allowed to cool to room temperature. The pressure vessel was placed in a –84 °C bath (ethyl acetate/LN_2) for 15 min and then carefully vented using a metering valve. THF (0.5 mL) was added through the venting valve of the pressure vessel to wash any residual liquids/solids into the vessel. The vessel was then opened, 1,3,5-trimethoxybenzene (0.178 mmol, 300 µL of 0.593 M solution in DMSO-d_6) was added as a ^{1}H NMR standard, and the contents of the vessel were diluted with DMSO-d_6. Approximately 50 µL of the resulting solution was added to an NMR tube, diluted further with DMSO-d_6, and neutralized with HCl. The sample was then analyzed by ^{1}H NMR spectroscopy.

Procedure for the Hydrogenation of CO_2 to Methanol with Ru-PNP^R (Table 3.3)

In a N_2-atmosphere dry box, a Parr reactor bottom (containing an octagon magnetic stirbar), glass pipettes, a 1 mL syringe, a 5 mL syringe, and a 20 gauge needle were placed into

the –37 °C freezer for 45 minutes. K_3PO_4 (250 µmol) was weighed and transferred to the reactor bottom that was placed back into the freezer. Next, [Ru] (5 µmol) was weighed into a 4 mL vial and transferred to the reactor bottom. The reactor bottom and 4 mL vial were placed into the –37 °C freezer. THF (0.2 mL) that had been stored in the freezer was added to the 4 mL vial via a 1 mL syringe. Dimethylamine (3.8 mL of 2.0 M in THF stored in the freezer in a sure seal) was then added to the 4 mL vial via a 5 mL syringe and needle before being transferred to the reactor bottom with a glass pipette. The reactor was immediately sealed and removed from the glovebox. The vessel was connected to the Parr Multiple Reactor System, and the manifold was thoroughly purged (1 minute and then vented 15 times) with bone dry grade CO_2 (99.9%). The vessel was then pressurized to 2.5 bar with CO_2. The manifold was then thoroughly purged (1 minute and then vented 15 times) with ultra-high purity H_2 (99.999%). The vessel was then pressurized with 50 bar ultra-high purity grade H_2 at room temperature to reach a total pressure of 52.5 bar. The reaction was heated at 95 °C with a stir rate of 800 RPM. The heating was conducted using Specview software. After 18 hours of heating, the temperature was increased to 155 °C for 22 hours before the reaction mixture was allowed to cool to room temperature. The pressure vessel was placed in a –84 °C bath (ethyl acetate/LN_2) for 15 min and then carefully vented using a metering valve. THF (0.5 mL) was added through the venting valve of the pressure vessel to wash any residual liquids/solids into the vessel. The vessel was then opened, 1,3,5-trimethoxybenzene (0.178 mmol, 300 µL of 0.593 M solution in DMSO-d_6) was added as a ^{1}H NMR standard, and the contents of the vessel were diluted with DMSO-d_6. Approximately 50 µL of the resulting solution was added to an NMR tube, diluted further with DMSO-d_6, and neutralized with HCl. The sample was then analyzed by ^{1}H NMR spectroscopy.

Procedure for the Hydrogenation of CO_2 to Methanol at Varied Ru Loadings (Table 3.4)

In a N_2-atmosphere dry box, a Parr reactor bottom (containing an octagon magnetic stirbar), glass pipettes, a 1 mL syringe, a 5 mL syringe, and a 20 gauge needle were placed into the –37 °C freezer for 45 minutes. K_3PO_4 (250 μmol) was weighed and transferred to the reactor bottom that was placed back into the freezer. Next, Ru-PNP^R (2.5–10 μmol) was weighed into a 4 mL vial and transferred to the reactor bottom. The reactor bottom and 4 mL vial were placed into the –37 °C freezer. THF (0.2 mL) that had been stored in the freezer was added to the 4 mL vial via a 1 mL syringe. Dimethylamine (3.8 mL of 2.0 M in THF and stored in the freezer in a sure seal) was then added to the 4 mL vial via a 5 mL syringe and needle before being transferred to the reactor bottom with a glass pipette. The reactor was immediately sealed and removed from the glovebox. The vessel was connected to the Parr Multiple Reactor System, and the manifold was thoroughly purged (1 minute and then vented 15 times) with bone dry grade CO_2 (99.9%). The vessel was then pressurized to 2.5 bar with CO_2. The manifold was then thoroughly purged (1 minute and then vented 15 times) with ultra-high purity H_2 (99.999%). The vessel was then pressurized with 50 bar with ultra-high purity grade H_2 at room temperature to reach a total pressure of 52.5 bar. The reaction was heated at 95 °C with a stir rate of 800 RPM. The heating was conducted using Specview software. After 18 hours of heating, the temperature was increased to 155 °C for 22 hours before the reaction mixture was allowed to cool to room temperature. The pressure vessel was placed in a –84 °C bath (ethyl acetate/LN_2) for 15 min and then carefully vented using a metering valve. THF (0.5 mL) was added through the venting valve of the pressure vessel to wash any residual liquids/solids into the vessel. The vessel was then opened, 1,3,5-trimethoxybenzene (0.178 mmol, 300 μL of 0.593 M solution in DMSO-d_6) was added as a ^{1}H NMR standard, and the contents of the vessel were diluted with DMSO-d_6. Approximately 50 μL of the resulting

solution was added to an NMR tube, diluted further with DMSO-d_6, and neutralized with HCl. The sample was then analyzed by ^{1}H NMR spectroscopy.

Procedure for the Hydrogenation of CO_2 to Methanol Studying the Influence of K_3PO_4 (Tables 3.5, 3.6, and 3.7)

In a N_2-atmosphere dry box, a Parr reactor bottom (containing an octagon magnetic stirbar), glass pipettes, a 1 mL syringe, a 5 mL syringe, and a 20 gauge needle were placed into the –37 °C freezer for 45 minutes. If appropriate, K_3PO_4 (250 μmol) was weighed and transferred to the reactor bottom that was placed back into the freezer. Next, Ru-PNP^R (2.5–10 μmol) was weighed into a 4 mL vial and transferred to the reactor bottom. The reactor bottom and 4 mL vial were placed into the –37 °C freezer. THF (0.2 mL) that had been stored in the freezer was added to the 4 mL vial via a 1 mL syringe. Dimethylamine (3.8 mL of 2.0 M in THF and stored in the freezer in a sure seal) was then added to the 4 mL vial via a 5 mL syringe and needle before being transferred to the reactor bottom with a glass pipette. The reactor was immediately sealed and removed from the glovebox. The vessel was connected to the Parr Multiple Reactor System, and the manifold was thoroughly purged (1 minute and then vented 15 times) with bone dry grade CO_2 (99.9%). The vessel was then pressurized to 2.5 bar with CO_2. The manifold was then thoroughly purged (1 minute and then vented 15 times) with ultra-high purity H_2 (99.999%). The vessel was then pressurized with 50 bar with ultra-high purity grade H_2 at room temperature to reach a total pressure of 52.5 bar. The reaction was heated at 95 °C with a stir rate of 800 RPM. The heating was conducted using Specview software. After 18 hours of heating, the temperature was increased to 155 °C for 22 hours before the reaction mixture was allowed to cool to room temperature. The pressure vessel was placed in a –84 °C bath (ethyl acetate/LN_2) for 15 min and then carefully vented using a metering valve. THF (0.5 mL) was added through the venting valve of the pressure vessel to wash any residual

liquids/solids into the vessel. The vessel was then opened, 1,3,5-trimethoxybenzene (0.178 mmol, 300 µL of 0.593 M solution in DMSO-d_6) was added as a ^{1}H NMR standard, and the contents of the vessel were diluted with DMSO-d_6. Approximately 50 µL of the resulting solution was added to an NMR tube, diluted further with DMSO-d_6, and neutralized with HCl. The sample was then analyzed by ^{1}H NMR spectroscopy.

Procedure for the Hydrogenation of CO_2 to Methanol: Cooperative Reactions (Figures 3.3, 3.4, and 3.5)

In a N_2-atmosphere dry box, a Parr reactor bottom (containing an octagon magnetic stirbar), glass pipettes, a 1 mL syringe, a 5 mL syringe, and a 20 gauge needle were placed into the –37 °C freezer for 45 minutes. If appropriate, K_3PO_4 (250 µmol) was weighed and transferred to the reactor bottom that was placed back into the freezer. Next, Ru-PNP^R (2.5 µmol) was weighed into a 4 mL vial and transferred to the reactor bottom. Then, Ru-PNP$^{R'}$ (2.5 µmol) was weighed into a separate 4 mL vial and transferred to the reactor bottom. The reactor bottom and 4 mL vials were placed into the –37 °C freezer. THF (0.2 mL) that had been stored in the freezer was added to one of the 4 mL vials via a 1 mL syringe. Dimethylamine (3.8 mL of 2.0 M in THF and stored in the freezer in a sure seal) was then added to the other 4 mL vial via a 5 mL syringe and needle before being transferred to the 4 mL vial with THF whose solution was then immediately transferred to the reactor bottom with a glass pipette. The reactor was quickly sealed and removed from the glovebox. The vessel was connected to the Parr Multiple Reactor System, and the manifold was thoroughly purged (1 minute and then vented 15 times) with bone dry grade CO_2 (99.9%). The vessel was then pressurized to 2.5 bar with CO_2. The manifold was then thoroughly purged (1 minute and then vented 15 times) with ultra-high purity H_2 (99.999%). The vessel was then pressurized with 50 bar with ultra-high purity grade H_2 at room temperature to reach a total pressure of 52.5 bar. The reaction was

heated at 95 °C with a stir rate of 800 RPM. The heating was conducted using Specview software. After 18 hours of heating, the temperature was increased to 155 °C for 22 hours before the reaction mixture was allowed to cool to room temperature. The pressure vessel was placed in a –84 °C bath (ethyl acetate/LN_2) for 15 min and then carefully vented using a metering valve. THF (0.5 mL) was added through the venting valve of the pressure vessel to wash any residual liquids/solids into the vessel. The vessel was then opened, 1,3,5-trimethoxybenzene (0.178 mmol, 300 µL of 0.593 M solution in DMSO-d_6) was added as a ^{1}H NMR standard, and the contents of the vessel were diluted with DMSO-d_6. Approximately 50 µL of the resulting solution was added to an NMR tube, diluted further with DMSO-d_6, and neutralized with HCl. The sample was then analyzed by ^{1}H NMR spectroscopy.

Procedure for the Hydrogenation of CO_2 to Methanol: Additive Reactions at the Same Ruthenium Loading (Figure 3.3)

In a N_2-atmosphere dry box, a Parr reactor bottom (containing an octagon magnetic stirbar), glass pipettes, a 1 mL syringe, a 5 mL syringe, and a 20 gauge needle were placed into the –37 °C freezer for 45 minutes. If appropriate, K_3PO_4 (250 µmol) was weighed and transferred to the reactor bottom that was placed back into the freezer. Next, Ru-PNP^R (2.5 µmol) was weighed into a 4 mL vial and transferred to the reactor bottom. The reactor bottom and 4 mL vial were placed into the –37 °C freezer. THF (0.2 mL) that had been stored in the freezer was added to the 4 mL vial via a 1 mL syringe. Dimethylamine (3.8 mL of 2.0 M in THF and stored in the freezer in a sure seal) was then added to the 4 mL vial via a 5 mL syringe and needle before being transferred to the reactor bottom with a glass pipette. The reactor was immediately sealed and removed from the glovebox. The vessel was connected to the Parr Multiple Reactor System, and the manifold was thoroughly purged (1 minute and then vented 15 times) with bone dry grade CO_2 (99.9%). The vessel was then pressurized to 2.5 bar with

CO_2. The manifold was then thoroughly purged (1 minute and then vented 15 times) with ultra-high purity H_2 (99.999%). The vessel was then pressurized with 50 bar with ultra-high purity grade H_2 at room temperature to reach a total pressure of 52.5 bar. The reaction was heated at 95 °C with a stir rate of 800 RPM. The heating was conducted using Specview software. After 18 hours of heating, the temperature was increased to 155 °C for 22 hours before the reaction mixture was allowed to cool to room temperature. The pressure vessel was placed in a –84 °C bath (ethyl acetate/LN_2) for 15 min and then carefully vented using a metering valve. THF (0.5 mL) was added through the venting valve of the pressure vessel to wash any residual liquids/solids into the vessel. The vessel was then opened, 1,3,5-trimethoxybenzene (0.178 mmol, 300 µL of 0.593 M solution in DMSO-d_6) was added as a ^{1}H NMR standard, and the contents of the vessel were diluted with DMSO-d_6. Approximately 50 µL of the resulting solution was added to an NMR tube, diluted further with DMSO-d_6, and neutralized with HCl. The sample was then analyzed by ^{1}H NMR spectroscopy. All additive reactions were ran concurrently such that both Ru-PNP^R and Ru-PNP$^{R'}$ were both set up on the same day.

Procedure for the Hydrogenation of CO_2 to Methanol: Additive Reactions at the Same Ruthenium Concentration (Figures 3.4 and 3.5)

In a N_2-atmosphere dry box, a Parr reactor bottom (containing an octagon magnetic stirbar), glass pipettes, a 1 mL syringe, a 5 mL syringe, and a 20 gauge needle were placed into the –37 °C freezer for 45 minutes. If appropriate, K_3PO_4 (250 µmol) was weighed and transferred to the reactor bottom that was placed back into the freezer. Next, Ru-PNP^R (5 µmol) was weighed into a 4 mL vial and transferred to the reactor bottom. The reactor bottom and 4 mL vial were placed into the –37 °C freezer. THF (0.2 mL) that had been stored in the freezer was added to the 4 mL vial via a 1 mL syringe. Dimethylamine (3.8 mL of 2.0 M in THF and stored in the freezer in a sure seal) was then added to the 4 mL vial via a 5 mL syringe and

needle before being transferred to the reactor bottom with a glass pipette. The reactor was immediately sealed and removed from the glovebox. The vessel was connected to the Parr Multiple Reactor System, and the manifold was thoroughly purged (1 minute and then vented 15 times) with bone dry grade CO_2 (99.9%). The vessel was then pressurized to 2.5 bar with CO_2. The manifold was then thoroughly purged (1 minute and then vented 15 times) with ultra-high purity H_2 (99.999%). The vessel was then pressurized with 50 bar with ultra-high purity grade H_2 at room temperature to reach a total pressure of 52.5 bar. The reaction was heated at 95 °C with a stir rate of 800 RPM. The heating was conducted using Specview software. After 18 hours of heating, the temperature was increased to 155 °C for 22 hours before the reaction mixture was allowed to cool to room temperature. The pressure vessel was placed in a –84 °C bath (ethyl acetate/LN_2) for 15 min and then carefully vented using a metering valve. THF (0.5 mL) was added through the venting valve of the pressure vessel to wash any residual liquids/solids into the vessel. The vessel was then opened, 1,3,5-trimethoxybenzene (0.178 mmol, 300 µL of 0.593 M solution in DMSO-d_6) was added as a ^{1}H NMR standard, and the contents of the vessel were diluted with DMSO-d_6. Approximately 50 µL of the resulting solution was added to an NMR tube, diluted further with DMSO-d_6, and neutralized with HCl. The sample was then analyzed by ^{1}H NMR spectroscopy. All additive reactions were ran concurrently such that both Ru-PNP^R and Ru-PNP$^{R'}$ were both set up on the same day.

Isothermal Cooperative for the Conversion of CO_2 to Methanol (Table 3.8)

In a N_2-atmosphere dry box, a Parr reactor bottom (containing an octagon magnetic stirbar), glass pipettes, a 1 mL syringe, a 5 mL syringe, and a 20 gauge needle were placed into the –37 °C freezer for 45 minutes. K_3PO_4 (250 µmol) was weighed and transferred to the reactor bottom that was placed back into the freezer. Next, Ru-PNP^{Cy} (2.5 µmol) was weighed into a 4 mL vial and transferred to the reactor bottom. Then, Ru-PNP^{Ph} (2.5 µmol) was weighed

into a separate 4 mL vial and transferred to the reactor bottom. The reactor bottom and 4 mL vials were placed into the –37 °C freezer. THF (0.2 mL) that had been stored in the freezer was added to one of the 4 mL vials via a 1 mL syringe. Dimethylamine (3.8 mL of 2.0 M in THF and stored in the freezer in a sure seal) was then added to the other 4 mL vial via a 5 mL syringe and needle before being transferred to the 4 mL vial with THF whose solution was then immediately transferred to the reactor bottom with a glass pipette. The reactor was quickly sealed and removed from the glovebox. The vessel was connected to the Parr Multiple Reactor System, and the manifold was thoroughly purged (1 minute and then vented 15 times) with bone dry grade CO_2 (99.9%). The vessel was then pressurized to 2.5 bar with CO_2. The manifold was then thoroughly purged (1 minute and then vented 15 times) with ultra-high purity H_2 (99.999%). The vessel was then pressurized with 50 bar with ultra-high purity grade H_2 at room temperature to reach a total pressure of 52.5 bar. The reaction was heated to the desired temperature with a stir rate of 800 RPM. After the allocated amount of time, the reaction mixture was allowed to cool to room temperature. The pressure vessel was placed in a –84 °C bath (ethyl acetate/LN_2) for 15 min and then carefully vented using a metering valve. THF (0.5 mL) was added through the venting valve of the pressure vessel to wash any residual liquids/solids into the vessel. The vessel was then opened, 1,3,5-trimethoxybenzene (0.178 mmol, 300 µL of 0.593 M solution in DMSO-d_6) was added as a ^{1}H NMR standard, and the contents of the vessel were diluted with DMSO-d_6. Approximately 50 µL of the resulting solution was added to an NMR tube, diluted further with DMSO-d_6, and neutralized with HCl. The sample was then analyzed by ^{1}H NMR spectroscopy.

3.5.3. Hydrogenation Reactions with 3.8 M $HNMe_2$

Procedure CO_2 Hydrogenation for Comparison to Literature Values (Table 3.10)

In a N_2-atmosphere dry box, a Parr reactor bottom (containing an octagon magnetic stirbar), glass pipettes, a 1 mL syringe, a 5 mL syringe, and a 20 gauge needle were placed into the –37 °C freezer for 45 minutes. K_3PO_4 (250 µmol) was weighed and transferred to the reactor bottom that was placed back into the freezer. Next, Ru-PNP^{Ph} (5 µmol) was weighed into a 4 mL vial and transferred to the reactor bottom. The reactor bottom and 4 mL vial were placed into the –37 °C freezer. Dimethylamine (2 mL of 3.8 M in THF) was then added to the 4 mL vial via a 5 mL syringe and needle before being transferred to the reactor bottom with a glass pipette. The reactor was immediately sealed and removed from the glovebox. The vessel was connected to the Parr Multiple Reactor System, and the manifold was thoroughly purged (1 minute and then vented 15 times) with bone dry grade CO_2 (99.9%). The vessel was then pressurized to 2.5 bar with CO_2. The manifold was then thoroughly purged (1 minute and then vented 15 times) with ultra-high purity H_2 (99.999%). The vessel was then pressurized with 50 bar with ultra-high purity grade H_2 at room temperature to reach a total pressure of 52.5 bar. The reaction was heated at 95 °C with a stir rate of 800 RPM. The heating was conducted using Specview software. After 18 hours of heating, the temperature was increased to 155 °C for 18 hours before the reaction mixture was allowed to cool to room temperature. The pressure vessel was placed in a –84 °C bath (ethyl acetate/LN_2) for 15 min and then carefully vented using a metering valve. THF (0.5 mL) was added through the venting valve of the pressure vessel to wash any residual liquids/solids into the vessel. The vessel was then opened, 1,3,5-trimethoxybenzene (0.178 mmol, 300 µL of 0.593 M solution in DMSO-d_6) was added as a ^{1}H NMR standard, and the contents of the vessel were diluted with DMSO-d_6. Approximately 50 µL of the resulting solution was added to an NMR tube, diluted further with DMSO-d_6, and neutralized with HCl. The sample was then analyzed by ^{1}H NMR spectroscopy.

Procedure for DMC Hydrogenation with Ru-PNP^{R} (Table 3.11)

In a N_2-atmosphere dry box, a Parr reactor bottom (containing an octagon magnetic stirbar), glass pipettes, a 1 mL syringe, a 5 mL syringe, and a 20 gauge needle were placed into the –37 °C freezer for 45 minutes. K_3PO_4 (250 µmol) was weighed and transferred to the reactor bottom that was placed back into the freezer. Next, Ru-PNP^{Ph} (5 µmol) was weighed into a 4 mL vial and transferred to the reactor bottom. The reactor bottom and 4 mL vial were placed into the –37 °C freezer. DMC (2.6 mL of 1.89 M in THF) was added directly to the reactor bottom. Dimethylamine (2 mL of 3.8 M in THF) was then added to the 4 mL vial via a 5 mL syringe and needle before being transferred to the reactor bottom with a glass pipette. The reactor was immediately sealed and removed from the glovebox. The vessel was connected to the Parr Multiple Reactor System, and manifold was then thoroughly purged (1 minute and then vented 15 times) with ultra-high purity H_2 (99.999%). The vessel was then pressurized with 50 bar with ultra-high purity grade H_2 at room temperature to reach a total pressure of 50 bar. The reaction was heated at 95 °C with a stir rate of 800 RPM. The heating was conducted using Specview software. After 18 hours of heating, the temperature was increased to 155 °C for 18 hours before the reaction mixture was allowed to cool to room temperature. The pressure vessel was placed in a –84 °C bath (ethyl acetate/LN_2) for 15 min and then carefully vented using a metering valve. THF (0.5 mL) was added through the venting valve of the pressure vessel to wash any residual liquids/solids into the vessel. The vessel was then opened, 1,3,5-trimethoxybenzene (0.178 mmol, 300 µL of 0.593 M solution in DMSO-d_6) was added as a ^{1}H NMR standard, and the contents of the vessel were diluted with DMSO-d_6. Approximately 50 µL of the resulting solution was added to an NMR tube, diluted further with DMSO-d_6, and neutralized with HCl. The sample was then analyzed by ^{1}H NMR spectroscopy.

Cooperative Hydrogenation of DMC to Methanol (Table 3.12)

In a N_2-atmosphere dry box, a Parr reactor bottom (containing an octagon magnetic stirbar), glass pipettes, a 1 mL syringe, a 5 mL syringe, and a 20 gauge needle were placed into the –37 °C freezer for 45 minutes. K_3PO_4 (250 µmol) was weighed and transferred to the reactor bottom that was placed back into the freezer. Next, Ru-PNP^{iPr} (2.5 µmol) was weighed into a 4 mL vial and transferred to the reactor bottom. Then, Ru-PNP^{Ph} (2.5 µmol) was weighed into a separate 4 mL vial and transferred to the reactor bottom. The reactor bottom and 4 mL vials were placed into the –37 °C freezer. DMC (2.6 mL of 1.89 M in THF) that had been stored in the freezer was added to one of the 4 mL vials via a 1 mL syringe. Dimethylamine (2.0 mL of 3.8 M in THF) was then added to the other 4 mL vial via a 5 mL syringe and needle before being transferred to the 4 mL vial with DMC whose solution was then immediately transferred to the reactor bottom with a glass pipette. The reactor was quickly sealed and removed from the glovebox. The vessel was connected to the Parr Multiple Reactor System, and the manifold was thoroughly purged (1 minute and then vented 15 times) with ultra-high purity H_2 (99.999%). The vessel was then pressurized with 50 bar with ultra-high purity grade H_2 at room temperature to reach a total pressure of 50 bar. The reaction was heated to 95 °C with a stir rate of 800 RPM. After 3 hours the reaction temperature was increased to 155 °C for 14 hours before the reaction mixture was allowed to cool to room temperature. The pressure vessel was placed in a –84 °C bath (ethyl acetate/LN_2) for 15 min and then carefully vented using a metering valve. THF (0.5 mL) was added through the venting valve of the pressure vessel to wash any residual liquids/solids into the vessel. The vessel was then opened, 1,3,5-trimethoxybenzene (0.178 mmol, 300 µL of 0.593 M solution in DMSO-d_6) was added as a ^{1}H NMR standard, and the contents of the vessel were diluted with DMSO-d_6. Approximately 50 µL of the resulting solution was added to an NMR tube, diluted further with DMSO-d_6, and neutralized with HCl. The sample was then analyzed by ^{1}H NMR spectroscopy.

Cooperative Hydrogenation of CO_2 to DMF at 2.5 bar of CO_2 (Table 3.13)

In a N_2-atmosphere dry box, a Parr reactor bottom (containing an octagon magnetic stirbar), glass pipettes, a 1 mL syringe, a 5 mL syringe, and a 20 gauge needle were placed into the –37 °C freezer for 45 minutes. Next, Ru-PNP^{iPr} (2.5 µmol) was weighed into a 4 mL vial and transferred to the reactor bottom. Then, Ru-PNP^{Ph} (2.5 µmol) was weighed into a separate 4 mL vial and transferred to the reactor bottom. The reactor bottom and 4 mL vials were placed into the –37 °C freezer. Dimethylamine (2 mL of 3.8 M in THF) was then added to a 4 mL vial via a 5 mL syringe and needle before being transferred to the other 4 mL vial that was then immediately transferred to the reactor bottom with a glass pipette. The reactor was quickly sealed and removed from the glovebox. The vessel was connected to the Parr Multiple Reactor System, and the manifold was thoroughly purged (1 minute and then vented 15 times) with bone dry grade CO_2 (99.9%). The vessel was then pressurized to 2.5 bar with CO_2. The manifold was then thoroughly purged (1 minute and then vented 15 times) with ultra-high purity H_2 (99.999%). The vessel was then pressurized with 50 bar with ultra-high purity grade H_2 at room temperature to reach a total pressure of 52.5 bar. The reaction was heated to 95 °C with a stir rate of 800 RPM. After 4 hours, the reaction mixture was allowed to cool to room temperature. The pressure vessel was placed in a –84 °C bath (ethyl acetate/LN_2) for 15 min and then carefully vented using a metering valve. THF (0.5 mL) was added through the venting valve of the pressure vessel to wash any residual liquids/solids into the vessel. The vessel was then opened, 1,3,5-trimethoxybenzene (0.178 mmol, 300 µL of 0.593 M solution in DMSO-d_6) was added as a ^{1}H NMR standard, and the contents of the vessel were diluted with DMSO-d_6. Approximately 50 µL of the resulting solution was added to an NMR tube, diluted further with DMSO-d_6, and neutralized with HCl. The sample was then analyzed by ^{1}H NMR spectroscopy.

Procedure CO_2 Hydrogenation to DMF at Varied Loadings of Ru-PNP^{Ph} (Table 3.14)

In a N_2-atmosphere dry box, a Parr reactor bottom (containing an octagon magnetic stirbar), glass pipettes, a 1 mL syringe, a 5 mL syringe, and a 20 gauge needle were placed into the –37 °C freezer for 45 minutes. Next, Ru-PNP^{Ph} (2.5 – 10 μmol) was weighed into a 4 mL vial and transferred to the reactor bottom. The reactor bottom and 4 mL vial were placed into the –37 °C freezer. Dimethylamine (2 mL of 3.8 M in THF) was then added to the 4 mL vial via a 5 mL syringe and needle before being transferred to the reactor bottom with a glass pipette. The reactor was immediately sealed and removed from the glovebox. The vessel was connected to the Parr Multiple Reactor System, and the manifold was thoroughly purged (1 minute and then vented 15 times) with bone dry grade CO_2 (99.9%). The vessel was then pressurized to 1 bar with CO_2. The manifold was then thoroughly purged (1 minute and then vented 15 times) with ultra-high purity H_2 (99.999%). The vessel was then pressurized with 50 bar with ultra-high purity grade H_2 at room temperature to reach a total pressure of 51 bar. The reaction was heated at 95 °C with a stir rate of 800 RPM. The heating was conducted using Specview software. After 16 hours of heating, the reaction mixture was allowed to cool to room temperature. The pressure vessel was placed in a –84 °C bath (ethyl acetate/LN_2) for 15 min and then carefully vented using a metering valve. THF (0.5 mL) was added through the venting valve of the pressure vessel to wash any residual liquids/solids into the vessel. The vessel was then opened, 1,3,5-trimethoxybenzene (0.178 mmol, 300 μL of 0.593 M solution in DMSO-d_6) was added as a ^{1}H NMR standard, and the contents of the vessel were diluted with DMSO-d_6. Approximately 50 μL of the resulting solution was added to an NMR tube, diluted further with DMSO-d_6, and neutralized with HCl. The sample was then analyzed by ^{1}H NMR spectroscopy.

CO_2 Hydrogenation to DMF with Research Grade H_2 (Table 3.15 & 3.16)

In a N_2-atmosphere dry box, a Parr reactor bottom (containing an octagon magnetic stirbar), glass pipettes, a 1 mL syringe, a 5 mL syringe, and a 20 gauge needle were placed into the –37 °C freezer for 45 minutes. Where appropriate, K_3PO_4 (250 µmol) was weighed and transferred to the reactor bottom that was placed back into the freezer. Next, Ru-PNP^{Ph} (5 µmol) was weighed into a 4 mL vial and transferred to the reactor bottom. The reactor bottom and 4 mL vial were placed into the – 37 °C freezer. Dimethylamine (2 mL of 3.8 M in THF) was then added to the 4 mL vial via a 5 mL syringe and needle before being transferred to the reactor bottom with a glass pipette. The reactor was immediately sealed and removed from the glovebox. The vessel was connected to the Parr Multiple Reactor System, and the manifold was thoroughly purged (1 minute and then vented 15 times) with bone dry grade CO_2 (99.9%). The vessel was then pressurized to 2 bar with CO_2. The manifold was then thoroughly purged (1 minute and then vented 15 times) with Research Grade H_2 (99.9999%). The vessel was then pressurized with 50 bar with Research Grade H_2 at room temperature to reach a total pressure of 52 bar. The reaction was heated at 95 °C with a stir rate of 800 RPM. The heating was conducted using Specview software. After 16 hours of heating, the reaction mixture was allowed to cool to room temperature. The pressure vessel was placed in a –84 °C bath (ethyl acetate/LN_2) for 15 min and then carefully vented using a metering valve. THF (0.5 mL) was added through the venting valve of the pressure vessel to wash any residual liquids/solids into the vessel. The vessel was then opened, 1,3,5-trimethoxybenzene (0.178 mmol, 300 µL of 0.593 M solution in DMSO-d_6) was added as a ^{1}H NMR standard, and the contents of the vessel were diluted with DMSO-d_6. Approximately 50 µL of the resulting solution was added to an NMR tube, diluted further with DMSO-d_6, and neutralized with HCl. The sample was then analyzed by ^{1}H NMR spectroscopy.

Cooperative Hydrogenation of CO_2 to Methanol at 1 bar of CO_2 (Figure 3.6 and 3.7)

In a N_2-atmosphere dry box, a Parr reactor bottom (containing an octagon magnetic stirbar), glass pipettes, a 1 mL syringe, a 5 mL syringe, and a 20 gauge needle were placed into the –37 °C freezer for 45 minutes. Next, Ru-PNP^{iPr} (2.5 µmol) was weighed into a 4 mL vial and transferred to the reactor bottom. Then, Ru-PNP^{Ph} (2.5 µmol) was weighed into a separate 4 mL vial and transferred to the reactor bottom. The reactor bottom and 4 mL vials were placed into the –37 °C freezer. Dimethylamine (2 mL of 3.8 M in THF) was then added to a 4 mL vial via a 5 mL syringe and needle before being transferred to the other 4 mL vial that was then immediately transferred to the reactor bottom with a glass pipette. The reactor was quickly sealed and removed from the glovebox. The vessel was connected to the Parr Multiple Reactor System, and the manifold was thoroughly purged (1 minute and then vented 15 times) with bone dry grade CO_2 (99.9%). The vessel was then pressurized to 1 bar with CO_2. The manifold was then thoroughly purged (1 minute and then vented 15 times) with Research Grade H_2 (99.9999%). The vessel was then pressurized with 50 bar with Research Grade H_2 at room temperature to reach a total pressure of 51 bar. The reaction was heated to 95 °C with a stir rate of 800 RPM. After 18 hours, the temperature was increased to 155 °C for an additional 24 hours before the reaction mixture was allowed to cool to room temperature. The pressure vessel was placed in a –84 °C bath (ethyl acetate/LN_2) for 15 min and then carefully vented using a metering valve. THF (0.5 mL) was added through the venting valve of the pressure vessel to wash any residual liquids/solids into the vessel. The vessel was then opened, 1,3,5-trimethoxybenzene (0.178 mmol, 300 µL of 0.593 M solution in DMSO-d_6) was added as a ^{1}H NMR standard, and the contents of the vessel were diluted with DMSO-d_6. Approximately 50 µL of the resulting solution was added to an NMR tube, diluted further with DMSO-d_6, and neutralized with HCl. The sample was then analyzed by ^{1}H NMR spectroscopy.

3.6. References

1. Rezayee, N. M.; Huff, C. A.; Sanford, M. S. *J. Am. Chem. Soc.* **2015**, *137*, 1028.

2. Yang, H.; Xu, Z.; Fan, M.; Gupta, R.; Slimane, R. B.; Bland, A. E.; Wright, I. *J. Environ. Sci.* **2008**, *20*, 14.

3. MacDowell, N.; Florin, N.; Buchard, A.; Hallett, J.; Galindo, A.; Jackson, G.; Adjiman, C. S.; Williams, C. K.; Shahb, N.; Fennell, P. *Energy Environ. Sci.* **2010**, *3*, 1645.

4. Figueroa, J. D.; Fout, T.; Plasynski, S.; McIlvried, H.; Srivastava, R. D. *Int. J. Greenh. Gas Con.* **2008**, *2*, 9.

5. Jessop, P. G. Homogeneous Hydrogenation of Carbon Dioxide In *The Handbook of Homogeneous Hydrogenation*; Wiley-VCH Verlag GmbH & Co., **2007**, p 489.

6. Huff, C. A.; Sanford, M. S. *J. Am. Chem. Soc.* **2011**, *133*, 18122.

7. Lohr, T. L.; Marks, T. J. *Nature Chem.* **2015**, *7*, 477.

8. Kroutil, W.; Rueping, M. *ACS Catal.* **2014**, *4*, 2086.

9. Fogg, D. E.; dos Santos, E. N. *Coord. Chem. Rev.* **2004**, *248*, 2365.

10. Wasilke, J.-C.; Obrey, S. J.; Baker, R. T.; Bazan, G. C. *Chem. Rev.* **2005**, *105*, 1001.

11. Denard, C. A.; Huang, H.; Bartlett, M. J.; Lu, L.; Tan, Y.; Zhao, H., Hartwig, J. F. *Angew. Chem. Int. Ed.* **2014**, *53*, 465.

12. Air Products and Chemicals, Inc. BIP gases – Cost savings: more usable gas. http://www.airproducts.com/microsite/uk/BIP/Cost_effectiveness.htm (accessed Jan. 22, 2018)

13. Zhang, L.; Han, Z.; Zhao, X.;Wang, Z.; Ding, K. *Angew. Chem. Int. Ed.* **2015**, *54*, 6186.

14. Kothandaraman, J.; Goeppert, A.; Czaun, M.; Olah, G. A.; Prakash, G. K. S. *J. Am. Chem. Soc.*, **2016**, *138*, 778.

15. Khusnutdinova, J. R.; Garg, J. A.; Milstein, D. *ACS Catal.*, **2015**, *5*, 2416.

16. Artz, J.; Müller, T. E.; Thenert, K.; Kleinekorte, J.; Meys, R.; Sternberg, A.; Bardow, A.; Leitner, W. *Chem. Rev.* **2018**, *118*, 434.

17. Sordakis, K.; Tang, C.; Vogt, L. K.; Junge, H.; Dyson, P. J.; Beller, M.; Laurenczy, G. *Chem. Rev.* **2018**, *118*, 372.

18. Kar, S.; Sen, R.; Goeppert, A.; Prakash, G. K. S. *J. Am. Chem. Soc.* **2018**, *140*, 1580.

19. Ahmad, N.; Levison, J. J.; Robinson, S. D.; Uttley, M. F.; Wonchoba, E. R.; Parshall, G. W. Complexes of Ruthenium, Osmium, Rhodium, and Iridium Containing Hydride

Carbonyl, or Nitrosyl Ligands. In *Inorganic Syntheses*; Parshall, G. W. McGraw-Hill: New York, **1974**; Vol. 15, p 48.

20. Bertoli, M.; Choualeb, A.; Lough, A. J.; Moore, B.; Spasyuk, D.; Gusev, D. G. *Organometallics* **2011**, *30*, 3479.

21. Kuriyama, W.; Matsumoo, T.; Ino, Y.; Ogata, O. (Takasago International Corporation) Ruthenium carbonyl complex having tridentate ligand, its production method and use. U.S. Patent 8,471,048. June 25, 2013.

CHAPTER 4

Towards Homogeneous-Heterogeneous Cooperative Conversion of Carbon Dioxide to Methanol via an Ester Intermediate[1]

4.1. Introduction

In 2011, the Sanford group reported the cascade conversion of carbon dioxide (CO_2) to methanol (CH_3OH) via an ester intermediate (Scheme 4.1).[2] First Catalyst A, a ruthenium catalyst is responsible for hydrogenating CO_2 to formic acid (Scheme 4.1, step i). The resulting formic acid undergoes a Lewis acid catalyzed esterification reaction with methanol to produce methyl formate (Scheme 4.1, step ii). A second ruthenium catalyst, Catalyst C, then hydrogenates the ester yielding methanol and regenerating the alcohol (Scheme 4.1, step iii). Excitingly, this system was the first homogeneous catalyzed conversion of CO_2 to methanol.[2]

Scheme 4.1. Conversion of CO_2 to Methanol via an Ester Cascade Pathway

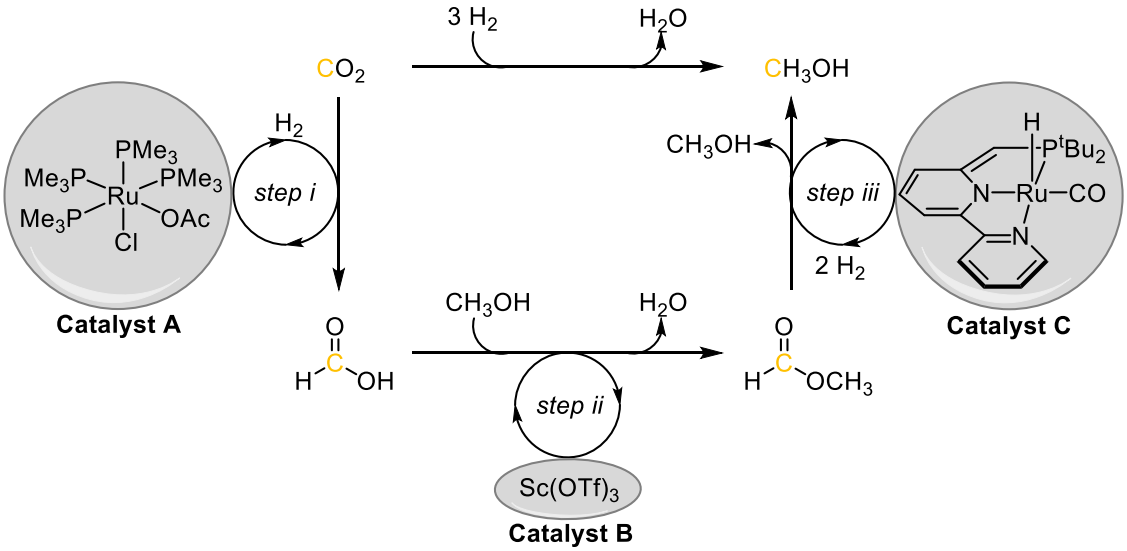

Interestingly, each of the three catalysts in Scheme 4.1 (Catalysts A–C) were independently reported and studied before use in the ester cascade system. Catalyst A was reported by Jessop and co-workers and was capable of hydrogenating >10,000 turnovers of CO_2.[3] Lewis acid catalyzed esterification is a well-established organic reaction.[4] Finally, Catalyst C, a Ru-pincer complex reported by Milstein and co-workers was well studied in ester hydrogenation.[5] The main advantage to the ester cascade system revolved around the fact that each catalyst and mechanism were thoroughly and independently studied, laying a stable framework for the realization of the ester cascade system.[6]

The inspiration behind the ester cascade system's utilization of three separate catalysts was derived from nature. In naturally occurring catalytic reactions, such as enzymatic reactions, multiple active sites are used to perform a single overall transformation.[7] Often, each enzyme's active site performs a single step along a pathway consisting of multiple enzymes and active sites.[7] In particular, the functionalization of CO_2 naturally occurs through a series of proton coupled electron transfers at 11 different active sites (Figure 4.1).[8]

Figure 4.1. Autotrophic Fixation of CO_2 in the Reductive Pentose Phosphate Cycle[8]

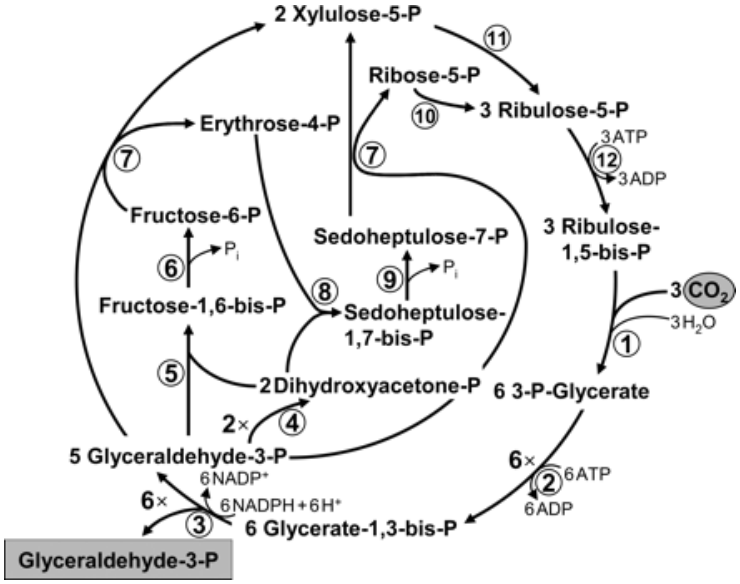

The uncatalyzed conversion of CO_2 to methanol would require prohibitively harsh conditions (Figure 4.2, Path 1). There are many heterogeneous catalysts capable of this reaction

(Figure 4.2, Path 2).[9,10,11] In order to overcome high activation barriers, harsh conditions are used, namely running the reactions at high temperatures (>200 °C).[12,13,14] Heterogeneous catalysts often contain multiple active sites with each type of active site performing a single step.[15,16,17] In order to use homogeneous catalysts for the conversion of CO_2 to methanol, we decided to mimic nature wherein three catalysts were employed, each with a relatively lower activation barrier compared to the heterogenous system (Figure 4.2, Path 3). These lower activation barriers allow for lower operating temperatures which is critical for homogeneous catalysts as they tend to undergo thermal decomposition.[18] By taking a leaf out of nature's handbook, we circumvented the need to find a single homogeneous catalyst capable of performing a variety of proton coupled electron transfers which in turn allowed for lower operating temperatures making homogenous catalysts an ideal candidate for this transformation.

Figure 4.2. Reaction Coordinate Diagram for Converting CO_2 to Methanol

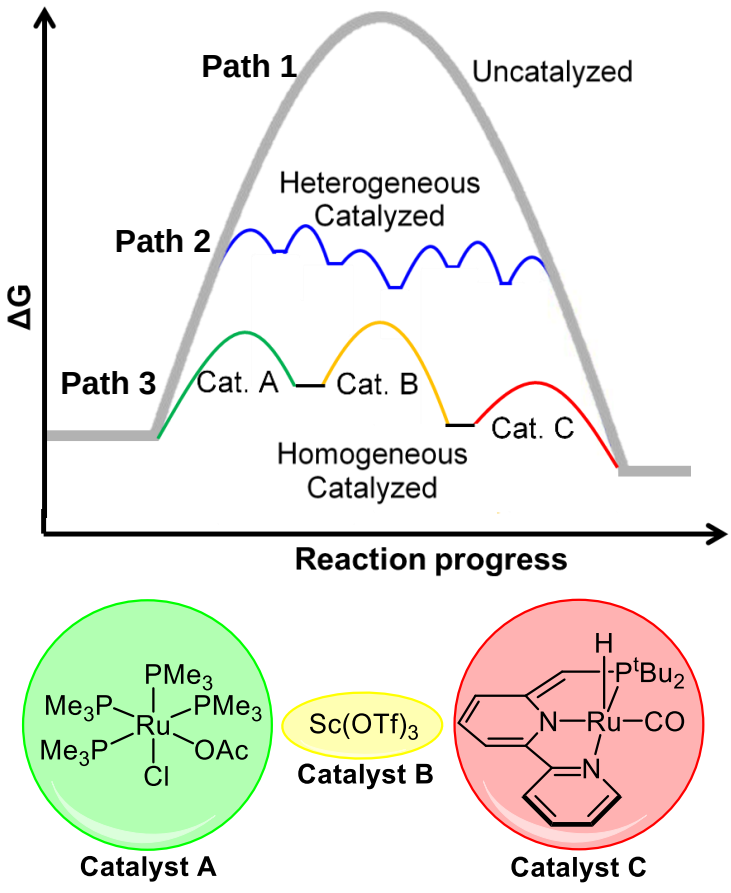

Even though the ester cascade system was a significant advancement in the conversion of CO_2 to methanol, this system produced very low turnovers of methanol allowing for a significant opportunity for improvement. When all three catalysts were in a single pot (one-well) together, only trace (2.5) turnovers of methanol were detected.[2] This low reactivity was primarily due Catalyst B inhibiting Catalyst C.[2,19,20] To improve the reactivity, a one-pot, two-well system was utilized wherein Catalyst A and Catalyst B were allowed to react in the same solution and generate methyl formate (Scheme 4.2, step i and ii). Then a temperature ramp was used to transfer the methyl formate from the inner well to the outer well where Catalyst C could then hydrogenate the ester onto methanol (Scheme 4.2, step iii). This new system improved the turnovers of methanol up to 21 turnovers.[2] Although this low-tech solution improved reactivity, we sought to further boost the ester cascade system in order to exploit the excellent reactivity of these homogeneous catalysts.

Scheme 4.2. Ester Cascade System Employing a One-Pot, Two-Well Setup

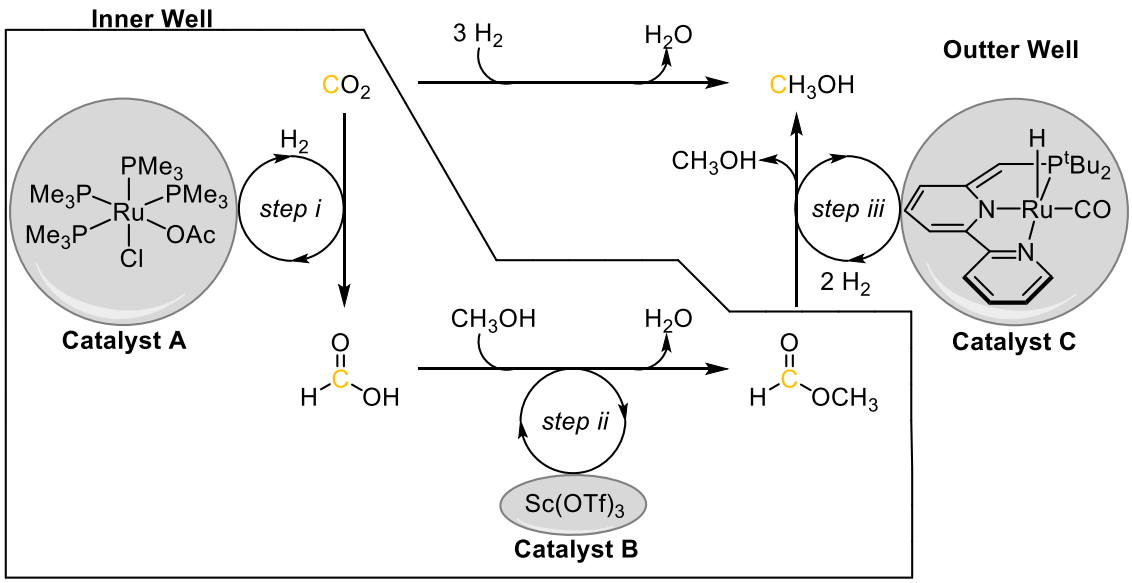

In initial attempts to generate a second-generation ester cascade system, new suites of catalysts were studied. The primary focus revolved around identifying an ester hydrogenation catalyst which was compatible with Lewis acids. Work from the Goldberg group identified Ir-complexes that were not only operable with Lewis acid, but also, exhibited increased reactivity

when $Sc(OTf)_3$ was present (Scheme 4.3).[21,22] This discovery led us to exchange our Catalyst C for IrCp*Bpy now improving our cascade system by having Catalyst B be compatible with the ester hydrogenation catalyst. Unfortunately, we were disappointed to see that Catalyst A and IrCp*Bpy were incompatible (Scheme 4.4). This second-generation cascade system produced 8 turnovers of methanol in a one-pot, one-well set-up, only a modest improvement from the original system's 2.5 turnovers of methanol.

Scheme 4.3. IrCp*Bpy Catalyzed Ethyl Formate Hydrogenation

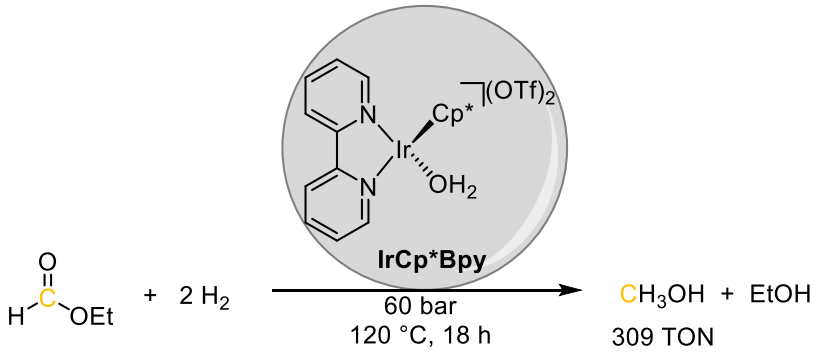

Scheme 4.4. Second-generation Ester Cascade System

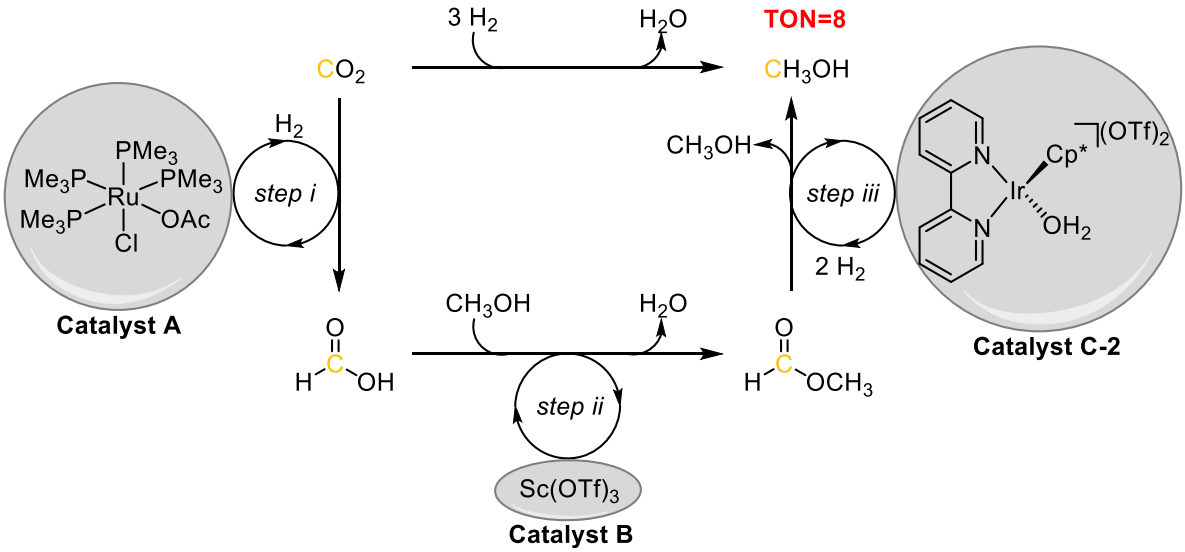

We hypothesized that we could generate an improved ester hydrogenation system by implementing a few key changes. First, we reasoned that simplification of the system was necessary. In all the suites of three catalysts that were tested, two-way compatibility was trivial, and issues occurred when attempting to find three-way compatibility. By simplifying the

system to two catalysts, we would increase the number of catalysts available. At the same time, this required one catalyst to perform two steps. We predicted that finding a single catalyst to do both hydrogenations (steps i and iii) would be possible but difficult. An easier route would be if one of the hydrogenation catalysts (Catalyst A or C), could also act as Catalyst B, removing the need for a simple Lewis acid. A second key change involved identifying an excellent Catalyst C. Catalyst A is extremely active, capable of converting >10,000 turnovers of CO_2.[3] We sought to combine an excellent CO_2 hydrogenation catalyst (Catalyst A) with a superior and more active ester hydrogenation catalyst (Catalyst C).

We identified heterogeneous catalysts, typically Lewis acidic in nature, as a possible solution to an improve ester cascade system (Scheme 4.5). Concurrently, they also are well established to hydrogenate intermediates similar to esters.[23,24,25,26] We thought that these two characteristics of heterogeneous catalysts would allow one to replace Catalyst B, the esterification catalyst, as well as Catalyst C, the ester hydrogenation catalyst (Scheme 4.5, steps ii and iii).

Scheme 4.5. Utilization of a Heterogeneous Catalyst in Place of Catalyst B & C

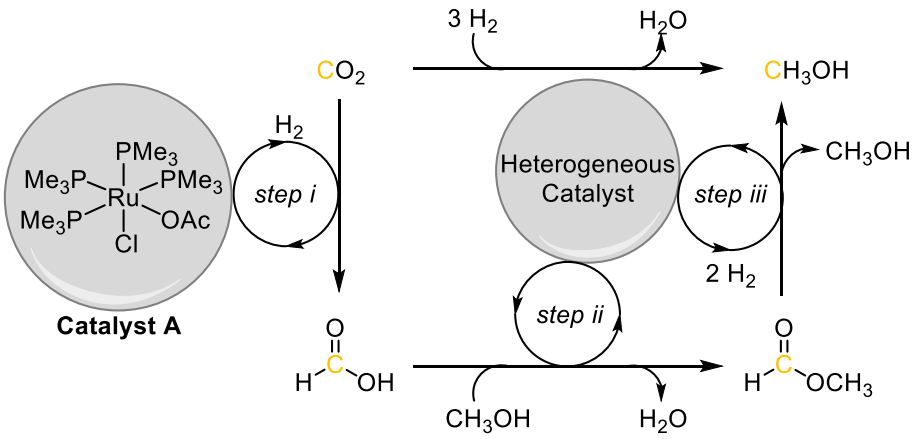

Importantly, we did not aim to utilize all heterogeneous catalysts or typical heterogeneous catalyst conditions in our ester cascade system; instead, we sought to couple homogeneous and heterogeneous catalysts. Heterogeneous catalyzed conversion of CO_2 to methanol is well established and is industrially operable at the George Olah plant in Iceland.[27]

The heterogeneous catalyst used is an extremely active cooper and zinc-based catalyst. Generating another heterogeneous conversion of CO_2 to methanol would not present a unique solution. Additionally, we desired to use lower reaction temperatures and pressures as this would allow for the continued utilization of homogeneous Catalyst A. Additionally, the hydrogenation of CO_2 is more favorable at low temperatures ($\Delta G=\Delta H-T\Delta S$) due to the reaction being entropically unfavorable ($-\Delta S$) and enthalpically favorable ($-\Delta H$).[9] Ultimately, we hoped to exploit the advantageous of both homogeneous and heterogeneous catalysis under mild conditions to generate more methanol than either catalyst alone.

4.2. Results and Discussion

4.2.1. Cu/Mo_2C for Homogeneous-Heterogeneous Coupled CO_2 Hydrogenation via an Ester Intermediate

Before studying the homogeneous-heterogenous coupled conversion of CO_2 to methanol, we needed to identify a suitable model system (Scheme 4.6). In the model system, ethanol (EtOH) is used as the reaction solvent as opposed to methanol like in the published system.[2] This is due to two main reasons. First, using ethanol as the solvent allows for easy identification of our methanol product which otherwise would be extremely hard to identify as only a small percentage of the methanol present at the end of the reaction would be derived from CO_2. In our published ester cascade system, this challenge was overcome by using expensive isotopically labelled materials, such as $^{13}CO_2$ or $^{13}CH_3OH$, which is not financially feasible for exploratory studies.[2] Secondly, when studying ethyl formate hydrogenation in ethanol, one can easily identify the methanol formed as resulting from hydrogenation as opposed to hydrolysis.

Scheme 4.6. Model System for Exploration of CO_2 to Methanol Catalyzed via a Homogeneous and Heterogeneous Catalyst

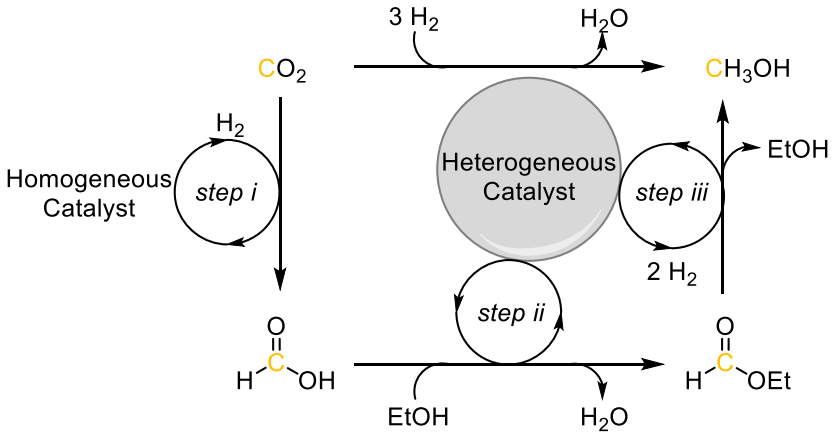

Our first step in generating a homogeneous-heterogeneous coupled ester cascade system focused on identifying a heterogeneous catalyst that was operable under low temperatures and pressures. In collaboration with Professor Levi Thompson's group at the University of Michigan, we worked closely with former graduate student Yuan Chen. The Thompson group was able to test a variety of heterogeneous catalysts they had on hand for ethyl formate hydrogenation.[28] Excitingly, they found that Cu/Mo_2C was very active for this reaction giving high selectivity for methanol production at the mild conditions employed in our original ester cascade system (135 °C, 30 bar H_2).

With Cu/Mo_2 identified as a suitable catalyst for ethyl formate hydrogenation at mild conditions, we sought to study its reactivity as a CO_2 hydrogenation catalyst. Even though we aimed to use Cu/Mo_2C as the ester hydrogenation catalyst, we also needed to identify if it was active for CO_2 hydrogenation at these mild conditions since CO_2 will be present in the ester cascade system. Surprisingly, Cu/Mo_2C was indeed active for the conversion of CO_2 to methanol at just 135 °C and 30 bar of H_2 primarily resulting in methanol, but with some intermediate ethyl formate still present. Unfortunately, variability plagued this system with large variation between runs (Table 4.1). Before continuing with further experimentation, we required to resolve the variability.

Table 4.1. Low Temperature CO_2 Hydrogenation with Cu/Mo_2C

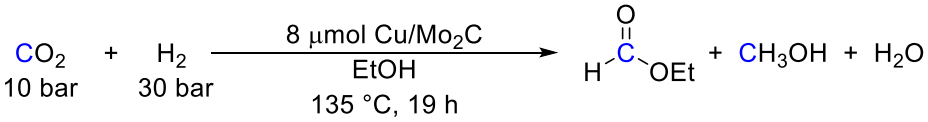

Entry[a]	TON Ethyl Formate	TON Methanol	Standard Deviation	Relative Standard Deviation
1	4	109	21	26%
2	3	58		
3	5	96		
4	7	72		

[a]**Conditions:** 8 μmol Cu/Mo_2C catalyst, 3 mL of EtOH, 10 bar CO_2, 30 bar H_2, 135 °C for 19 h, stirred at 800 RPM. Yields determined by ^1H NMR spectroscopy. Max TON ~2300.

Post-catalysis, we observed that the heterogeneous catalyst's appearance had changed. Pre-reaction, the material was a purple-red granule, but after catalysis, the material was a black powder. The material was not undergoing thermal decomposition due to the ester hydrogenation reactions studied in the Thompson group employing the same temperature without any change in the material. After thorough investigation, we realized a key difference between the Thompson lab set-up and our reaction set-up was the reactor design. The Thompson lab's Parr reactor utilized an overhead stirrer to mix the reaction solution. Our reactors were not equipped with such a device and instead utilized stir bars (see section 4.4.1 for more information). We hypothesized the mechanical pulverization of the material was causing collapse of the porous structure of the Mo_2C unit.[28]

We next sought to study different stir bars in attempt to generate a more reproducible system while maintaining the structure and reactivity of the heterogeneous catalyst. We moved from using Spinbar® magnetic stirring fleas (3 x 10 mm) to using octagon stir bars with a pivot ring (7.9 x 12 mm). Unfortunately, our variability did not improve (Table 4.2, Entries 1–4). We also utilized another variation of stir bar (oval, 5 x 10 mm), but to no avail (Table 4.2, Entries 5–7). We realized that the difference between our reactions and those of the Thompson group was the stirring method, but overcoming this difference was non-trivial.

Table 4.2. Stirring Investigation for Low Temperature CO_2 Hydrogenation with Cu/Mo_2C

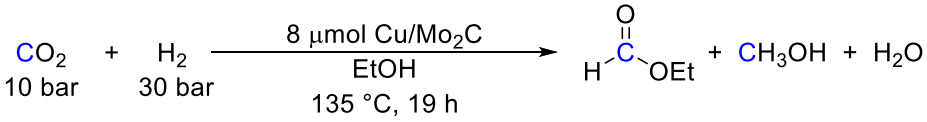

Entry[a]	Stirbar	TON Ethyl Formate	TON Methanol	Relative Standard Deviation
1	Octagon	5	137	27%
2	Octagon	4	73	
3	Octagon	6	121	
4	Octagon	9	91	
5	Oval	5	19	36%
6	Oval	6	40	
7	Oval	3	28	

[a]**Conditions:** 8 μmol Cu/Mo_2C catalyst, 3 mL of EtOH, 10 bar CO_2, 30 bar H_2, 135 °C for 19 h, stirred at 800 RPM. Yields determined by ^1H NMR spectroscopy. Max TON ~2300.

Since it was not possible to reproduce the Thompson group's stirring method without purchasing an expensive Parr reactor, we attempted to run the reactions without any stirring. Although at first glance this seems entirely preposterous as our catalyst was heterogeneous, we hypothesized that since so little solvent (1.5 mL in contact with the catalyst inside of a 45 mL reactor) was utilized compared to our substrates (CO_2 and H_2) which are present in high pressures, mass transport to the catalyst may not be limiting. Additionally, our intermediates as well as products were completely soluble in ethanol such that our reaction solution was homogeneous. Running Cu/Mo_2C catalyzed CO_2 hydrogenation without stirring, we found the reaction to be extremely reproducible (Table 4.3). Excellent reproducibility could be achieved between eight separate runs (relative standard deviation 5%). With our reproducibility solved, we now sought to continue our exploration into Cu/Mo_2C.

Table 4.3. No Stirring in Low Temperature CO_2 Hydrogenation with Cu/Mo_2C

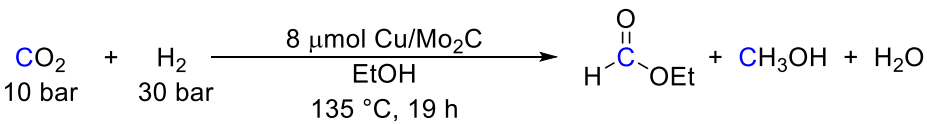

Entry[a]	TON Ethyl Formate	TON Methanol	Relative Standard Deviation
1	4	136	5%
2	10	155	

3	9	146
4	9	151
5	8	148
6	9	157
7	11	136
8	5	143

[a]**Conditions:** 8 µmol Cu/Mo_2C catalyst, 3 mL of EtOH, 10 bar CO_2, 30 bar H_2, 135 °C for 19 h. Yields determined by ^1H NMR spectroscopy. Max TON ~2300.

The lifetime of Cu/Mo_2C was next studied in order to identify the ideal reaction time. Applying Cu/Mo_2C in CO_2 hydrogenation, we found that Cu/Mo_2C was extremely active even after multiple days (Table 4.4). A substantial increase in the turnovers of methanol was observed when increasing the reaction from just 6 hours to 19 hours (Table 4.4, Entries 1 and 3). Continuing the reaction from 19 hours to nearly four days, Cu/Mo_2C continued to produce methanol once again generating over double the amount as compared to 19 hours (Table 4.4, Entries 3 and 4). Finally, after running the reaction for over 13 days, additional turnovers of methanol were observed, but it was apparent that the catalyst was no longer as active (Table 4.4, Entry 5). We further investigated the lifetime of Cu/Mo_2C by looking at the turnover frequency (TOF) at various points (Figure 4.3). It was apparent that sometime around two days, the TOF decreased significantly.

Table 4.4. Cu/Mo_2C Lifetime for CO_2 Hydrogenation

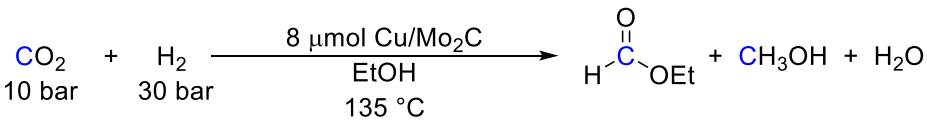

Entry[a]	Time (h)	TON Ethyl Formate	TON Methanol
1	6	14	72
2	16	10	126
3	19	9	147
4	94	3	328
5	314	1	440

[a]**Conditions:** 8 µmol Cu/Mo_2C catalyst, 3 mL of EtOH, 10 bar CO_2, 30 bar H_2, 135 °C. Yields determined by ^1H NMR spectroscopy. Max TON ~2300.

Figure 4.3. Cu/Mo_2C TOF Lifetime[a]

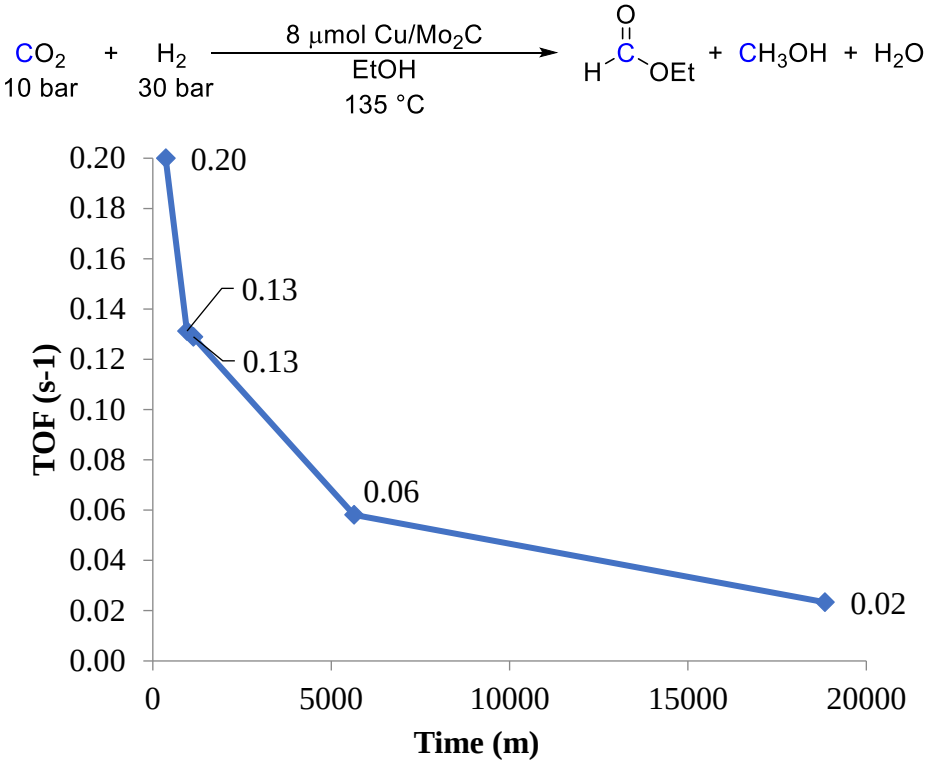

[a]**Conditions:** 8 µmol Cu/Mo_2C catalyst, 3 mL of EtOH, 10 bar CO_2, 30 bar H_2, 135 °C. Yields determined by ^{1}H NMR spectroscopy. Max TON ~2300.

Once identifying 19 hours or less as an optimal reaction time for Cu/Mo_2C to obtain high turnovers of methanol, we next coupled this heterogeneous catalyst with homogeneous catalysts (Figure 4.4). Catalyst **1** is an excellent CO_2 hydrogenation catalyst.[3,6] Additionally, we sought to study how Cu/Mo_2C was impacted by the homogeneous Lewis acid and esterification catalyst **2**.[4] Complex **3** is capable of converting CO_2 to methanol under acidic conditions so we hypothesized the presence of the Lewis acidic heterogeneous catalyst may result in a synergistic effect resulting in more methanol.[29,30] The ruthenium complex **4** is a good CO_2 hydrogenation catalyst; albeit, not as active as complex **1**, but we thought the increased ligand denticity may be beneficial for the complex's stability.[31] Finally, **5** is known to be aided by Lewis acids making it likely that the heterogenous catalyst could increase the homogeneous catalyst's reactivity.[21,22]

Figure 4.4. Homogeneous Catalysts of Interest to Couple with Cu/Mo_2C

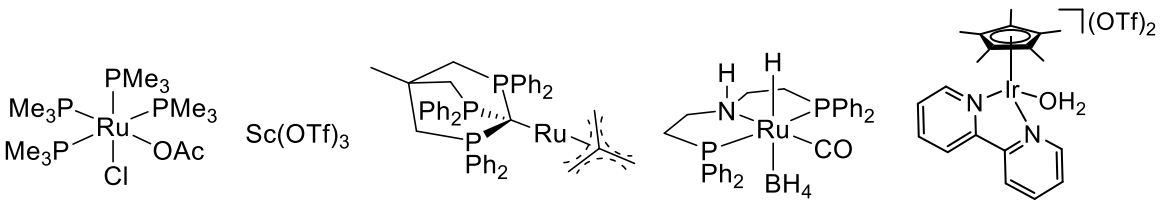

1 **2** **3** **4** **5**

Coupling Cu/Mo_2C with each homogeneous catalyst led to inhibition rather than synergy (Table 4.5). The heterogeneous catalyst alone produced the most methanol at 126 turnovers (Table 4.5, Entry 1). Adding in 10 μmol of **1** led to a significant decrease in the amount of methanol formed. Dropping the loading of homogeneous complex to 5 μmol led to improved turnovers of methanol, but still did not out compete the heterogeneous catalyst alone (Table 4.5, Entries 1–3). Moving on to a simple Lewis acid, $Sc(OTf)_3$ once again inhibition was observed (Table 4.5, Entry 4). Interestingly, **2** inhibited the heterogeneous catalyst more than **1** which contains very Lewis basic, phosphine ligands, while **2** only contains relatively non-coordinating triflates. Moving on to the homogeneous catalysts baring tridentate ligands, **3** and **4**, an improvement in the TON was not obtained (Table 4.5, Entries 5 and 6). Tri-dentate Complex **3** inhibited Cu/Mo_2C more than **1** which contains only monodentate ligands; this was surprising to us as we thought the monodentate ligands were more likely to come off the ruthenium and bind strongly to open sites on Cu/Mo_2C. Complex **4** is extremely stable and under normal reaction conditions does not shed ligands besides $-BH_3$ to generate the active species. We hypothesized that $-BH_3$ or complex **4**'s nitrogen in the PNP-backbone may be binding to Cu/Mo_2C's active sites shutting down the Cu/Mo_2C's reactivity, at the same time as making **4** inactive. Coupling Cu/Mo_2C with **5** which is stable in both Lewis acids and Brønsted-Lowery acids,[22] resulted in inhibition once again. This was perplexing as Cu/Mo_2C is not extremely water sensitive (water is generated as a side-product in the reaction) and water is the

only ligand lost to generate the active species of **5**. Ultimately, our first attempts at coupling a homogeneous and heterogenous catalyst were unfruitful.

Table 4.5. Cooperative Homo-Heterogeneous CO_2 Hydrogenation

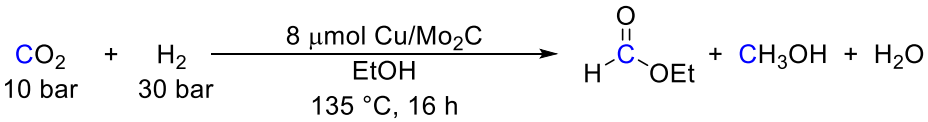

Entry[a]	Co-catalyst	Co-catalyst (μmol)	TON Ethyl Formate	TON Methanol
1	—	—	8	126
2	**1**	10	14	45
3	**1**	5	13	68
4	**2**	10	5	14
5	**3**	10	11	15
6	**4**	10	16	50
7	**5**	10	4	5

[a]**Conditions:** 8 μmol Cu/Mo_2C catalyst, 5-10 μmol homogeneous catalyst, 3 mL of EtOH, 10 bar CO_2, 30 bar H_2, 135 °C for 16 h. Yields determined by ^1H NMR spectroscopy. Max TON ~2300.

We proposed that the inhibition problem in Table 4.5 could be a result of catalyst loading. We thought that some of the homogeneous catalyst's ligands released to generate the active catalyst (**1**=OAc, **3**=alkene, **4**=BH_3, **5**=H_2O) were binding to active sites of the heterogeneous catalyst. To test this, we increased the heterogenous catalyst up to 11 μmol making it so there was more heterogeneous active site compared to the homogeneous catalysts (Table 4.6). Interestingly, we found that instead of seeing an improvement from Table 4.5 to Table 4.6, further inhibition was observed. For instance, from Cu/Mo_2C alone to the addition of **1**, in Table 4.5 the heterogeneous catalyst maintained 36% of its reactivity (Entries 1 and 2), but in Table 4.6 even though there are more active site compared to the homogeneous catalyst Cu/Mo_2C retained a similar 32% of its original reactivity. In all cases, Cu/Mo_2C maintained its reactivity better when there are only 8 μmol compared to 11 μmol of active sites. When 5 μmol of **1** were present, Cu/Mo_2C maintained 54% of its original reactivity at 8 μmol compared to 11 μmol where only 48% of its original reactivity was retained (see Entry 3 in Tables 4.5 and 4.6). Comparing the reactions with 10 μmol of **4** present, Cu/Mo_2C maintained 40% of its

original reactivity with 8 μmol of Cu/Mo_2C vs 17% of original reactivity with 11 μmol of Cu/Mo_2C (Entry 6 in Tables 4.5 and 4.6).

Table 4.6. Increasing Heterogeneous Catalyst Loading for Cooperative Homogeneous-Heterogeneous Catalysis

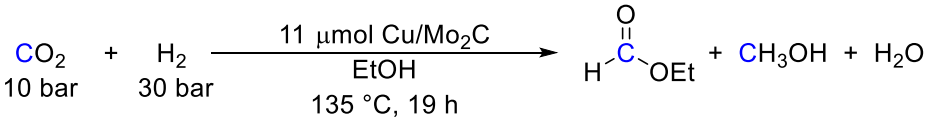

Entry[a]	Cocatalyst	Cocatalyst (μmol)	TON Ethyl Formate	TON Methanol
1	—	—	6	100
2	**1**	10	10	32
3	**1**	5	9	48
4	**2**	10	5	10
5	**3**	10	8	11
6	**4**	10	6	17
7	**5**	10	5	5

[a]**Conditions:** 11 μmol Cu/Mo_2C catalyst, 5–10 μmol homogeneous catalyst, 3 mL of EtOH, 10 bar CO_2, 30 bar H_2, 135 °C for 19 h. Yields determined by ^{1}H NMR spectroscopy. Max TON ~1600.

Next, we endeavoured to see how quickly inhibition of Cu/Mo_2C was occurring. We hypothesized that perhaps over time the homogeneous catalysts were decomposing and shedding their ligands, causing the inhibition of Cu/Mo_2C. We decreased the reaction time to 6 hours and once again observed inhibition of Cu/Mo_2C when a homogeneous catalyst was present (Table 4.7). In the 6-hour reactions (Table 4.7, Entries 4 and 6), the tridentate-baring homogeneous catalysts **3** and **4** inhibited Cu/Mo_2C by a lesser amount (78% and 75% drop in reactivity) as compared to the 19-hour reactions which exhibited an 89% and 83% drop in reactivity, respectively (Table 4.6, Entries 5 and 6). This seemed to support the idea that these homogeneous catalysts are decomposing over time either from temperature or from interaction with the heterogeneous catalyst. At shortened reaction times, the homogeneous complex **1** baring monodentate phosphines and a chloride saw as much inhibition as the tridentate-based homogeneous catalysts, which was opposite from that seen in Table 4.6 where less inhibition was seen with **1**.

Table 4.7. Decreasing Reaction Time for Cooperative Homogeneous-Heterogeneous Catalysis

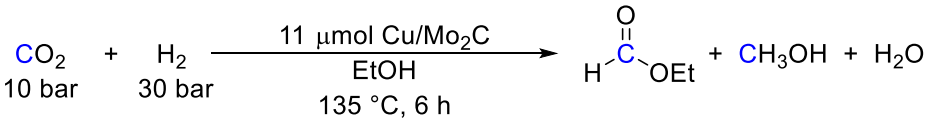

Entry[a]	Cocatalyst	Cocatalyst (mmol)	TON Ethyl Formate	TON Methanol
1	—	—	10	51
2	**1**	10	8	12
3	**1**	8	8	12
4	**1**	2	7	15
5	**3**	10	8	11
6	**4**	10	6	13

[a]**Conditions:** 11 μmol Cu/Mo_2C catalyst, 2–10 μmol homogeneous catalyst, 3 mL of EtOH, 10 bar CO_2, 30 bar H_2, 135 °C for 6 h. Yields determined by ^1H NMR spectroscopy. Max TON ~1600.

Initial attempts to couple Cu/Mo_2C with various homogeneous catalysts were unsuccessful, but still provided a wealth of knowledge. Somewhat orthogonal to traditional heterogeneous catalysis, we discovered that the most reproducible reactions occurred when no stirring was employed. We found that Cu/Mo_2C was indeed active in CO_2 hydrogenation to methanol at 135 °C and 30 bars of H_2 which are extremely mild operating conditions for a heterogeneous catalyst. Coupling Cu/Mo_2C with homogeneous catalysts lead to inhibition in all cases attempted. Moving from monodentate to tridentate ligands on the homogeneous catalysts seemed to have little improvement on the compatibility with the heterogeneous catalyst. Shorter reaction times led to less inhibition of Cu/Mo_2C, but it was still significant. Ultimately, we were unable to generate a homogeneous-heterogeneous catalytic ester cascade system.

4.2.2. Exploration of Different Heterogeneous Catalysts for Cooperative CO_2 Hydrogenation via an Ester Intermediate

We next explored different heterogeneous catalysts in an attempt to develop an improved ester cascade system that utilized both a homogeneous and heterogeneous catalyst. We hypothesized that the immense sensitivity of Cu/Mo_2C could be derived from

the Mo_2C support, the Cu moiety, or both. It was seemed as if Cu/Mo_2C was indeed binding the ligands of the homogeneous catalyst, but we sought to get a better idea of where such binding was occurring to try to alleviate the issue. If the issue was that the Mo_2C support was sensitive, we could move to other heterogeneous catalysts. On the other hand, if the sensitivity was derived from the Cu, we envisioned utilizing a different metal-Mo_2C, such as Ru/Mo_2C or Pd/Mo_2C.

We next turned our attention to Mo_2C as the heterogeneous catalyst of interest allowing for the direct comparison to Cu/Mo_2C and to determine if Cu was causing the sensitivity to the homogeneous catalysts. We found that this heterogeneous catalyst was indeed active at mild conditions, but less active than its Cu-analogue (Table 4.8). Interestingly, Mo_2C maintained its reactivity better when **1** was present (53%) as compared to Cu/Mo_2C which only retained 24% of the heterogeneous-only reactivity (Table 4.8, Entries 1 and 2 compared to 3 and 4). This seemed to indicate that both the Mo_2C support and the copper are responsible for the sensitivity to the homogeneous catalyst. Unfortunately, the Cu is also responsible for increased reactivity of the material overall (Table 4.8, Entries 1 and 3).

Table 4.8. Comparing Cu/Mo_2C and Mo_2C in Cooperative Homogeneous-Heterogeneous Catalyzed CO_2 Hydrogenation

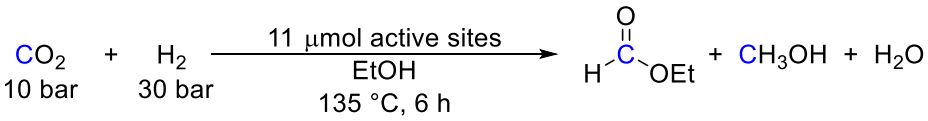

Entry[a]	Hetero Catalyst	Cocatalyst	Cocatalyst (μmol)	TON Ethyl Formate	TON Methanol
1	Cu/Mo_2C	—	—	10	51
2	Cu/Mo_2C	**1**	10	8	12
3	Mo_2C	—	—	6	32
4	Mo_2C	**1**	10	10	17

[a]**Conditions:** 11 μmol heterogeneous catalyst, 10 μmol homogeneous catalyst, 3 mL of EtOH, 10 bar CO_2, 30 bar H_2, 135 °C for 6 h. Yields determined by ^1H NMR spectroscopy. Max TON ~1600.

Interestingly, when running inductively coupled plasma optical emission spectrometry (ICP-OES) on the Mo_2C after the reaction with co-catalyst **1** present, we observed the presence of phosphine, chloride, and ruthenium. The results indicated the presence of Ru (0.3 wt%) and

P (0.7 wt%). This evidence supported the hypothesis that the homogeneous catalyst was decomposing and occupying the active sites of the heterogeneous complex. If all the homogeneous catalyst, both the Ru and P, was deposited onto Mo_2C that would result in a wt% of 3.0 for Ru and 3.7 for P. Interestingly, only 10% of the maximum Ru was deposited onto Mo_2C, while only 19% of the P was deposited. This was somewhat surprising as only a small amount of **1** was deposited onto the material and yet the reactivity dropped by half (Table 4.8, Entries 3 and 4). At most, only 66% of active sites should be unavailable (if each Ru and P bond independently to a single active site) leaving about 34% of Mo_2C's active sites open for catalysis. It was interesting that the turnovers of methanol were not higher seeing as there were still many active sites open on the heterogeneous catalyst and only a small fraction of the homogeneous catalyst was deposited onto the metal.

Next, we sought to utilize a different heterogeneous catalyst, copper zinc aluminium oxide (CZA). This heterogeneous catalyst was developed during the 1960s and used by Imperial Chemical Industries for methanol production from syngas.[9] This catalyst enabled the use of significantly lower temperatures (200–300 °C compared to 300–400 °C) and pressures (50–100 atm compared to 250–300 atm).[9,11] After the advent of CZA, many industrial copper-based catalysts are still used for industrial production of methanol.[9]

Our initial studies into CZA focused on utilizing even more mild reaction conditions. Studying ethyl formate hydrogenation at just 40 bar of H_2 and 135 °C, led to 75% yield of methanol in just 6 hours (Scheme 4.7). This corresponds to 63 turnovers of methanol, which is surprisingly high for such low operating conditions for CZA. With this reactivity in hand, we were excited to further explore CZA in our ester cascade system.

Scheme 4.7. CZA Catalyzed Ethyl Formate Hydrogenation at Low Temperature

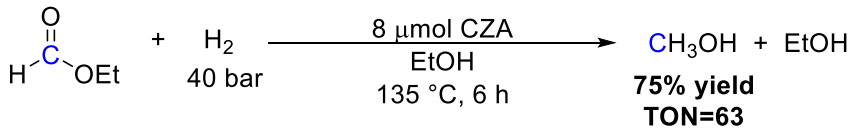

The next phase of CZA exploration focused on utilizing CZA in CO_2 hydrogenation. We initially thought that CZA would only perform ester hydrogenation but based on its excellent reactivity we were not surprised to see that CZA was also active for CO_2 hydrogenation at low temperatures (Table 4.9). Although CZA was inactive at 80 °C (Table 4.9, Entry 1), at just 110 °C and 40 bar, 36 turnovers of methanol and 11 turnovers of ethyl formate were obtained (Table 4.9, Entry 2). Increasing the temperature up to 135 °C, 135 turnovers of methanol and 18 turnovers of ethyl formate were obtained in just 6 hours (Table 4.9, Entry 3). This excellent reactivity was far superior compared to that of Cu/Mo_2C which gave 72 turnovers of methanol and 14 turnovers of ethyl formate.

Table 4.9. Low Temperature CZA CO_2 Hydrogenation

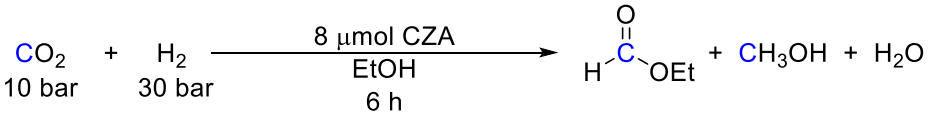

Entry[a]	Temperature (°C)	TON Ethyl Formate	TON Methanol
1	80	0	0
2	110	11	36
3	135	18	135

[a]**Conditions:** 8 μmol CZA catalyst, 3 mL of EtOH, 10 bar CO_2, 30 bar H_2, 6 h. Yields determined by ^1H NMR spectroscopy. Max TON ~2300.

Once identifying CZA as the most active heterogeneous catalyst tested, it was next coupled with a homogeneous catalyst in the ester cascade system (Table 4.10). Coupling CZA with **1** resulted in no methanol formation, while CZA alone produced 135 turnovers of methanol (Table 4.10, Entries 1 and 2). When CZA and **4** were used together, inhibition was once again observed, and very little methanol was produced (Table 4.10). Overall, the results in Table 4.10 were consistent with those previously seen; the homogeneous catalyst severely inhibited the heterogeneous catalyst.

Table 4.10. CZA in Cooperative Homogeneous-Heterogeneous Catalyzed CO_2 Hydrogenation

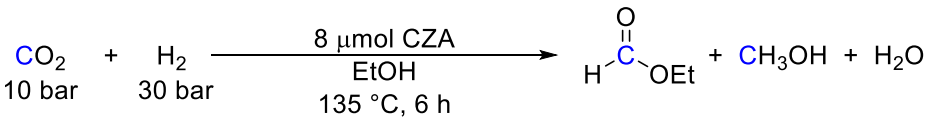

Entry[a]	Cocatalyst	Cocatalyst (µmol)	TON Ethyl Formate	TON Methanol
1	—	—	18	135
2	**1**	10	10	0
3	**4**	10	15	7

[a]**Conditions:** 8 µmol CZA catalyst, 3 mL of EtOH, 10 bar CO_2, 30 bar H_2, 6 h. Yields determined by ^{1}H NMR spectroscopy. Max TON ~2300.

Directly comparing Cu/Mo_2C, Mo_2C, and CZA, it was apparent that each catalyst was inhibited by the homogeneous catalyst **1**, but to varying degrees (Figure 4.5). The most active catalyst for generating methanol, CZA, was also the most inhibited when **1** was present, dropping the turnovers of methanol from 135 to 0 (Figure 4.5). On the other hand, Cu/Mo_2C retained some of its reactivity when **1** was present (76% decrease in turnovers of methanol). Finally, Mo_2C was the most active when **1** was present generating 17 turnovers of methanol (only a 47% decrease in reactivity); although, it was still inhibited by **1**. Overall, there was a correlation between the more active heterogeneous hydrogenation catalysts also being the most inhibited by the presence of a homogeneous catalyst.

Figure 4.5. Comparing Inhibition of **1** on Each Heterogeneous Catalyst[a]

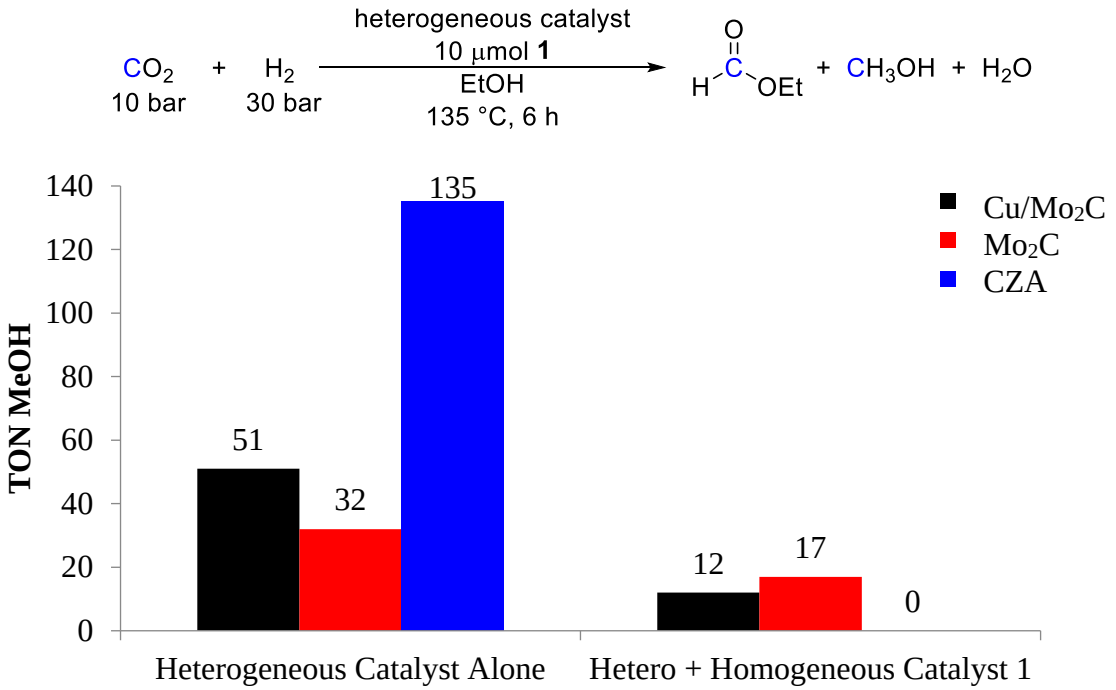

[a]**Conditions:** 11 µmol of Cu/Mo_2C or Mo_2C or 8 µmol CZA catalyst, 10 µmol **1** [$Ru(PMe_3)_4(OAc)Cl$], 3 mL of EtOH, 10 bar CO_2, 30 bar H_2, 135 °C, 6 h. Yields determined by ^{1}H NMR spectroscopy. Max TON ~1600 or ~2300.

4.2.3. Exploration of Different Pathways for Cooperative CO_2 Hydrogenation via an Ester Intermediate

Thus far, we had been unsuccessful in generating a functional heterogeneous-homogeneous catalyzed ester cascade system, let alone an improved ester cascade system. Even after studying a variety of homogeneous and heterogeneous catalyst, we were unable to circumvent the homogeneous catalyst inhibiting the heterogeneous catalyst. At this point we directed our attention to utilizing a different cascade pathway (Scheme 4.8). Having seen no success with the ester pathway, we focused on accessing the formic acid, formate, or amide[31] cascade pathway, all of which share formic acid as a common intermediate (Scheme 4.8).

Scheme 4.8. Different CO_2 to Methanol Cascade Pathways

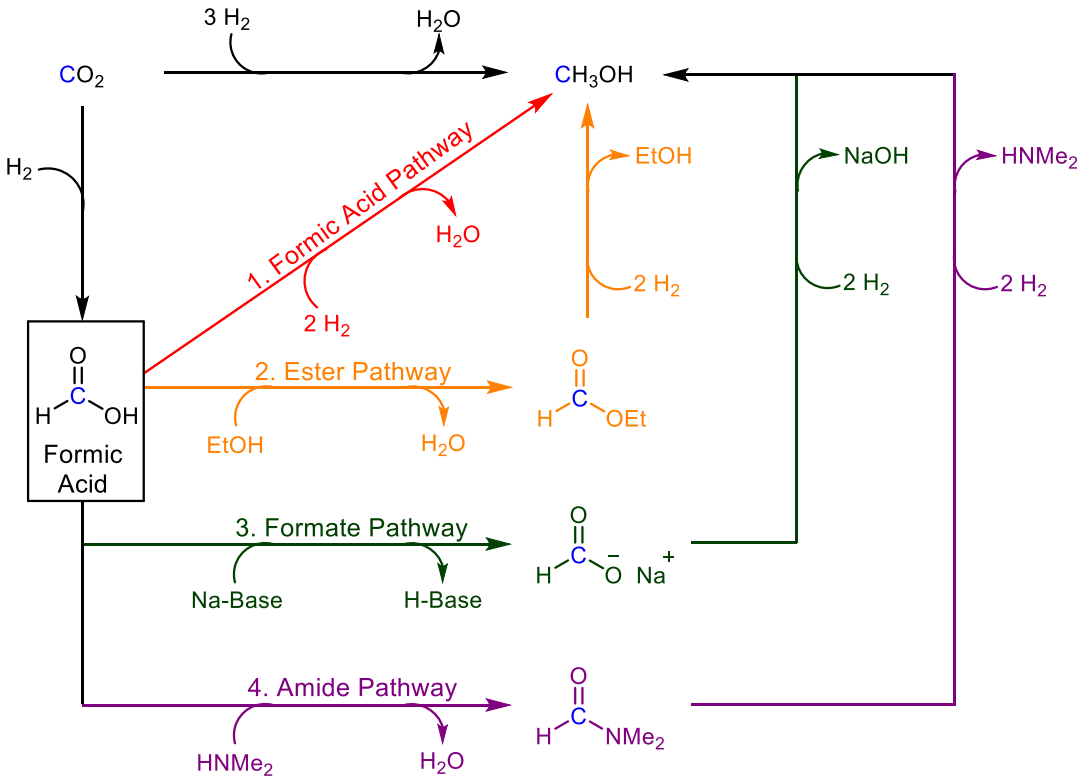

We first investigated whether Cu/Mo_2C was active in the formic acid pathway (Table 4.11). It is important to note that although the reaction was no longer ran in ethanol, once a single hydrogenation of formic acid occurs, the alcohol can then undergo an esterification reaction with formic acid to generate the ester which can then be hydrogenated; effectively,

once Cu/Mo_2C hydrogenates a single molecule of formic acid the pathway can switch from the formic acid pathway (Scheme 4.8, Path 1) to the ester cascade pathway (Scheme 4.9, Path 2).

Testing Cu/Mo_2C for formic acid hydrogenation, we were pleased to see that Cu/Mo_2C was indeed active in the formic acid pathway generating 49 turnovers of methanol, corresponding to 70% yield in 6 hours (Table 4.11, Entry 1). Importantly, no methyl formate was observed. Next, Cu/Mo_2C was studied for CO_2 hydrogenation through the formic acid cascade pathway (Table 4.11, Entries 2–4). Increased activity was seen when using THF as the solvent compared to water, which we hypothesized could be a result of water coordinating to the active sites of the heterogeneous catalyst. Moving to a solvent free system, we found the highest turnovers of methanol at 73 (Table 4.11, Entry 4). We proposed that this increased reactivity was a result of a higher concentration of the substrates (CO_2 and H_2) at the active site of the catalyst. Finally, when coupling Cu/Mo_2C with the homogenous catalyst **5** in water, we once again saw inhibition of the heterogeneous catalyst dropping the turnovers of methanol from 16 to 7 (Table 4.11, Entry 5). Although Cu/Mo_2C was active in the formic acid cascade pathway, we were still unable to generate a cooperative heterogeneous-homogeneous system.

Table 4.11. Cu/Mo_2C in the Formic Acid Pathway

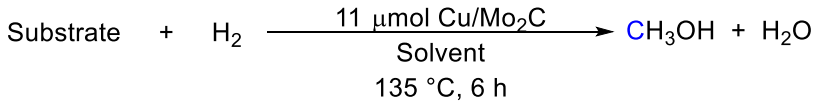

Entry[a]	Substrate	Homogeneous Catalyst	Solvent	TON Methanol
1[b]	Formic acid	—	THF	49
2	CO_2	—	THF	39
3	CO_2	—	H_2O	16
4	CO_2	—	—	73
5	CO_2	**5**	H_2O	7

[a]**Conditions:** 11 μmol heterogeneous catalyst, 3 mL of solvent, 10 bar CO_2, 30 bar H_2, 135 °C for 6 h. Yields determined by ^{1}H NMR spectroscopy. Max TON for Entry 1 ~70 and Entries 2–4 ~1600. [b]0.77 mmol formic acid, 40 bar H_2.

We next compared Cu/Mo_2C, Mo_2C, and CZA in the formic acid pathway. Consistent with previously results, CZA was the most active heterogeneous catalyst for this transformation

(Table 4.12, Entry 3). Also, Mo_2C was again the least active producing only 20 turnovers of methanol (Table 4.12, Entry 2). Methyl formate was not observed in any of the reactions. Additionally, the ester cascade system was more active generating higher turnovers of methanol (up to 135 TON) with all three heterogeneous catalysts tested.

Table 4.12. Comparing Cu/Mo_2C, Mo_2C, and CZA in the Formic Acid Pathway

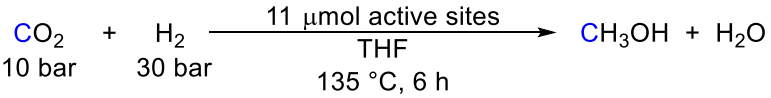

Entry[a]	Hetero Catalyst	TON Methyl Formate	TON Methanol
1	Cu/Mo_2C	0	39
2	Mo_2C	0	20
3	CZA	0	78

[a]**Conditions:** 11 μmol Cu/Mo_2C or Mo_2C or 8 μmol of CZA, 3 mL of THF, 10 bar CO_2, 30 bar H_2, 135 °C for 6 h. Yields determined by ^1H NMR spectroscopy. Max TON ~1600.

Next, Cu/Mo_2C and CZA were investigated for DMF hydrogenation, a key step in the amide cascade pathway (Scheme 4.8, Pathway 4). The hydrogenation of DMF presented an interesting selectivity challenge (Scheme 4.9). Either the C–O or the C–N bond of the amide can be cleaved, generating either trimethylamine (C–O cleavage) or methanol and dimethylamine (C–N cleavage). Ultimately, we desired to selectivity cleave the C-N bond as our target product was methanol. We found that both Cu/Mo_2C and CZA were active for DMF hydrogenation at mild conditions (Table 4.13). Interestingly, both heterogeneous catalysts gave a mixture of C–O and C–N bond cleavage products at approximately 70% yield (Table 4.13, Entries 1 and 4). Curiously, both catalysts produced nearly the same percentage of methanol out of all the products formed (68% with Cu/Mo_2C and 67% with CZA) meaning that about 2/3 of the DMF in either case underwent the desired C–N bond cleavage.

Scheme 4.9. Selectivity for DMF Hydrogenation

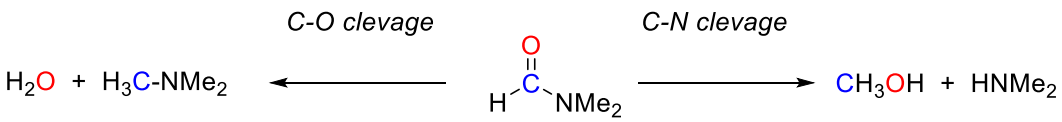

We delve into further studies of the amide cascade system with Cu/Mo_2C. We hypothesized that Cu/Mo_2C was likely sensitive to the basic amines being produced. To test this, an addition of 0.8 mmol of dimethylamine resulted in decreased reactivity of Cu/Mo_2C (from 71% to 66% yield). Additionally, a change in selectivity was observed with Cu/MO_2C producing only trimethylamine and no methanol (Table 4.13, Entries 1 and 2). This confirmed that the amine was inhibiting the heterogeneous catalyst's ability to generate methanol. We next sought to couple Cu/Mo_2C with a homogeneous catalyst in the amide cascade system. Upon addition of **4**, the original catalyst in the amide cascade system,[31] the yield dropped significantly from 71% to 42% (Table 4.13, Entries 1 and 3). Interestingly, the ratio of C–N compared to C–O shifted from about 66% to 75% of the products derived from C–N bond cleavage. Although this shift in selectivity could be trivial and simply a result of the lower yield, it could also indicate something impactful about the heterogeneous catalyst; ultimately, this could indicate that there are two separate active sites on the heterogeneous catalyst with the homogeneous catalyst preferentially binding to the sites for C–O cleavage over the C–N sites. Overall, the amide cascade pathway was operable with both Cu/Mo_2C and CZA, but with the homogeneous catalyst still inhibited the heterogeneous catalyst.

Table 4.13. Exploring Cu/Mo_2C and CZA in Amide Hydrogenation

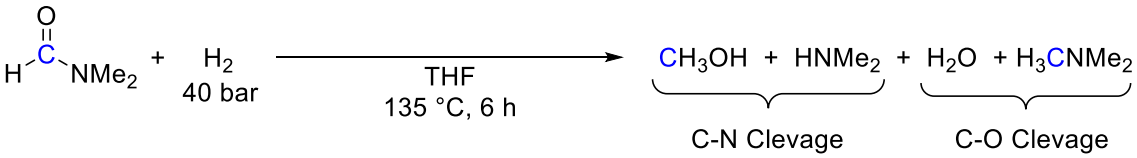

Entry[a]	Hetero Catalyst	Additive	TON Methanol	TON Trimethylamine	Max TON	Yield (%)
1	Cu/Mo_2C	—	36	17	70	71
2[b]	Cu/Mo_2C	$HNMe_2$	0	46	70	66
3[c]	Cu/Mo_2C	**4**	22	7	70	42
4	CZA	—	49	24	100	73

[a]**Conditions:** 11 µmol Cu/Mo_2C or 8 µmol of CZA, 3 mL of THF, 0.8 mmol DMF, 40 bar H_2, 135 °C for 6 h. Yields determined by ^{1}H NMR spectroscopy. [b] 0.21 mL (0.8 mmol) of 3.8 M $HNMe_2$. [c] 10 µmol of **4**.

Exploration of the amide cascade system continued via study of dimethylammonium dimethylcarbamate (DMC). Ultimately, DMC is simply a CO_2 source as it is in equilibrium with CO_2 (the substrate) and dimethylamine (Scheme 4.10) with DMC formation being favored

Scheme 4.10. DMC Equilibrium with Free CO_2 and Dimethylamine

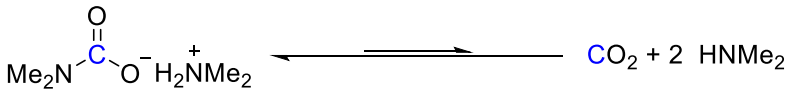

at room temperature and CO_2 being favored at elevated temperatures. The use of DMC allowed for the delay in utilizing a solution of dimethylamine which is tedious to prepare. Once again, both Cu/Mo_2C and CZA were active for hydrogenating DMC (Table 4.14). In terms of selectivity, CZA was much better at hydrogenating the DMF produced, primarily generating the C–O bond cleavage products (Table 4.14, Entry 2). On the other hand, Cu/Mo_2C was worse at DMF hydrogenation, leaving 49 turnovers of DMF and only cleaving 12 turnovers of DMF that was produced (Table 4.14, Entry 1). Once again, $CuMo_2C$ favored C–O bond cleavage in roughly the same ratio as that seen with CZA.

Table 4.14. Exploring Cu/Mo_2C and CZA in DMC Hydrogenation

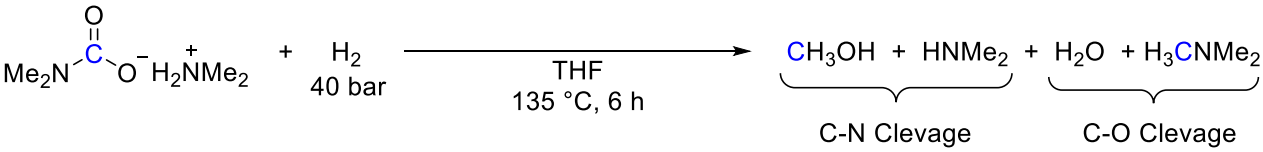

Entry[a]	Hetero Catalyst	TON DMF	TON Methanol	TON Trimethylamine	Max TON	Conversion (%)
1	Cu/Mo_2C	49	1	11	73	84
2	CZA	4	4	45	100	53

[a]**Conditions:** 11 µmol Cu/Mo_2C or 8 µmol of CZA, 3 mL of THF, 0.8 mmol DMC, 40 bar H_2, 135 °C for 6 h. Yields determined by ^{1}H NMR spectroscopy.

Both Cu/Mo_2C and CZA were applied to the amide cascade system starting from CO_2 (Table 4.15). In accordance with Table 4.14, CZA was a better DMF hydrogenation catalyst compared to Cu/Mo_2C converting nearly all the DMF produced onto methanol (Table 4.15, Entries 3 and 4). Interestingly, Cu/Mo_2C outperformed CZA for the first time in the three pathways studied producing higher turnovers of DMF and methanol (Table 4.15). With 0.8

mmol of dimethylamine present, Cu/Mo_2C generated 76 turnovers of products, while CZA generated 38 turnovers (Table 4.15, Entry 1 compared to 3). At increased amounts of dimethylamine, Cu/Mo_2C once again gave higher turnovers of products (Table 4.14, Entry 2 compared to 4). We attributed this phenomenon of CZA being less active than Cu/Mo_2C to the fact that CZA has proven to be more sensitive and more easily inhibited than Cu/Mo_2C in our previous studies (see Figure 4.5 and Tables 4.10, 4.13, and 4.14). At lower amounts of dimethylamine, both catalysts had about the same selectivity for C–N compared to C–O bond cleavage, with both slightly favouring C–O (Table 4.15, Entries 1 and 3). Increasing the dimethylamine, a change in selectivity was seen (Table 4.15, Entries 2 and 4); now both catalysts strongly favor C–O cleavage.

Table 4.15. Exploring Cu/Mo_2C and CZA in the Amide Cascade System Hydrogenation

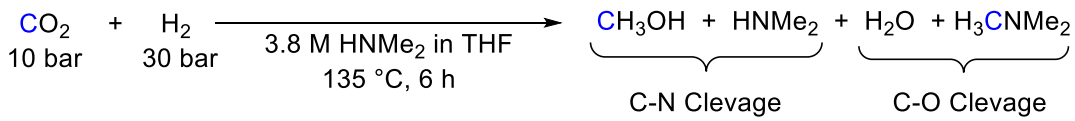

Entry	Hetero Catalyst	mmol $HNMe_2$	TON DMF	TON Methanol	TON Trimethylamine	Total TON
1	Cu/Mo_2C	0.8	46	12	18	76
2[b]	Cu/Mo_2C	1.6	99	0	28	127
3	CZA	0.8	7	12	19	38
4[b]	CZA	1.6	9	3	94	106

[a]**Conditions:** 11 µmol Cu/Mo_2C or 8 µmol of CZA, 3 mL of THF, 0.21 mL of 3.8 M $HNMe_2$ in THF, 10 bar CO_2, 30 bar H_2, 135 °C for 6 h. Yields determined by ^{1}H NMR spectroscopy. [b]0.42 mL of 3.8 M $HNMe_2$ in THF.

No attempt was made to couple Cu/Mo_2C or CZA with a homogeneous catalyst in the amide cascade system starting from CO_2. The only homogenous catalyst active in the amide cascade system at the time was **4**, Our findings in Table 4.13, showed that under nearly analogous conditions, **4** inhibited Cu/Mo_2C. Due to CZA's sensitivity to homogeneous catalysts and dimethylamine, coupling it with a homogeneous catalyst was also not explored.

Ultimately, the study of different CO_2 to methanol cascade pathways showed the breadth and limitations of these heterogeneous catalysts. All three heterogeneous catalysts, Cu/Mo_2C, Mo_2C, and CZA were active in the formic acid pathway, with CZA being the most

active and Mo_2C being the least. The formic acid pathway was less active than the ester cascade pathway. Both Cu/Mo_2C and CZA were studied in the amide cascade pathway looking at DMF, DMC, and CO_2 hydrogenation. Once again, CZA outperformed Cu/Mo_2C when starting with DMF, but when dimethylamine was present in large amounts (both DMC and CO_2 hydrogenation), Cu/Mo_2C was able to outperform CZA , likely due to CZA's sensitivity to Lewis bases. Even when changing the pathway from CO_2 to methanol, all attempts to couple these heterogeneous catalysts with homogeneous catalysts were unsuccessful, leading to inhibition in all cases.

4.3. Conclusions

Although a homogeneous-heterogeneous cascade system could not be realized due to inhibition, there were several important findings. The three heterogeneous catalysts that were tested, Cu/Mo_2C, Mo_2C, and CZA were all active in the ester pathway at very mild conditions for a heterogeneous catalyst (135 °C and 40 bar) with CZA being the most active and Mo_2C being the least reactive. None of the heterogeneous catalysts studied worked cooperatively with the homogeneous catalysts explored (**1**–**5**) and instead, significant inhibition was seen. The most active catalyst, CZA was the most inhibited by homogeneous catalyst **1**, while Mo_2C, the least active catalyst was the least inhibited maintaining 50% of its original reactivity. All three heterogeneous catalysts were active in the formic acid pathway with CZA once again being the most active and Mo_2C being the least active. Attempts to couple the heterogeneous catalysts with homogenous catalyst **5** once again lead to severe inhibition. Finally, Cu/Mo_2C and CZA were tested in the amide cascade system and DMF hydrogenation. Both were active for DMF hydrogenation, giving nearly the same selectivity (~68%) for C–N bond scission to generate methanol. In the full amide cascade system starting from CO_2, it was apparent that CZA was better at hydrogenating DMF compared to Cu/Mo_2C. Ultimately, the large amounts of $HNMe_2$

amine present in the amide cascade system likely led to inhibition of the heterogeneous catalysts. Overall, attempts to couple a homogeneous and heterogeneous catalyst to reap the benefits of both was non-trivial and led to only the catalysts inhibiting one another.

4.4. Experimental Procedures

4.4.1. General Procedures and Materials and Methods

General Procedures

All manipulations were carried out under a nitrogen atmosphere using standard Schlenk line or glove box techniques unless otherwise noted. All high-pressure reactions were carried out using a Parr Model 5000 Multiple Reactor system that includes six 45 mL vessels equipped with flat-gaskets and head mounting valves. All reactors were equipped with glass liners that were manufactured to fit the well of the reactor; however, there was a small gap between the outer side of glass liner and the reactor well. This dead space required 1.5 mL of solvent to fill it. This was done to precautionarily prevent the solvent or reaction products from distilling out of the glass liner and getting stuck in the dead space where reaction with the catalyst was not possible. The system was operated by a 4871process controller and SpecView version 2.5 software. All pressures are reported from the SpecView interface at room temperature. NMR spectra were obtained on Varian VNMRs: 400 MHz (400 MHz for ^{1}H) or 700 MHz (700 MHz for ^{1}H). Chemical shifts are reported in parts per million (ppm) and are referenced to an internal standard. Unless otherwise noted, the NMR yields were based on methanol (δ= 3.16 ppm) and were quantified using DMF (δ= 7.93 ppm) or 1,3,5-trimethoxybenzene (δ= 6.02 ppm) as an internal standard in dimethylsulfoxide-d_6 (DMSO-d_6). For each NMR experiment, 4 scans were collected, a 35 second relaxation delay was used, and a pulse angle of 90° was applied.

Materials and Methods

Tetrahydrofuran (THF) was purified using an Innovative Technologies (IT) solvent purification system consisting of a copper catalyst, activated alumina, and molecular sieves. Dimethylsulfoxide-d_6 (DMSO-d_6, Cambridge Isotope Laboratories) was purchased from the supplier and used as received. Ethanol (200 proof, anhydrous, ≥99.5%) was purchased from Sigma Aldrich in a Sure/Seal™ bottle. Homogeneous catalysts **1**,[3] **3**,[29] **5**[21] were synthesized according to literature procedure. Scandium (III) triflate (99%), **2**, was purchased from Sigma Aldrich. The catalyst, Ru-Macho, **4** was purchased from Strem Chemicals (98%) and used as received. Formic acid (>95%) was purchased from Sigma Aldrich, degassed, and used without further purification. Deionized water was degassed for 1 hour before use. Anhydrous N,N-dimethylformamide (DMF, 99.8%) was obtained from Alfa Aesar and used without further purification. Dimethylamine (99%) was purchased from Sigma Aldrich and used to prepare a 3.8 M in THF solution according to literature procedure.[31] Dimethylammonium dimethylcarbamate (DMC) was purchased from Sigma Aldrich, degassed, and used without further purification. Ultra-high purity hydrogen (99.999%) and carbon dioxide (99.9%) were purchased from Metro Welding.

Reactor Descriptions

A single Parr reactor type was employed. All are 45 mL and are composed of a well (in which the solid and liquid reagents are charged) and a head, which contains various attachments as described below. Each is made of Hastelloy C, and the wells are 7.5 cm tall and 3 cm in diameter. The heads consist of a pressure transducer and two inlet/outlet valves that can connect to a Parr Model 5000 Multiple Reactor system described above, a safety release valve, and a well for a thermocouple (Figure 4.6).

Figure 4.6. Picture of Reactor with the Parts of the Reactor Labeled

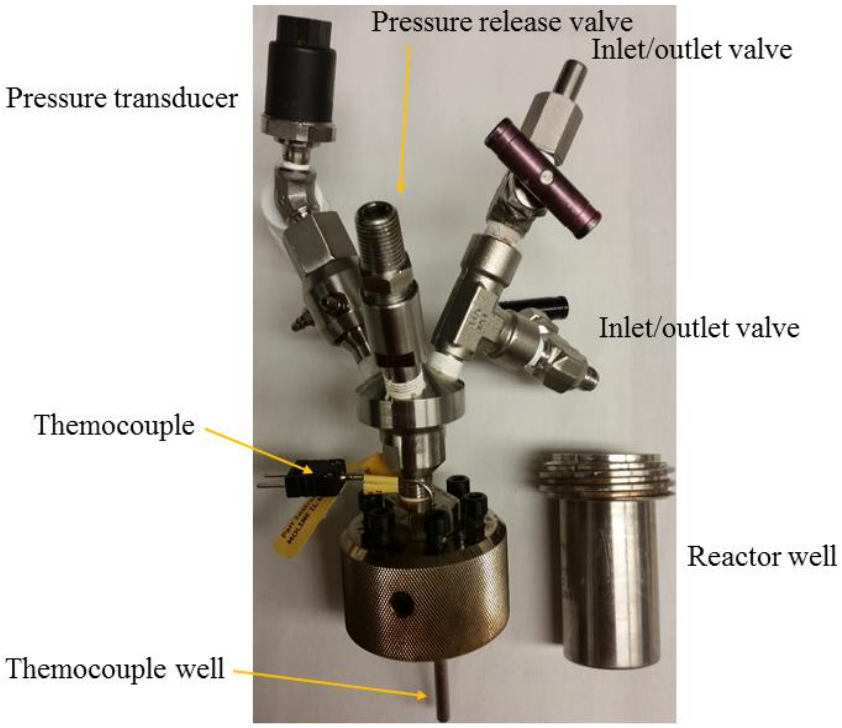

Reaction Work-up

At the reaction end time, the reactors were removed from the Parr Multiple Reactor system. The reactors were transferred to a fume hood where they were secured by clamps and cooled for 10 minutes at room temperature before work-up. In the meantime, each Parr reactor's overnight status was checked by looking at the plot charting the continuous temperature and pressure read from each reactor. Any abnormalities, such as large changes greater than 5 °C or 3 bar, were noted. The small cold traps that were used for condensing the reaction products were removed from the oven and allowed to cool. Liquid nitrogen was obtained and a dewar was filled to cool the Schlenk line trap as well as the reactor's small cold trap.

Once the small trap was cool, the work-up was started (see Figure 4.7). Metering valves were attached to the reactor's inlet/outlet valve. The metering valve's tubing was attached to the outer opening of the cold trap and the trap was placed into a liquid nitrogen dewar where it chilled for about 5 minutes. The reactor was then opened via the inlet/outlet valve while the

metering valve was closed. The metering valve was then used to slowly and carefully release excess pressure from the reactor. The CO_2 that was released condensed inside the cold trap. After about 3 minutes, the pressure coming through the trap was minimal, the metering valve was shut and Schlenk line tubing was attached to the other, central tube of the small trap. Vacuum was then applied to the trap. Once the vacuum had stabilized, the Schlenk line was closed resulting in static vacuum within the small trap between the Schlenk line and metering valve. Next, the metering valve was opened all the way and closed. The trap equilibrated for 2 minutes, before opening the Schlenk line again to pull active vacuum. This cycling was repeated until the vacuum has stabilized and did not significantly increase when opened to the Schlenk line (normally 6 cycles).

Figure 4.7. Picture of Reactor Being Worked-up

Next, the reactors were transferred to water baths set to 50 °C. After two minutes, vacuum was then applied to the cold trap (still in liquid nitrogen). Once the vacuum had stabilized, the Schlenk line was closed resulting in static vacuum within the small trap between the Schlenk line and metering valve. Next, the metering valve was opened all the way and

closed. After 2 minutes of equilibration, the Schlenk line was opened to pull active vacuum. This cycling was repeated until the vacuum had stabilized and did not significantly increase when opened to the Schlenk line. At this time, the metering valve was opened (exposing the reactor interior to active vacuum) and the vacuum was monitored to ensure that there was no increase in the pressure. The system remained open to active vacuum for 5 minutes at which time the metering valve and Schlenk line were closed.

The cold trap was then removed from the liquid nitrogen bath to thaw. The tubing to the Schlenk line and metering valve were carefully, but immediately removed. The cold trap was placed into a beaker to thaw. DMF (80 μL) was immediately added to the center opening of the trap followed by 0.2 mL of d_6-DMSO.

The reactors were cleaned while the cold trap was thawing. The reactors were removed from the water bath and metering valve removed. The reactor top was then disassembled. If the vac transfer was performed properly, the bottom of the reactor only contained the solid, dry heterogeneous catalyst. The liner was removed, and catalyst color and consistency were noted. The catalyst was transferred to a tarred vial where the mass was then recorded. The glass liners were cleaned with aqua regia, rinsed thoroughly with water and acetone, and dried and stored in the oven. The reactor was wiped clean before being rinsed with acetone followed by water and finally rinsed with acetone. The reactor was wiped dry. The reactor was then scrubbed with scour pads before being rinsed with acetone, water, and acetone. The reactor bottom dried in the oven for 10–15 minutes. The reactor's headspace within the top portion was thoroughly cleaned with acetone and water by passing solvent through the inlet/outlet value through the headspace and out of the bottom of the reactor top. Nitrogen was then passed through outlet valve to dry the reactor top interior.

While the vessels were being cleaned, the cold traps were consistently monitored. When the solution in the trap was still cold, but unfrozen, the trap was mixed well to ensure a

homogenous solution. The solution was then poured into a 4 mL vial and sealed with a Teflon cap. NMR tubes were charged with 0.5 mL of d_6-DMSO. Once the vial of reaction solution was at room temperature 3–4 drops of the solution were added to the NMR tube, which was then capped and thoroughly shaken to ensure mixing. If large amounts of base ($HNMe_2$) were present, the solution was neutralized with HCl.

4.4.2. Catalyst Preparation[28]

The Mo_2C catalyst was synthesized from an ammonium molybdate precursor (Alfa Aesar) using a temperature programmed reaction (TPR) technique. The Mo_2C was prepared by reducing ammonium molybdate in H_2 at 350 °C for 12 h, followed by treatment in 15% CH_4/H_2 at 590 °C for 2h, and the resulting material was then quenched to room temperature. Other details regarding the synthesis procedures have been described in previous reports.[26,28] All the freshly-synthesized Mo_2C-based catalysts were transferred to and stored in an H_2O and O_2 free glovebox filled with Ar (MBraun, H_2O <0.1 ppm, O_2 < 5ppm) prior to use to avoid any exposure to O_2.

Metals were deposited onto the Mo_2C supports using a wet impregnation technique. The carbides were passivated prior to exposure to air to avoid bulk oxidation of the material. To avoid passivation and deposit metals directly onto the native Mo_2C surfaces (as opposed to a passivated surface), the freshly-synthesized materials were transferred under an inert gas (CH_4/H_2 or He) into an aqueous solution containing a target concentration of $Cu(NO_3)_2$ then allowed to interact for at least 20 h. Argon was continuously purging through the solutions (during the wet impregnation process) to deaerate and agitate the solution. The synthesized Cu/Mo_2C catalyst showed pyrophoricity, indicating the absence of surface passivation on the final materials. The resulting catalyst slurry was dried at 110 °C for 2 h and reduced in flowing H_2 (400 mL/min) at 300 °C for 4 h to decompose the nitrate and produce the Cu domains.

CZA ($Cu/ZnO/Al_2O_3$) was acquired from commercial vendors (SüdChemie/Clariant) and used after pretreatment. CZA was pretreated in 4% H_2/N_2 (200 ml/min) by first heating the material from 25 °C to 200 °C at a rate of 4 °C/min and holding at 200 °C for 4 h. The material was cooled to room temperature after the pretreatment and transferred to a glovebox.

Surface areas of the materials were determined from N_2 physisorption isotherms collected using a Micromeritics ASAP 2010 analyzer. The isotherms were analyzed using the Brunauer–Emmett–Teller (BET) method. Prior to the measurements, the catalysts were degassed (< 5 mm Hg) for at least 4 h at elevated temperatures (350 °C for the Mo_2C-based catalysts, 200 °C for CZA). The bulk crystalline structures of the catalysts were characterized using X-ray diffraction performed using a Rigaku Miniflex diffractometer with Cu Kα radiation (λ = 1.5418 Å). The diffraction patterns were obtained by scanning 2θ from 10 to 90° at a scan rate of 5 °/min. Inductively coupled plasma (ICPOES, Varian 710-ES analyzer) was used to determine the metal compositions for Mo_2C.

All the heterogeneous catalysts were prepared and characterized in the Thompson Lab at the UM Chemical Engineering Department. The catalysts were placed in vials and then packed in a secondary container under Ar to be transferred (in an oxygen-free environment) to Sanford Lab at UM Chemistry Department for activity measurement.

4.4.3. Hydrogenation Reactions

Stirred CO_2 to Methanol Ester Cascade Reactions (Tables 4.1–4.2)

The heterogeneous catalyst Cu/Mo_2C (24 mg, 8 μmol of active sites) was weighed and loaded directly into a glass liner containing the appropriate stir bar (either a flea, octagon, or oval Spinbar). Ethanol (1.5 mL) was placed into the well of the reactor. The glass liner was then placed into the reactor and charged with 1.5 mL of ethanol. The reactor was immediately sealed and removed from the glovebox. The vessel was connected to the Parr Multiple Reactor

System, and the manifold was thoroughly purged (1 minute and then cycled 8 times) with bone dry grade CO_2 (99.9%). The vessel was then pressurized to 10 bar with CO_2. The manifold was then thoroughly purged (1 minute and then vented 15 times) with Ultra High Purity H_2 (99.999%). The vessel was then pressurized with 30 bar with Ultra High Purity H_2 at room temperature to reach a total pressure of 41 bar. The reaction was heated at 135 °C with a stir rate of 800 rotations per minute (RPM). The heating was conducted using Specview software. After 19 hours of heating, the reactor was worked-up as described in Section 4.4.1.

Non-Stirred CO_2 to Methanol Ester Cascade Reactions (Tables 4.3)

The heterogeneous catalyst Cu/Mo_2C (24 mg, 8 μmol of active sites) was weighed and loaded directly into a glass liner. Ethanol (1.5 mL) was placed into the well of the reactor. The glass liner was then placed into the reactor and charged with 1.5 mL of ethanol. The reactor was immediately sealed and removed from the glovebox. The vessel was connected to the Parr Multiple Reactor System, and the manifold was thoroughly purged (1 minute and then cycled 8 times) with bone dry grade CO_2 (99.9%). The vessel was then pressurized to 10 bar with CO_2. The manifold was then thoroughly purged (1 minute and then vented 15 times) with Ultra High Purity H_2 (99.999%). The vessel was then pressurized with 30 bar with Ultra High Purity H_2 at room temperature to reach a total pressure of 41 bar. The reaction was heated at 135 °C with a stir rate of 800 RPM (regardless of the absence of a stir bar). The heating was conducted using Specview software. After the appropriate amount of time at temperature, the reactor was treated as described in the "Reaction Work-up" section above (see 4.4.1.).

Exploration of Catalyst Lifetime in CO_2 to Methanol Ester Cascade Reactions (Table 4.4 and Figure 4.3)

The heterogeneous catalyst Cu/Mo_2C (24 mg, 8 μmol of active sites) was weighed and loaded directly into a glass liner. Ethanol (1.5 mL) was placed into the well of the reactor. The glass liner was then placed into the reactor and charged with 1.5 mL of ethanol. The reactor was immediately sealed and removed from the glovebox. The vessel was connected to the Parr Multiple Reactor System, and the manifold was thoroughly purged (1 minute and then cycled 8 times) with bone dry grade CO_2 (99.9%). The vessel was then pressurized to 10 bar with CO_2. The manifold was then thoroughly purged (1 minute and then vented 15 times) with Ultra High Purity H_2 (99.999%). The vessel was then pressurized with 30 bar with Ultra High Purity H_2 at room temperature to reach a total pressure of 41 bar. The reaction was heated at 135 °C with a stir rate of 800 RPM (regardless of the absence of a stir bar). The heating was conducted using Specview software. After the appropriate amount of time (6–314 h) at 135 °C, the reactor was treated as described in the "Reaction Work-up" section above (see 4.4.1.).

Coupling Cu/Mo_2C with homogeneous catalysts in CO_2 to Methanol Ester Cascade Reactions (Tables 4.5–4.7)

The heterogeneous catalyst Cu/Mo_2C (24 mg, 8 μmol of active sites for Table 4.5 and 33 mg, 11 μmol of active sites for Tables 4.6 and 4.7) was weighed and loaded directly into a glass liner. Ethanol (1.5 mL) was placed into the well of the reactor. The glass liner was then placed into the reactor. A solution of the homogeneous catalyst was prepared in a 4 mL vial with 1.5 mL of ethanol and added to the glass liner. The reactor was immediately sealed and removed from the glovebox. The vessel was connected to the Parr Multiple Reactor System, and the manifold was thoroughly purged (1 minute and then cycled 8 times) with bone dry grade CO_2 (99.9%). The vessel was then pressurized to 10 bar with CO_2. The manifold was

then thoroughly purged (1 minute and then vented 15 times) with Ultra High Purity H_2 (99.999%). The vessel was then pressurized with 30 bar with Ultra High Purity H_2 at room temperature to reach a total pressure of 41 bar. The reaction was heated at 135 °C with a stir rate of 800 RPM (regardless of the absence of a stir bar). The heating was conducted using Specview software. After the appropriate amount of time at 135 °C (16 h for Table 4.5, 19 h for Table 4.6, and 6 h for Table 4.7), the reactor was treated as described in the "Reaction Work-up" section above (see 4.4.1.).

Utilization of Cu/Mo_2C or Mo_2C with homogeneous catalysts in CO_2 to Methanol Ester Cascade Reactions (Table 4.8, Entries 1 and 3): Without Homogeneous Catalyst

The heterogeneous catalyst Cu/Mo_2C (33 mg, 11 μmol of active sites) or Mo_2C (28 mg, 11 μmol of active sites) was weighed and loaded directly into a glass liner. Ethanol (1.5 mL) was placed into the well of the reactor. The glass liner was then placed into the reactor and charged with 1.5 mL of ethanol. The reactor was immediately sealed and removed from the glovebox. The vessel was connected to the Parr Multiple Reactor System, and the manifold was thoroughly purged (1 minute and then cycled 8 times) with bone dry grade CO_2 (99.9%). The vessel was then pressurized to 10 bar with CO_2. The manifold was then thoroughly purged (1 minute and then vented 15 times) with Ultra High Purity H_2 (99.999%). The vessel was then pressurized with 30 bar with Ultra High Purity H_2 at room temperature to reach a total pressure of 41 bar. The reaction was heated at 135 °C with a stir rate of 800 RPM (regardless of the absence of a stir bar). The heating was conducted using Specview software. After 6 h at 135 °C, the reactor was treated as described in the "Reaction Work-up" section above (see 4.4.1.).

Utilization of Cu/Mo_2C or Mo_2C with homogeneous catalysts in CO_2 to Methanol Ester Cascade Reactions (Table 4.8, Entries 2 and 4): With Homogeneous Catalyst

The heterogeneous catalyst Cu/Mo_2C (33 mg, 11 µmol of active sites) or Mo_2C (28 mg, 11 µmol of active sites) was weighed and loaded directly into a glass liner. Ethanol (1.5 mL) was measured via a 1 mL syringe and placed into the well of the reactor. The glass liner was then placed into the reactor. The homogeneous catalyst was weighed into a 4 mL vial and 1.5 mL of ethanol were added via a 1 mL syringe. The solution was transferred to the glass liner. The reactor was immediately sealed and removed from the glovebox. The vessel was connected to the Parr Multiple Reactor System, and the manifold was thoroughly purged (1 minute and then cycled 8 times) with bone dry grade CO_2 (99.9%). The vessel was then pressurized to 10 bar with CO_2. The manifold was then thoroughly purged (1 minute and then vented 15 times) with Ultra High Purity H_2 (99.999%). The vessel was then pressurized with 30 bar with Ultra High Purity H_2 at room temperature to reach a total pressure of 41 bar. The reaction was heated at 135 °C with a stir rate of 800 RPM (regardless of the absence of a stir bar). The heating was conducted using Specview software. After 6 h at 135 °C, the reactor was treated as described in the "Reaction Work-up" section above (see 4.4.1.).

Exploration of CZA for Ethyl Formate Hydrogenation (Scheme 4.7)

The heterogeneous catalyst CZA (41 mg, 8 µmol of active sites) was weighed and loaded directly into a glass liner. Ethanol (1.5 mL) was placed into the well of the reactor. The glass liner was then placed into the reactor and charged with 1.5 mL of ethanol and 50 µL (0.63 mmol) of ethyl formate. The reactor was immediately sealed and removed from the glovebox. The vessel was connected to the Parr Multiple Reactor System, and the manifold was thoroughly purged (1 minute and then vented 15 times) with Ultra High Purity H_2 (99.999%). The vessel was then pressurized with 40 bar with Ultra High Purity H_2 at room temperature to

reach a total pressure of 41 bar. The reaction was heated at 135 °C with a stir rate of 800 RPM (regardless of the absence of a stir bar). The heating was conducted using Specview software. After 6 h at 135 °C, the reactor was treated as described in the "Reaction Work-up" section above (see 4.4.1.).

Utilization of CZA in CO_2 to Methanol Ester Cascade Reactions (Table 4.9)

The heterogeneous catalyst CZA (41 mg, 8 μmol of active sites) was weighed and loaded directly into a glass liner. Ethanol (1.5 mL) was placed into the well of the reactor. The glass liner was then placed into the reactor and charged with 1.5 mL of ethanol. The reactor was immediately sealed and removed from the glovebox. The vessel was connected to the Parr Multiple Reactor System, and the manifold was thoroughly purged (1 minute and then cycled 8 times) with bone dry grade CO_2 (99.9%). The vessel was then pressurized to 10 bar with CO_2. The manifold was then thoroughly purged (1 minute and then vented 15 times) with Ultra High Purity H_2 (99.999%). The vessel was then pressurized with 30 bar with Ultra High Purity H_2 at room temperature to reach a total pressure of 41 bar. The reaction was heated to the appropriate temperature with a stir rate of 800 RPM (regardless of the absence of a stir bar). The heating was conducted using Specview software. After 6 h at the desired temperature, the reactor was treated as described in the "Reaction Work-up" section above (see 4.4.1.).

Utilization of CZA with homogeneous catalysts in CO_2 to Methanol Ester Cascade Reactions (Table 4.10)

The heterogeneous catalyst CZA (41 mg, 8 μmol of active sites) was weighed and loaded directly into a glass liner. Ethanol (1.5 mL) was measured via a 1 mL syringe and placed into the well of the reactor. The glass liner was then placed into the reactor. The homogeneous catalyst was weighed into a 4 mL vial and 1.5 mL of ethanol were added via a 1 mL syringe.

The solution was transferred to the glass liner. The reactor was immediately sealed and removed from the glovebox. The vessel was connected to the Parr Multiple Reactor System, and the manifold was thoroughly purged (1 minute and then cycled 8 times) with bone dry grade CO_2 (99.9%). The vessel was then pressurized to 10 bar with CO_2. The manifold was then thoroughly purged (1 minute and then vented 15 times) with Ultra High Purity H_2 (99.999%). The vessel was then pressurized with 30 bar with Ultra High Purity H_2 at room temperature to reach a total pressure of 41 bar. The reaction was heated at 135 °C with a stir rate of 800 RPM (regardless of the absence of a stir bar). The heating was conducted using Specview software. After 6 h at 135 °C, the reactor was treated as described in the "Reaction Work-up" section above (see 4.4.1.).

Comparing Cu/Mo_2C, Mo_2C, and CZA with homogeneous catalyst 1 in CO_2 to Methanol Ester Cascade Reactions (Figure 4.5)

The heterogeneous catalyst Cu/Mo_2C (33 mg, 11 μmol of active sites) or Mo_2C (28 mg, 11 μmol of active sites) or CZA (41 mg, 8 μmol of active sites) was weighed and loaded directly into a glass liner. Ethanol (1.5 mL) was measured via a 1 mL syringe and placed into the well of the reactor. The glass liner was then placed into the reactor. The homogeneous catalyst was weighed into a 4 mL vial and 1.5 mL of ethanol were added via a 1 mL syringe. The solution was transferred to the glass liner. The reactor was immediately sealed and removed from the glovebox. The vessel was connected to the Parr Multiple Reactor System, and the manifold was thoroughly purged (1 minute and then cycled 8 times) with bone dry grade CO_2 (99.9%). The vessel was then pressurized to 10 bar with CO_2. The manifold was then thoroughly purged (1 minute and then vented 15 times) with Ultra High Purity H_2 (99.999%). The vessel was then pressurized with 30 bar with Ultra High Purity H_2 at room temperature to reach a total pressure of 41 bar. The reaction was heated at 135 °C with a stir

rate of 800 RPM (regardless of the absence of a stir bar). The heating was conducted using Specview software. After 6 h at 135 °C, the reactor was treated as described in the "Reaction Work-up" section above (see 4.4.1.).

Exploration of Cu/Mo_2C for Formic Acid Hydrogenation (Table 4.11, Entry 1)

The heterogeneous catalyst Cu/Mo_2C (33 mg, 11 μmol of active sites) was weighed and loaded directly into a glass liner. THF (1.5 mL) was placed into the well of the reactor. The glass liner was then placed into the reactor and charged with 1.5 mL of THF and 0.77 mmol of formic acid. The reactor was immediately sealed and removed from the glovebox. The vessel was connected to the Parr Multiple Reactor System, and the manifold thoroughly purged (1 minute and then vented 15 times) with Ultra High Purity H_2 (99.999%). The vessel was then pressurized with 40 bar with Ultra High Purity H_2 at room temperature to reach a total pressure of 41 bar. The reaction was heated at 135 °C with a stir rate of 800 RPM (regardless of the absence of a stir bar). The heating was conducted using Specview software. After 6 h at 135 °C, the reactor was treated as described in the "Reaction Work-up" section above (see 4.4.1.).

Exploration of Cu/Mo_2C in the Formic Acid Pathway (Table 4.11, Entries 2–3)

The heterogeneous catalyst Cu/Mo_2C (33 mg, 11 μmol of active sites) was weighed and loaded directly into a glass liner. THF or H_2O (1.5 mL) was measured via a 1 mL syringe and placed into the well of the reactor. The glass liner was then placed into the reactor. To the glass liner, 1.5 mL of THF or H_2O were added via a 1 mL syringe. The reactor was immediately sealed and removed from the glovebox. The vessel was connected to the Parr Multiple Reactor System, and the manifold was thoroughly purged (1 minute and then cycled 8 times) with bone dry grade CO_2 (99.9%). The vessel was then pressurized to 10 bar with CO_2. The manifold was

then thoroughly purged (1 minute and then vented 15 times) with Ultra High Purity H_2 (99.999%). The vessel was then pressurized with 30 bar with Ultra High Purity H_2 at room temperature to reach a total pressure of 41 bar. The reaction was heated to 135 °C with a stir rate of 800 RPM (regardless of the absence of a stir bar). The heating was conducted using Specview software. After 6 h at 135 °C, the reactor was treated as described in the "Reaction Work-up" section above (see 4.4.1.).

Solvent-Free Exploration of Cu/Mo_2C in the Formic Acid Pathway (Table 4.11, Entry 4)

The heterogeneous catalyst Cu/Mo_2C (33 mg, 11 µmol of active sites) was weighed and loaded directly into a glass liner. The glass liner was then placed into the reactor. The reactor was immediately sealed and removed from the glovebox. The vessel was connected to the Parr Multiple Reactor System, and the manifold was thoroughly purged (1 minute and then cycled 8 times) with bone dry grade CO_2 (99.9%). The vessel was then pressurized to 10 bar with CO_2. The manifold was then thoroughly purged (1 minute and then vented 15 times) with Ultra High Purity H_2 (99.999%). The vessel was then pressurized with 30 bar with Ultra High Purity H_2 at room temperature to reach a total pressure of 41 bar. The reaction was heated at 135 °C with a stir rate of 800 RPM (regardless of the absence of a stir bar). The heating was conducted using Specview software. After 6 h at 135 °C, the reactor was treated as described in the "Reaction Work-up" section above (see 4.4.1.).

Coupling of Cu/Mo_2C and a homogeneous catalyst in the Formic Acid Pathway (Table 4.11, Entry 5)

The heterogeneous catalyst Cu/Mo_2C (33 mg, 11 µmol of active sites) was weighed and loaded directly into a glass liner. H_2O (1.5 mL) was measured via a 1 mL syringe and placed into the well of the reactor. The glass liner was then placed into the reactor. The

homogeneous catalyst was weighed into a 4 mL vial and 1.5 mL of H_2O were added via a 1 mL syringe. The solution was transferred to the glass liner. The reactor was immediately sealed and removed from the glovebox. The vessel was connected to the Parr Multiple Reactor System, and the manifold was thoroughly purged (1 minute and then cycled 8 times) with bone dry grade CO_2 (99.9%). The vessel was then pressurized to 10 bar with CO_2. The manifold was then thoroughly purged (1 minute and then vented 15 times) with Ultra High Purity H_2 (99.999%). The vessel was then pressurized with 30 bar with Ultra High Purity H_2 at room temperature to reach a total pressure of 41 bar. The reaction was heated at 135 °C with a stir rate of 800 RPM (regardless of the absence of a stir bar). The heating was conducted using Specview software. After 6 h at 135 °C, the reactor was treated as described in the "Reaction Work-up" section above (see 4.4.1.).

Comparing Heterogeneous Catalysts in the Formic Acid Pathway (Table 4.12)

The heterogeneous catalyst Cu/Mo_2C (33 mg, 11 µmol of active sites) or Mo_2C (28 mg, 11 µmol of active sites) or CZA (41 mg, 8 µmol of active sites) was weighed and loaded directly into a glass liner. THF (1.5 mL) placed into the well of the reactor. The glass liner was then placed into the reactor and charged with1.5 mL of THF. The reactor was immediately sealed and removed from the glovebox. The vessel was connected to the Parr Multiple Reactor System, and the manifold was thoroughly purged (1 minute and then cycled 8 times) with bone dry grade CO_2 (99.9%). The vessel was then pressurized to 10 bar with CO_2. The manifold was then thoroughly purged (1 minute and then vented 15 times) with Ultra High Purity H_2 (99.999%). The vessel was then pressurized with 30 bar with Ultra High Purity H_2 at room temperature to reach a total pressure of 41 bar. The reaction was heated to 135 °C with a stir rate of 800 RPM (regardless of the absence of a stir bar). The heating was conducted using Specview software. After 6 h at 135 °C, the reactor was treated as described in the "Reaction

Work-up" section above (see 4.4.1.) with neutralization included: after adding 3–4 drops of the reaction solution to the NMR tube, the solution was neutralized with HCl due to the presence of large amounts of base ($HNMe_2$). The tube was then capped and thoroughly shaken to ensure mixing.

Exploration of Cu/Mo_2C and CZA for DMF Hydrogenation (Table 4.13, Entries 1, 2, and 4)

The heterogeneous catalyst Cu/Mo_2C (33 mg, 11 μmol of active sites) or CZA (41 mg, 8 μmol of active sites) was weighed and loaded directly into a glass liner. THF (1.5 mL) was placed into the well of the reactor. The glass liner was then placed into the reactor and charged with 1.5 mL of THF and 60 μL (0.8 mmol) of DMF where placed directly into the glass liner. If appropriate, 0.21 mL of 3.8 M $HNMe_2$ in THF were also added to the glass liner. The reactor was immediately sealed and removed from the glovebox. The vessel was connected to the Parr Multiple Reactor System, and the manifold was thoroughly purged (1 minute and then vented 15 times) with Ultra High Purity H_2 (99.999%). The vessel was then pressurized with 40 bar with Ultra High Purity H_2 at room temperature to reach a total pressure of 41 bar. The reaction was heated to 135 °C with a stir rate of 800 RPM (regardless of the absence of a stir bar). The heating was conducted using Specview software. After 6 h at 135 °C, the reactor was treated as described in the "Reaction Work-up" section above (see 4.4.1.) besides the following variation: after adding 3–4 drops of the reaction solution to the NMR tube, the solution was neutralized with HCl due to the presence of large amounts of base ($HNMe_2$). The tube was then capped and thoroughly shaken to ensure mixing.

Coupling of Cu/Mo_2C and a homogeneous catalyst in the DMF Hydrogenation (Table 4.13, Entry 4)

The heterogeneous catalyst Cu/Mo_2C (33 mg, 11 µmol of active sites) was weighed and loaded directly into a glass liner. THF (1.5 mL) was placed into the well of the reactor. The glass liner was then placed into the reactor and charged with a solution of the homogeneous catalyst in 1.5 mL of THF and 60 µL (0.8 mmol) of DMF where placed directly into the glass liner. The reactor was immediately sealed and removed from the glovebox. The vessel was connected to the Parr Multiple Reactor System, and the manifold was thoroughly purged (1 minute and then vented 15 times) with Ultra High Purity H_2 (99.999%). The vessel was then pressurized with 40 bar with Ultra High Purity H_2 at room temperature to reach a total pressure of 41 bar. The reaction was heated at 135 °C with a stir rate of 800 RPM (regardless of the absence of a stir bar). The heating was conducted using Specview software. After 6 h at 135 °C, the reactor was treated as described in the "Reaction Work-up" section above (see 4.4.1.) besides the following variation: after adding 3–4 drops of the reaction solution to the NMR tube, the solution was neutralized with HCl due to the presence of large amounts of base ($HNMe_2$). The tube was then capped and thoroughly shaken to ensure mixing.

Exploration of Cu/Mo_2C and CZA for DMC Hydrogenation (Table 4.14)

The heterogeneous catalyst Cu/Mo_2C (33 mg, 11 µmol of active sites) or CZA (41 mg, 8 µmol of active sites) was weighed and loaded directly into a glass liner. THF (1.5 mL) was measured placed into the well of the reactor. The glass liner was then placed into the reactor and charged with 1.5 mL of THF and 108 mg (0.8 mmol) of DMC. The reactor was immediately sealed and removed from the glovebox. The vessel was connected to the Parr Multiple Reactor System, and the manifold was thoroughly purged (1 minute and then vented 15 times) with Ultra High Purity H_2 (99.999%). The vessel was then pressurized with 40 bar

with Ultra High Purity H_2 at room temperature to reach a total pressure of 41 bar. The reaction was heated to 135 °C with a stir rate of 800 RPM (regardless of the absence of a stir bar). The heating was conducted using Specview software. After 6 h at 135 °C, the reactor was treated as described in the "Reaction Work-up" section above (see 4.4.1.) besides the following variation: after adding 3–4 drops of the reaction solution to the NMR tube, the solution was neutralized with HCl due to the presence of large amounts of base ($HNMe_2$). The tube was then capped and thoroughly shaken to ensure mixing.

Exploration of Cu/Mo_2C and CZA in the Amide Cascade Pathway (Table 4.15)

The heterogeneous catalyst Cu/Mo_2C (33 mg, 11 μmol of active sites) or CZA (41 mg, 8 μmol of active sites) was weighed and loaded directly into a glass liner. THF (1.5 mL) was placed into the well of the reactor. The glass liner was then placed into the reactor and charged with 1.5 mL of THF and 3.8 M $HNMe_2$ (0.21 mL or 0.42 mL) in THF. The vessel was connected to the Parr Multiple Reactor System, and the manifold was thoroughly purged (1 minute and then cycled 8 times) with bone dry grade CO_2 (99.9%). The vessel was then pressurized to 10 bar with CO_2. The manifold was then thoroughly purged (1 minute and then vented 15 times) with Ultra High Purity H_2 (99.999%). The vessel was then pressurized with 30 bar with Ultra High Purity H_2 at room temperature to reach a total pressure of 41 bar. The reaction was heated at 135 °C with a stir rate of 800 RPM (regardless of the absence of a stir bar). The heating was conducted using Specview software. After 6 h at 135 °C, the reactor was treated as described in the "Reaction Work-up" section above (see 4.4.1.) besides the following variation: after adding 3–4 drops of the reaction solution to the NMR tube, the solution was neutralized with HCl due to the presence of large amounts of base ($HNMe_2$). The tube was then capped and thoroughly shaken to ensure mixing.

4.5. References

1. This chapter presents work done in collaboration with Professor Levi Thompson and Yuan Chen at the University of Michigan. The Thompson group prepared the heterogeneous catalysts discussed while the Sanford group ran all catalytic reactions appearing herein. Some overlap may occur with Yuan Chen's dissertation and publications.

2. Huff, C. A.; Sanford, M. S. *J. Am. Chem. Soc.* **2011**, *133*, 18122.

3. Munshi, P.; Main, A. D.; Linehan, J. C.; Tai, C. C.; Jessop, P. G. *J. Am. Chem. Soc.* **2002**, *124*, 7963.

4. Barrett, A.G.M.; Braddock, D.C. *Chem. Commun.* **1997**, 351.

5. Zhang, J.; Leitus, G.; Ben-David, Y.; Milstein, D. *Angew. Chem. Int. Ed*. **2006**, *45*, 1113.

6. Getty, A. D.; Tai, C.-C.; Linehan, J. C.; Jessop, P. G.; Olmstead, M. M.; Rheingold, A. L. *Organometallics*, **2009**, *28*, 5466.

7. Nelson, D. L.; Lehniger, A. L. Cox, M. M. *Lehninger Principles of Biochemistry*, 5th ed.; W. H. Freeman and Company, **2008**.

8. Berg, I. A. *Appl. Environ. Microbiol.* **2011**, *77*, 1925.

9. Olah, G. A.; Goeppert, A.; Prakash, G. K. S. *Beyond Oil and Gas: The Methanol Economy*, 1st ed.; Wiley-VCH, **2006**.

10. Hansen, J. B.; Nielsen, P. E. H. *Handbook of Heterogenous Catalysis*, 2nd ed.; Wiley-VCH, **2008**.

11. Waugh, K.C. *Catal. Letters*, **2012**, *142*, 1153.

12. Li, Y. N.; Ma, R.; He, L. N.; Diao, Z. F. *Catal. Sci. Technol*. **2014**, *4*, 1498.

13. Martino, G.; Courty, P.; Marcilly, C.; Kochloefl, K.; Lunsford, J. H. *Handbook of Heterogeneous Catalysis*; Wiley-VCH: Weinheim, **1997**.

14. Spencer, M. S. *Top. Catal.* **1999**, *8*, 259.

15. Gröger, H. *Chem. Eur. J.* **2001**, *7*, 5246.

16. Kusunoki, Y.; Miyazawa, T.; Kunimori, K.; Tomishige, K. *Catal. Commun.* **2005**, *6*, 645.

17. Sun, K.; Lu, W.; Qiu, F.; Liu, S.; Xu, X. *Appl. Catal., A* **2003**, *252*, 243.

18. Miessler, G. L.; Fischer, P. J.; Tarr, D. A. *Inorganic Chemistry*, 5th ed.; Pearson, **2013.**

19. Huff, C. A.; Kampf, J. W.; Sanford, M. S. *Organometallics* **2012**, 31, 4643.

20. Huff, C. A.; Kampf, J. W.; Sanford, M. S. *Chem. Comm*. **2013**, *49*, 7147.

21. Brewster, T. P.; Rezayee, N. M.; Culakova, Z.; Sanford, M. S.; Goldberg, K. I. *ACS Catal.* **2016**, *6*, 3113.

22. Brewster, T. P.; Miller, A. J. M.; Heinekey, D. M.; Goldberg, K. I. *J. Am. Chem. Soc.* **2013**, *135*, 16022.

23. Grabow, L.C.; Mavrikakis, M. *ACS Catal.* **2013**, 365.

24. Gormley, R. J.; Rao, V. U. S.; Soong, Y.; Micheli, E. *Appl. Catal., A* **1992**, *87*, 81.

25. Iwasa, N.; Terashita, M.; Arai, M.; Takezawa, N. *React. Kinet. Catal. Lett*. **2001**, *74*, 93.

26. Chen, Y.; Choi, S.; Thompson, L.T. *ACS Catal.* **2015**, *5*, 1717.

27. Olah, G. A.; Prakash, G. K. S.; Goeppert, A. *J. Am. Chem. Soc*. **2011**, *133*, 12881.

28. Chen, Y. "Designing Heterogeneous-Based Cascade Catalytic Systems for Carbon Dioxide Hydrogenation." Ph.D. Dissertation, University of Michigan, Ann Arbor, MI, **2016**.

29. Wesselbaum, S.; von Stein, T.; Klankermayer, J.; Leitner, W. *Angew. Chem. Int. Ed.* **2010**, *21*, 7499.

30. Wesselbaum, S.; Moha, V.; Markus, M.; Brosinski, S.; Thenert, K. M.; Kothe, J.; von Stein, T.; Englert, U.; Holscher, M.; Klankermayer, J.; Leitner, W. *Chem. Sci.* **2015**, *6*, 693.

31. Rezayee, N. M.; Huff, C. A.; Sanford, M. S. *J. Am. Chem. Soc*. **2015**, *137*, 1028.

CHAPTER 5

Heterogenized-Homogeneous Catalysts for Ester Hydrogenation

5.1. Introduction

The catalytic hydrogenation of formate esters is a critical step in the cascade conversion of carbon dioxide (CO_2) to methanol (CH_3OH) via the ester cascade system (Scheme 5.1).[1] In the reported system, Catalyst A is responsible for hydrogenating CO_2 to formic acid (Scheme 5.1, step i). Formic acid then undergoes an esterification reaction with methanol catalyzed by the Lewis acidic Catalyst B to produce methyl formate (Scheme 5.1, step ii). Finally, Catalyst C is responsible for hydrogenation of the ester to afford methanol and regenerate the alcohol (Scheme 5.1, step iii). Although this represents the first homogeneous conversion of CO_2 to methanol, this system was limited by incompatibilities between catalysts B and C, as well as the low activity of Catalyst C.[1]

Scheme 5.1. Conversion of CO_2 to Methanol via an Ester Cascade Pathway

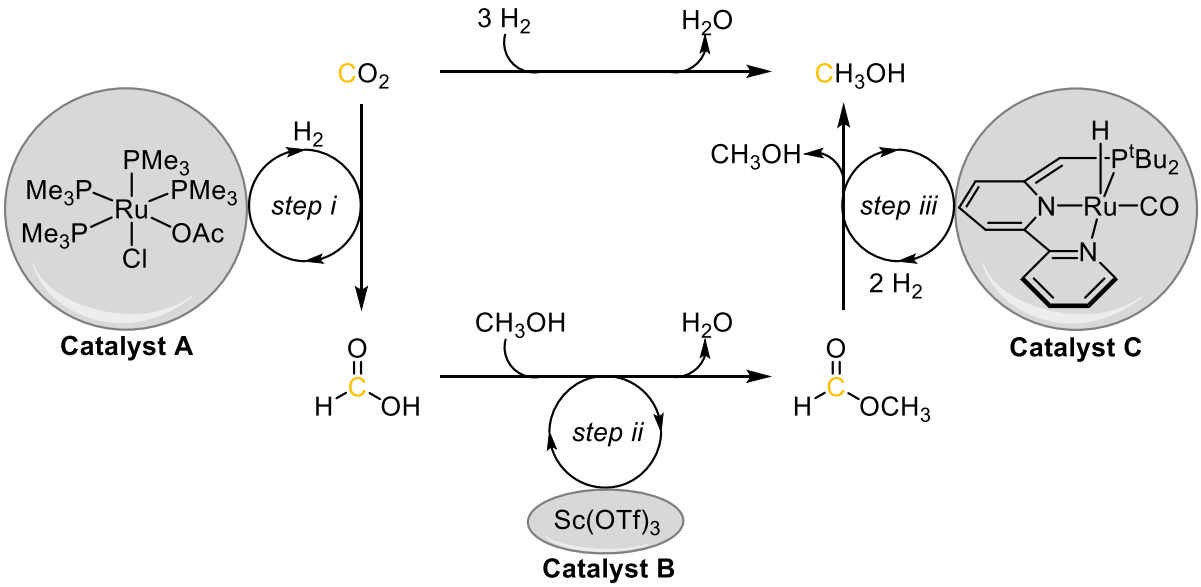

In Chapter 4 we focused on generating a superior cascade system with higher turnovers of methanol and conversions of CO_2 by utilizing a heterogeneous catalyst as both Catalyst B and C (Scheme 5.2, step ii and step iii). This allowed for the system to be simplified, requiring only two catalysts, the heterogeneous catalyst and a homogeneous catalyst, to be compatible. We hypothesized that the Lewis acidic nature of heterogeneous catalysts would allow them to act as the esterification catalyst (Scheme 5.2, step ii). Additionally, there are heterogeneous catalysts for ester hydrogenation (Scheme 5.2, step iii). Gratifyingly, the three heterogeneous catalysts tested were indeed active as the esterification catalyst and ester hydrogenation catalyst under mild reaction conditions. However, all homogeneous CO_2 hydrogenation catalysts examined proved incompatible with the heterogeneous systems, and inhibition was observed in every case. Analysis of the heterogeneous catalyst post-catalysis showed that the homogenous catalyst had decomposed and deposited on the heterogenous catalyst, explaining the low turnovers. We hypothesized that decomposition of the homogeneous catalyst was occurring *at the active site* of the heterogeneous catalyst.

Scheme 5.2. Homogenous and Heterogeneous Catalyzed Ester Cascade Pathway

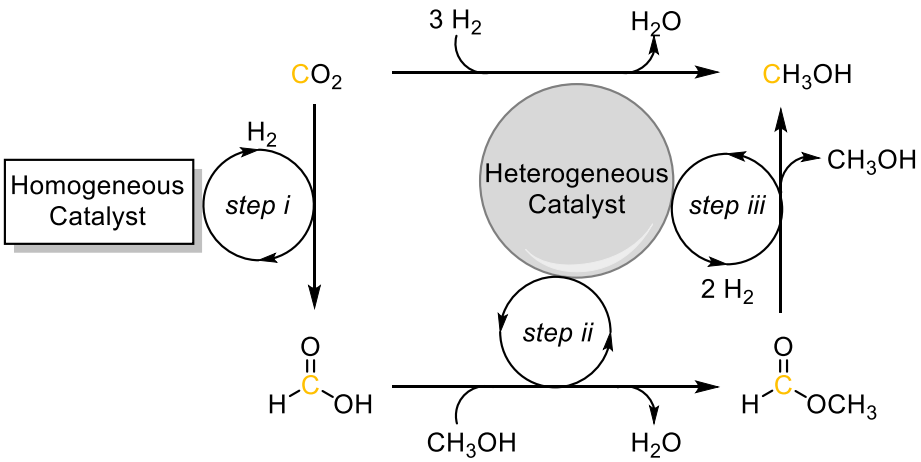

As such, we sought an alternative approach to coupling a homogenous and a heterogeneous catalyst in a single system for CO_2 hydrogenation.[2] We hypothesized that site-isolation of the active catalysts would be critical. By preventing the active site of the

homogenous and heterogeneous catalysts from interacting, we anticipated that the two catalysts would maintain their active forms and be able to co-exist in a single pot. Although there are a variety of ways to accomplish site-isolation, we focused on size-exclusion. By utilizing a porous heterogeneous catalyst with the active site protected in the interior of the pore, selection of an appropriate homogeneous catalyst that is too large to enter the pore of the heterogeneous catalyst would allow for a homogeneous-heterogeneous catalytic system with the active sites isolated from one another.

In line with our previous attempts at a homogeneous-heterogeneous catalytic ester cascade system, we sought to utilize a homogeneous CO_2 hydrogenation catalyst. The extensive CO_2 hydrogenation literature shows a vast array of catalysts with varying sizes, as well as highly active complexes capable of >10,000 turnovers.[3,4,5,6] For our new site-isolated homogeneous-heterogeneous catalytic system, it was necessary to select a homogenous catalyst where the active catalyst is generated with loss of only non-coordinating ligands. Additionally, once the active species is formed, its ligands must be non-labile. If either of these ligands dissociate from the homogeneous complex, diffusion into the heterogeneous catalyst's pore would be possible. Ultimately, these ligands could bind to the interior heterogeneous active site and inhibit the heterogeneous catalyst. We believed that the extensive homogeneous catalysis literature for CO_2 hydrogenation would render selection of such a homogenous catalyst relatively straightforward.

Metal-organic frameworks (MOFs) stood out as an ideal class of porous heterogeneous catalysts to explore. There are many examples of porous MOFs that have found applications in gas storage, separations, and catalysis.[7] MOFs are a "class of coordination polymers comprising organic linkers wherein metal−ligand interaction/bonding leads to 2D or 3D crystalline network structures".[8] MOFs are comprised of two components: the node and the framework linker.[7] The nodes are typically inorganic metal clusters or ions, while framework

linkers are organic moieties often appended with multiple carboxylic acids. The polytopic nature of the framework linkers result in three-dimensional structures with nodes attached to one another via the framework linkers.

One key advantage of MOF-based supports is their tunability at both the node and linker.[7] There are many examples of MOFs that can be synthesized with different metal precursors to generate a series of MOFs with the same overall structure, but with a different node metal.[9,10] Equally relevant, different framework linkers can be employed in MOF synthesis, generating MOFs with the same node and connectivity, but a different linker, and hence different pore dimensions.[11,12] Post-synthetic modification is another powerful strategy for tuning MOF reactivity.[12,13,14] Once the MOF is formed, post-synthetic modification can be employed to generate open coordination sites at the node,[15] to append moieties to the framework linker or node,[12] or to undergo ligand exchange with a different, exogeneous framework linker.[16] This tunability of MOFs make them attractive heterogeneous catalyst supports for our ester cascade system.

We proposed that MOFs would be an ideal candidate for the active-site isolated homogeneous-heterogeneous cascade ester system. We hypothesized that the Lewis acidic nodes of MOFs could catalyze the esterification of formic acid (Scheme 5.3, step ii). Additionally, we proposed to incorporate an ester hydrogenation catalyst within the pore of the MOF (Scheme 5.3, step iii). By incorporating a catalytic site for ester hydrogenation inside the pore, size exclusion can be utilized to maintain separation between the CO_2 homogeneous hydrogenation catalyst (Scheme 5.3, step i) and heterogeneous active site. Ultimately, we envisioned that MOFs could simplify the system to only two components, while also allowing for the desired site-isolation (Scheme 5.3).

Scheme 5.3. Homogeneous and MOF Catalyzed Ester Cascade System

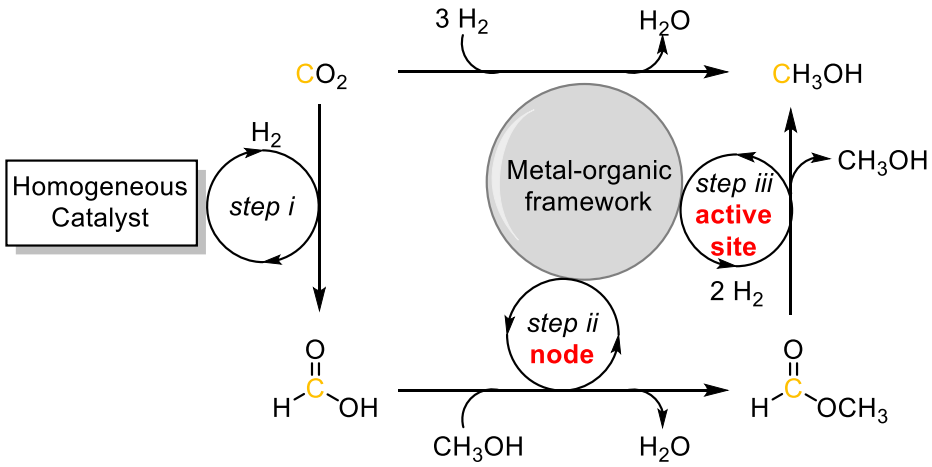

There are three general approaches to incorporate a catalytic active site into a MOF: incorporation at the framework linker, at the node, or in the pore (Scheme 5.4).[17,18,19] Often, a ligand is incorporated directly as the linker during synthesis (Scheme 5.4, a). For instance, a bipyridine-based carboxylic acid has been used to generate a UiO-type MOF wherein the linker can be post-synthetically metallated to generate a catalytically active Ir complex.[20] Although comparatively less common, active sites can also be generated at the nodes of the MOF. The metal-clusters that make up the nodes often have open sites wherein an exogenous catalytic metal can be incorporated (Scheme 5.4, b). One such example involves removal of a proton from the node and replacement with Co to generate a catalyst for benzylic C-H borylation, benzylic C-H silylation, and alkene hydrogenation amongst others.[15] Alternatively, one can replace labile ligands at the nodes with pendant linkers. Pendant linkers comprise both a moiety for binding to the node, such as a carboxylic acid, and a portion that can ligate a metal to generate a catalytic active site (Scheme 5.4, c).[21] Finally, catalysts can be incorporated via ionic interactions (Scheme 5.4, d). By incorporating a charge into the MOF, a catalytically active moiety can be incorporated via ion exchange.[22] One example of this involved incorporating a

cationic Rh-complex into MIL-101-SO_3 that contains a negative charge on the framework linker and utilizing the resulting material for alkene hydrogenation.[23] Each of these methods presents unique challenges and advantages.

Scheme 5.4. Strategies for Incorporating a Catalyst into a MOF

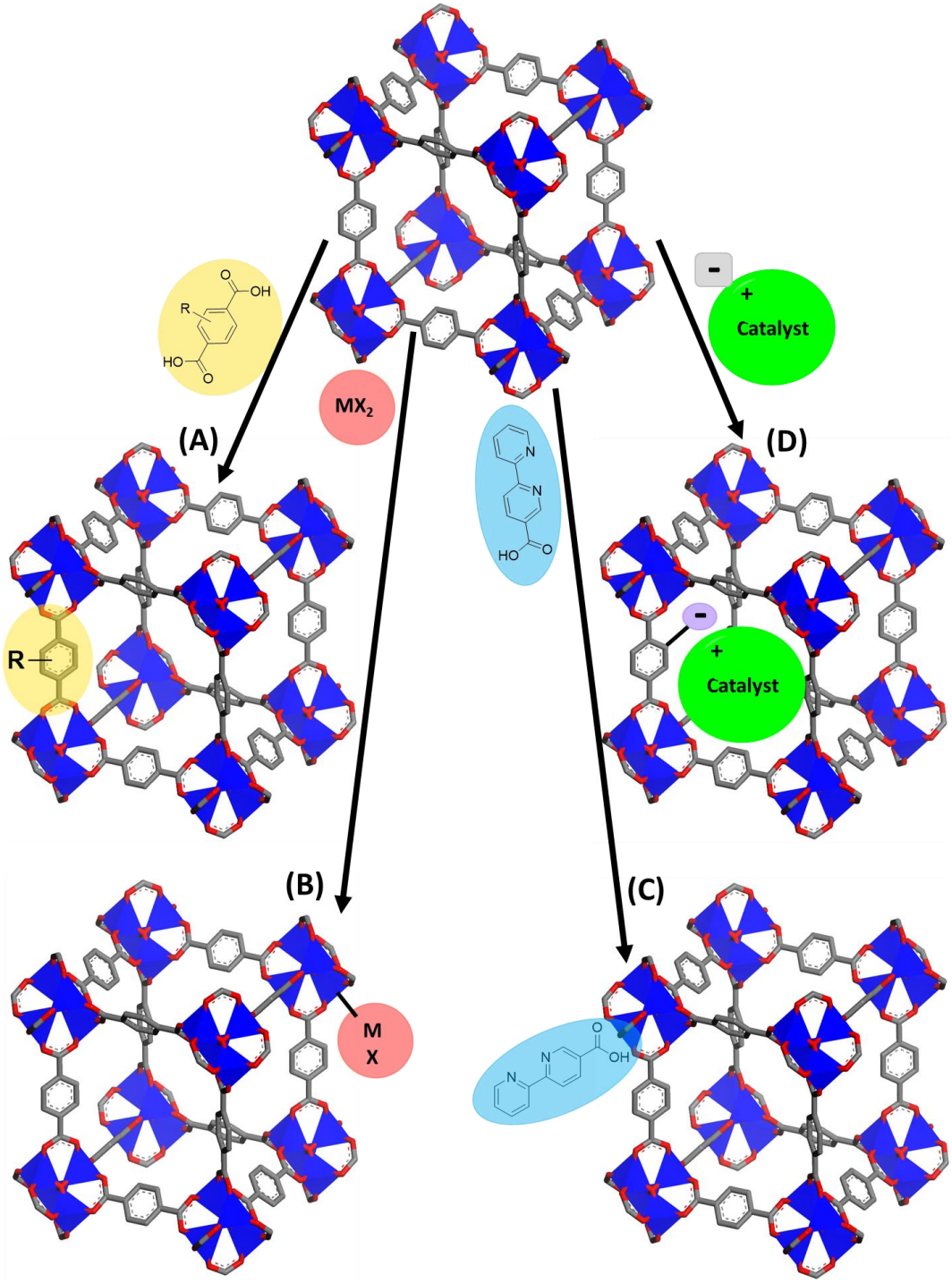

Characterization of the MOF active site is often non-trivial. To characterize the active site, X-ray absorption techniques such as XANES (X-ray absorption near edge structure) and EXAFS (extended X-ray absorption fine structure) are typically used to probe the oxidation state and ligand environment. Single crystal X-ray diffraction is used much less frequently due to the challenges of growing a MOF single crystal. All of these X-ray techniques are typically conducted on the MOF after catalyst incorporation, not in solution. This is a disadvantage as the catalytic species that is active in solution may not be formed or observable in the solid-state. Another method of active site characterization involves digestion of the material. Either strong base or strong acid can be used to digest the MOF and the resulting solution is frequently then analyzed via NMR and other solution-based techniques such as MS. Unfortunately, many homogeneous catalysts are not stable under such harsh conditions, making identification of the true active site difficult. Overall, characterization of the active site inside of catalytic MOFs is often time consuming, costly, and occurs under conditions very different to those employed in catalytic reactions.

We hypothesized that by incorporating a discrete homogeneous catalyst into a MOF via ion-exchange, characterization of the active site may be more straightforward. By selecting a homogeneous catalyst bearing a cationic charge, the discrete complex can undergo ion-exchange into an anionic MOF, supporting the homogeneous catalyst inside of the MOF. Once in the MOF, the complex can be exchanged back out, either pre- or post-catalysis to easily identify the speciation of the metal center. We hypothesized that this incorporation technique would allow for facile and readily available characterization of the ligand-sphere of the catalytic active site.

Beyond the ease of characterizing the active site, the heterogenized-homogeneous catalyst generated via ion exchange would reap the benefits of both heterogeneous and homogeneous catalysis.[2,24] This catalyst would have a single, well-defined active site, unlike

that of most heterogeneous catalysts.[2,24] Once the active site is characterized via ion-exchange, elucidation of the reaction mechanism can be accomplished by running the analogous homogeneous complex under the same reaction conditions. We also proposed that the heterogenized-homogeneous catalyst may be more stable than the corresponding homogeneous analog due to limited accessibility of bimolecular decomposition pathways. Additionally, the catalyst should be recyclable, allowing for easy separation from the reaction products.[2,24] This could also allow for the heterogenized-homogeneous catalyst to be employed in packed bed flow reactors, something that true homogeneous catalysts are not suitable for. Ultimately, we hypothesized that by heterogenizing a homogeneous catalyst inside of a MOF via ion-exchange, the catalyst could not only be thoroughly and straightforwardly studied, but also could generate a superior catalyst compared to the homogeneous analog.

The homogeneous catalyst and MOF chosen were $IrCp^*Bpy^{2+}$ and MIL-101-SO_3, respectively (Scheme 5.5). $IrCp^*Bpy^{2+}$ was an ideal candidate to put into a MOF via ionic interactions and this complex has been well studied as an ester hydrogenation catalyst.[25] Importantly, the catalyst is cationic and remains so throughout the proposed catalytic cycle.[26] Additionally, this homogeneous catalyst is not only stable to Lewis acids like those found in the nodes of MOFs, but is aided by them.[26] For the MOF, MIL-101-SO_3 was an excellent candidate due to its stability, pore window size, and anionic linker.[22,23,27] It was critical to select a MOF that could withstand the ester cascade system reaction conditions of 135 °C and 40 bar H_2, and MIL-101-SO_3 is known to be thermally stable up to 300 °C.[27] The pore window of MIL-101-SO_3 is large enough that $IrCp^*Bpy^{2+}$ can fit through the pore window with its ligand sphere intact, but also small enough that a variety of homogeneous CO_2 hydrogenation catalysts (mainly bearing bulky, tridentate ligands) would not be able to fit inside of the pore window, thus allowing the homogeneous catalyst to be size-excluded and the active sites to be site-isolated. Ultimately, the incorporation and heterogenization of $IrCp^*Bpy^{2+}$ into MIL-101-SO_3

via ionic interactions and coupling of the resulting doped-MOF (Ir@MIL) with a homogeneous CO_2 hydrogenation catalyst may allow for the realization of a homogeneous and heterogeneous coupled ester cascade pathway.

Scheme 5.5. IrCp*Bpy Incorporation into MIL-101-SO_2 to Generate Ir@MIL

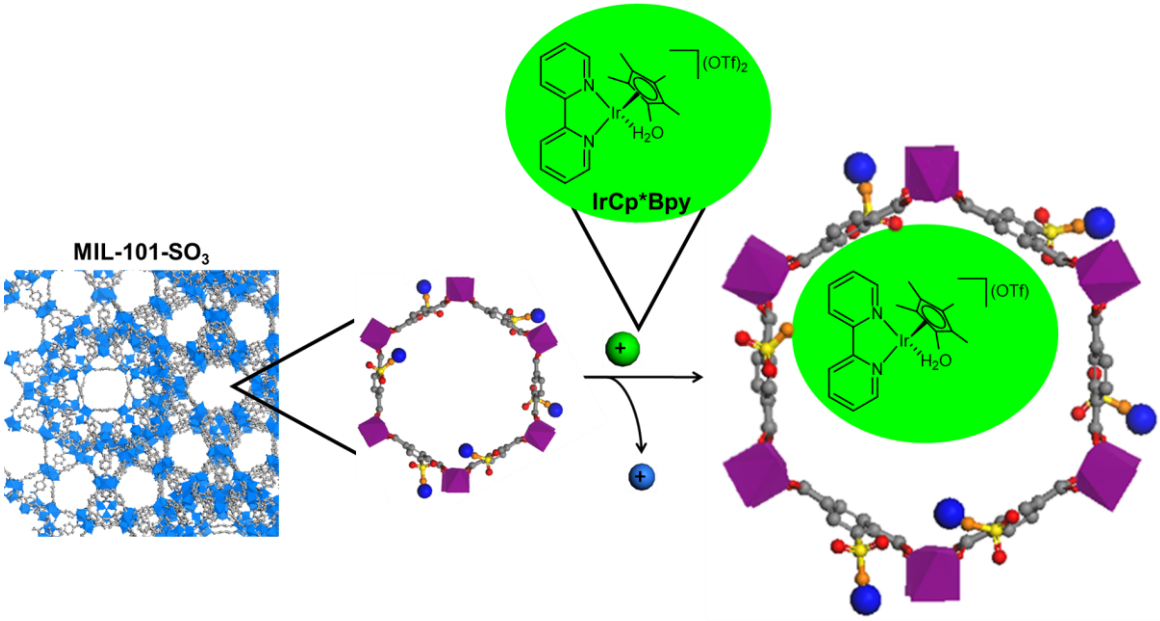

5.2. Results and Discussion[28]

5.2.1. Incorporation of IrCp*Bpy into MIL-101-SO_3 and Catalysis

Before an improved ester cascade system could be developed, the heterogenized-homogeneous catalyst needed to be prepared. This was accomplished by combining the homogeneous catalyst, IrCp*Bpy^{2+}, in DMF with MIL-101-SO_3 for four days. At this time, any Ir complex not bound to the framework was removed via washing with DMF. Analysis of the loaded MOF (Ir@MIL) via powder X-ray diffraction (PXRD) showed that the MOF maintained its crystallinity due to retention of low angle peaks (Figure 5.1). Thermogravimetric Analysis (TGA) was performed on Ir@MIL, and the collected data looked different than that reported for the parent MOF MIL-101-SO_3.[27] The reported TGA shows two major weight loss

events: (1) decomposition of the MOF at 600 K (327 °C) and (2) water loss occurring below 380 K (107 °C) accounting for about 45 wt%.[27] In contrast, the TGA of Ir@MIL showed a significant loss in weight percent (~40 wt%) steadily over a large temperature range (27–600 °C) (Figure 5.2). We attributed this steady loss in weight to a combination of: (1) solvent loss (between 0 and 41 molecules of H_2O per unit cell as reported) and (2) $IrCp^*Bpy^{2+}$ decomposition. Notably, $IrCp^*Bpy^{2+}$ is known to decompose at around 135 °C. Thus, the weight loss (5.33 wt%) below this temperature was attributed to solvent loss. ICP-OES analysis was carried out to determine the weight percent of Ir in Ir@MIL. It was necessary to consider solvent in the weight percent calculation, such that the wt % of water found by TGA was used to back-calculate the molecules of water per unit cell to obtain an accurate contribution from the solvent in the MOF. By comparing the ratio of Cr to Ir from the ICP (1:0.322 mg/L), and taking the weight loss of solvent into account, the weight percent of Ir was found to be 2.8% (Equation 5.1).

Figure 5.1. PXRD of Ir@MIL and MIL-101-SO_3

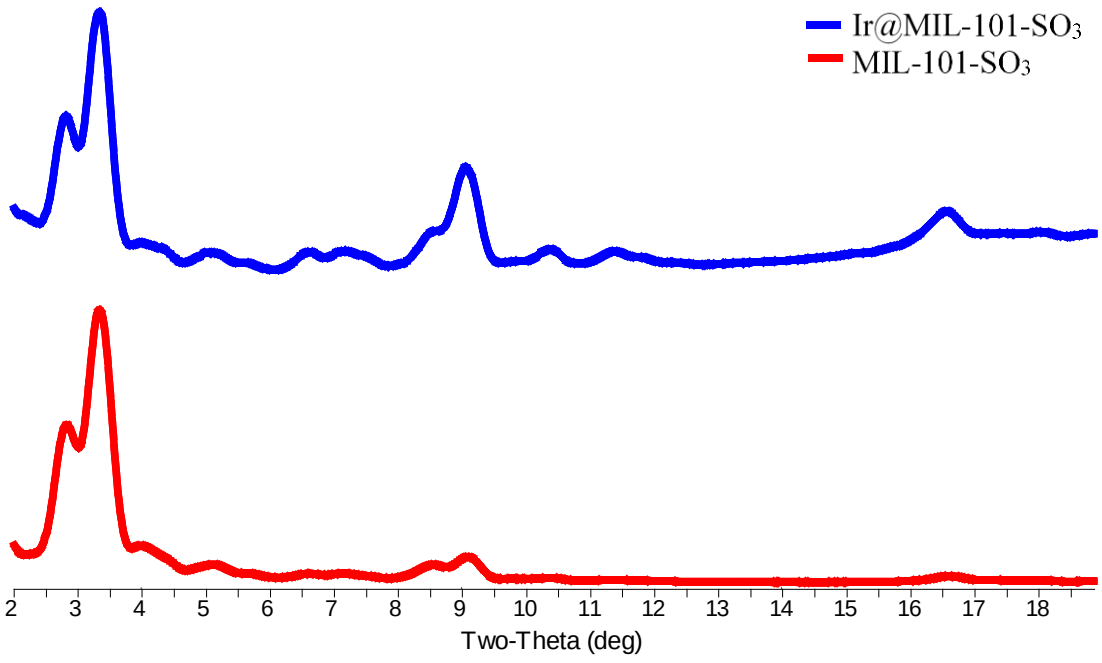

Figure 5.2. TGA of Ir@MIL

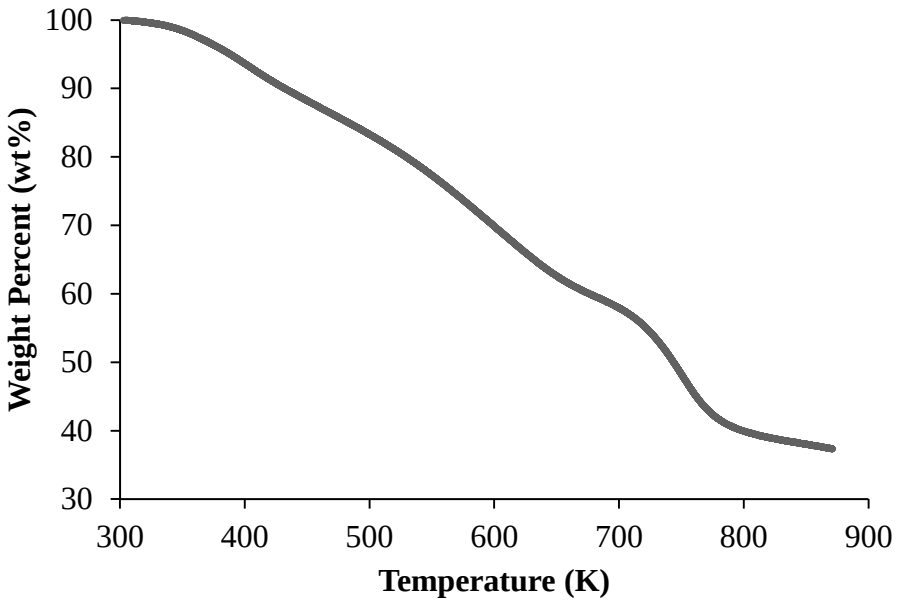

Equation 5.1. Weight Percent Calculation Accounting for Water

$$wt\%\ Ir = \frac{mg\ Ir}{mg\ IrCp * Bpy + mg\ MIL - 101 - SO_3 + mg\ H_2O}$$

With Ir@MIL in hand we set out to study its catalytic activity for the hydrogenation of ethyl formate (Figure 5.3). This transformation enables the easy identification of methanol as deriving from catalytic hydrogenation as opposed to hydrolysis. It should be noted that once methanol is formed, a transesterification can take place at the Lewis acidic node of the MOF, generating methyl formate. As a control, MIL-101-SO_3 itself was tested for ethyl formate hydrogenation, and it was found to be inactive (Figure 5.3). Next, the homogeneous analogue (IrCp*Bpy^{2+}) was studied under these conditions and yielded 402 turnovers of methyl formate and 278 turnovers of methanol (i.e., 680 turnovers of hydrogenation products). A final control reaction involved studying IrCp*Bpy^{2+} in the presence of added MIL-101-SO_3. Here, the Ir-complex was not pre-loaded into the MOF; instead, the two discrete moieties were loaded into the same reactor. Interestingly, the presence of MIL-101-SO_3 actually inhibited the

homogeneous catalyst, resulting in decreased turnovers of both methyl formate and methanol (Figure 5.3). This was surprising, as IrCp*Bpy^{2+}, has been reported to perform better in the presence of Lewis acids, leading us to anticipate the MOF would aid in ester hydrogenation. Finally, Ir@MIL was studied under analogous conditions, and was found to outperform all of the control reactions, producing 542 turnovers of methyl formate and 203 turnovers of methanol (Figure 5.3).

Figure 5.3. Controls and Ir@MIL Catalytic Ethyl Formate Hydrogenation[a]

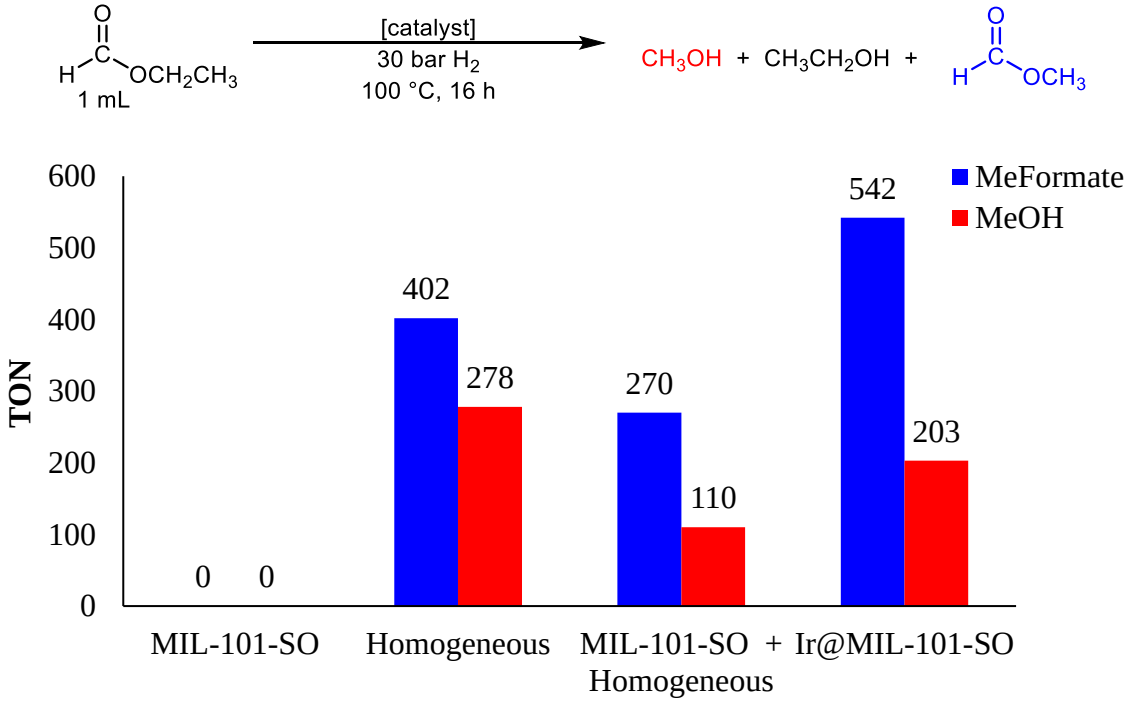

[a]**Conditions:** 1 mL of ethyl formate, 30 bar H_2, 100 °C, 16 h

Next, we sought to study the recyclability of Ir@MIL. We hypothesized that site isolating our homogeneous catalyst inside of a MOF would enhance the stability of IrCp*Bpy^{2+}. Specifically, bimolecular decomposition could be avoided due to the fact the homogeneous catalysts are ionically bond to the framework and should not be able interact with one another. Unfortunately, even though fresh Ir@MIL showed high reactivity, the recycled the material showed a significant drop in reactivity (Figure 5.4).

Figure 5.4. Recyclability of Ir@MIL in Catalytic Ethyl Formate Hydrogenation[a]

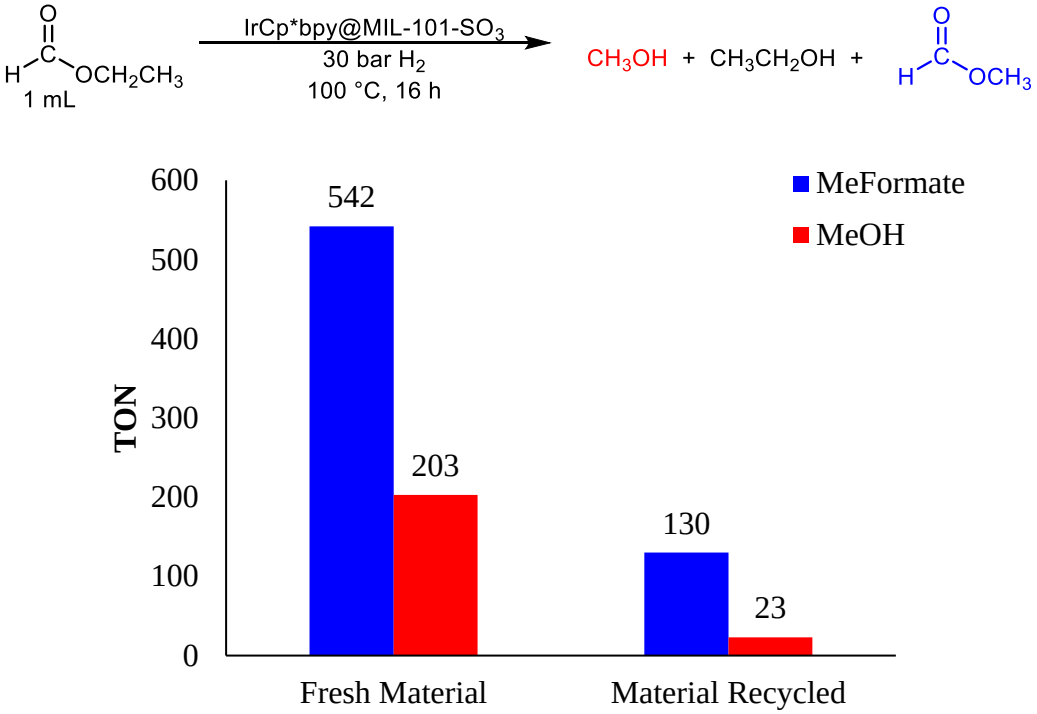

[a]**Conditions:** 11.8 mg of Ir@MIL, 1 mL of ethyl formate, 30 bar H_2, 100 °C, 16 h; Recycled reaction: after work-up, material was ran again with 1 mL of fresh ethyl formate, 30 bar H_2, 100 °C, 16 h.

Our focus shifted to identifying the reason that Ir@MIL was not maintaining its reactivity after recycling. We noted that the post-catalysis reaction solution was yellow, the same color as IrCp*Bpy when in solution. This led us to hypothesize that Ir was leaching from Ir@MIL during catalysis; as such, ICP analysis was carried out on the post-catalysis material. Interestingly, instead of seeing the Ir decreasing, the ratio of Cr:Ir actually increased from 1 Cr per 0.322 Ir mg/L to 1 Cr per 0.552 mg/L. Since there was no additional source of Ir in the reaction, we reasoned the Cr content must have decreased as a result of MOF degradation, which would release Cr into solution. According to PXRD, the material maintained crystallinity (Figure 5.5), however, as PXRD is a bulk technique, it is not capable of identifying any surface collapse that may have occurred. Additionally, PXRD would not be able to identify the loss of Cr that was washed away in solution. We hypothesized that MOF degradation could

be the result of ethyl formate. At the time, we hypothesized that ethyl formate may be exchanging with the framework linker at the node of the MOF. After all framework linkers have been substituted out with ethyl formate, the Cr would then be in solution instead of as a solid. Another hypothesis was that IrCp*Bpy could be hydrogenating the carboxylic acids of the framework linkers allowing Cr to be bound to ethyl formate and ultimately reside in solution instead of as part of the MOF.

Figure 5.5. PXRD Ir@MIL Post-Catalysis and Native MIL-101-SO_3

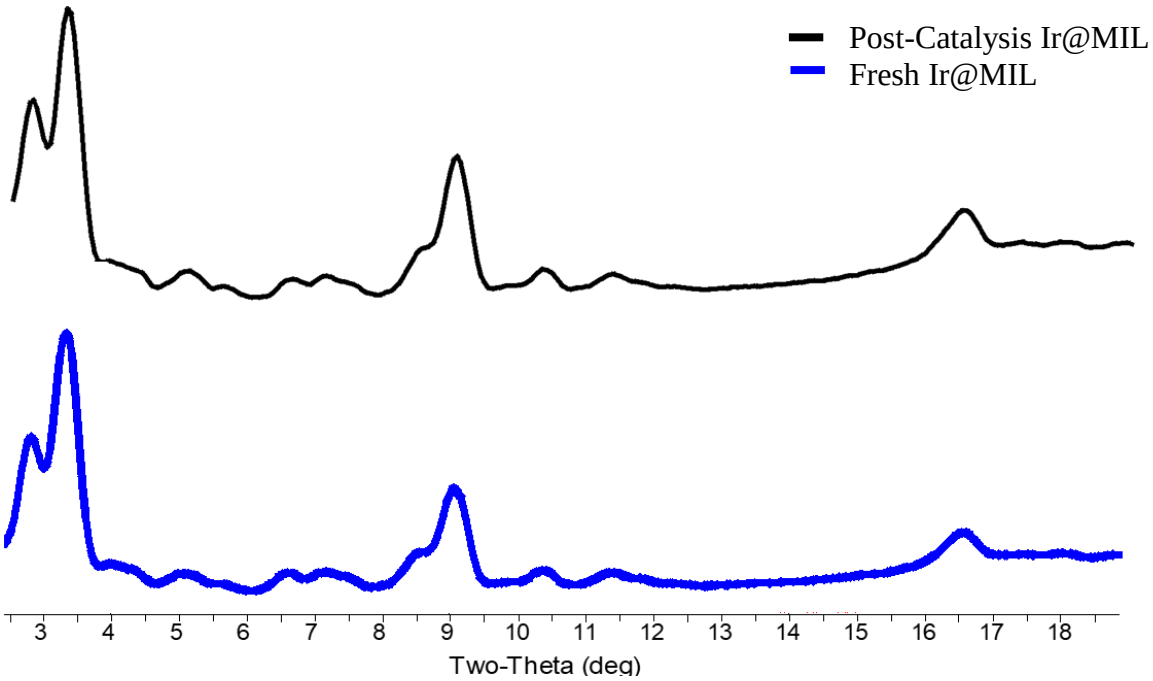

In an attempt to prevent Ir leaching and MOF decomposition, we utilized non-neat reactions employing hexane and benzene as the solvent. We hypothesized that decreasing the concentration of ethyl formate in the reaction might enhance the stability of the material. Although Ir@MIL outperformed the homogeneous catalyst under these new solvent conditions, only low yields were obtained (Figure 5.6). The previous results in Figures 5.3 and 5.4 gave 9% yield, which is line with the reactions in hexane and benzene at 10% yield. Notably, the post-catalysis reaction solutions were both clear and colorless. When attempting

to recycle Ir@MIL in benzene a 16% decrease in reactivity was observed indicating that at least one other route of decomposition was occurring in addition to possible ethyl formate derived decomposition.

Figure 5.6. Ir@MIL Catalytic Ethyl Formate Hydrogenation in Solvents[a]

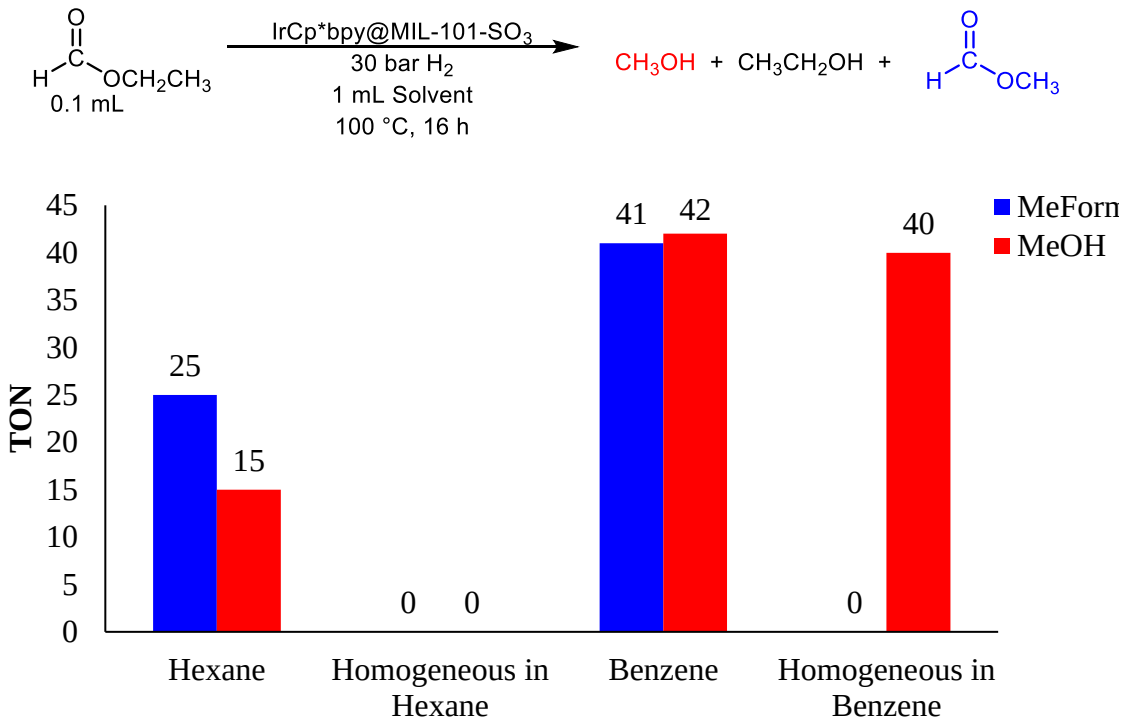

[a]**Conditions:** 11.8 mg of Ir@MIL, 0.1 mL of ethyl formate, 0.9 mL of n-hexane or benzene, 30 bar H_2, 100 °C, 16 h.

Although it is clear that Ir@MIL is catalytically active for ester hydrogenation, batch to bath issues were discovered once the material from the first batch, Batch A, was consumed (Figure 5.7). Within each batch of Ir@MIL, the results were reproducible, but moving from one batch to the other, the results varied significantly. The first batch of Ir@MIL was more than twice as reactive than the third batch even though the same procedure was followed. The variation between batches was concerning and halted all further experimentation until the issue was resolved.

Figure 5.7. Batch Issues with Ir@MIL Catalytic Ethyl Formate Hydrogenation[a]

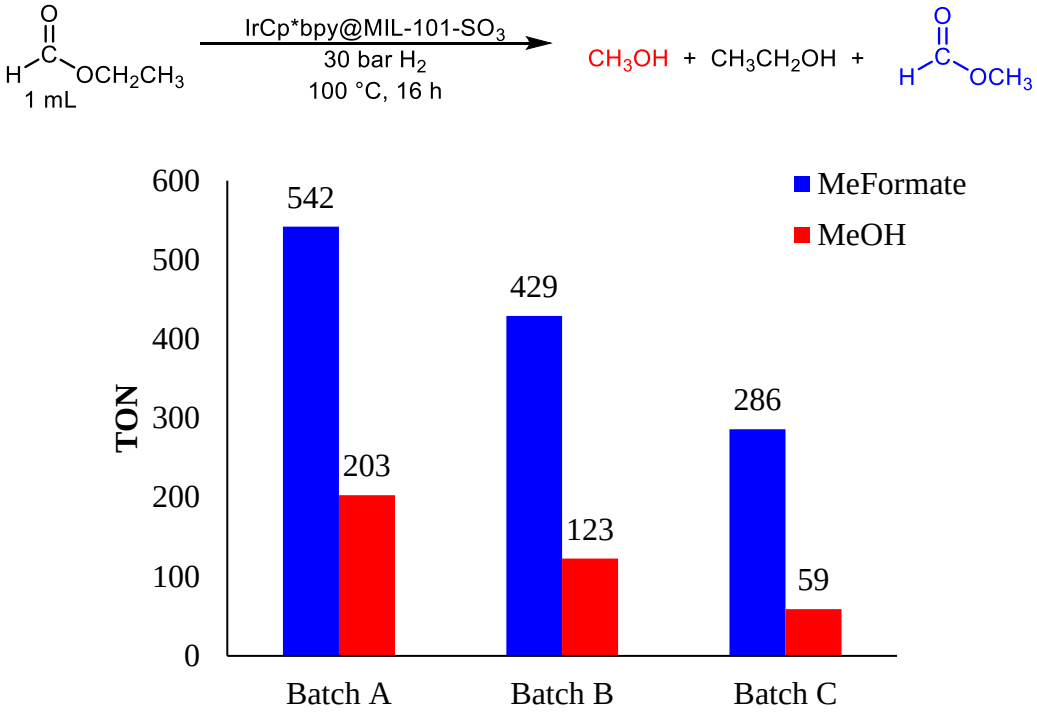

[a]**Conditions:** 11.8 mg of Ir@MIL, 1 mL of ethyl formate, 30 bar H_2, 100 °C, 16 h

5.2.2. DMF and Ir@MIL

To elucidate the cause of batch-to-batch variability with Ir@MIL, we first sought to directly study the catalyst via ion-exchange. By employing a procedure similar to that used when loading $IrCp^*Bpy^{2+}$ into MIL-101-SO_3, it would allow us to confirm the speciation of the Ir-complex and hopefully eliminate the source of the batch-to-batch issues. By using 300 equiv. of HCl and exchanging for the same amount of time used for loading $IrCp^*Bpy^{2+}$ into MIL-101-SO_3, we hoped to obtain the Ir complex with its bipyridine and Cp* ligands still bound (Scheme 5.6). MIL-101-SO_3 is extremely stable to dilute acids, so utilizing HCl to recover the homogeneous catalyst presented no danger of MOF degradation.[27] We anticipated that the large excess of Cl ions present would replace both the OTf counter ion and the H_2O ligand. Importantly, these would not appear in ^1H NMR spectrum of the exchanged material and would be the direct result of ion-exchange of the complex out of MOF.

Scheme 5.6. Retrieving IrCp*Bpy from Ir@MIL via Exchange with HCl

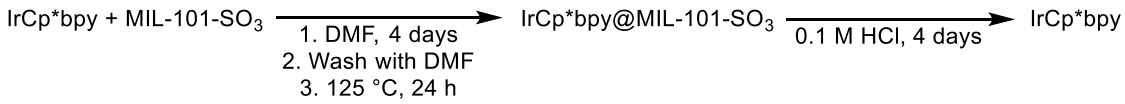

After exposing Ir@MIL to HCl for 4 days, a ^{1}H NMR spectrum of the resulting solution was collected (Figure 5.8, A). As a control, the homogeneous complex was exposed to dilute HCl for the same duration, and the ^{1}H NMR spectrum of this solution was also obtained (Figure 5.8, B). Additionally, a ^{1}H NMR spectrum of the homogeneous complex in DMSO-d_6 was obtained for reference (Figure 5.8, C). In the presence of HCl, the bipyridine and Cp* peaks shifted slightly upfield. Very good overlap was observed between the peaks of IrCp*Bpy^{2+} treated with acid and the solution from the Ir@MIL HCl-exchange (Figure 5.8, A and B). This indicates that the IrCp*Bpy^{2+} maintains both its bipyridine and Cp* ligands when incorporated into the MOF. Notably, this HCl exchange to remove the homogeneous catalyst occurred without decomposition of the MIL-101-SO_3, which retained its crystallinity after this process as determined by PXRD (Figure 5.9).

Figure 5.8. ^{1}H NMR of Ir@MIL Exchange with HCl

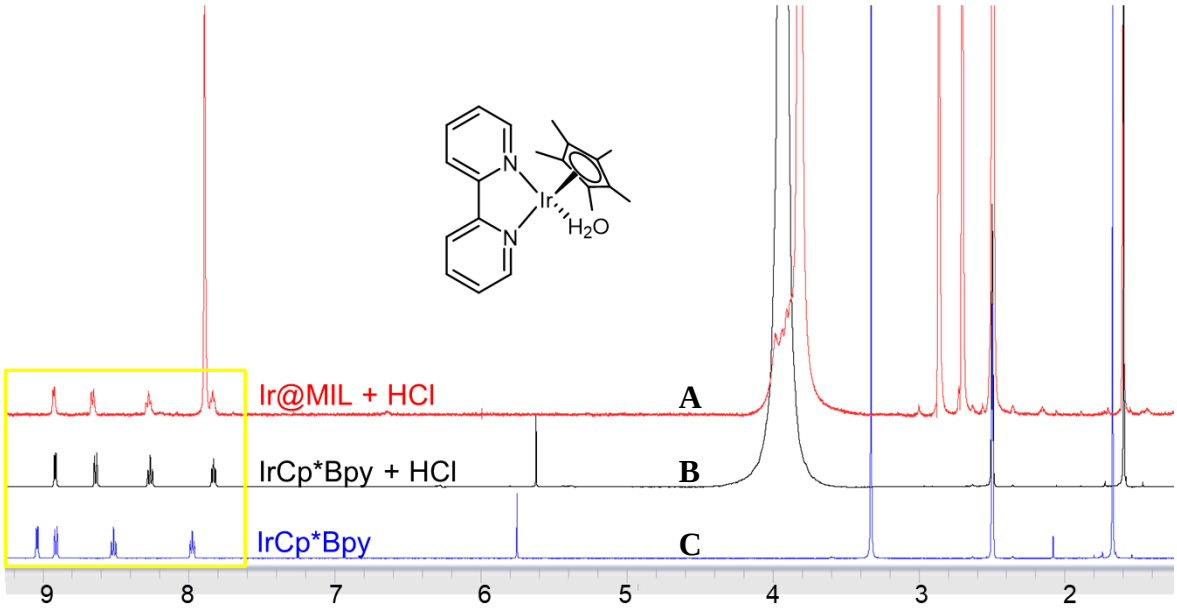

Figure 5.9. PXRD Ir@MIL Post-HCl Exchange and Fresh MIL-101-SO_3

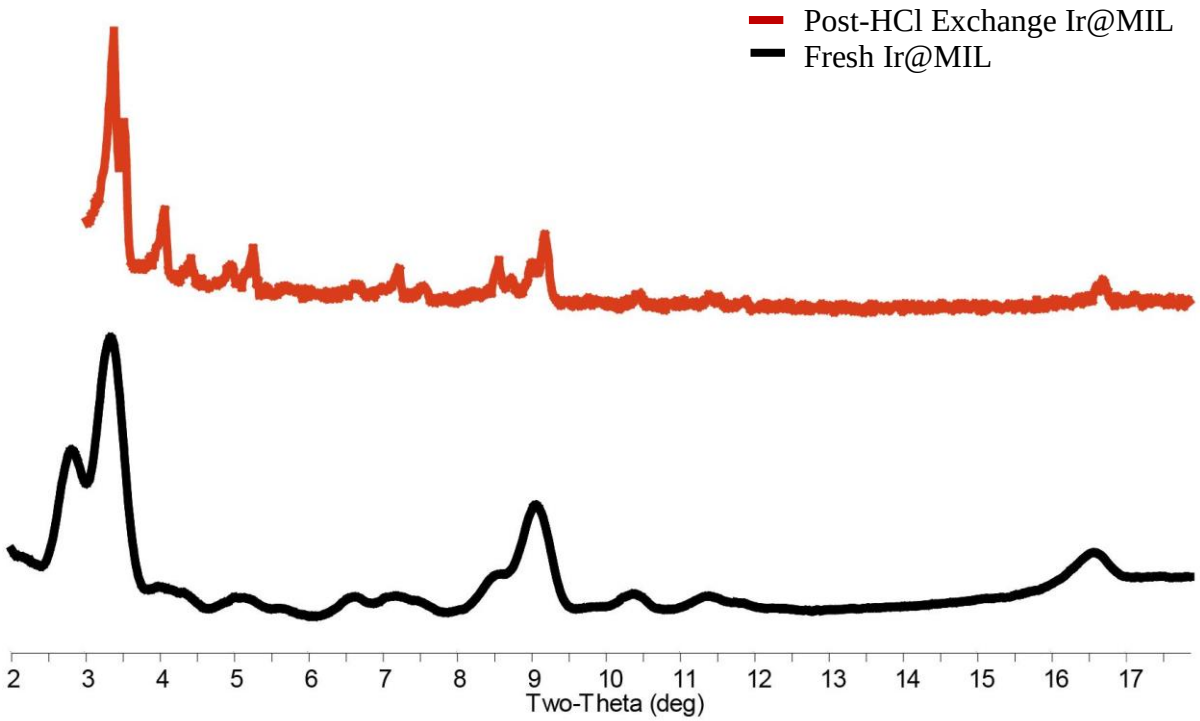

This exchange reaction also showed the presence of DMF (Figure 5.8, A, δ = 7.92, 2.89, and 2.77 ppm). We noted that the catalyst was loaded in DMF, and the MOF is also washed with DMF following the loading procedure. Previous reports suggested that activation of the MOF at 125 °C under high vacuum for 24 hours led to loss of all exogenous solvent; however, this was clearly not the case in this system.[23] Typically, TGA would be the first indication of the presence of solvent in the material, but due to the low thermal stability of IrCp*Bpy^{2+}, it was not clear whether the mass loss from TGA derived from solvent or the decomposition of the complex. However, this HCl exchange procedure allowed us to identity not only the presence of solvent, but also the exact amount (22 equivalents of DMF per Ir for Ir@MIL used in Figures 5.3, 5.4, and 5.5). The finding that DMF is present in Ir@MIL led to a recalculation of the Ir loading from 2.8 wt% to 1.9 wt%. This means that the TONs with this catalyst are actually higher than initially calculated (see Table 5.2 in 5.4.4. below for adjusted turnovers), which even further distinguishes Ir@MIL as superior to its homogeneous analogue.

Furthermore, the discovery of DMF in the material further explained both batch-to-batch issues, as well as the finding that the amount of Ir compared to Cr increased post-catalysis despite the fact that the Ir appeared to be leaching. The batch-to-batch issues can be explained by varying amounts of DMF in each batch. Although MIL-101-SO_3 has excellent acid stability, it is very unstable to bases. We hypothesized that, upon heating Ir@MIL during catalysis, that DMF was destroying the MOF via generation of basic dimethylamine.

We next sought to study how DMF impacted the reactivity of the homogeneous catalyst IrCp*Bpy^{2+}. With 22 equivalents of DMF added, the reactivity of IrCp*Bpy^{2+} decreased dramatically, and no methanol was formed under our standard conditions (Figure 5.10). This indicated that DMF is detrimental to the reactivity of IrCp*Bpy^{2+}, which is consistent with previous reports showing that IrCp*Bpy^{2+} is sensitive to Lewis bases.[25,26] Interestingly, this study also explains the previous finding that the homogeneous catalyst is inhibited by the

Figure 5.10. Influence of DMF on IrCp*Bpy Catalyzed Ester Hydrogenation[a]

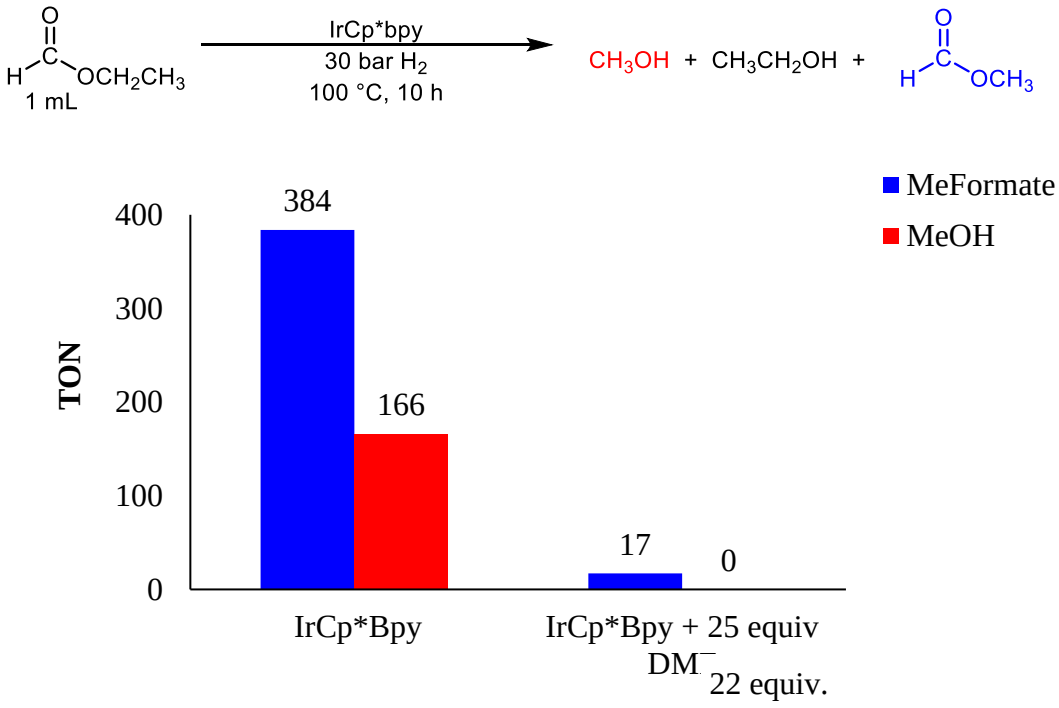

[a]**Conditions:** 3 µmol of IrCp*Bpy, 5 µL of DMF, 1 mL of ethyl formate, 30 bar H_2, 100 °C, 10 h

presence of MIL-101-SO_3 (Figure 5.3). This inhibition is likely due to the presence of DMF in MIL-101-SO_3, which shuts down the reactivity of the homogeneous catalyst.

To address these issues, we synthesized DMF-free Ir@MIL by washing MIL-101-SO_3 post-synthesis with water and THF and also using THF as the loading solvent. This DMF-free material Ir@MIL showed very high activity, at 611 turnovers of methyl formate and 513 turnovers of methanol (Figure 5.11). As a control, IrCp*Bpy and MIL-101-SO_3 were loaded into the same reactor. Importantly, this reaction produced more hydrogenation products when compared to the homogeneous catalyst alone (Figure 5.11). This finding was consistent with the activity of $IrCp^*Bpy^{2+}$ being enhanced in the presence of Lewis acids. Overall, Ir@MIL was 65% more reactive than the homogeneous catalyst alone and 37% more reactive than the homogeneous catalyst used in conjunction with MIL-101-SO_3. Ultimately, supporting of $IrCp^*Bpy^{2+}$ in MIL-101- SO_3 led to both increased reactivity, as well as synergistic effect between the $IrCp^*Bpy^{2+}$ and MIL-101-SO_3.

Figure 5.11. DMF-Free Ir@MIL Ethyl Formate Hydrogenation[a]

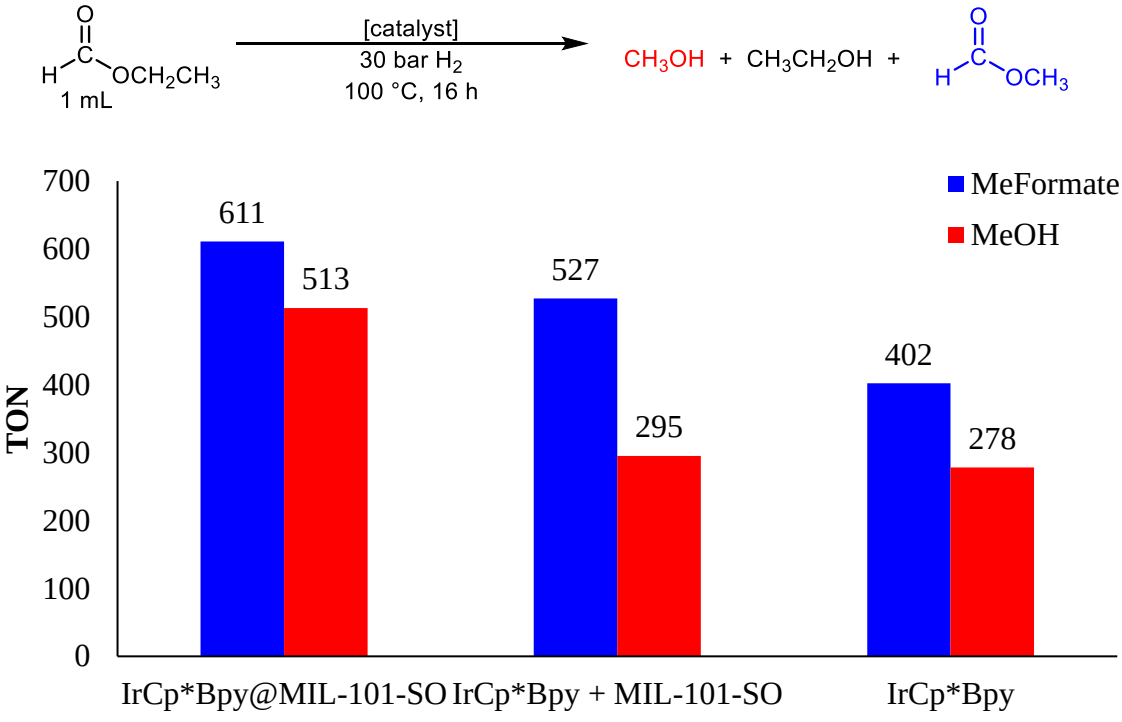

[a]**Conditions:** 1 mL of ethyl formate, 30 bar H_2, 100 °C, 16 h

5.2.3. Leaching Studies of Ir@MIL

Although removal of DMF from Ir@MIL resolved many of the issues outlined above, recycling the material still led to a significant decrease in reactivity from 1223 turnovers of hydrogenation products down to just 72 (Figure 5.12). At the end of the recycled reaction, the reaction solution was yellow, suggesting that the $IrCp^*Bpy^{2+}$ was likely leaching from the material. We hypothesized that decreasing the reaction temperature might decrease the amount of leaching and lead to better retention of reactivity. Unfortunately, when dropping the reaction temperature from 100 ºC to 80 °C or 60 ºC did not improve recyclability (Figure 5.12).

Figure 5.12. Ir@MIL Ethyl Formate Hydrogenation at Different Temperatures[a]

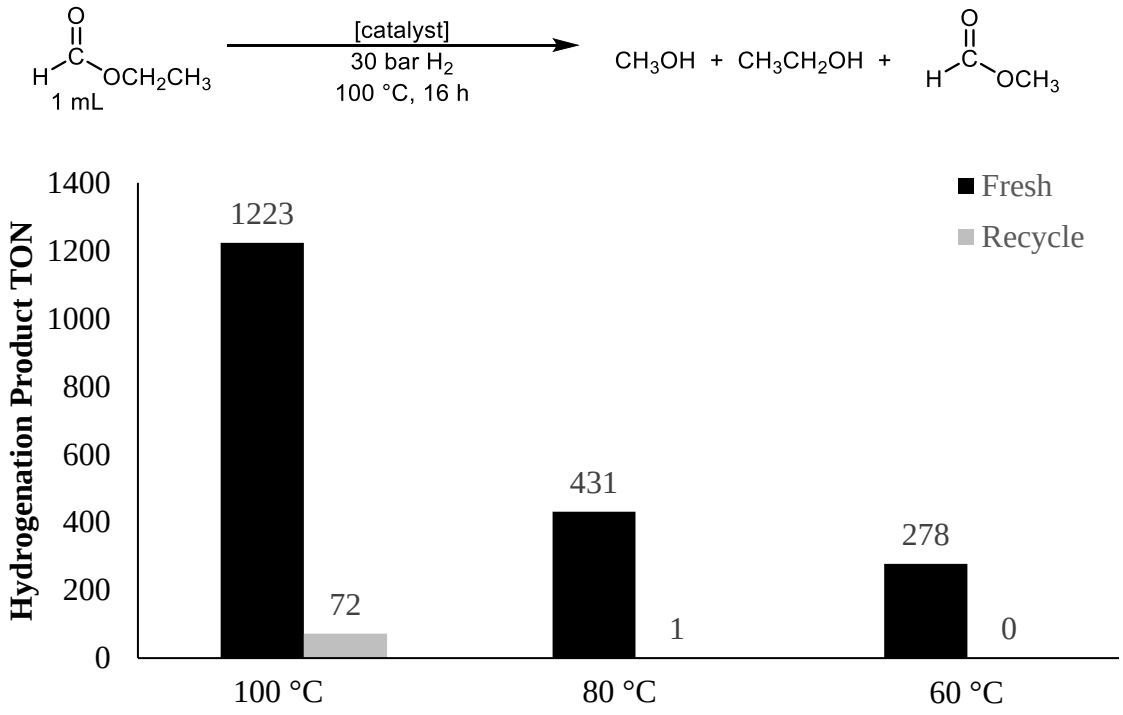

[a]**Conditions:** 1 mL of ethyl formate, 30 bar H_2, 16 h. The 100 °C reaction utilized 1.33 µmol Ir and the 80 °C and 60 °C reactions used 1.37 µmol Ir.

We next probed how much Ir leached from Ir@MIL at 100, 80, and 60 °C (Figure 5.13). Before catalysis, the material used for the 100 °C reactions had 4.56 wt% Ir while the 80 and 60 °C reactions contained 4.54 wt% Ir. The materials were retrieved post-catalysis, washed

with acetone, and dried at elevated temperature before ICP-MS was used to quantify the wt% Ir. At all three temperatures, the wt% of Ir in the material decreased. At 100, 80, and 60 °C the Ir decreased by 31%, 26%, and 25%, respectively. This finding was consistent with our hypothesis that less leaching would occur at lower temperature, although the effect was not very dramatic.

Figure 5.13. Weight Percent Ir in Ir@MIL Pre- and Post-Ethyl Formate Hydrogenation[a]

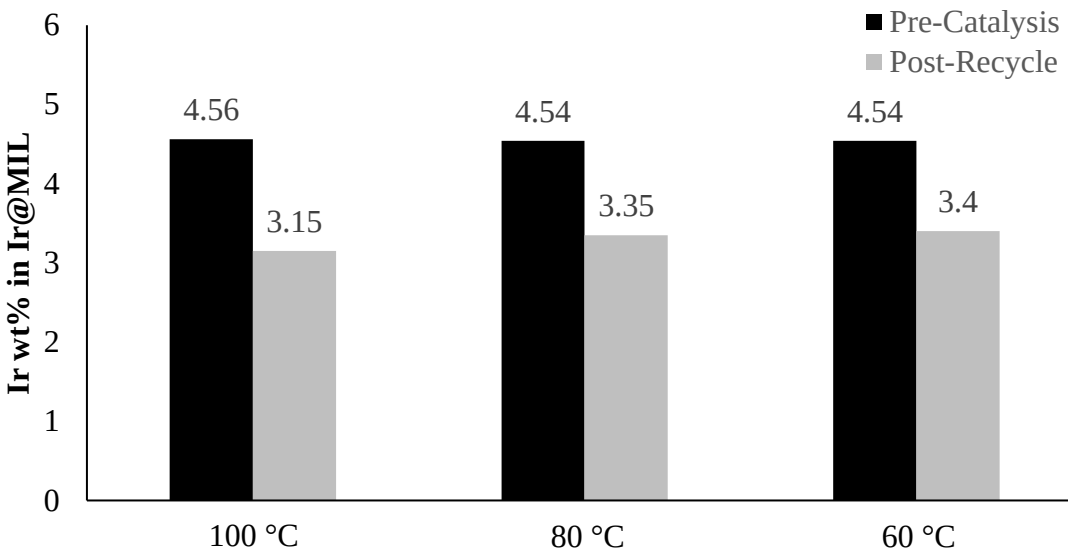

In order to identify the origin of the leaching, we performed a series of leaching tests where Ir@MIL was exposed to different solvents, at different temperatures, and with or without H_2 present (Table 5.1). Comparing ethyl formate and benzene as solvents, both Ir@MIL samples exhibited a small amount of leaching (Table 5.1, Entries 1 and 4). Increasing the temperature from room temperature to 100 °C resulted in a relatively small increase in leaching (Table 5.1, Entries 1 and 2). Interestingly, the combination system of ethyl formate and benzene led to more leaching than either of the two separately (Table 5.1, Entry 4), but ultimately, these values were all within the range of the error of the ICP-MS instrument (Table 5.1, Entries 1, 4, and 5). Interestingly, a significant decrease in Ir loading (21% and 25%) was seen when H_2 was present at room temperature with both ethyl formate and a mixture of ethyl formate and benzene as the solvent (Table 5.1, Entry 3 and 8). These leaching values are in

line with the Ir leaching observed during catalysis at 80 °C (26%) and 60 °C (25%). The leaching observed in Figure 5.9 and the other leaching studies in Table 5.1 suggest that the presence of H_2 is responsible for the majority of the observed Ir leaching.

Table 5.1. Leaching Studies for Ir@MIL

Entry	Solvent	Temperature (°C)	Additive	Starting wt% Ir	Ending wt% Ir	Decrease (%)
1		23	—	4.54	4.19	8
2	Ethyl Formate	100	—	4.54	4.14	9
3		23	H_2	4.54	3.56	21
4	Benzene	23	—	4.54	4.14	9
5	0.1 mL Ethyl	23	—	4.54	4.03	11
6	Formate +	100	—	4.54	3.82	16
7	0.9 mL Benzene	23	H_2	4.54	3.40	25

The proposed reaction mechanism provides an explanation for why H_2 induces Ir leaching from Ir@MIL.[26] As shown in Scheme 5.7, this mechanism involves initial reaction of $IrCp^*Bpy^{2+}$ with hydrogen to generate a dihydrogen complex (Scheme 5.7, b), which can protonate the substrate, causing the charge of the Ir complex to change from 2^+ to 1^+ (Scheme 5.7, c). In homogeneous catalysis, this charge change has little impact; however, for Ir@MIL catalysis, this change in charge has significant implications (Scheme 5.8). In the homogeneous

Scheme 5.7. IrCp*Bpy Proposed Hydride Generation

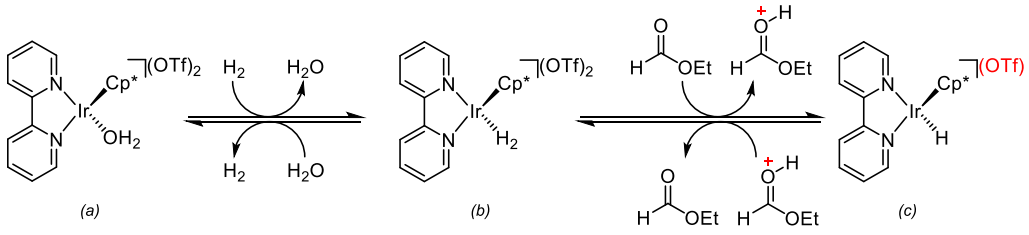

Scheme 5.8. Ir@MIL Proposed Hydride Generation

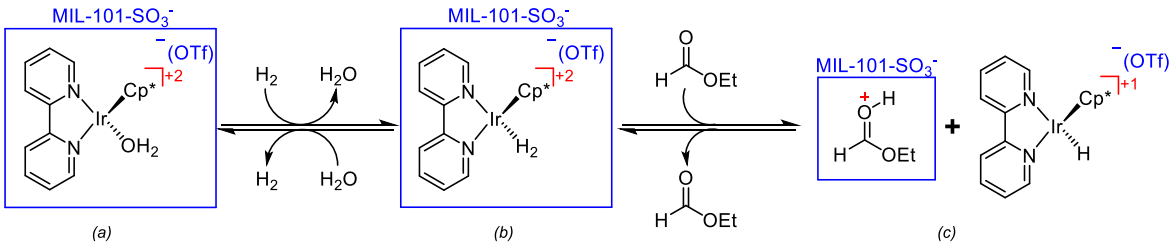

catalyst, the 2^+ charge is balanced by two triflates (one inner sphere and one outer sphere). In contrast, in Ir@MIL, we expect that the 2^+ charge is balanced by an inner sphere triflate and a SO_3^- from the MOF linker (Scheme 5.8, a). As such, when the charge changes from 2^+ to 1^+, the charge balance from the MOF is no longer necessary, which could enable the IrCp*Bpy to diffuse more easily throughout or out of MIL-101-SO_3. In addition, since the organic substrate is now protonated, it could participate in an ion exchange with the MOF/Ir catalyst. We hypothesized that this was likely the origin Ir leaching during catalysis. Further studies are underway to more thoroughly support this hypothesis. If it is found that the mechanism of hydrogenation is indeed the cause of leaching, different reactions will be explored with Ir@MIL, as it will not be possible to prevent leaching for ester hydrogenation.

5.3. Conclusions

A heterogenized-homogeneous Ir ester hydrogenation catalyst was generated via ion-exchange. This catalyst, Ir@MIL, was found to be active for ethyl formate hydrogenation. Poor recyclability and batch-to-batch issues led to more thorough characterization of Ir@MIL via HCl exchange. This exchange revealed that the catalyst retained its bipyridine and Cp* ligands. It also indicated the presence of large amounts of DMF, which was not identified by traditional materials characterization techniques. The DMF was found to significantly inhibit the homogeneous catalyst. Once eliminating DMF from Ir@MIL synthesis, the material was found to be more reactive and reproducible.

Ultimately, heterogenizing IrCp*Bpy inside of MIL-101-SO_3 provided a significantly more reactive catalyst than the homogeneous analogue. However, Ir@MIL is not readily recyclable, as the activity of this material decreases significantly when it is reused. Post-catalysis analysis of Ir@MIL indicated that the weight percent of Ir had decreased. Leaching studies pointed to H_2 as the cause of leaching. Further studies are currently underway to identify

if the mechanism of hydrogenation is indeed causing leaching of Ir from Ir@MIL. Continuing studies are underway to realize the goal of using Ir@MIL as both the esterification and ester hydrogenation catalyst for the cascade ester pathway.

5.4. Experimental Procedures

5.4.1. General Procedures and Materials and Methods

General Procedures

All manipulations were carried out under a nitrogen atmosphere using standard Schlenk line or glove box techniques unless otherwise noted. Centrifugation was carried out on a Sorval ST 16 centrifuge from ThermoScientific. A TA Instrument Q50 thermogravimetric analyzer was used for TGA. The samples were heated in a platinum holder from 30 °C to 600 °C at a ramp rate of 5 °C/min under a N_2 atmosphere and the weight change was recorded as a function of temperature. ICP-OES data was obtained on a Perkin-Elmer Optima 2000 DV with Winlab software. For analysis, the MOF was dissolved in nitric acid. Alternatively, ICP-MS data was obtained on Perkin-Elmer NexION 2000 with Syngistix 2.0 software where the MOF was dissolved in Piranha solution at 100 °C for 1 hour and cooled before ICP was performed. It

Equation 5.2. Weight Percent Calculation When No Solvent Is Present

$$wt\%\ Ir = \frac{mg\ Ir}{mg\ IrCp * Bpy + mg\ MIL - 101 - SO_3}$$

was necessary to include the same concentration of piranha in the blanks and calibration standards to account for matrix effects. For ICP, the Ir:Cr ratio was used to back calculate mg of IrCp*bpy and mg of MIL-101-SO_3 and plugged into Equation 5.2. when the material was activated and TGA showed no solvent present (see Equation 5.1 for when solvent is present). Powder x-ray diffraction (PXRD) patterns were collected at room temperature using a Rigaku R-Axis Spider diffractometer with an image plate detector and graphite monochromated Cu-

Kα radiation (λ = 1.54187 Å). Samples were mounted on a CryoLoop, and images were collected for three minutes while rotating the sample about the φ-axis at 10°/s, oscillating ω between 120° and 180° at 1°/s with χ fixed at 45°. Images were integrated from 2 to 70° with a 0.01° step size using AreaMax 2.0 software (Rigaku). Powder patterns were processed using Jade 8 XRD Pattern Processing, Identification & Quantification analysis software (Materials Data, Inc). All high-pressure reactions were pressurized using a Parr Model 5000 Multiple Reactor system that includes six 45 mL vessels equipped with flat-gaskets and head mounting valves. The system was operated by a 4871 process controller and SpecView version 2.5 software. All pressures are reported from the SpecView interface at room temperature. Reactions were heated in a fume hood in a stainless-steel heating block where the reaction temperature corresponded to the block temperature. NMR spectra were obtained on Varian VNMRs: 400 MHz (400 MHz for ^{1}H) or 700 MHz (700 MHz for ^{1}H). Chemical shifts are reported in parts per million (ppm) and are referenced to an internal standard. Unless otherwise noted, the NMR yields were based on methanol (δ= 3.16 ppm) and methyl formate (δ= 1.22, 4.14, and 8.19 ppm) and were quantified using 1,3,5-trimethoxybenzene (δ= 6.02 ppm) as an internal standard in dimethylsulfoxide-d_6 (DMSO-d_6). For each NMR experiment, 4 scans were collected, a 35 second relaxation delay was used, and a pulse angle of 90° was applied.

Materials and Methods

The metal-organic framework, MIL-101-SO_3[23] and homogeneous catalyst[26] were synthesized according to literature procedures. Tetrahydrofuran (THF) was purified using an Innovative Technologies (IT) solvent purification system consisting of a copper catalyst, activated alumina, and molecular sieves. Anhydrous N,N-dimethylformamide (DMF, 99.8%) was obtained from Alfa Aesar and used without further purification. Ethyl formate (98+%) in an AcroSeal bottle was purchased from Fisher Scientific and used without purification. n-

hexane, extra dry, over molecular sieves in an AcroSeal bottle was purchased from Fisher Scientific and used as received. Benzene anhydrous, 99.8% in a Sure/Seal was purchased from Sigma Aldrich and used without purification. 1,3,5-Trimethoxybenzene (99%) was purchased from Acros. Hydrochloric acid was purchased from MilliporeSigma. Dimethylsulfoxide-d_6 (DMSO-d_6, Cambridge Isotope Laboratories) was purchased from the supplier and used as received. Ultra-high purity hydrogen (99.999%) was purchased from Metro Welding.

Reactor Descriptions

A single Parr reactor type was employed. All are 45 mL and are composed of a well (in which the solid and liquid reagents are charged) and a head, which contains various attachments as described below. Each is made of Hastelloy C, and the wells are 7.5 cm tall and 3 cm in diameter. The heads consist of a pressure transducer and two inlet/outlet valves that can connect to a Parr Model 5000 Multiple Reactor system described above, a safety release valve, and a well for a thermocouple (Figure 5.14).

Figure 5.14. Picture of Reactor with the Parts of the Reactor Labeled

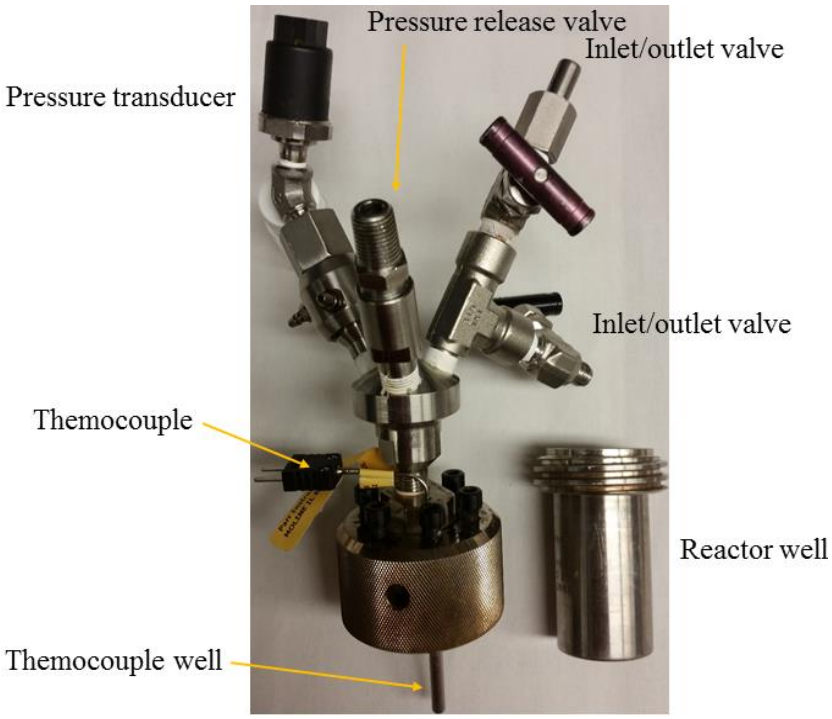

Reaction Work-up (see below for reactions that will be recycled)

At the reaction end time, the reactors were removed from the heating block and cooled for 10 minutes at room temperature. The pressure vessel was placed in a –84 °C bath (ethyl acetate/LN_2) for 15 min and then carefully vented using a metering valve. THF (0.5 mL) was added through the venting valve of the pressure vessel to wash any residual liquids/solids into the vessel. The vessel was then opened, 1,3,5-trimethoxybenzene (0.178 mmol, 300 µL of 0.593 M solution in DMSO-d_6) was added as a ^{1}H NMR standard. Approximately 50 µL of the resulting solution was added to an NMR tube containing 0.5 mL of DMSO-d_6. The sample was then analyzed by ^{1}H NMR spectroscopy.

Reaction Work-up for Recycled Reactions

At the reaction end time, the reactors were removed from the heating block and cooled for 10 minutes at room temperature before work-up. Small cold traps that were used for condensing the reaction products were removed from the oven and allowed to cool. Once the small trap was cool, the work-up was started (see Figure 5.15). Metering valves were attached to the reactor's inlet/outlet valve. The metering valve's tubing was attached to the outer opening of the cold trap and the trap was placed into a liquid nitrogen dewar where it cooled for about 5 minutes. The reactor was then opened via the inlet/outlet valve while the metering valve was closed. The metering valve was then used to slowly and carefully release excess pressure from the reactor. After about 3 minutes, the pressure coming through the trap was minimal, the metering valve was shut and Schlenk line tubing was attached to the other, central tube of the small trap. Vacuum was then applied to the trap. Once the vacuum had stabilized, the Schlenk line was closed resulting in static vacuum within the small trap between the Schlenk line and metering valve. Next, the metering valve was opened all the way and closed. The trap equilibrated for 2 minutes, before opening the Schlenk line again to pull active

vacuum. This cycling was repeated until the vacuum has stabilized and did not significantly increase when opened to the Schlenk line (normally 6 cycles).

Figure 5.15. Picture of Reactor Being Worked-up when Recycling Ir@MIL

The reactors were then transferred to the heating block at 100 °C. After two minutes, vacuum was then applied to the cold trap (still in liquid nitrogen). Once the vacuum had stabilized, the Schlenk line was closed resulting in static vacuum within the small trap between the Schlenk line and metering valve. Next, the metering valve was opened all the way and closed. After 2 minutes of equilibration, the Schlenk line was opened to pull active vacuum. This cycling was repeated until the vacuum had stabilized and did not significantly increase when opened to the Schlenk line. At this time, the metering valve was opened (exposing the reactor interior to active vacuum) and the vacuum was monitored to ensure that there was no increase in the pressure. The system remained open to active vacuum for 5 minutes at which time the metering valve, reactor inlet valve, and Schlenk line were closed.

The cold trap was then removed from the liquid nitrogen bath to thaw. The tubing to the Schlenk line and metering valve were carefully, but immediately, removed. The cold trap was placed into a beaker to thaw. 1,3,5-trimethoxybenzene (0.178 mmol, 300 μL, 0.593 M in DMSO-d_6) was immediately added to the center opening of the trap followed by 0.2 mL of DMSO-d_6. When the solution in the trap was still cold, but unfrozen, the trap was mixed well

to ensure a homogenous solution. The solution was then poured into a 4 mL vial and sealed with a Teflon cap. NMR tubes were charged with 0.5 mL of DMSO-d_6. Once the vial of reaction solution was at room temperature 3-4 drops of the solution were added to the NMR tube, which was then capped and thoroughly shaken to ensure mixing.

The metering valve was removed from the closed reactor and both were pumped into the glovebox. Once inside the glovebox, the metering valve was then placed back onto the reactor and the reactor was slowly vented via the metering valve. The reactor was then opened, and more substrate/solvent were added. The reactor was then closed and removed from the glovebox before being sealed and pressurized as normal.

5.4.2. Catalyst Preparation

MIL-101-SO_3 Synthesis and Work-up with DMF

Concentrated hydrochloric acid (0.69 mL) was loaded into a jar containing 45 mL of deionized water. Monosodium 2-sulfoterephthalic acid (3.01 g) and CrO_3 (1.16 g) were added to the jar. The jar was sealed with a Teflon cap and thoroughly shaken before being sonicated for 20 minutes. The solution was divided into three portions and each placed into a 20 mL Teflon-lined stainless-steel autoclaves. The autoclaves were each heated at 180 ºC in an oven for 6 d. The oven was then turned off, the door opened, and the autoclaves and oven cooled to room temperature. The resulting green solids were washed with DMF (4 x 40 mL). The solids were then dried at room temperature under high vacuum for 24 h. The MOF was ground with mortar and pestle and stored on bench top in sealed 20 mL vials.

Ir@MIL-101-SO_3 Synthesis with DMF

The homogeneous complex, IrCp*Bpy (40.6 mg) was weighed into a 20 mL vial and 1.36 mL of DMF were added. MIL-101-SO_3 (69.1 mg) was weighed into a separate 20 mL

vial. DMF (2.05 mL) was added to the MOF and the homogeneous catalyst solution was transferred to the MOF vial. The 20 mL vial was capped and placed on a shaker for 4 days. The contents of the vial were then transferred to centrifuge tubes, centrifuged, and the solid was then washed with DMF (4 x 6 mL). The solid was dried at room temperature under high vacuum for 24 hours, before being dried at 125 °C under high vacuum for 24 hours. ICP-OES found the Ir:Cr to be 0.33 which corresponded to 2.8 wt% when DMF was not taken into consideration.

MIL-101-SO_3 Synthesis and Work-up without DMF

Concentrated hydrochloric acid (0.69 mL) was loaded into a jar containing 45 mL of deionized water. Monosodium 2-sulfoterephthalic acid (3.01 g) and CrO3 (1.16 g) were added to the jar. The jar was sealed with a Teflon cap and thoroughly shaken before being sonicated for 20 minutes. The solution was divided into three portions and each placed into a 20 mL Teflon-lined stainless-steel autoclaves. The autoclaves were each heated at 180 ºC in an oven for 6 d. The oven was then turned off, the door opened, and the autoclaves and oven cooled to room temperature. The resulting green solids were washed with H_2O (4 x 40 mL). The solids were then dried at room temperature under high vacuum for 24 h. The material was then transferred into three 20 mL vials and dried at 125 °C under high vacuum for 24 h. The MOF was then transferred into a N_2-filled glovebox under vacuum. The MOF was ground with mortar and pestle and stored in the water and oxygen free environment.

Ir@MIL-101-SO_3 Synthesis without DMF

The homogeneous complex, IrCp*Bpy (40.6 mg) was weighed into a 20 mL vial and THF (4.54 mL) was added. MIL-101-SO_3 (69.1 mg) was weighed into a separate 20 mL vial. THF (2.05 mL) was added to the MOF and the homogeneous catalyst solution was transferred

to the MOF vial. The 20 mL vial was capped and placed on a shaker for 4 days. The contents of the vial were then transferred to centrifuge tubes, centrifuged, and the solid was then washed with THF (5 x 10 mL). The solid was then dried at room temperature under high vacuum for 24 hours, before being dried at 125 °C under high vacuum for 24 hours. The Ir@MIL material was then transferred into a N_2-filled glovebox under vacuum where it was stored in the water and oxygen free environment.

5.4.3. Hydrogenation Reactions

Ethyl Formate Hydrogenation with MIL-101-SO_3

The appropriate amount of MIL-101-SO_3 was weighed into a 4 mL vial. For Figure 5.3, 11.4 mg of MIL-101-SO_3 containing 22 equivalents of DMF were used and for Figure 5.11, 3.8 mg of MIL-101-SO_3 were used. The contents of the vial were transferred to the well of the reactor. The vial was charged with 1.0 mL of ethyl formate via a 1 mL syringe and transferred via pipette to the well of the reactor. The reactor was immediately sealed and removed from the glovebox. The vessel was connected to the Parr Multiple Reactor System, and the manifold was thoroughly purged (1 minute and then cycled 15 times) with Ultra High Purity H_2 (99.999%). The vessel was then pressurized with 30 bar with Ultra High Purity H_2 at room temperature to reach a total pressure of 30 bar. The reaction was placed into a preheated block at 100 °C. After 16 hours of heating, the reactor was treated as described in the "Reaction Work-up" section above (see 5.4.1.).

Ethyl Formate Hydrogenation with IrCp*Bpy

The appropriate amount of IrCp*Bpy was weighed into a 4 mL vial. For Figure 5.3, 1.8 mg IrCp*Bpy (2.3 μmol) were used and for Figure 5.9, 1.7 mg (2.1 μmol) of IrCp*Bpy were used. The contents of the vial were transferred to the well of the reactor. The vial was charged

with 1.0 mL of ethyl formate via a 1 mL syringe and transferred via pipette to the well of the reactor. The reactor was immediately sealed and removed from the glovebox. The vessel was connected to the Parr Multiple Reactor System, and the manifold was thoroughly purged (1 minute and then cycled 15 times) with Ultra High Purity H_2 (99.999%). The vessel was then pressurized with 30 bar with Ultra High Purity H_2 at room temperature to reach a total pressure of 30 bar. The reaction was placed into a preheated block at 100 °C. After 16 hours of heating, the reactor was treated as described in the "Reaction Work-up" section above (see 5.4.1.).

Ethyl Formate Hydrogenation with Ir + MIL-101-SO_3

The appropriate amount of IrCp*Bpy was weighed into a 4 mL vial. For Figure 5.3, 1.8 mg IrCp*Bpy (2.3 μmol) were used and for Figure 5.11, 1.7 mg (2.1 μmol) of IrCp*Bpy were used. In a separate 4 mL vial, MIL-101-SO_3 was weighed out. For Figure 5.3, 11.4 mg of MIL-101-SO_3 containing 22 equivalents of DMF were used and for Figure 5.9, 3.8 mg of MIL-101-SO_3 were used. The contents of both vials were transferred to the well of the reactor. Each vial was charged with 0.5 mL of ethyl formate via a 1 mL syringe and transferred via pipette to the well of the reactor. The reactor was immediately sealed and removed from the glovebox. The vessel was connected to the Parr Multiple Reactor System, and the manifold was thoroughly purged (1 minute and then cycled 15 times) with Ultra High Purity H_2 (99.999%). The vessel was then pressurized with 30 bar with Ultra High Purity H_2 at room temperature to reach a total pressure of 30 bar. The reaction was placed into a preheated block at 100 °C. After 16 hours of heating, the reactor was treated as described in the "Reaction Work-up" section above (see 5.4.1.).

Ethyl Formate Hydrogenation with Ir@MIL

The appropriate amount of Ir@MIL was weighed into a 4 mL vial. For Figure 5.3, Ir@MIL (11.8 mg of 1.9 wt%, 1.1 μmol) containing 22 equivalents of DMF were used and for Figure 5.11, 5.5 mg of Ir@MIL (7.3 wt%, 2.1 μmol) were used. The contents of the vial were transferred to the well of the reactor. The vial was charged with 1.0 mL of ethyl formate via a 1 mL syringe and transferred via pipette to the well of the reactor. The reactor was immediately sealed and removed from the glovebox. The vessel was connected to the Parr Multiple Reactor System, and the manifold was thoroughly purged (1 minute and then cycled 15 times) with Ultra High Purity H_2 (99.999%). The vessel was then pressurized with 30 bar with Ultra High Purity H_2 at room temperature to reach a total pressure of 30 bar. The reaction was placed into a preheated block at 100 °C. After 16 hours of heating, the reactor was treated as described in the "Reaction Work-up" section above (see 5.4.1.).

Recycling Studies with Ir@MIL (Figure 5.4)

The appropriate amount of Ir@MIL was weighed into a 4 mL vial. For Figure 5.4, Ir@MIL (11.8 mg of 1.9 wt%, 1.1 μmol) containing 22 equivalents of DMF were used. The contents of the vial were transferred to the well of the reactor. The vial was charged with 1.0 mL of ethyl formate via a 1 mL syringe and transferred via pipette to the well of the reactor. The reactor was immediately sealed and removed from the glovebox. The vessel was connected to the Parr Multiple Reactor System, and the manifold was thoroughly purged (1 minute and then cycled 15 times) with Ultra High Purity H_2 (99.999%). The vessel was then pressurized with 30 bar with Ultra High Purity H_2 at room temperature to reach a total pressure of 30 bar. The reaction was placed into a preheated block at 100 °C. After 16 hours of heating, the reactor was treated as described in the "Reaction Work-up for Recycled Reactions" section above (see 5.4.1.). After work-up and upon bringing the reactor into the glovebox, the reactor was

recharged with 1.0 mL of ethyl formate via a 1 mL syringe. The reactor was immediately sealed and removed from the glovebox. The vessel was connected to the Parr Multiple Reactor System, and the manifold was thoroughly purged (1 minute and then cycled 15 times) with Ultra High Purity H_2 (99.999%). The vessel was then pressurized with 30 bar with Ultra High Purity H_2 at room temperature to reach a total pressure of 30 bar. The reaction was placed into a preheated block at 100 °C. After 16 hours of heating, the reactor was treated as described in the "Reaction Work-up" section above (see 5.4.1.).

Ethyl Formate Hydrogenation in Benzene (Figure 5.6)

The appropriate amount of catalyst, either IrCp*Bpy (1.8 mg, 2.3 μmol) or Ir@MIL (11.8 mg of 1.9 wt%, 1.1 μmol), was weighed into a 4 mL vial. The contents of the vial were transferred to the well of the reactor. The vial was charged with 0.9 mL of benzene and 0.1 mL of ethyl formate via a 1 mL syringe and transferred via pipette to the well of the reactor. The reactor was immediately sealed and removed from the glovebox. The vessel was connected to the Parr Multiple Reactor System, and the manifold was thoroughly purged (1 minute and then cycled 15 times) with Ultra High Purity H_2 (99.999%). The vessel was then pressurized with 30 bar with Ultra High Purity H_2 at room temperature to reach a total pressure of 30 bar. The reaction was placed into a preheated block at 100 °C. After 16 hours of heating, the reactor was treated as described in the "Reaction Work-up" section above (see 5.4.1.).

Ethyl Formate Hydrogenation in n-Hexane (Figure 5.6)

The appropriate amount of catalyst, either IrCp*Bpy (1.8 mg, 2.3 μmol) or Ir@MIL (11.8 mg of 1.9 wt%, 1.1 μmol), was weighed into a 4 mL vial. The contents of the vial were transferred to the well of the reactor. The vial was charged with 0.9 mL of hexane and 0.1 mL of ethyl formate via a 1 mL syringe and transferred via pipette to the well of the reactor. The

reactor was immediately sealed and removed from the glovebox. The vessel was connected to the Parr Multiple Reactor System, and the manifold was thoroughly purged (1 minute and then cycled 15 times) with Ultra High Purity H_2 (99.999%). The vessel was then pressurized with 30 bar with Ultra High Purity H_2 at room temperature to reach a total pressure of 30 bar. The reaction was placed into a preheated block at 100 °C. After 16 hours of heating, the reactor was treated as described in the "Reaction Work-up" section above (see 5.4.1.).

Ethyl Formate Hydrogenation with Different Batches of Ir@MIL (Figure 5.7)

11.8 mg of Ir@MIL was weighed into a 4 mL vial. For Batch A, Ir@MIL contained 22 equivalents of DMF per Ir, while Batch B had 28 equivalents of DMF to Ir (Batch C's DMF content was not determined). The contents of the vial were transferred to the well of the reactor. The vial was charged with 1.0 mL of ethyl formate via a 1 mL syringe and transferred via pipette to the well of the reactor. The reactor was immediately sealed and removed from the glovebox. The vessel was connected to the Parr Multiple Reactor System, and the manifold was thoroughly purged (1 minute and then cycled 15 times) with Ultra High Purity H_2 (99.999%). The vessel was then pressurized with 30 bar with Ultra High Purity H_2 at room temperature to reach a total pressure of 30 bar. The reaction was placed into a preheated block at 100 °C. After 16 hours of heating, the reactor was treated as described in the "Reaction Work-up" section above (see 5.4.1.).

Influence of DMF on Ethyl Formate Hydrogenation with IrCp*Bpy (Figure 5.10)

The appropriate amount of IrCp*Bpy was weighed into a 4 mL vial. The contents of the vial were transferred to the well of the reactor. The vial was charged with 1 mL of ethyl formate via a 1 mL syringe. To the solution, 5 µL of DMF via a 10-µL syringe were added to the vial. The solution was transferred via pipette to the well of the reactor. The reactor was

immediately sealed and removed from the glovebox. The vessel was connected to the Parr Multiple Reactor System, and the manifold was thoroughly purged (1 minute and then cycled 15 times) with Ultra High Purity H_2 (99.999%). The vessel was then pressurized with 30 bar with Ultra High Purity H_2 at room temperature to reach a total pressure of 30 bar. The reaction was placed into a preheated block at 100 °C. After 16 hours of heating, the reactor was treated as described in the "Reaction Work-up" section above (see 5.4.1.).

5.4.4. Ion Exchange of IrCp*Bpy Out of Ir@MIL

Into a 4 mL vial, 9.7 mg of Ir@MIL 2.8 wt% were added. To the vial, 0.5 mL of DMSO-d_6 and 95 µL of 0.1 M HCl were added. The vial was closed and placed on a shaker plate for 4 days. After 4 days, the solution was clear and yellow. The vial was opened and 1,3,5-trimethoxybenzene (0.178 mmol, 300 µL of 0.593 M solution in DMSO-d_6) was added. The solution was then transferred into an NMR tube and ^{1}H NMR was collected (see Figure 5.8).

In parallel with the above experiment, 2.5 mg of IrCp*Bpy were added to a separate 4 mL vial. To the vial, 0.5 mL of DMSO-d_6 and 95 µL of 0.1 M HCl were added. The vial was closed and placed on a shaker plate for 4 days. After 4 days, the solution was clear and yellow. The vial was opened and 1,3,5-trimethoxybenzene (0.178 mmol, 300 µL of 0.593 M solution in DMSO-d_6) was added. The solution was then transferred into an NMR tube and ^{1}H NMR was collected (see Figure 5.8).

These HCl exchange studies found the material used in Figures 5.3, 5.4, and 5.6 to have 22 equivalents of DMF. The weight percent equation therefore needed to be adjusted to account for the mass of DMF (Equation 5.3). In Figure 5.7, Batch A is the same as Figures 5.3, 5.4, and 5.6, while Batch B had 28 equivalents, and Batch C was not determined. Due to DMF present, the weight percent of Ir@MIL was truly 1.9 wt% Ir, not 2.8 wt%. Corrected hydrogenation

products for Figures 5.3, 5.4, and 5.6 appear below in Table 5.2. Ultimately, this finding, though important, didn't change any of the previous conclusions.

Equation 5.3. Weight Percent Calculation Accounting for DMF

$$wt\%\ Ir = \frac{mg\ Ir}{mg\ IrCp * Bpy + mg\ MIL - 101 - SO_3 + mg\ DMF}$$

Table 5.2. Corrected TONs for Ir@MIL Catalysis in Figures 5.3, 5.4, and 5.6

Figure	Conditions	Reported TON		Corrected TON	
		Methyl Formate	Methanol	Methyl Formate	Methanol
5.3	Ir@MIL	542	203	835	314
5.4	Fresh	542	203	835	314
	Recycle	130	23	200	35
5.5	Benzene	41	42	63	65
	Hexane	25	15	39	23

5.4.5. Post-Catalysis ICP

For materials that were analyzed post-catalysis via ICP, all materials were thoroughly washed and dried to ensure no inference occurred with the ICP-MS. Each MOF was filtered, rinsed with acetone (3 mL), and allowed to air dry on the filter paper. The MOF was then transferred to a 4 mL vial where it was dried under high vacuum for approximately 4 hours. Finally, the 4 mL vial was placed inside a 20 mL vial and dried under high vacuum at 125 °C for 24 hours. The material was then digested as described above (see 5.4.1).

5.5. References

1. Huff, C. A.; Sanford, M. S. *J. Am. Chem. Soc.* **2011**, *133*, 18122.

2. Miessler, G. L.; Fischer, P. J.; Tarr, D. A. *Inorganic Chemistry*, 5th ed.; Pearson, **2013.**

3. Munshi, P.; Main, A. D.; Linehan, J. C.; Tai, C. C.; Jessop, P. G. *J. Am. Chem. Soc.* **2002**, *124*, 7963.

4. Kar, S.; Kothandaraman, J.; Goeppert, A.; Prakash, G. K. S. *J. CO_2 Util.* **2018**, *23*, 212.

5. Sodakis, K.; Tang, C.; Vogt, L. K.; Junge, H.; Dyson, P. J.; Beller, M.; Laurenczy, G. *Chem. Rev.* **2018**, *118*, 372.

6. Artz, J.; Müller, T. E.; Thenert, K. *Chem. Rev.* **2018**, *118*, 434.

7. Zhou, H.-C.; Long, J. R.; Yaghi, O. M. *Chem. Rev.* **2012**, *112*, 673.

8. Seth, S.; Matzger, A. J. *Cryst. Growth Des.* **2017**, *17*, 4043.

9. Mitchell, L.; Gonzalez-Santiago, B.; Mowat, J. P. S.; Gunn, M. E.; Williamson, P.; Acerbi, N.; Clarke, M. L.; Wright, P. A. *Catal. Sci. Technol.* **2013**, *3*, 606.

10. Xu, C.; Peng, Y.; Han, X.; Liu, Y.; Lin, X.; Cui, Y. *Nat. Commun*. **2017**, *8*, 2171.

11. Lu, W.; Wei, Z.; Gu, Z.-Y.; Liu, T.-F.; Park, J.; Park, J.; Tian, J.; Zhang, M.; Zhang, Q.; Gentle, T.; Bosch, M.; Zhou, H.-C. *Chem. Soc. Rev.* **2014**, *43*, 5561.

12. Kim, M.; Cohen, S. M. *CrystEngComm.* **2012,** *14*, 4096.

13. Ahnfeldt, T.; Gunzelmann, D.; Wack, J.; Senker, J.; Stock, N. *CrystEngComm.* **2012,** *14*, 4126.

14. Burrows, A. D.; Keenan, L. L. *CrystEngComm.* **2012,** *14*, 4112.

15. Manna, K.; Ji, P.; Lin, Z.; Greene, F. X.; Urban, A.; Thacker, N. C.; Lin, W. *Nat. Commun.* **2016**, *7*, 12610.

16. Kim, M.; Cahill, J. F.; Su, Y.; Prather, K. A.; Cohen, S. M. *Chem. Sci.* **2012**, *3*, 126.

17. Rogge, S. M. J.; Bavykina, A.; Hajek, J.; Garcia, H.; Olivos-Suarez, A. I.; Sepúlveda-Escribano, A.; Vimont, A.; Clet, G.; Bazin, P.; Kapteijn, F.; Daturi, M.; Ramos-Fernandes, E. V.; Llabrés I Xamena, F. X.; Van Speybroeck, V.; Gascon, J. *Chem. Soc. Rev.* **2017**, *46*, 3134.

18. Sawano, T.; Thacker, N. C.; Lin, Z.; McIsaac, A. R.; Lin, W. *J. Am. Chem. Soc.* **2015**, *137*, 12241.

19. Manna, K.; Zhang, T.; Greene, F. X.; Lin, W. *J. Am. Chem. Soc.* **2015** *137*, 2665.

20. Sawano, T.; Lin, Z.; Boures, D.; An, B.; Wang, C.; Lin, W. *J. Am. Chem. Soc.* **2016**, *138*, 9783.

21. Rimoldi, M.; Nakamura, A.; Vermeulen, N. A.; Henkelis, J. J.; Blackburn, A. K.; Hupp, J. T.; Stoddart, J. F.; Farha, O. K. *Chem. Sci.* **2016**, *7*, 4980.

22. Genna, D. T.; Wong-Foy, A. G.; Matzger, A. J.; Sanford, M. S. *J. Am. Chem. Soc.* **2013**, *135*, 10586.

23. Genna, D. T.; Pfund, L. Y.; Samblanet, D. C.; Wong-Foy, A. G.; Matzger, A. J.; Sanford, M. S. *ACS Catal.* **2016**, *6*, 3569.

24. Hartwig, J. F. *Organotransition Metal Chemistry*: *From Bonding to Catalysis*. University Science Books, **2010**.

25. Brewster, T. P.; Miller, A. J. M.; Heinekey, D. M.; Goldberg, K. I. *J. Am. Chem. Soc.* **2013**, *135*, 16022.

26. Brewster, T. P.; Rezayee, N. M.; Culakova, Z.; Sanford, M. S.; Goldberg, K. I. *ACS Catal.* **2016**, *6*, 3113.

27. Akiyama, G.; Matsuda, R.; Sato, H.; Takata, M.; Kitagawa, S. *Adv. Mater.* **2011**, *23*, 3294.

28. Portions of this work were completed in collaboration with undergraduate Zohaib Siddiq of the Sanford lab with characterization aid by Jake Boissonnault from Professor Adam Matzger's Group at the University of Michigan.